Technical University of Denmark

DTU

Coordinated Frequency Control of Wind Turbines in Power Systems with High Wind Power Penetration

Tarnowski, Germán Claudio; Sørensen, Poul Ejnar; Østergaard, Jacob; Carne Kjær, Philip

[Link back to DTU Orbit](#)

DTU Library
Technical Information Center of Denmark

Technical University of Denmark

DTU

Germán Claudio Tarnowski

Coordinated Frequency Control
of
Wind Turbines in Power Systems
with High Wind Power Penetration

PhD Thesis, November 2011

DTU Electrical Engineering
Department of Electrical Engineering

Germán Claudio Tarnowski

Coordinated Frequency Control
of
Wind Turbines in Power Systems
with High Wind Power Penetration

PhD Thesis, November 2011

Coordinated Frequency Control of Wind Turbines in Power Systems with High Wind Power Penetration,

Author:
Germán Claudio Tarnowski

Supervisors:
Professor Jacob Østergaard, Centre for Electric Technology, DTU Elektro.
Dr. Philip Carne Kjær, Chief Specialist, Vestas Wins Systems A/S.
Professor Poul Ejnar Sørensen, DTU Wind Energy, Risø DTU.

Department of Electrical Engineering	**Global Research Department**
Centre for Electric Technology (CET)	Power Plant R&D / Engineering
Technical University of Denmark	Vestas Wind Systems A/S
Elektrovej 325	Dusager 4
DK-2800 Kgs. Lyngby	DK-8200 Aarhus N
Denmark	Denmark
www.elektro.dtu.dk/cet	www.vestas.com
Tel: (+45) 45 25 35 00	Tel: (+45) 97 30 00 00
Fax: (+45) 45 88 61 11	
E-mail: cet@elektro.dtu.dk	

"Querer es poder"

(*"To want is to be able to"*)

A mis padres, hermano y hermanas.

(*To my parents, brother and sisters*)

ABSTRACT

The integration of large amounts of wind power in power systems presents huge challenges. In particular, with the increase of wind power generation, more regulation reserves would be necessary, the capability of the power system to offer conventional regulating power would be reduced and the dynamic stability of the grid frequency under large disturbances would be compromised.

The aim of this study is to investigate the integration of large scale wind power generation in power systems and its active power control. Novel methods and solutions dealing specifically with the electric frequency stability and high wind power penetration or in islanding situations are addressed.

The review of relevant theoretical concepts is supported by measurements carried out on an isolated power system characterized by high wind power penetration. Different mathematical and simulation models are used in several particular views. These models were developed and verified during this work, based around a particular manufacturer's wind turbine and on said isolated power system with wind power.

The capability of variable speed wind turbines for providing Inertial Response is analysed. To perform this assessment, a control algorithm for wind turbine inertial response is developed and the performance is simulated for a single wind turbine. It is shown that wind power is able to provide valuable inertial response when combining a large number of wind turbines in a wind plant.

Active power control architectures for wind power generation were studied considering a large share of wind power in the system. Results show the abilities of the architectures to manage the variability of the generated wind power, reducing the impact on the grid frequency and providing suitable frequency regulation service when required.

The coordination between the developed control systems and the conventional plants responses is studied. A methodology for determining the necessary wind power reserve and control parameters such as frequency response characteristic (droop) and deadband is presented. The performance and the capability for supporting the grid in normal operation and during large load events are demonstrated with accurate computational simulations.

RESUMÉ PÅ DANSK

Dette ErhvervsPhD projekt har udviklet reguleringsstrategier med det formål at facilitere en forøget andel af vindkraft i elektriske elforsyningssystemer. Disse reguleringsstrategier er målrettet frekvensstabilitet problemet, der kan forårsages af store andele vindkraft i elforsyningssystemet eller når elforsyningssystemet er i ø-drift.

Konventionelle kraftværker er normalt ansvarlige for at regulere frekvensen i elektriske elforsyningssystemer. Med høje andele af vindkraft kan der opstå balance problemer med den aktive effekt, der vanskeliggør frekvensreguleringen. Dette forværres af, at en høj andel af vindkraft fortrænger konventionelle kraftværker fra systemet. Det er nødvendigt at finde løsninger til disse problemer for at muliggøre at betydelige mængder vindkraft kan integreres i verdens elforsyningssystemer.

I dette projekt er det blevet undersøgt, hvorledes vindkraftværker kan deltage i frekvensreguleringen og hvilke egenskaber deres respons skal have. Formålet med projektet har været at finde en metodik for frekvensregulering med vindmøller, at udvikle en reguleringsarkitektur for realtidsbalancering af vindmøllernes produktion og at foreslå en metodik til at koordinere frekvensreguleringen fra vindkraftværkerne med de konventionelle kraftværkers eksisterende frekvensreserver. Det Bornholmske elforsyningssystem under ø-drift har været benyttet som et eksempel på et svagt forbundet elforsyningssystem med en betydelig andel af vindkraft. De udviklede løsninger er blevet verificeret med en simuleringsmodel af dette system, men vil ikke desto mindre også være brugbare for et stort elforsyningssystem.

De vigtigste resultater viser, at vindmøller kan bidrage til både frekvensreguleringen og frekvensstabiliteten ved at benytte en kombination af aktiv effektregulering og inertirespons. Muligheden for at lave inertirespons med vindmøller afhænger kraftigt af den øjeblikkelige vindstyrke, men responset kan forbedres ved et hensigtsmæssigt design af vindmøllens reguleringssystem. Den udviklede reguleringsarkitektur kombinerer funktionaliteter på systemniveau til at bidrage med services, der forbedrer frekvensstabiliteten i elforsyningssystemer med en høj andel af vindkraft. Den udviklede koordineringsmetode kan levere rammen for den reguleringsarkitektur, der tillader et samspil med de eksisterende frekvensreserver.

Dette projekt har udviklet løsninger til at integrere vindkraftværker, understøttet fremtidige arkitekturer for elforsyningssystemer som for eksempel tilsigtet ø-drift og har bidraget med ny viden til både Vestas Wind Systems A/S og til DTU.

RESUMEN EN CASTELLANO

La integración de grandes cantidades de generación eólica en los sistemas de potencia presenta enormes desafíos. En particular, con el aumento de generación eólica en un sistema de potencia, mayores cantidades de reservas de regulación serían necesarias, la capacidad del sistema de potencia de ofrecer potencia regulante convencional se reduciría y la estabilidad dinámica de la frecuencia de la red bajo grandes perturbaciones quedaría comprometida.

El objetivo de este trabajo es investigar la integración de generación eólica a gran escala en los sistemas de potencia y su control de potencia activa. Nuevos métodos y soluciones que tratan específicamente con la estabilidad de la frecuencia eléctrica con altos niveles de penetración de generación eólica, o en situaciones de isla, son atendidos.

La revisión de los conceptos teóricos relevantes se apoya en mediciones realizadas sobre un sistema de potencia aislado caracterizado por poseer altos niveles de penetración de generación eólica. Diferentes modelos matemáticos y de simulación son utilizados en varios análisis particulares. Estos modelos fueron desarrollados y verificados durante este trabajo, en torno a una turbina eólica de un fabricante en particular y sobre dicho sistema eléctrico aislado con generación eólica.

La capacidad de los aerogeneradores de velocidad variable para proporcionar Respuesta Inercial es analizada. Para llevar a cabo esta evaluación, un algoritmo de control para la respuesta inercial de aerogeneradores es desarrollado y su desempeño es simulado. Se muestra que la generación eólica es capaz de proporcionar una respuesta inercial valiosa para el sistema de potencia cuando se combina un gran número de turbinas eólicas en una central eólica.

Arquitecturas para el control de la potencia activa de grandes cantidades de generación eólica en el sistema de potencia fueron estudiadas. Los resultados muestran las distintas capacidades de las arquitecturas estudiadas para gestionar la variabilidad de la potencia eólica generada, reduciendo el impacto en la frecuencia de la red y proporcionando un servicio adecuado de regulación de frecuencia cuando es requerido.

La coordinación entre los sistemas de control desarrollados y las respuestas de las plantas convencionales es estudiada. Es desarrollada una metodología para la determinación de la potencia de reserva eólica necesaria y los parámetros de control, como ser la característica de la respuesta de frecuencia (proporcionalidad) y la banda muerta de frecuencia. El rendimiento y la capacidad para soportar la red durante el funcionamiento normal y durante los grandes eventos de carga son demostrados con simulaciones computacionales precisas.

PREFACE

ACKNOWLEDGEMENTS

TABLE OF CONTENTS

ACRONYMS, ABREVIATIONS & SYMBOLS

Symbol	Unit	Definition
AC	-	Alternating Current
AGC	-	Automatic Generation Control
C	-	Constant
C_P, C_{PN}	-	Respectively: WTG coefficient of aerodynamical power (efficiency) and WTG coefficient at nominal power.
DB	Hz; pu	Frequency dead-band
DC	-	Direct Current
DFIG	-	Doubly-Fed Induction Generator
DR	MW	Disturbance reserve (large frequency events).
DSO	-	Distribution system operator
D_i	pu	Damping coefficient of the machine i
D_{sys}	pu	Coefficient of load-frequency dependency
da/db	[a]/[b]; pu	Derivative of a with respect to b
d_{DT}	pu/rad/s	Drive train friction between masses
E_{Aero}	J; pu	Aerodynamical energy obtained from WTG rotor
$E_{Eletric}$	J; pu	Electrical energy injected into the grid
E_i	V; pu	Internal voltage in a SG, machine i
$E_{Inertia}$	J; pu	Electrical energy obtained from kinetic energy
$E_{Kinetic}$	J; pu	Kinetic energy in rotating mass
E_{Losses}, $E_{Losses-Mech}$, $E_{Losses-Gen}$	J; pu	Respectively: total lost energy, lost energy in mechanical system and lost energy in generator
E_{Self}	J, pu	Energy self-consumed by WTG (auxiliary systems)
EC	MW-h; pu	Energy consumption in the power system.
FR	-	Frequency Response
FSM	-	Frequency Sensitive Mode
F_{DT}	pu/(rad/s)^2	Drive train speed dependant losses coefficient
f	Hz; pu	Frequency; grid frequency.
f_{meas}	Hz; pu	Measured terminal's frequency
f_0	Hz; pu	Nominal grid frequency
f_{PLL}	Hz; pu	Frequency value as output from the PLL
f_{ss}	Hz; pu	Steady state grid frequency
f_T	N; pu	Thrust force generated on the rotor's blades

G , G1	$1/\Omega$; pu	Conductance. Generator 1.
GC	-	Grid code(s)
G_{EIR}	-	Gain for the energy delivered during IR
H, H_i	s	Machine inertia constant based on machine's rating
H'	s	Machine inertia constant based on power system base power
H_{sys}	s	Inertia constant of the power system, based on power system base power
IR	-	Inertial response (of the WTG/WPP)
i	-	Element of a set
ini	-	Instant of time immediately after the event
I_{dqs}	A; pu	Stator currents in the d-q system
I_{dqr}	A; pu	Rotor currents in the d-q system
I_{dr-ref} , I_{qr-ref}	A; pu	Reference values for rotor currents controller (d or q axis)
ICa	MW	Installed capacity of wind power
$Is\_Connected\_WPS\text{-}i$	-	Flag indicating connection of WPS-i
$Is\_Higher\_than\_Pmean\_WPS\text{-}i$	-	Flag indicating production is higher than mean
$Is\_regulated\_WPS\text{-}i$	-	Flag indicating WPS-i production is being regulated
J, J_t	kgm^2	Moment of inertia and WTG total moment of inertia
K_{Aero}	pu	Constant of the turbine rotor which includes swept area, air density, and mathematical constants.
K_{p_PLL}	Pu	Proportional gain for the PI of the PLL implemented for IR
K_{i_PLL}	pu	Integrator gain for the PI of the PLL implemented for IR
K_{sys}	MW/Hz; pu	System stiffness
L, L	-	Load
LFSM	-	Limited Frequency Sensitive Mode
LVRT	-	Low Voltage Ride Through functionality
NPS	-	Nordic Power System
N_{HiMean}	-	Number of sources i with production higher than mean
$NWPS$	-	Number of WPS
$NWPS_{Fluct}$	-	Number of WPS with fluctuating output
$NWPS_{Reg}$	-	Number of WPS with regulated output
PCC	-	Point of Common Coupling

PFC	-	Primary frequency control
PI	-	Proportional-Integral controller
PLL	-	Phase-Locked Loop (device or algorithm)
PS	-	Power system
PS1, PS2, PS3	-	Power system models 1, 2 and 3
P	MW; pu	Active power
P_{Aero}, P_{AeroN}	MW; pu	Respectively: aerodynamical power being developed in the WTG rotor and aerodynamical power at nominal operation
P_{Ava}, P_{AvaWTG}, P_{AvaMin}	MW; pu	Respectively: available wind power possible to be generated at the moment and minimum available power for allowing IR operation.
$P_{conv-ref}$	MW; pu	Reference for the power converter of the WTG
P_{Curt}	MW; pu	Power that has been curtailed (limited) from P_{Ava}
$P^*_{DemandWPGS}$	MW; pu	Reference for the WPGS
$P_{demandWTG}$	MW; pu	Demanded power to the WTG. Reference
P^*_{ExtWPS}		External reference, absolute constraint, for the generated power from the WPS
P_e, $P_{Electric}$	MW; pu	Generator's electrical power
P_{elWTG}, P_{elWPS}	MW; pu	Respectively: active power output from the WTG and from a WPS
$P_{ext-ref}$	MW; pu	Reference from external command
$P_{Inertia}$, ΔP_{IR}	MW; pu	Active power component coming from kinetic energy. Power output due to IR actuation
$P_{Kinetic}$	MW; pu	Mechanical power from kinetic energy transformation
P_L, P_{Lnet}	MW; pu	Power consumed by the load (or net load)
P_{Losses}	MW; pu	Lost power due to irreversible transformation
P_m	MW; pu	Mechanical power. Prime mover output
P_{MaxOL}, P_{MaxTOL},	MW; pu	Respectively: maximum allowed power overload and power that creates a T_{MaxOL} for the given ω_t
P_{maxWTG}	MW; pu	The maximum external reference acceptable for the WTG
P_{mdq}, P_{md}, P_{mq}	pu	Switching duty cycle of the power electronics represented in the d-q reference frame
P_{meas}	MW; pu	Measured active power output
P_{Min}, P_{minWTG}	MW; pu	The minimum external reference acceptable for the WTG

P_{msys}	MW; pu	Mechanical power of the equivalent prime mover seen from the system point of view
P_{opt}	MW; pu	Optimal power from available wind
P_{Ref}	MW; pu	Reference for the active power controller
P_{ResWPS}	MW; pu	Amount of power reserve (curtailment) in the WPS
P_{Sij}	MW/rad; pu	Synchronizing power coefficient between grid node i and grid node j
P_t, P_{tN}	MW; pu	Respectively: turbine power output and nominal turbine power
$P_{WindMax}$	MW; pu	Is an upper limitation for the wind power at system level
$P_{WindMin}$	MW; pu	The minimum possible power to be generated for the next period of time
Q	MVAr; pu	Reactive power
Q_{meas}	MVAr; pu	Measured reactive power (for controller input)
Q_{ref}	MVAr; pu	Reference for the power converter of the WTG
ROCOF	Hz/s; pu/s	Rate of change of grid frequency
RR	MW	Normal regulation reserves
R_i (R_{SGi})	pu	Droop of the governor of machine i
R_{HF}, R_{LF}, R_{wind}	pu	Droop of wind power frequency control (High Frequency, Low Frequency and Wind (in general))
R_{sys}	pu	Equivalent droop seen from the system point of view
R_t	m; pu	WTG's rotor radius
SFC	-	Secondary frequency control
SG	-	Synchronous generator(s)
SRM	-	System regulation margin
t	s	Time
T_{Boost}	s	Period of time during first stage of IR operation
T_G	s	Governor's time constant
Thf_{Hi}, Thf_{Lo}	Hz; pu	Threshold values for Hi and Low frequency event detection, respectively.
$Thdf_{Hi}, Thdf_{Lo}$	Hz/s; pu/s	Threshold values for Hi and Low ROCOF event detection, respectively.
T_{MaxTOL}	Nm; pu	Maximum allowed mechanical torque overload
$T_{Recovery}$	S	Period of time for WTG recovery action after first stage of

		IR operation
$T_{r\,WPP}$, $T_{r\,WTG}$	-	Transformer of WPP and WTG
T_{sWPP}	s	Sampling time of the WPPC
T_{sWPS}	s	Sampling time of the WPS controller
T_{sWTG}	s	Sampling time of the WTG controller
T_{sys}	s	Time constant of equivalent prime mover seen from the system point of view
TOL	%	Allowed torque overload in % of nominal torque
TSO	-	Transmission system operator
U1; U2; U3	V; pu	Grid voltage of phase 1, phase 2 and phase 3 respectively
UCTE	-	Union for the Co-ordination of Transmission of Electricity
v_{nacY}	m/s; pu	Lineal speed of the nacelle on the shaft's axis direction (y).
v_{wind}	m/s; pu	Wind speed
V_d; V_q	V; pu	Voltage magnitude in the d and q axis respectively
V_{dqs}	V; pu	Stator voltages in the d-q system
V_{dqr}	V; pu	Rotor voltages in the d-q system
V_L	V; pu	Voltage magnitude in the load
V_w, V_{wN}	m/s; pu	Respectively: wind speed and wind speed at nominal operation
VSWT	-	Variable speed wind turbine
WP, WP_E, WP_C, WP_{Sh}, WP_I	-	Wind power penetration level: Energy, Capacity, Share, Instantaneous
WPG	-	Wind power generation
WPGS	-	Wind power generation system: the total, controllable, wind power generation in the power system
WPP	-	Wind power plant
WPPC	-	Wind power plant controller
WPS	-	Wind power source: a source of wind power to the power system, i.e. a WTG, a WPP or a Cluster.
WTG	-	Wind turbine generator
X_{SL}	Ω; pu	Reactance seen from the bus L, which is the parallel of all the reactances between the generators and the bus L
X_{12}	Ω; pu	Equivalent reactance between points 1 and 2

$\forall$	-	*For all…*
$\partial x / \partial y$	$[x]/[y]$	Partial of x with respect to y
$\dot{a}$	$[a]/s$	Derivative of a with respect to time t
Δx	-	Delta: variation of a variable x from a steady state condition
ΔE_{Boost}	MWs; pu·s	Energy released by the WTG during first stage of IR
$\Delta F_{WindFluct}$	Hz; pu	Specified, allowed, grid frequency variation due to wind power fluctuations
$\Delta P_{WindFluct}$	MW; pu	Allowed wind power fluctuation at system level
ΔP_{Drop}, $\Delta P_{DropMax}$	MW; pu	Respectively: power drop below pre-event value after T_{Boost} and maximum allowed
ΔP_{FC}	MW; pu	Power response to frequency deviation
δ_i	rad; pu	Rotor angle of the machine i
δ_L	rad; pu	Voltage angle of the load
δ_{ij}	rad; pu	Difference between voltage's angles of node i and node j
λ	-	Blade's tip speed ratio
η_{DT}	-	Drive train torque dependant losses coefficient (<1)
θ, θ_{opt}, θ_{ref}	deg	Respectively: pitch angle of WTG's blades, optimal pitch angle for maximum mechanical power at given wind, reference for the pitch angle controller.
τ_{Aero}	Nm; pu	Aerodynamical torque generated on the rotor's blades
τ_e	Nm; pu	Electromagnetic torque generated in the generator's air gap
ω, ω_g, ω_{ref}, ω_{Min}, ω_{DynMax}	rad/s; pu	Respectively: SG's rotational speed, rotational speed of the generator's rotor, reference for the rotational speed controller, minimum allowed speed and maximum dynamic allowed speed.
ω_r (ω_t), ω_{tN}	rad/s; pu	Respectively: rotational speed of the turbine's rotor (.) and WTG speed at nominal operation.

1
INTRODUCTION

This thesis presents the development and analysis of methodologies for frequency control of modern wind power generation aiming at integrating large amounts of wind power in the power system. New methods and solutions dealing specifically with the frequency stability problem with high wind power penetration or in islanding situations are developed.

1.1 Background

The global energy challenge is to satisfy the growing demand, to secure the energy sources and, at the same time, to face the threat equally urgent of climate change. In this sense, renewable energies promise to be an important source for mankind. They are safe, clean and plentiful. Unlike conventional fuels, renewable energies are permanently available in almost every country in the world. Of renewable technologies, wind power currently has the most potential to make the largest impact. Wind power generation in large quantities is a reality in the global energy matrix, particularly in countries that have seriously implemented plans to integrate these renewable energy sources in the electricity system, taking advantage of their available wind resources. But still many questions surrounding this type of generation, particularly on how to manage it in the most convenient way, do not have a clear answer yet.

1.1.1 Definitions of wind power penetration

It is essential to characterize in first place the different concepts of "penetration level of wind power", to have a clear definition of them. The efforts on wind power integration, such as operation methodologies, costs and decision-making are directly related these definitions. Wind penetration (WP) can be defined in a number of ways. At least four different measures are commonly used: Energy penetration (WP_E), capacity penetration (WP_C), share of power penetration (WP_{Sh}) and instantaneous penetration (WP_I), which are defined as follows:

Energy penetration (WP_E): Ratio of the amount of energy obtained from the wind generation to the total energy consumed in the power system, normally on an annual basis:

$$WP_E = \frac{Total\ wind\ energy\ produced\ (TWh)}{Total\ energy\ consumptio\ n\ (TWh)} \tag{1.1}$$

Capacity penetration (WP_C): Ratio of the installed wind power capacity (nominal power) to the peak load consumption, normally on a specified time period:

$$WP_C = \frac{Installed\ wind\ power\ (MW)}{Peak\ load\ consumptio\ n\ (MW)} \tag{1.2}$$

Share of power penetration (WP_{Sh}): Ratio of maximum wind power production to the summation of the minimum demand plus the exportation capacity of the system:

$$WP_{Sh} = \frac{Maximum\ wind\ power\ production\ (MW)}{Minimum\ load + Exportatio\ n\ capacity\ (MW)} \tag{1.3}$$

Instantaneous penetration (WP_I): Ratio of the present wind power production to the present system load:

$$WP_I = \frac{Actual\ wind\ power\ production\ (MW)}{Actual\ system\ load\ (MW)} \tag{1.4}$$

The WP_{Sh} reflects the capacity of the power system for balancing the wind. This measure must remain below 1 (i.e. below 100%) to ensure the correct power balance in the system; the nearer to 1 (100%), the closer the system is to its limit for balancing the *daily* variations of the wind. A $WP_{Sh} > 1$ means that the wind power production would need to be curtailed at some point on its operation period.

The WP_C is linked to the WP_E by the system Load Factor (*LF*) and the wind power plant Capacity Factor (*WCF*):

$$LF = \frac{Total\ energy\ consumptio\ n\ (TWh)}{Peak\ load\ consumptio\ n\ (TW) \cdot 8600\ (h)} \tag{1.5}$$

$$WCF = \frac{Total\ wind\ energy\ produced\ (TWh)}{Installed\ wind\ power\ (TW) \cdot 8600\ (h)} \tag{1.6}$$

Therefore:

$$WP_C = \frac{LF}{WCF} \cdot \frac{1}{WP_E} \tag{1.7}$$

1.1.2 Wind power in the world

World's wind power resources are enormous and could cover a larger share of the global electricity consumption. This is already happening in a few regions in the world with large installed capacity of wind turbine generators. **Table 1-1** shows the WP_C and the WP_E for various countries leading the share of wind in Europe in 2010. The reference loads are set out in the System Adequacy Forecast (January 2007) for the Union for the Co-ordination of Transmission of Electricity (UCTE) area [69]. Other places in the world have less share of wind power, but they are leaders in installed capacity, such as China with 42.3 GW and the USA with 40.2 GW (2010). **Figure 1-1** shows the wind power growth in the EU and the World in 2010. Complete information of the European and global status of wind power in 2010 can be found in [1] and [2].

While wind energy in the EU has covered around 5.5 % of its electricity demand in 2010, EWEA targets for 2020 and 2030 estimate a WP_E of up to 15.7 % and up to 28 % respectively [1].

The WP_{Sh} is already high in certain areas of Europe, for example West Denmark (57 %) and the German state of Schleswig-Holstein (44 %), but the system can *still* absorb additional wind power before it reaches the limit for conventional operation. However, with increasing amounts of wind power installed, improvements are required in the power exchange capacities between various countries.

Table 1-1: Wind power penetration in various European countries (2010) [1] [69]

Country	Reference load (GW) (2007)	Installed capacity (GW)	WP$_C$	WP$_E$
W. Denmark	3.8	2.5	66 %	25.6 %
Spain	43.0	20.67	48 %	15 %
Portugal	8.5	3.9	46 %	15.4 %
Germany	74.0	27.2	36 %	8 %
Netherlands	16.1	2.24	14 %	4.1 %
France	80.0	5.66	7 %	2.3 %
Ireland	4.4 [(1)]	1.43	-	12.9 %

[(1)] Obtained from [4].
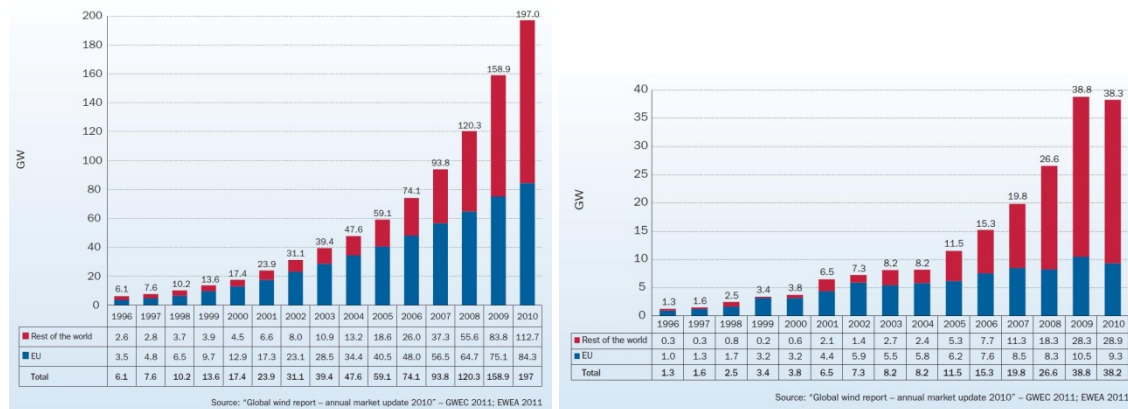
Figure 1-1: Global wind power capacity evolution in 2010. Cumulative capacity (left) and annual capacity (right) [1].

1.1.3 Main integration issues

The fluctuating nature of wind power introduces several challenges to reliable operation of power systems. During the first two decades of wind turbines being connected to the public grid (1980-2000), a fairly strong grid was assumed and the turbines and controls were simple and designed accordingly. With increased integration of wind power to the transmission network, modern wind power plants employ variable-speed wind turbines (VSWT) and are required and designed to fulfil increasingly demanding grid codes [3]-[17]. Looking at the current levels of wind power in large power systems, if the transmission capability is available, it is clearly feasible to integrate wind power to a significant extent without major system changes. Power system studies conclude that 20% wind energy penetration can be reliably accommodated in the actual system. The 80 GW of wind power already installed in Europe (2010) is characterized by: (i) areas of high, medium and low penetration levels; (ii) different conditions and (iii) bottlenecks and operational challenges. Challenges exist for the various stakeholders involved: Generation, transmission, distribution, power trading and consumers.

The following areas characterize the issues that need to be addressed in order to integrate wind power into the power system [69]:

a- **Design and operation of the power system:** Power reserve capacities and power balance management, short-term forecasting of wind power, demand-side management and energy storage, and optimization of system flexibility for power generation;

b- **Grid infrastructure issues:** Optimization of present network infrastructure, new lines to remote locations, extensions and reinforcements, offshore grids, and improved interconnections;

c- **Grid connection of wind power:** Grid codes for wind turbines (and wind power plants), power quality and wind power plant capabilities;

    d- **Market redesign issues:** Market aggregation and adapted market rules increasing the market flexibility, especially for cross-border exchange and operating the system closer to the delivery hour;

    e- **Institutional issues:** Stakeholder incentives, non-discriminatory third party grid access and socialization of costs.

1.1.4 Challenges on power balance and frequency control

The increase of wind power generation (WPG) in Power Systems (PS) brings new challenges for the system operation, particularly regarding active power balance and frequency control. In some European countries, penetration levels of $WP_l \approx$ 50-60% have already been achieved for short periods of time [69]. But the stability and control of traditional PS still relies on the characteristics and controllability of conventional power plants. In particular, these power plants are also responsible for controlling the electrical frequency in the grid, and perform major actions for balancing the power consumption in the PS.

The actual concern is how to develop the future power system so that wind power can be integrated efficiently and economically. One challenge lies in reliably balancing generation and load with a large portion of generation coming from wind, which, unlike many traditional power sources, cannot be dispatched *in the traditional sense*.

How wind can be reliably accommodated into power systems operation and planning? There are many *proposals*. But a common *practice* for Transmission System Operators (TSO) today is to ensure that sufficient reserves from other power sources are available all the time, for keeping the system in balance upon wind power fluctuations and forecast errors. Such a strategy increases the operating cost of the system [40]-[48].

But in future power systems with high wind power penetration, conventional power plants will be displaced. Thus the sources of conventional reserve available to the system will be reduced and fewer conventional plants will be available on-line to share the regulation burden. Reserve management by conventional plants will be difficult, especially in isolated power systems, which has no interconnection and limited capability of power regulation. Consequently, wind power fluctuations might introduce large power imbalances leading to power system frequency control and operational issues [44] [106]. Additionally, modern wind power plants (WPP) are equipped with Variable Speed Wind Turbines (VSWT) technologies, which are interfaced with power electronics converters. The common configuration of these converters completely decouples the turbine's rotational speed from the grid frequency. Therefore variations in grid frequency are not seen by the generator's rotor and the VSWTs do not contribute with the system inertia [19] [21]. The power system inertia will be reduced; greater rates of frequency change will be observed during system contingencies; and conventional prime

movers will have less time to react in order to keep the frequency stable. If the penetration level of WPG increases above certain value, it will become technically difficult and economically expensive to maintain the actual regulation strategy and grid security by means of conventional generation.

Summarizing, if wind power in the power system increases:
1- More regulation reserves will need to be allocated in the PS to compensate wind power forecast errors and to balance wind power fluctuations.
2- Conventional power plants on-line will be replaced by WPP, therefore the capability of the PS to offer conventional regulating power may be reduced.
3- Considering the previous, the rotating inertia of synchronously isolated PS will also be reduced; therefore the dynamic stability of the grid frequency under large disturbances may be compromised.

The issues above mentioned are much more evident in islanded power systems without interconnections to other systems [4] [8] [63] [106].

While modern WPG has lately being required to provide frequency response in the most evolved PS, it has not achieved the same participation level than conventional plants yet. In some PS, mainly with weak interconnections and/or high wind power penetration, frequency reserves can be more valuable to the system than maximizing the WPG yield [40] [69] [106]. In future PS, WPG will have to provide fast regulating power and a reliable, deterministic and repeatable frequency response to support the grid and decrease costs of conventional power reserve.

It is evident, then, that modern WPG should have equivalent functionalities than conventional power plants in order (but not limited) to:
1- Regulate power fluctuations caused by wind power itself.
2- Provide with regulation reserves and static frequency response for supporting the PS, balancing the load changes.
3- Provide with active power response for supporting the dynamic stability of the grid frequency in case of large load imbalances.

The importance of developing methods for control and operation of WPG under different scenarios considering, on one hand, the uncertainties associated with wind speed and, on the other hand, the requirements for system stability, power quality and contractual obligations is highlighted.

The characteristics of controllability offered by actual wind power technologies make possible to elaborate and develop control strategies with different objectives. But any kind of power control on WPG other than optimal production means a reduction on pro-

duced electrical energy. Therefore the functionalities above mentioned, if implemented on WPG, shall produce the lowest impact on revenues as possible.

Taking the case of the Danish island of Bornholm [108], about 30MW of WPG are installed in its power system –among other conventional generators– in contrast with its 55 MW peak load, but still it has been shown that the wind power resources cannot be fully exploited in island operation. It is necessary to find solutions to the system stability problems in order to allow the integration of significant amounts of WPG. In this PhD project, the Bornholm power system in island operation is used as example and experimental platform of an islanded/weakly interconnected network with significant wind power penetration, and the developed solutions are inspired on this system.

1.2 State of the art

With high wind power penetration, wind power does not only need to reduce its impact on the system, but also contribute with frequency response. The need for wind turbines to participate in frequency regulation has been identified in several studies. But wind turbines can only supply ancillary services associated with active power to a limited extent, depending on wind conditions. Power contribution for frequency stability attending a system event is possible inside these boundaries. Some works have studied the reduction of the impact of fluctuating wind power on the system by using control strategies for smoothening the power output of variable speed wind turbines (VSWT) [29]-[33]. They all make use of the capability of the VSWT for varying the rotor speed. A loss of wind energy is associated with these techniques.

Many studies have been conducted regarding frequency control of wind power in the last 5-6 years. Initially, the control was studied as implemented at WTG level, and the studies were focused on a single wind turbine response [84]. Later, the frequency control migrated to the WPP level due to controllability reasons, in order to obtain the desired response at the point of common coupling (PCC) and increase the performance of the WPP [110] [111] [115]. The WPP frequency controllers are designed to attend the requirements from the grid codes. Today, frequency control from WPP is well developed [62] and the requirements are well established [6] [3] [9]. However, the WPP are operated (and responding) independently from each other. Considering the integration issues discussed in the previous sections, the power system must be operated with balance and reliability, taking into account the aggregated behaviour of all of its loads and generation operating together. Overall, from the balance and frequency control point of view, it is the net system power that must be balanced, however, not an individual load or generation source in isolation. Few works investigating the possibilities and limitations of controlling the wind power production at system level, by implementing power control architectures were found, e.g. [117] [118], yet, they do not really control the WPG but instead adapt the conventional production around wind power. In [116] an

interesting approach is carried out, where the WPPs are grouped in "clusters" and controlled from an "upper" level. This allows a better use of the wind power to provide regulation reserves for frequency control from the cluster. An approach that was not considered, however, is controlling the *whole* wind power production in the power system with the same philosophy. This PhD work investigates solutions in this direction. Furthermore, the control architecture derived in this PhD project should be coordinated with the actual capability of conventional power plants in the system.

Recently, new ideas and methods to solve the issues of power balance and reduction in system inertia have emerged. Some of these new ideas work on the system load side, e.g. by manipulating electro-thermal loads during the grid frequency event. This is many time referred as Demand as Frequency-control Reserve (DFR) [119]. Other ideas work on energy storage technologies interfaced by power converters, where the controllable and fast actuation device is used for delivering or absorbing power to/from the grid during frequency events. Some of these utilize electric vehicles [120] or Virtual Power Plants [121]. But one of the most interesting and studied ideas is the use of modern win power generators to contribute with extra power during the grid frequency events, which is many times referred as inertial response. This is one of the focuses of this PhD work.

VSWT has the ability to generate a desired power output –inside limits- through fast control actions, which can be used to offer superior performance concerning system stability during disturbances. Several controllers have been proposed for producing an inertial response from wind turbines to support frequency drops [20]-[24], [38]. In [20] and [21] different controlled responses of WPP to large frequency deviations are investigated, but the implemented controllers do not consider in detail the *capabilities* of the VSWT to deliver energy from the turbine's rotor. Simplification by using aggregated model of the WPP for inertial response is also used. Despite of showing the impact of the produced waveform on the grid, this power does not reflect a realistic response from the VSWT or the WPP. Nevertheless, there is a clarification on further work to be done. The same observations can be derived in a number of recent publications such as [22]-[27]. In [28] the mechanical output from the turbine's rotor is considered in the overall response of the WTG and the impact on the grid, however the control algorithm for injecting extra energy does not consider the characteristics of the grid frequency, therefore the response of the turbine is not adapted in real time to the *needs of the system*. Other control methodologies consider the grid frequency as input, therefore generating a corresponding waveform. This can be given by the frequency derivative (*df/dt*) in an attempt to emulate synchronous machines response, e.g. [22] [23] [25], or it can be a combination of *df/dt* plus a term proportional to frequency deviation Δ*f*, e.g. [24] [35]. However, in all the reviewed bibliography regarding inertial response from wind turbines, [18]-[37], it was not found any case where the capability of VSWT for delivering

kinetic energy at different wind conditions is considered for designing the controller for this functionality. Furthermore, all the analyses consider a constant wind speed and/or an aggregated response from the WPP as if it were similar to a single VSWT, which gives unrealistic behaviour of the VSWT, especially during the recovery period, i.e. the period following the initial power injection.

It is clear then, that a deeper analysis of the capabilities of the VSWT is necessary. This study should consider the impacts of aerodynamical power, mechanical structure, overloads, operational limits, etc. in order to have a clear picture of what can really be done with a VSWT. Furthermore, these capabilities should be considered together with the characteristics of the grid frequency event for generating a suitable power waveform, in order to contribute with frequency stabilization and satisfy the *needs of the system.*

Despite the high attention on wind power inertial response, there are almost no specifications or exact details available in any grid codes. At the time of writing this thesis, no grid code contained any tangible requirements specification on inertial response from wind power. Neither has any commercial project used it so far. Only general requirements and responses equivalent to synchronous machines are evaluated or specified [13] [14]. An actual rough overview on these can be found in [66].

1.3 Project objectives and limitations

Considering the issues previously mentioned, the aim of this PhD work is to develop and study control methodologies for integrating an increased share of wind power generation in the PS, dealing specifically with the frequency stability problem with high wind power penetration. These control methodologies shall provide equivalent effect on the PS to the two main standard mechanisms for frequency stability and control: (i) inertial response and (ii) primary frequency control.

Specifically, the objectives defined for this PhD work are:
- To study the capability of WTGs for injecting a suitable power waveform towards stabilization of grid frequency drops, referred as inertial response, and to develop a control algorithm for providing the WTGs with this functionality.
- To develop and study control methodologies for wind power production in the PS, aiming at reducing the impact of wind power fluctuations on the grid frequency and at providing with suitable frequency regulation service to the system when required.
- To study control architectures for wind power systems that implement, in a combined manner, the developed methodologies previously mentioned.
- To study a methodology for coordination of the developed wind power control with the conventional power generation, interplaying with frequency activated reserves in the system, and to study the overall combined response.

Project Limitations

From the issues listed in Section 1.1.3, system power reserves, system balance management, short-term wind power forecasting and wind power plant capabilities and control are related to the studies in this work. Here, special attention is paid to the period of time where the two frequency stability and control mechanisms abovementioned take place in the system, typically within 0.1s to 15 min. Therefore, the models used in this investigation were developed to perform RMS simulations. Time periods beyond the typical for these mechanisms are not considered here since it is assumed a *proper* secondary frequency control acting at higher level in the power system. Effects of damping power oscillations [97]- [102], synchronizing power, voltage control [112]-[114] and severe faults in the grid (such as short circuits) are out of the scope. Wind power plants were modelled with individual wind turbines (not lumped) and realistic wind speeds (measured and/or simulated). In this PhD project, the power system of the Danish Island of Bornholm during island operation is used as example of islanded/weakly interconnected network with significant wind power penetration. Extensive measurements were carried out on this system for characterization and the solutions here developed are based on verified models of this system. Extensive data of a particular manufacturer's wind turbine with its constraints were used for the studies.

1.4 Contributions

The main contributions of this PhD work are listed below:

- *Study and characterization of the capability of variable speed wind turbines for providing inertial response.*
- *Development of control algorithm for wind turbines inertial response.*
- *Study and characterization of the capability of wind power plants (wind farms) for providing inertial response.*
- *Proposal and development of a frequency controller for wind power generation.*
- *Proposal and development of control functionality for wind power production aiming at reducing the overall power fluctuations injected to the grid.*
- *Study of control architectures for wind power generation.*
- *Method for coordinating the developed frequency response functionalities with conventional generation in the system.*

1.5 Structure of the Thesis

Chapters 1, 2 and 3 describe the background, overviews and tools necessary for the development of the main part of this work. The main contributions of this work are divided in chapters 4, 5 and 6. The overall thesis structure is listed below.

Chapter 1: Presents the background, review, projects objectives and limitations, contributions and thesis outline.

Chapter 2: Presents an overview of main concepts regarding frequency control mechanisms, performance of system frequency response, impact of wind power on power system balance, survey on relevant grid codes, measurements in islanded situation with high wind power penetration –performed during this work– and proposed requirements for wind power control.

Chapter 3: Briefly describes the different modelling used in this work. Different modelling approaches were used in order to obtain particular conclusions on different issues. Detailed modelling of a multimegawatt variable speed wind turbine and an isolated real power system were developed, adjusted and verified against measurements.

Chapter 4: Studies the capability of variable speed wind turbines for inertial response and develops a control algorithm for wind turbine inertial response. The performance is tested through accurate computational simulations with realistic conditions. The capability of wind power plants for inertial response is assessed in the same way.

Chapter 5: Control functionalities for wind power production at system level are proposed, developed and studied in this chapter. The control functionalities are implemented in different architectures. The performance of the architectures is assessed through accurate computational simulations.

Chapter 6: Studies the coordination between the control functionalities developed in the previous two chapters and the standard regulation mechanisms in power systems. The performance and the capability for supporting the grid during large load events are evaluated through computational simulations.

Chapter 7: Summarizes and concludes the work done, the findings and the suggested future work.

1.6 Publications and patent applications

1.6.1 Publications

1- Tarnowski, G. C; Kjær, P. C.; Sørensen, P. E.; Østergaard, J., "Study on Variable Speed Wind Turbines Capability for Frequency Response". In Proc. European Wind Energy Conference EWEC 2009, 16-19 March, Marseille, France, 2009.

2- Tarnowski, G.C.; Kjær, P.C.; Sorensen, P.E.; Østergaard, J.; "Variable speed wind turbines capability for temporary over-production". In Proc. *Power & Energy Society General Meeting PES '09 IEEE*, 26-30 July, Calgary, Canada, 2009.

3- Tarnowski, G.C.; Kjær, P.C.; Dalsgaard, S.; Nyborg, A.; "Regulation and frequency response service capability of modern wind power plants". In Proc. *Power and Energy Society General Meeting, 2010 IEEE* , 25-29 July, Minneapolis, USA, 2010.

4- Tarnowski, G. C.; Kjær, P. C.; Østergaard, J. and Sørensen, P. E., Frequency Control in Power Systems with High Wind Power Penetration. In proc. 9th International Workshop on large-scale integration of wind power into power systems, 2010. 18-29 Oct., Québec, Canada, 2010.

1.6.2 Patent applications

1- Wind Turbine Providing Grid Support. WO 2011/000531. Publication 06 January 2011.

2- Method for Emulation of Synchronous Machine. WO 2011/092193. Publication 04 August 2011.

3- Wind Power Production with Reduced Power Fluctuations. WO 2012/019613. Publication 16 February 2012.

4- Systems and Methods for Generating and Inertial Response to a Change in the Voltage of an Electrical Grid. Pending public disclosure.

5- Wind Power Plant Frequency Control. Pending public disclosure.

6- Dispatching Algorithm for Wind Power System Generation. Pending public disclosure.

7- Method for coordinating Frequency Control Characteristics between Conventional Plants and Wind Power. Pending public disclosure.

2

FREQUENCY CONTROL AND WIND POWER IMPACT – AN OVERVIEW

This chapter presents an overview of main concepts of frequency control in power systems and wind power impact on the power balance. The standard mechanisms for frequency stability and control in present power systems are addressed. The average performance of the system frequency response upon a load imbalance and its dependence on different characteristic parameters are analysed. This study provides a basis and understanding for further analyses in this work. The different impacts of wind power on power balance and grid frequency are described, highlighting relevant issues with high wind power penetration. A survey on representative grid codes with requirements on frequency control for wind power is carried out. Some of these requirements are used as basis for this work. Results from measurements carried out during this investigation are presented. The measurements were conducted on a small isolated power system characterized by a large share of wind power generation, providing evidence of some of the main issues with high wind power penetration. Based on the overviews, observations and discussions along this chapter, requirements for wind power frequency control with high wind power penetration are finally elaborated.

2.1 Standard mechanisms for frequency stability and control

In an AC power system with synchronous generators (SG), the frequency of the network is dictated by their rotational speed. A change in the grid frequency is produced by a change in the speed of those SG generators which, in turns, is caused by an imbalance between electrical power output (consumption) and mechanical power input (generation).

In order to maintain the security and integrity of the power system the TSO must operate it properly, ensuring –among others– adequate frequency control so to achieve operation within frequency limits at all times. Since the consumption in the network changes all the time (even small changes), the grid frequency also changes all the time. This is because the mechanical power applied to the SG's shaft cannot follow the same rhythm of the consumption change. Thus the rotating inertias in generators are *energy buffers* between mechanical generation and electrical consumption. The grid frequency deviation is then taken normally as an indication that the grid load has changed. Upon fre-

quency deviation detection, proper regulation mechanisms are activated and applied to the SG's mechanical input in order to balance the load change in the grid and maintain the grid frequency inside a narrow range. The Grid Codes (GC) establish strong requirements for maintaining the grid frequency inside those boundaries (as described in Section 2.4).

Load changes (imbalances) in the network are divided in two main groups:
1. Continuous operation: Normal connection and disconnection of consumers.
2. Disturbances: Unexpected and undesirable power imbalances produced by e.g. generator trip, tie line trip, large consumption trip. Also referred as *contingency*.

Wind power generation also produces changes in the electrical load seen by the SG's, due to its fluctuating nature. This is enclosed under "continuous operation" imbalances.

From the moment that a load imbalance is produced in the network to the moment where the grid frequency is fully stabilized, several mechanisms take place in the power system during different stages, which depend on the duration of the dynamics involved. Those stages are:
1. Distribution of power impact and inertial response.
2. Primary frequency control (or governor response).
3. Secondary frequency control.
4. Multi-level frequency control.

Figure 2-1 shows the typical response and duration of the first three mechanisms of frequency stability and control when a large change in the system load is produced (disturbance), together with the performance response of the average grid frequency. This power system has three SG machines characterized by: Constant mechanical power input (red line), governor response (blue line) and secondary frequency control (green line). The steady state deviation (Δf_{ss}), the rate of change of frequency (ROCOF) and the bottom point of the frequency deviation (*nadir*), are among the main performance indicators [58]. *The basic task of frequency control is to maintain the grid frequency inside specified boundaries.* In the next subsections each one of the previous mechanisms is briefly described.

2.1.1 Distribution of power impact and inertial response [70] [71]

Consider the **Figure 2-2**. The first stage in a frequency disturbance is initiated with a change in system load, ΔP_L. The concern here is to estimate the magnitude of the power impact in each generator in the system and their speed variations during the first moments of load change. The analysis done in this subsection is based on the classical modelling described in Appendix A.1. The estimates are approximate, according to the model assumptions, yet instructive.
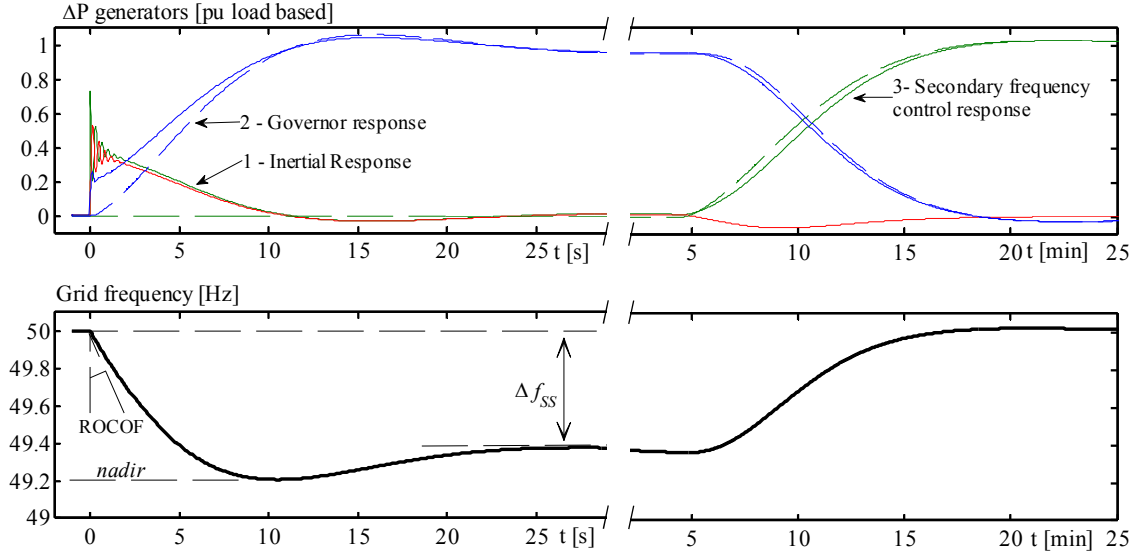
Figure 2-1: Typical power system response to a large load change. Top: generator without governor response (red), generator with governor response (blue), generator with secondary control (green), electric power (solid) and mechanical power (dashed).
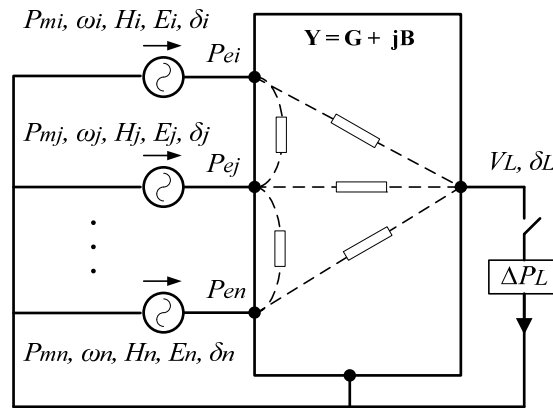
Figure 2-2: Representation of a multimachine system for load impact (classical model).

2.1.1.1 Initial power impact

When the load impact ΔP_L first occurs in a busbar L in the system, the SG's rotors angle cannot change immediately because of the inertias, therefore initially $\Delta \delta_i = 0$ and $\Delta \omega_i = 0$. Equally, the governors are not activated, thus the change in prime movers mechanical output $\Delta P_{mi} = 0$. Working the expressions (**A.3**)-(**A.6**) in the Appendix A.1, the initial values (*ini*) of the *changes* are:

$$\Delta \delta_L (ini) = -\frac{\Delta P_L}{\displaystyle\sum_{j=1}^{n} P_{SjL}} \tag{2.8}$$

$$\Delta P_{ei}(ini) = \frac{P_{SiL}}{\displaystyle\sum_{j=1}^{n} P_{SjL}} \cdot \Delta P_L \tag{2.9}$$

$$\Delta \dot{\omega}_i(ini) = -\frac{\Delta P_{ei}(ini)}{2H'_i} \tag{2.10}$$

$$\Delta \dot{\delta}_i(ini) = 0 \tag{2.11}$$

From the last expressions, important observations can be derived:

- At the instant of the load impact, generators rotor's angles cannot move instantly due to the inertias, therefore the electric energy source cannot come instantaneously from the kinetic energy stored in the masses.
- At the instant of the load impact, the source of energy is the energy stored in the magnetic fields of the synchronous generators.
- The power given by (2.9) indicates that the load imbalance ΔP_L is *immediately* shared by the synchronous generators in the system (if timing of travelling waves in lines is neglected).
- The power impact is distributed among SGs according to their synchronizing power coefficients, P_{SiL}, with respect to the load bus L.
- The machines electrically close to the point of impact (lower impedance) will pick up the greater share of the load, *independently of their inertial size*.
- The share of initial power of a given generator initiates a change on its rotor speed indicated by (2.10) (acceleration or deceleration).
- After the initial power impact, the synchronous machines will decelerate or accelerate *at different rates*, according to individual inertias H_i and electrical *location* given by the synchronizing power coefficient, P_{SiL}.

A better visualization of the previous observations can be achieved by simple analysis of the two-machine system shown in **Figure 2-3**. Assuming that the voltage magnitudes and initial angles are more or less equal, i.e. $E_1 \approx E_2 \approx V_L$ and $cos\ \delta_{1L0} \approx cos\ \delta_{2L0}$, we have:

$$\Delta P_{e1}(ini) = \frac{\dfrac{1}{X_{1L}}}{\left(\dfrac{1}{X_{1L}} + \dfrac{1}{X_{2L}}\right)} \cdot \Delta P_L \;=\; \frac{X_{SL}}{X_{1L}} \cdot \Delta P_L \tag{2.12}$$

$$\Delta P_{e2}(ini) = \frac{\dfrac{1}{X_{2L}}}{\left(\dfrac{1}{X_{1L}} + \dfrac{1}{X_{2L}}\right)} \cdot \Delta P_L \;=\; \frac{X_{SL}}{X_{2L}} \cdot \Delta P_L \tag{2.13}$$

$$\Delta\dot{\omega}_1(ini) = -\frac{1}{2H'_1} \cdot \frac{X_{SL}}{X_{1L}} \cdot \Delta P_L \tag{2.14}$$

$$\Delta\dot{\omega}_2(ini) = -\frac{1}{2H'_2} \cdot \frac{X_{SL}}{X_{2L}} \cdot \Delta P_L \tag{2.15}$$

where the system reactance seen from the load bus, X_{SL}, is the parallel of the reactances between all the generators and the load bus.

It is shown in (2.14)-(2.15) and generalized in (2.10) that the sudden change ΔP_L produces different accelerations in the machines. This triggers an oscillatory transient in the power system before it settles to a new steady-state condition. But load changes occur continuously during normal operation of power systems, all the time, and the triggered oscillations are reflected in the power flows in lines and generators. Thus the *scheduled* power outputs from generators have random oscillations superimposed.
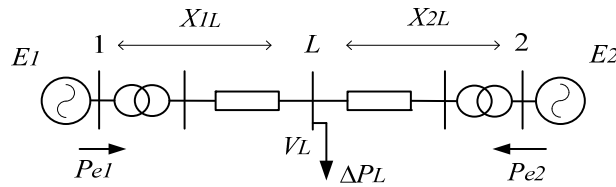
Figure 2-3: Two-machine system

2.1.1.2 Rotors swings

Shortly after the load change ΔP_L have been applied and the power impact have been distributed among the machines, each machine experiences a change in its speed, therefore $\Delta\omega_i \neq 0$ and rotor angles start changing values. However, governors are not acting yet. If the applied load change remains constant, the system response can be approximated –working on expressions (A.3)-(A.6) in the Appendix A.1– by:

$$\Delta\delta_L = -\frac{\Delta P_L}{\sum_{j=1}^{n} P_{SjL}} + \frac{\sum_{j=1}^{n} P_{SjL} \cdot \Delta\delta_j}{\sum_{j=1}^{n} P_{SjL}} \tag{2.16}$$

$$\Delta P_{ei} = \sum_{\substack{j=1 \\ j \neq i,L}}^{n} P_{Sij} \cdot \left(\Delta\delta_i - \Delta\delta_j\right) + P_{SiL} \cdot \left(\Delta\delta_i - \Delta\delta_L\right) \tag{2.17}$$

$$\Delta\dot{\omega}_i = -\frac{1}{2H'_i}\left(\Delta P_{ei} + D_i \cdot \Delta\omega_i\right) \tag{2.18}$$

$$\Delta\dot{\delta}_i = \Delta\omega_i \qquad\qquad\qquad (2.19)$$

Here, further observations can be done. Despite of having experienced a fixed load change in the system, the expression (**2.17**) shows that the power output from each machine has one component supplying the load (characterized by the synchronizing power coefficient P_{SiL}) and another component flowing among the other generators in the grid. This new power component (summation function in the right side of **2.17**) appears due to the differences between rotor angles deviations, and its main effect is to keep all the machines synchronized; tied. As shown in **Figure 2-4**, the machines start oscillating against each other, pulling and pushing with this power component, which depends on relative rotor deviations and synchronizing power coefficients, P_{Sij}. Meanwhile there is an overall reduction (or increase) of speeds in this period of time. We can say that at this time there is a change in the grid frequency. But that change *is different in different points in the system*, as long as generators are oscillating against each other. Only after damping those oscillations –by rotor damping windings, network losses and other devises such as PSS (not represented here) – the change in grid frequency becomes the same all over the system. In the modelling used here, the damping in each machine is represented by D_i.
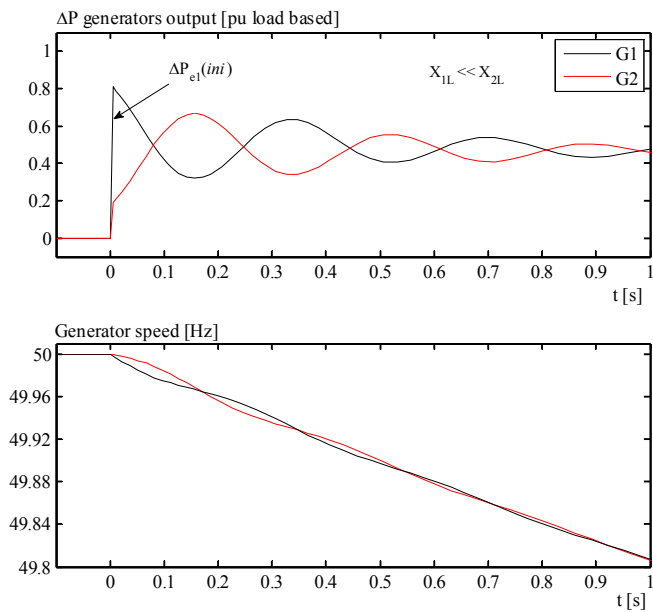
Figure 2-4: Power and speed swings of the two machines system when a load change is applied. The same oscillatory phenomenon is present, to different extents, in any multimachine system.

2.1.1.3 Average inertial response

The situation previously described can only last for few seconds during the first rotors swings. After settlement of rotors angles deviation, all the generators remain in synchronism, the rate of change in grid frequency (ROCOF) can be *averaged* all over the system and rotating masses slow down (or speed up) with the same acceleration. If the governors are still not responding, such average frequency rate of change is given by:

$$\Delta\dot{\omega}_i = \cdots = \Delta\dot{\omega}_n = -\frac{\Delta P_{ei}}{2H'_i} = \cdots = -\frac{\Delta P_{en}}{2H'_n} = -\frac{\Delta P_L}{2\sum_{j=1}^{n} H'_j} = -\frac{\Delta P_L}{2H_{sys}} \qquad (2.20)$$

where H_{sys} is the system inertia constant (defined by (**A.8**) in Appendix A.1). The power output from each machine is:

$$\Delta P_{ei} = \frac{H'_i}{H_{sys}} \cdot \Delta P_L \qquad (2.21)$$

More observations can be derived from these last expressions. At this stage, the power output from each synchronous machine can be expressed *just* on their inertia constants H'_i without considering the electrical distances [71] [72], which is a totally different criteria compared with the *initial* powers impact. Thus, while the acceleration is now the same for all the synchronized masses, the machines power output are different for different sizes of masses. The average rate of change of the grid frequency depends *just* on the size of the load change ΔP_L and the system inertia constant H_{sys}. If the rotors oscillations still persist to some degree, all the units oscillate around a mean speed given by an "inertial centre" in the grid.

2.1.2 Primary frequency control

Each synchronous generator has a speed controller, or governor, that can be engaged or disengaged. If engaged, it will detect the speed deviation $\Delta\omega_i$ (locally) after the processes described in the previous Section 2.1.1 and will start changing the prime mover power production, ΔP_{mi}, towards stabilization of the speed. This is the beginning of a new stage after the load change, aimed at *controlling* the grid frequency. As shown before in **Figure 2-1**, upon governor response (blue line) the speed deviations would level off after a few seconds to a constant value Δf_{ss} and the machine oscillations would eventually decay, depending on the speed controller and system dynamics. The same change in frequency is seen all over the grid at the same time.

The action of the prime-mover's governor due to grid frequency changes while all references are kept constant is referred as *primary frequency control* (PFC). This response corresponds to the power of the prime mover in **Figure 2-1**, dashed blue line. PFC and governor response are synonyms and these names are used indistinctly along this work.

Normally the governor will detect the frequency change when it deviates from nominal frequency f_o beyond a deadband, *DB*. The *static* response of the governor is normally *proportional* to the speed change (droop characteristic, R_i), thus the grid frequency deviation will stabilize at a steady state value f_{ss}, with an offset error from the nominal f_0, while the load change is compensated by the prime mover power change, ΔP_{mi}. **Figure 2-5** shows a typical (simple) governor-prime mover-generator configuration (left) and its static governor characteristic (right).

In order to maintain a good performance of frequency control at system level, the individual speed controllers *must* fulfil minimum requirements before connecting the generator to the grid, such as: response time, ramp rates, deadband, droop, etc., which are specified in the grid code (GC) as described in Section 2.4.
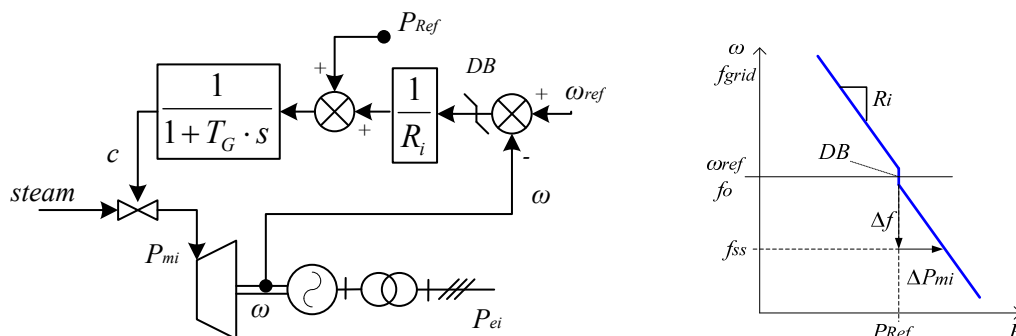

Figure 2-5: Typical diagram of speed governor (left) and its static characteristic (right).

2.1.3 Secondary frequency control

After PFC actuation, further actions are conducted in order to reduce the permanent frequency deviation, Δf_{ss}. This is accomplished by a further slowly change in prime movers load reference, P_{Ref}, towards reduction of Δf_{ss}. The action of adjusting the prime mover's load reference in order to reduce the grid frequency offset is referred as *secondary frequency control* (SFC) and it is exemplified in **Figure 2-1**, dashed green line.

In some grids, for example the Nordic, the SFC is done by manual adjustment on the load references of some selected generators [5]. In other types of systems, typically large systems, the adjustment of the P_{Ref} is automated in an integrated platform, referred as automatic generation control (AGC), as part of a multi-level frequency control mechanism in the power system. In isolated systems, the SFC can be limited to manual adjustments without the need for coordination with a central regulator [106] [107].
The SFC is much slower than the PFC. The time constant (or period) of SFC adjustment is typically 10-15 min. At power plant level, the main limitation on SFC is the capability of prime movers (normally thermal plants) to change the production, therefore only ramp rates of about 2-4-8 % of rated power *per minute* are allowed for the P_{Ref} [70] [72]. While the PFC stabilizes the frequency on f_{ss} with fast actuation, the SFC slowly adjusts the production to maintain the average grid frequency around f_o.

2.1.4 Multi-level frequency control and power dispatch

A typical example of multi-level frequency control (MLFC) is the AGC system [70] [72] [73]. The MLFC is a platform also for the tertiary frequency control (TFC) [72]. **Figure 2-6** shows an overall structure of the MLFC down to the generation level.

As mentioned previously, the AGC actuates at system level and automatically adjusts the P_{Ref} in generators based on system frequency deviation. In an interconnected system

with different areas A, the power flow between areas, P_{tie}, is also an input for the AGC. The adjustments on P_{Ref} made by the AGC are based on: (i) the *bias factor λ_A* –which is the designated proportion between the required production change over area A and the system frequency change; (ii) the error in the desired power flow P_{tie} and (iii) the *participation factors α_i* –which is the contribution of the generator i to the SFC in the area A, [70] [72] [73]. A controller, e.g. a PI, adjusts the load references towards reduction of the error (see **Figure 2-6**). The sum of regulation ranges speeds (%/min) of generators participating with SFC is referred to as the bandwidth of the SFC. The more generators participating, the larger the bandwidth is. A suitable bandwidth can restore a f_{ss} back to f_o in proper time, but it normally should not take more than 15 minutes.

Areas A are sometimes defined by the market zone [5], where system power dispatch is normally executed via an energy market [3] [9] [56]. Depending on the market structure, power plants either bid their prices in a centralized pool or arrange bilateral contracts directly with DSO's or large consumers. The TSO then adjusts the supplied bids or contracts at system level to make sure that the system constraints are satisfied and to allocate the required amount of System Regulating Margin (i.e. reserves for PFC and SFC from individual power plants). In such a market structure, the task of TFC is to adjust, manually or automatically, the P_{Ref} of individual governors in order to ensure:

    1- Spinning reserve in the units participating with PFC.
    2- Optimal dispatch of units participating with SFC.
    3- Restoration of the SFC bandwidth.

The restoration of the SFC bandwidth can also be assisted by automatic or manual connection/disconnection of reserve units which can get on-line within 15 min of requested.
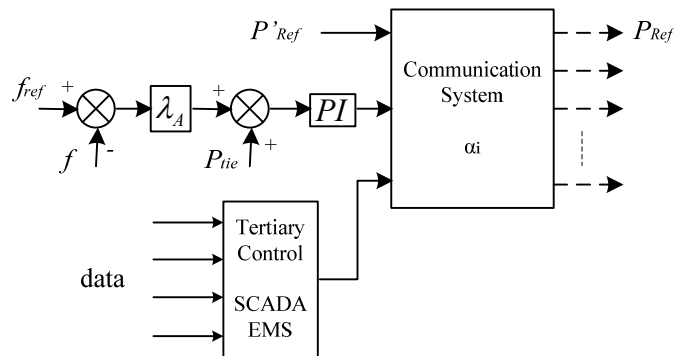

Figure 2-6: Multi-level control including AGC and Tertiary control [72].

2.1.5 System regulating margin

In order to maintain the grid frequency inside boundaries (specified in the grid code) when unpredicted load imbalances occur in the system (e.g. variations in demand forecast, sudden generation loss, wind power fluctuations, etc.), it is necessary to allocate

enough margin for frequency activated generation (system frequency response), referred many times as "system regulating margin" (SRM) [3] [5]. It is the amount of power reserve, provided by additional generation or demand reduction measures, available above (or below) the present system demand. *The allocation of SRM must not be constrained by the trading and settlement rules (market).* However, the SRM is traded in the Regulation Market [5] [9].

As example, in the Nordel System [5] the SRM is basically composed by:

1- Normal regulation reserve (RR): The amount of power that is automatically deployed by a frequency change equal to its normal deviation (e.g. at 49.9Hz or 50.1Hz in [5]). Basically, it is the summation of regulation reserves from all generators providing PFC, which is distributed between areas according to the annual consumption during the previous year, giving a total of RR = 600 MW.

2- Disturbance reserve (DR): The amount of power that must be automatically deployed by frequency changes within the disturbance range (e.g. 49.9-49.5 Hz in [5]). This power is determined by the *dimensioning fault* (normally given by the largest unit size) and by the load frequency dependence of the system, which is subtracted from the dimensioning fault. The objective is to hold the frequency nadir, and failure in delivering this power may end in load shedding.

3- Fast active disturbance reserve (FR): Is the power reserve necessary to release the RR or DR once they have been used. It can take minutes for its activation.

4- Slow active disturbance reserve (SR): Is the power reserve necessary to release the FR once it has been used. It can take several minutes to hours to activate.

Similar definitions can be found in other systems, e.g. [3] [9]. Regarding the SFC, the European UCTE system requires a total reserve in the range of 1% of the power generated in the area and at least equal to the largest generating unit in the area.

In power systems with high wind power penetration, the determination of the RR is not given by a fixed rule and it varies from system to system [44] [45]. In future power systems, conventional plants may be replaced by renewable power plants; therefore the SRM will have to be provided, at least partially, by these renewable power sources.

2.2 Performance of system frequency response

In this section, the average performance of the system frequency response upon load imbalance and its dependence on different characteristic parameters are analysed. The gained understanding provides a basis for further analyses and observations along this work.

It was shown that the dynamics of the average electrical frequency is strongly influenced by the global inertia constant H_{sys}. This is described by (**2.20**). For a given load

change, the bigger the inertia H_{sys} the slower the average frequency rate of change is. And vice versa, the smaller the inertia H_{sys} the faster the average grid frequency rate of change is.

Before governor's response upon load change, the power supply is fed with energy taken from synchronous machines rotating masses. Large H_{sys} implicates that prime movers do not need to be fast reacting for immediate compensation of the electrical load change. System inertia provides an *energy buffer* and guarantees sufficient time for governor response. Additionally the grid frequency does not experience large nadir. Low H_{sys} implicates faster and larger frequency deviations as consequence of electrical load changes, thus a power system with low inertia experiments a degradation of the quality of the frequency.

The extracted energy $\Delta E_{Inertia\text{-}i}$ from the rotating masses of a generator *i*, for a given frequency deviation Δf, is obtained by solving the following integral:

$$\Delta E_{Inertia-i} = \int_0^{t1} \Delta P_{ei}\, dt = 2H_i \int_{fo}^{f1} f\, df \tag{2.22}$$

Thus:

$$\Delta E_{Inertia-i} = 2H_i f_o \Delta f + H_i \Delta f^2 \;\; [\text{p.u.}] \tag{2.23}$$

Normally it is considered $f_o = 1$ p.u. and $\Delta f^2 \approx 0$. **Figure 2-7** left shows the energy delivered (or absorbed) from synchronous machine rotors due to frequency deviations for different inertia constants H_i. The larger the H_i, the more energy is released. The released energy is based to each machine's rated power. At the right it is shown the "average" inertial response versus grid frequency rate of change for different inertias.

During the period of governor's actuation, the performance of the grid frequency is also largely influenced by the governor's droop, R_i, and by the reaction time of the prime mover, T_G. Following, the impact of these three parameters in the grid frequency performance is assessed by using the modelling of the power system PS1, which is described in Section 3.3.2.
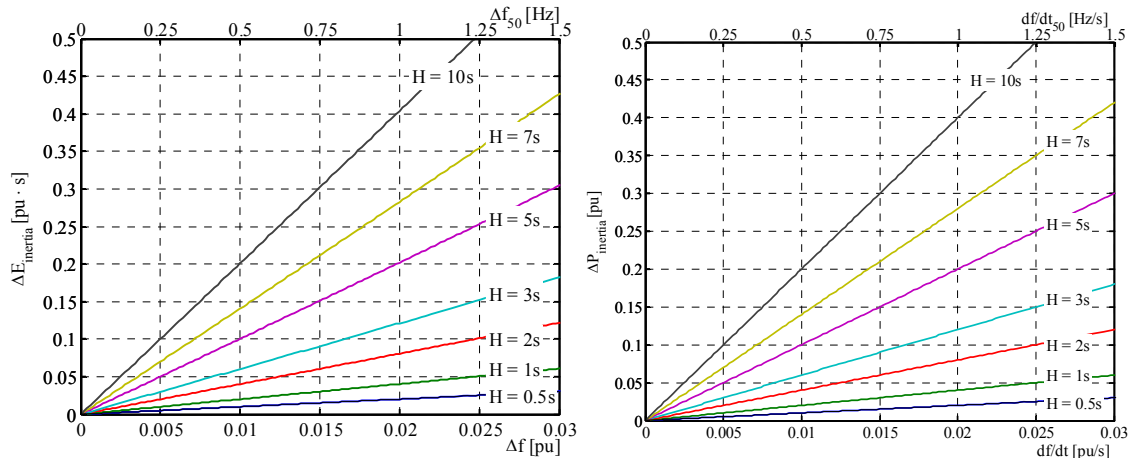
Figure 2-7: Synchronous machine released kinetic energy vs. grid frequency deviation (left) and average inertial response vs. ROCOF (right) for different inertia constants H.

2.2.1.1 Performance varying H, R, T, and D

From the normalized case presented in Section 3.3.2, independent changes through a gain k were applied on the system inertia constant $H_{sys} = k \cdot H_0$, the system equivalent governor droop $R_{sys} = k \cdot R_0$, the system equivalent prime mover time constant $T_{sys} = k \cdot T_0$ and the load-frequency constant $D_{sys} = k \cdot D_0$. All the other parameters were kept unchanged in each case. **Figure 2-8** shows the average power system performance when changing H_{sys} (left) and R_{sys} (right), and **Figure 2-9** shows the average power system performance when changing T_{sys} (left) and D_{sys} (right). Note that the scales are normalized to the time to minimum, t_{min}, steady state deviation Δf_{ss} and load change ΔP_{load}. In each plotting the values of the changes from the normalized case are specified and the arrows indicate the direction of the reduction on the given parameter. The normalized case is indicated in blue color.

Observe how the average grid frequency performance is affected in each case. The most significant impacts are produced by changes in H_{sys} and R_{sys}. **Figure 2-8** left and **Figure 2-10** show the increase in peak frequency deviation (nadir) when the system inertia constant is reduced. As example, 40% reduction in H_{sys} will produce ~21% increase in the nadir if all the other system parameters remain unchanged. Considering the UK power system as example, the minimum acceptable dynamic frequency value after a large generation loss is 49.2Hz [8] [9]. Thus, with a reduction of 40% of its inertia it would end with $49.2 - 0.21 \cdot (50 - 49.2) \approx 49.03$ Hz minimum frequency, which may be unacceptable. A 40% reduction in R_{sys} produces a similar *increase* in the nadir. The equivalent prime movers time constant also produces a significant impact. The load-frequency dependency D_{sys} produces the least significant effect.

2.2.1.2 Improving frequency performance when H_{sys} is reduced

When increasing wind power penetration, a reduction in the composite power system inertia H_{sys} can take place if conventional (synchronous) power plants are disconnected from the power system [60], which is explained by the expression (**2.20**). Similarly, the reduction in the number of conventional power plants may produce a reduction in the amount of regulating power (i.e. less machines providing PFC). In our analysis here, this is reflected as an increase in R_{sys}.

The issue of reduction in H_{sys} could be addressed by conventional means by re-adjusting (compensating) the system load-frequency control parameters such as R_{sys} or/and T_{sys}. Here, a simple analysis by using the model PS1 and the normalized case described in Section 3.3.2 was done as follows:
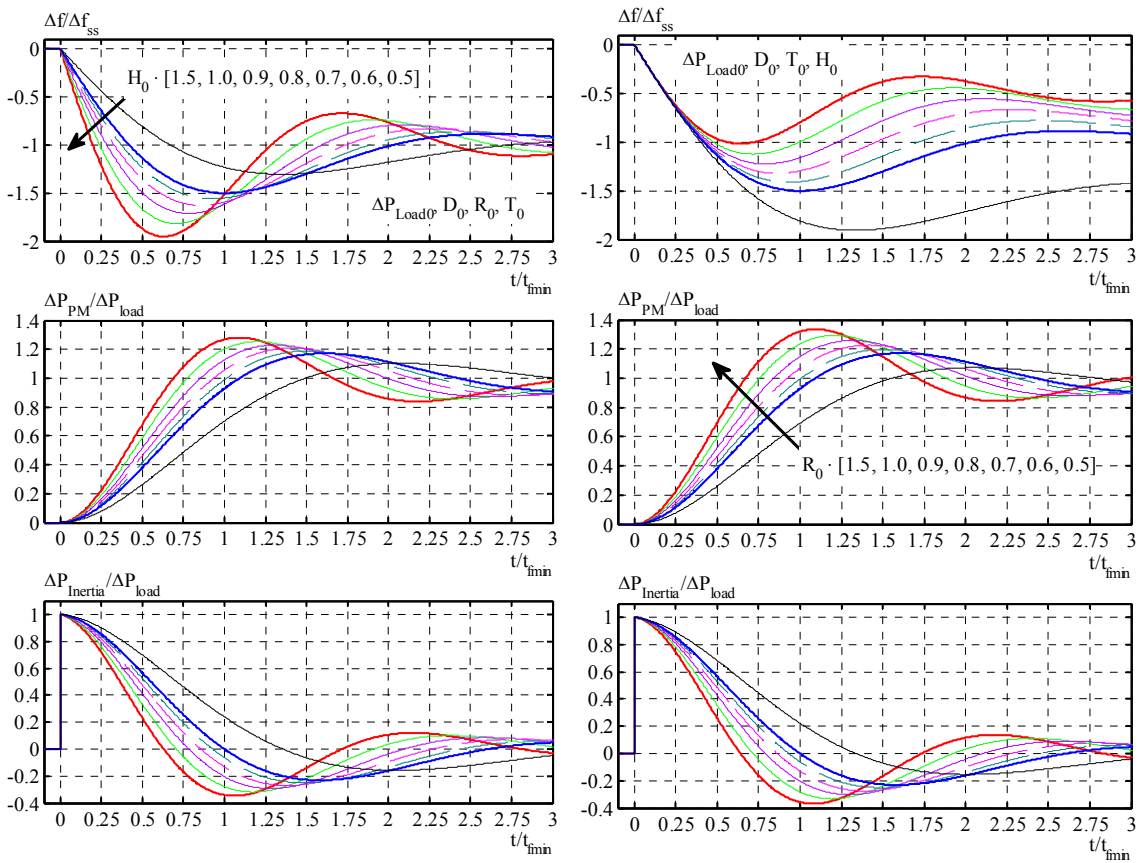
Figure 2-8: Average system response for different values of H_{sys} (left) and R_{sys} (right). Arrows indicate direction of reduction in respective parameter.
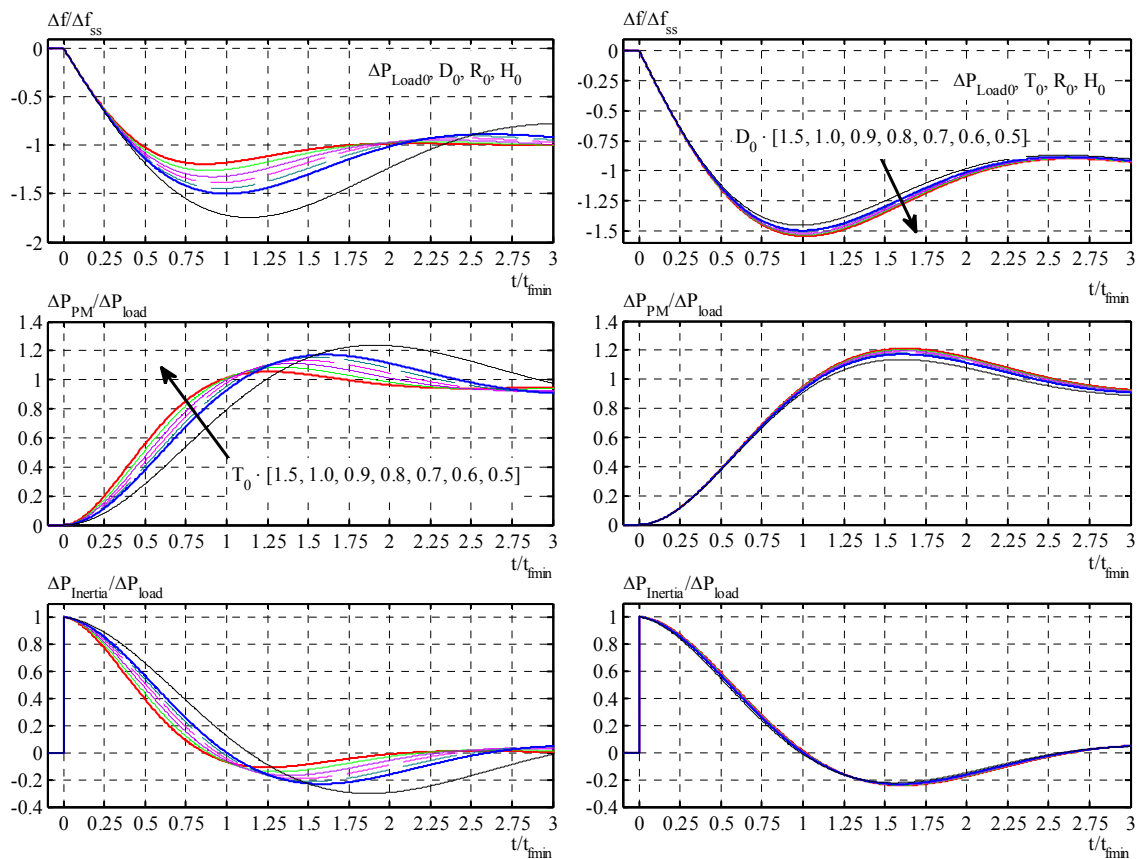
Figure 2-9: Average system response for different values of T_{sys} (left) and D_{sys} (right). Arrows indicate direction of reduction in respective parameter.

Figure 2-10: Increase in peak frequency deviation Δf_{max} (%) vs. reduction in system inertia constant ΔH_{sys} (%).

Figure 2-11 left shows an example of how the grid frequency performance is improved by decreasing the composite system droop R_{sys}: 1) First the system inertia is reduced

30% from the base case (blue to red), and then 2) the system droop is reduced ~22% in order to restore the maximum frequency deviation to 1.5 pu (red to green). This last action means to increase the system regulation capability in MW/Hz by i) reducing the droop R_i of generators online or ii) by connecting more generators with governor response. But doing any of these adjustments, there are economic implications in the system operation, since this type of actions is controlled in many countries by the corresponding Regulating Market or Balancing Market [55].

Figure 2-11 right shows an example of how the grid frequency deviation is improved by decreasing the time constant T_{sys} of the equivalent prime mover: 1) First the system inertia is reduced 30% from the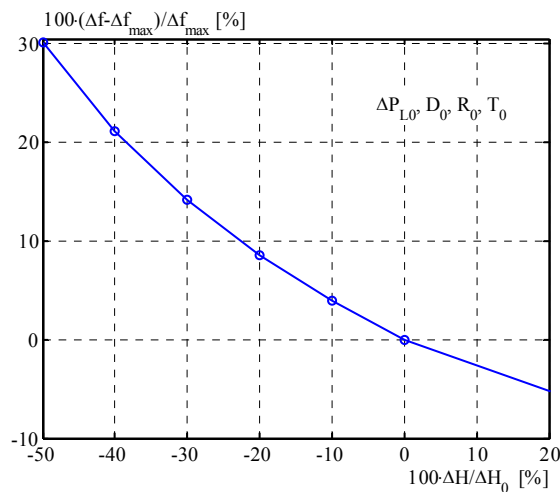 base case (blue to red), and then 2) the time constant is reduced in 30% in order to restore the maximum frequency deviation to 1.5 pu (red to green). As the prime movers time constant in most of the cases is not an adjustable parameter, it is more difficult to improve the grid frequency performance by this. Unless faster generating units, like gas turbine generators, replace the slow response prime movers, reducing the equivalent system time constant is an option many times unrealistic.

The necessary changes in R_{sys} and T_{sys} for maintaining a constant peak frequency deviation (nadir) can be better understood through graphical relationships. **Figure 2-12** shows these curves which were built with the normalized parameters in **Table A-1**, Appendix A.4. It can be seen how the relationship between $\Delta H/H_0$ and $\Delta R/R_0$ is practically linear, whereas the relationship between $\Delta H/H_0$ and $\Delta T/T_0$ is purely linear.
Other solutions need to be elaborated if it is desired to avoid the use of conventional plants for solving these wind power integration issues.
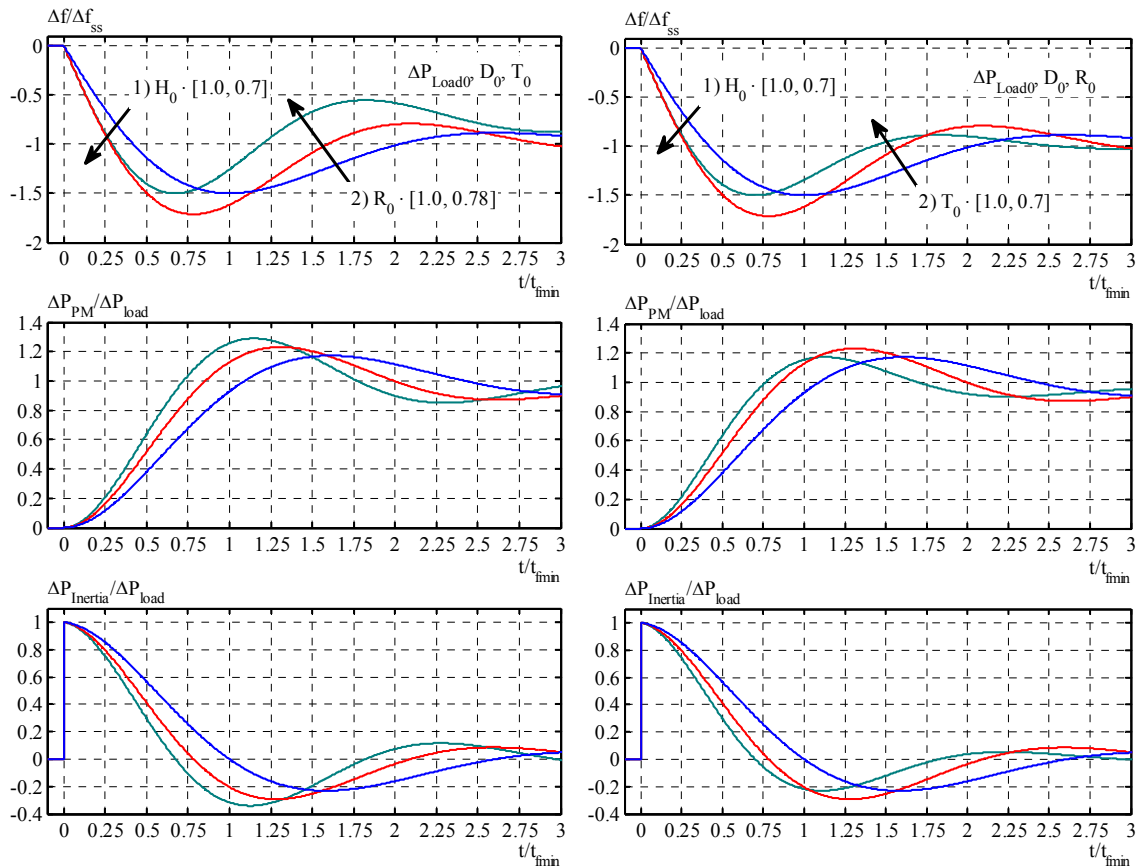
Figure 2-11: (left) 30% reduction in H_{sys} is compensated by ~22% reduction in R_{sys} in order to keep maximum frequency deviation Δf_{max} unchanged. (right) 30% reduction in H_{sys} is compensated by 30% reduction in T_{sys}.
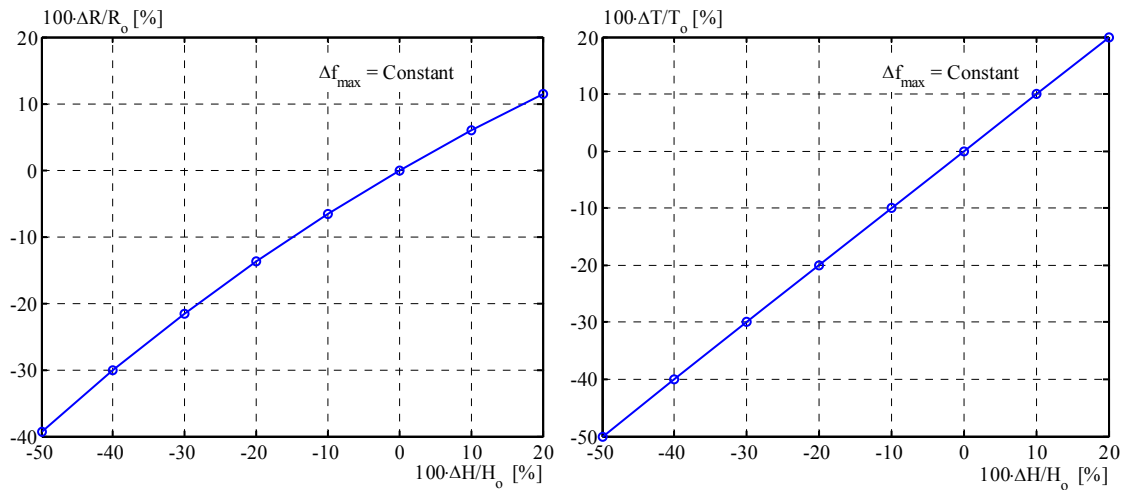
Figure 2-12: (left) Necessary change in R_{sys} when varying system inertia constant H_{sys} in order to keep maximum frequency deviation Δf_{max} unchanged. (right) Necessary change in T_{sys} when varying system inertia constant H_{sys} in order to keep maximum frequency deviation Δf_{max} unchanged.

2.3 Impact of wind power on power balance and frequency

Optimal wind power generation, when not combined with other technologies such as energy storage, unavoidable requires regulation capacity from the power system (MW/Hz) to balance the wind power fluctuations [40]-[55]. When increasing the wind power penetration, the characteristic of these fluctuations can change in different ways. For example, the overall fluctuations can be smoothened out in magnitude and/or frequencies [48]-[50], depending on the geographical distribution of the wind plants over the power system. In other cases, the generated wind power fluctuations can increase in magnitude and/or frequencies at such point that the normal regulation capacity cannot compensate them or the system operation becomes risky, as in islanded or small power systems [41] [106] [107] (Section 2.5).

2.3.1 Balancing and frequency impact

Power balance and frequency control are major technical problems in power systems with significant wind power production [40] [43]. Experiences demonstrate that difficulties maintaining balance between production and consumption under light-load and high wind conditions, i.e. cases of high wind power penetration, can exist. A real case example was studied during this work and presented in [63]. That study can be complemented with the measurements carried out in this work, presented in Section 2.5.

A wind power plant does not operate all the time, so system reserves are needed for when the wind is not blowing. This operation is normally managed day ahead, by combining forecast tools and market rules [45] [54]. Additionally during the wind plant operation, the normal wind power fluctuations in the range of tens of minutes and the errors in power forecast need to be balanced on-line by the regulation reserves, RR, [40] [41] [45] [63].

Reserves and balancing capacity come at a cost [43]. But an increase in installed wind capacity does not always means an increase of costs for operating the power system [40]. In most power systems today, wind power is not foreseen to impact the second-to-second regulation reserves. However, the impact is seen in the 15-minute balancing market for slower reserves for frequency control. In some systems there is *still* room for regulation capacity in the market, but in isolated systems this regulation market margin is limited due to the limited number of power plants.

Statistical studies carried out in [42] shows that when the penetration of the wind power in the system increases, an increasing amount of reserves need to be allocated. Theoretical analysis says that a 10% of wind penetration in the Nordic system would require an increase in reserves of 2.5-4% of the wind capacity. When the Nordic system works without transmission bottlenecks the impact of wind power becomes significant at 10% penetration level, i.e. ~2% of increase in reserves or 310-420MW. At 20% wind pene-

tration, the increase in reserves is 4% of the wind capacity or 1200-1600 MW. This is 2 to 2.5 times the actual required reserves of 600 MW [5], which is significant.

Like an individual consumer, a wind power plant is variable in output and less predictable than most other technologies. However, from a system operation view, the behaviour of a single wind plant is just as irrelevant as the demand behaviour of an individual consumer. *What is relevant however for balancing the power in the grid is the collective behaviour of consumers and all generating plants*. That has been the guiding principle of power balance since the grid inception (more than 100 years ago) and is likely to remain equal regardless the generation technologies we use. The basic principles of reserves, balancing, aggregation and forecasting still apply.

If the regulation reserves from conventional plants are to be kept limited when increasing the wind power penetration, then some mechanisms for reducing the wind power fluctuations and providing with wind power frequency reserves should be implemented. In some power systems, mainly with weak interconnections and/or high wind power penetration, frequency reserves provided by wind power can be more valuable to the system than maximizing the generation yield [62].

2.3.2 System inertia impact

The rotational speed of modern variable speed wind turbines is normally decoupled from the grid frequency by the power electronic converter configuration [21]-[26]. Therefore variations in grid load and frequency do –per default– not alter the turbine output power. This characteristic differs from synchronous machines, as described in Section 2.1.1. With high wind power penetration there is a risk that the power system inertia, H_{sys}, decreases, thus aggravating the grid frequency stability upon large load changes. The effect of inertia reduction may be even worse in power systems with slow PFC such as those with large amount of hydropower, or in small power systems with inherent low inertia such as islanded systems [41] [60].

As described in Section 2.1.1, the dynamical properties of the grid frequency during the first period following a load change depends largely on the amount of synchronous machines connected to the system and the network impedances linking those machines. These dynamical properties are affected if the amount of variable speed wind turbines is increased. For analysing briefly what would be such an impact, two hypothetical scenarios for a given power system can be addressed, which are:

- **Scenario A**: Increase of WPG following the growth of power consumption. Therefore the number of connected synchronous machines is most likely to remain constant.
- **Scenario B**: Increase of WPG by replacing conventional plants (synchronous machines) by wind power plants. Therefore the number of synchronous ma-

chines online is reduced while the average consumption is most likely to remain constant.

If the grid event is a load change ΔP_L, then in the Scenario A the power system average inertial response described by (2.20)-(2.21) *does not change*, because the number and type of synchronous machines remain unchanged. Therefore, if the size of ΔP_L is the same before and after the wind penetration in Scenario A, the system average inertial response *is not affected*. However, the power transfers over the transmission network might increase because of the use of existing lines to accommodate the wind power (e.g. wind generation located further away from the main load centres, as is the case for example in the United Kingdom [8]). Higher transfers mean larger voltage angle differences between network nodes, hence a reduction in synchronizing power coefficients between the generators closest to the wind plant and the rest of the system. This deteriorates the system dynamic properties. By taking expressions (2.9)-(2.10) and (A.2) in Appendix A.1, to assess the *initial* impact of a load change *Before* and *After* the wind plant connection to the same transmission line than the synchronous machine *i*, we obtain:

$$\left.\frac{\Delta \dot{\omega}_i(ini)\big|_{After}}{\Delta \dot{\omega}_i(ini)\big|_{Before}} = \frac{\Delta P_{ei}(ini)\big|_{After}}{\Delta P_{ei}(ini)\big|_{Before}} \approx \frac{P_{SiL}\big|_{After}}{P_{SiL}\big|_{Before}} = \frac{\cos\delta_{iL0}\big|_{After}}{\cos\delta_{iL0}\big|_{Before}}\right. \tag{2.24}$$

Expression (2.24) indicates that the initial power impact $\Delta P_{ei}(ini)$ is *reduced* when the line is more loaded (lower $\cos \delta_{iL0}$), i.e. when the wind plant is using the same line than generator *i*. If the generator *i* takes a lower (initial) share of the ΔP_L, then the other generators in the system will take a larger (initial) share of the ΔP_L. The same is for the initial rotor accelerations. In conclusion, this effect increases the initial intermachine oscillations following a load change (as shown in **Figure 2-4**), since the initial rotor acceleration is lower for generator *i* and higher for the other generators. As the initial oscillations are greater, more time (or effort) is needed for damping.

By taking expressions (2.20)-(2.21) to assess the *average* inertial response following a load change *Before* and *After* the wind plant connection, we obtain:

$$\frac{\Delta \dot{\omega}_i\big|_{After}}{\Delta \dot{\omega}_i\big|_{Before}} = \frac{\Delta P_{ei}\big|_{After}}{\Delta P_{ei}\big|_{Before}} = 1, \tag{2.25}$$

which indicates that the average inertial response remains unchanged in Scenario A.

An additional observation should be done. In order to allow higher wind power fluctuations in Scenario A, the system stiffness K_{sys} (or regulating capability, MW/Hz) may need to be increased by request of the system operator [40] [41] [43] [45] [63]. This action, in fact, would *improve* the grid frequency dynamic response, keeping the same

ROCOF but rising up the nadir. This can be visualized in **Figure 2-8** right (an increase in K_{sys} means a reduction in system droop, R_{sys}).

In the Scenario B the power system average inertial response described by (**2.20**)-(**2.21**) *is affected*, because the number of synchronous machines is reduced. If the size of ΔP_L is the same before and after the wind penetration in Scenario B, the system will experience a faster change in the average frequency because of the lower value of H_{sys}. This can be visualized in **Figure 2-8** left for constant ΔP_L and lower values of H_{sys} and in **Figure 2-10**. Thus Scenario B increases the risk of activating protection mechanisms in the system due to high ROCOF or low nadir. Regarding the power transfers over the transmission network, they might increase similarly to Scenario A if e.g. the replaced synchronous machine is distant from the new wind plant, or they might remain unchanged if the replacing wind plant is connected at the same bus than the decommissioned synchronous machine (which is very unlikely).

Let's assume the second case, where the power transfers (and voltage angle differences) are unchanged. By taking expressions (**2.9**)-(**2.10**) to assess the initial impact of a load change *Before* and *After* the disconnection of the synchronous machine *n*, we obtain:

$$
\frac{\Delta \dot{\omega}_i(ini)\big|_{After}}{\Delta \dot{\omega}_i(ini)\big|_{Before}} = \frac{\Delta P_{ei}(ini)\big|_{After}}{\Delta P_{ei}(ini)\big|_{Before}} = \frac{\sum\limits_{j=1}^{n} P_{SjL}\big|_{Before}}{\sum\limits_{j=1}^{n-1} P_{SjL}\big|_{After}} > 1
\tag{2.26}
$$

This expression shows that if a synchronous machine *n* is disconnected, the remaining machines *i* will take part of the load ΔP_L corresponding to *n*. The initial power impact in remaining machines is higher as well as the initial rotor acceleration, therefore the initial oscillations are larger.

By taking expressions (**2.20**)-(**2.21**) to assess the *average* inertial response following a load change *Before* and *After* the disconnection of the synchronous machine *n*, we obtain:

$$
\frac{\Delta \dot{\omega}_i\big|_{After}}{\Delta \dot{\omega}_i\big|_{Before}} = \frac{\sum\limits_{j=1}^{n} H'_j}{\sum\limits_{j=1}^{n} H'_j - H'_n} > 1
\tag{2.27}
$$

which indicates an increase in the average frequency rate of change when disconnecting machine *n*. Additionally, a disconnected synchronous machine cannot contribute with PFC. Therefore in Scenario B there would be a combination of effects: (i) a reduction in system inertia H_{sys} and (ii) an increase in system droop R_{sys}. If in this case the R_{sys} is attempted to be reduced (by increasing somehow regulation reserves RR, MW/Hz), the

original system frequency response might be partially "restored" by rising up the nadir. This can be visualized in **Figure 2-8** right and **Figure 2-11** left.

In conclusion, the average frequency performance in the power system is deteriorated *only* if synchronous machines are disconnected. In the other hand, with low wind speed conditions, the number of synchronous machines in the system may be higher, reducing the overall need for wind power inertial support.

Wind power will have to assume responsibility in maintaining the system frequency stability in high wind power penetration scenarios. This is technically possible, since modern wind turbines are indeed programmable power sources, and they present flexibility for very fast control of generated active and reactive powers, inside design limits. In [21] and [60] the impact of high wind power penetration on the grid frequency response upon load increase was studied. Additionally, the benefit of supporting the frequency stability implementing an enhancement in the control of wind turbines was also addressed. This enhancement is normally referred in the literature as "inertia emulation". Many recent works about the subject can be found in the literature, e.g. [22]-[38]. A contribution from this work is a particular Inertial Response controller (IR) for wind turbines. This is proposed and developed in Chapter 4.

2.4 Grid codes survey on frequency control for wind power

A survey of representative grid codes with requirements on frequency control for wind power is carried out. Some of these requirements are used as basis for this work.

The Grid Code (GC) is a technical document setting out the rules, responsibilities and procedures governing the operation, maintenance and development of the power system. It is a public document periodically updated with new requirements and it differs from operator to operator. Countries with large amount of wind power have issued dedicated GC for its connection to transmission and distribution levels, focused mainly on power controllability, power quality and fault ride-through capability [15] [16] [17]. In general, wind power plants at transmission level shall act as close as possible to conventional power plants, providing wide range of power output control based on TSO instructions. Participation in primary and secondary frequency control is also required.
Isolated power systems with lack of interconnection to others such as in Ireland [3] or Great Britain [9], or with very high wind power penetration such as in Denmark [6] or Spain [7], demand very strict requirements in terms of active power and frequency control (among others). Particularly Denmark establishes the most demanding requirements regarding active power control. Seven regulation functions are required [6], being the main ones: i) Absolute production constraint, ii) delta production constraint, iii) balance regulation, iv) power gradient constraint, and v) frequency regulation. In [10] a generic grid code for wind power plants aiming at unifying the requirements in Europe is provided.

Ireland and Great Britain have elaborated requirements for wind power frequency response that differs significantly from each other: Basically, in the Irish GC [3] the wind plant frequency response has a variable characteristic which depends on the available wind power, while in the British GC [9] the wind plant frequency response has a fixed characteristic similar to conventional plants, based on the installed capacity. All the other GC in the world are similar to one of the previously mentioned or are less demanding [6] [7] [11] [14]-[17]. For this reason, and because Ireland and Great Britain are isolated power systems that are planning large amounts of wind power, special attention is paid to their GC in this work. Following, a brief yet relevant description of these two is made.

2.4.1 EirGrid

EirGrid is the TSO in Ireland [3]. Its GC specifies various requirements in relation to frequency ranges and frequency control. Many aspects in the system as a whole are considered for establishing the requirements for the wind power plants [4]. In the Irish system, the loss of a typical 300 MW plant can have a very large effect on the system frequency [4]. The loss of a smaller generator has a significant effect as well. In this GC the addressed issues for wind power plants regarding grid frequency impact are: i) frequency regulation range, ii) frequency response characteristic, iii) production curtailment and iv) power ramp rates. The main requirements concerning frequency control for thermal plants as well as for wind power plants are summarized below [3]:

Conventional Power Plants
- *Primary frequency control* (PFC)*:* Takes place in the period of up to 30 seconds after a change in grid frequency and is achieved by automatic corrective responses on prime movers: (a) generators when synchronized to the grid shall operate at all times under the control of a Governor Control System (GCS), unless otherwise specified by the TSO; (b) no time delays other than those necessarily inherent in the design of the GCS shall be introduced; (c) a frequency deadband around the nominal (50 Hz) of no greater than ±15 mHz may be applied to the GCS; (d) normal governor regulation shall be between 3% and 5% (droop).
- *Secondary frequency control* (SFC)*:* Takes place in the time scale from 5 seconds up to 10 minutes after the change in grid frequency and it is achieved by a combination of automatic and manual actions on the load set point in each GCS. The Automatic Generation Control (AGC) is part of the SFC. Generators of 60 MW or larger shall be connected to the AGC. The SFC implements the dispatch instruction while the frequency feedback is closed at TSO level.
- *Frequency regulation:* The PFC operates normally in the range specified in **Table 2-2 A**, referred as "frequency regulation range" or "normal operating range". If the grid frequency goes beyond these limits it is considered a major disturbance (contingency). The contingency is solved by use of the Operating Reserves.

- *Power ramp rates:* Thermal generators shall have a power ramp rate not lower than 1.5 %/min.

- *Dispatching:* The SFC is normally used for setting the scheduled operation through a "dispatch instruction" related to the trading day. Additionally, the TSO monitors the system frequency and issues a dispatch instruction at any time in order to provide ancillary services to seek to regulate frequency (AGC).

- *Operating reserves:* Similar to as described in Section 2.1.5. The amount of operating reserves is calculated as part of the SRM. Here, demand disconnection is also part of the operating reserves, which is split into discrete MW blocks.

Wind Power Plants

The WPP should have a wind power plant controller (WPPC) to allow active power control and frequency response of the WPP as a whole.

- *Active power control:* The WPPC shall be capable of operating each WTG at a reduced production, when desired, by order sent on-line from the TSO. The new set-point shall commence implementation within 10 seconds from receipt, with a power ramp rate equal to the maximum setting. There are two settings of maximum ramp rate of active power output, each ranging from 1 to 30 MW/min. The first setting shall apply to the average output over 1 minute while the second setting applies to the average output over 10 minutes. The power response rate of each WTG should be a minimum of 1 %/min of rated capacity. The TSO acknowledges that falling wind speed may cause either of the maximum ramp rate settings to be exceeded.

- *Frequency response*: The frequency response (FR) from the WPP shall be characterized by the curve shown in **Figure 2-13** red line, by A-B-C-D-E. It specifies the WPP output as % of the available wind power, P_{Ava}, by continuously monitoring the grid frequency. The blue line is defined by the points (F_X, P_X). **Table 2-1** indicates the setting ranges for these points. For frequencies below F_B the power output increases as % of P_{Ava} with the slope A-B and for frequencies above F_C the power output decreases as % of P_{Ava} with the slope C-D-E. For frequencies between F_B-F_C –considered as the normal grid frequencies range –the power output does not respond to frequency changes (deadband). When the TSO constrains the WPP production to a value P_{Set} in MW, the points B, C and D are the minimum of: (i) P_{Set} converted to % of P_{Ava} or (ii) P_B, P_C, P_D. For values of P_{Set} (%) > P_B, the WPP production is not constrained to a fixed value but curtailed to a % of P_{Ava} (which is P_B-P_C). Different sites may have different settings for (F_X, P_X). Two FR curves shall be specified by the TSO. The WPPC shall be required to change between these two curves within 1 minute from receipt of the TSO instruction. The FR should be achieved without disconnecting WTGs except for frequencies beyond D-E. No time delays other than those necessarily inherent in the design of the FR control loop should be introduced.

The TSO requires that each WPP makes all the signals available at a remote terminal unit designed for that WPP. Wind plants above 30 MW should provide production forecast and available power values [4].
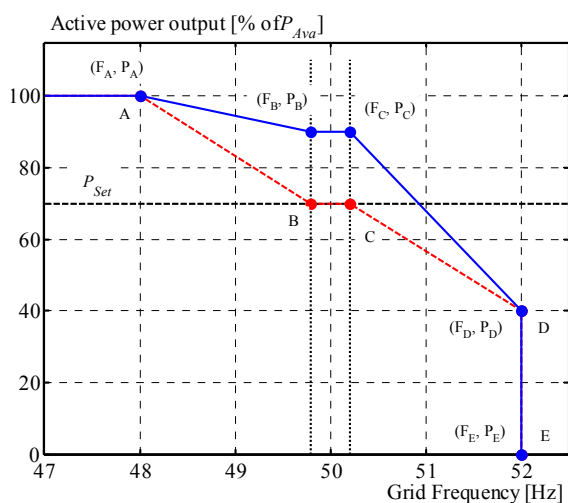

Active power output [% of P_{Ava}]

Figure 2-13: EirGrid GC specifications for WPP frequency response. In this curve, the P_{Set} is the WPP set point converted to % of P_{Ava} [3].

Table 2-1: Ranges of (F_X , P_X)for curve at left

Grid frequency range [Hz]			Setting ranges [% of P_{Ava}]	
			>10MW	<=10MW
F_A	47.0-51.0	P_A	50-100	100
F_B	49.5-51.0	P_B	50-100	100
F_C	49.5-51.0	P_C		
F_D	50.5-52.0	P_D	20-100	20-100
F_E		P_E	0	0
With: $F_A \leq F_B \leq F_C \leq F_D = F_E$ & $P_B = P_C$				

2.4.2 NGET

National Grid Electricity Transmission Company (NGET) is the TSO in Great Britain (GB). The GB power system and its overall inertia are comparatively small in relation to e.g. the wider European UCTE system [8]. Thus frequency control capability is an essential requirement for all types of generation here, especially due to the system size, range of the system demand and the expected volume of wind power in the near future [8]. The system frequency control is regulated by the Balancing Code (BC) [9]. The BC specifies the Balancing Mechanism process (BM), ruling the information exchanged for power and energy trading (gate closure), the processes post trading and the procedures and requirements regarding system frequency control. The system frequency control is provided by generating units participating in the BM, as part of the Ancillary Services (AS). Thus the effectiveness and consequences of the BM determine the requirements for frequency control.

Conventional power plants
This GC establishes similar frequency response requirements for all the generating units connected to the system, including wind power [9]. All the generators in the system, including WPP above 50 MW, shall have the capability of operating with two different modes, which are:

- Frequency Sensitive Mode (FSM): Power output shall change proportionally and opposite to positive or negative frequency deviations from the reference fre-

quency. Power reserve is needed upwards and downwards. The deadband around the nominal frequency (50 Hz) should not be greater than 30 mHz (±15 mHz).

- Limited Frequency Sensitive Mode (LFSM): Power output shall be insensitive to frequency changes except when the system frequency exceeds 50.4 Hz, point from which specific high frequency response must be provided.

Figure 2-14 summarizes the requirements for FSM and LFSM (applicable to all type of units). The frequency of the system shall be controlled normally in the range indicated in **Table 2-2 A**, unless exceptional circumstances prevail. The frequency controller must be capable to be set so to provide an overall droop between 3 % and 5 % of rated power. The minimum requirements for FSM and LFSM are dependent on the present loading of the unit, but in general should not be less than 2 % power change per 0.1 Hz change.
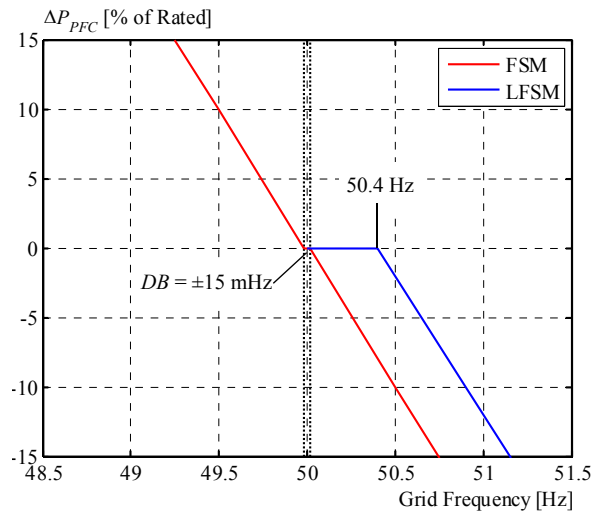

Figure 2-14: Requirements for FSM and LFSM in NGET Grid Code.

The frequency response performance of the generating unit is defined in terms of Primary Response, Secondary Response and High Frequency Response:

- The Primary Response performance is characterized by the minimum increase in active power output between 10 and 30 seconds after the start of a -0.05 Hz/s frequency ramp change. The power change shall start within 2 seconds and be capable of achieving 10% of nameplate capacity by 10 seconds.
- The Secondary Response performance is characterized by the minimum increase in active power output between 30 seconds and 30 minutes after the start of such frequency ramp change.
- The High Frequency Response performance is characterized by the decrease in active power output 10 seconds after the start of a +0.05 Hz/s frequency ramp change in the area of LFSM actuation. This power should change decreasingly with time over 0 to 10 seconds.

The generating units must be able to receive dispatching instructions from the TSO. Thus the system frequency in GB is controlled by (i) automatic response from generating units (and DC connections,) operating in LFSM or FSM, by (ii) the issuing of instructions to the generating units from the TSO and by (iii) control of demand.

Operating Reserves (OR) are determined one day in advance, on the basis of demand levels forecast, large power plants availability shortfalls and the loss of generation against which the transmission system must be secured, or loss of import from or sudden export to external interconnections. The GB's TSO allocates the OR to the appropriate units participating in the BM, fulfilling their requirements for AS. Thus AS for frequency control is activated by requesting to the generators to move to or from FSM. They will be specifically requested to operate providing primary response and/or secondary response and/or high frequency response. FSM requirements are not applicable to WPP of less than 50 MW. Each generating unit must operate –per default –at all times in LFSM, unless instructed to operate in FSM. Regulation under LFSM is not part of AS, but it is known as high frequency response.

Contingency reserves are decided by the TSO one day in advance, on the basis of historical trends of large power plants and demand. Its allocation in thermal plants is carried out through a combination of ancillary services instructions and bid-offer acceptances, consistent also with the dynamic capabilities of the power plant-allocated reserve and contractual arrangements. The disconnection of demand as AS starts with frequencies equal or below 48.8 Hz and it is split in discrete MW blocks.

Wind Power Plants

Similarly to conventional plants, WPP must be capable of contributing to frequency control by continuous modulation of active power output according to **Figure 2-14** when allowed by the wind. Frequency controllers for wind power may be located at WPP level, at individual WTG or be a combination of both. The WPP should produce power, P_{WPP}, according to an external set point, P_{Set}. If the available power, P_{Ava}, is lower than P_{Set}, then the P_{WPP} will be what is possible, following variations in P_{Ava}. Upon changes in P_{Set} the P_{WPP} should change with a predefined maximum ramp rate. On these characteristics, the WPP should be able to operate in FSM or LFSM, as follows:

- FSM: firstly, the P_{WPP} should be reduced externally by P_{Set} to provide head room for up-regulation. If the frequency crosses above 50.015 Hz the controller should take the actual $P_{WPP}(0)$ (memory function) and use this to reduce the production with a ΔP_{PFC} according to **Figure 2-14**, staying like this as long as frequency and P_{Ava} are both high. On the other hand, if the frequency falls below 49.985 Hz the controller should increase production from $P_{WPP}(0)$ (memory function) with a ΔP_{PFC} according to **Figure 2-14**, staying like this as long as frequency is low and P_{Ava} is high. If the demanded power to the WPP, $P_{Demand} = P_{set} + \Delta P_{PFC}$, is above P_{Ava} then the WPP will produce just what is possible. **Figure 2-15** left shows a WTG simulation responding to this characteristic when a fictitious frequency reduction is applied. Only when the frequency is between 50 ± 0.015 Hz the memory of $P_{WPP}(0)$ is *released* and the P_{WPP} is allowed to follow the minimum of $\{P_{Set}, P_{Ava}\}$.

- LFSM: The WPP produces what is possible, but the operator can impose a P_{Set} if wanted for grid balancing reasons. If the frequency crosses above 50.4 Hz the controller should take the actual $P_{WPP}(0)$ (memory function) and use this to reduce the production with ΔP_{PFC} according to **Figure 2-14**, staying like this as long as frequency and P_{Ava} are high. If the P_{Ava} falls below the demanded power, $P_{Demand} = P_{set} + \Delta P_{PFC}$, then the WPP will produce what is possible. **Figure 2-15** right shows a WTG simulation responding to LFSM characteristic when a fictitious frequency increase is applied. Only when the frequency is below 50.4 Hz the memory of $P_{WPP}(0)$ is *released* and allowed to follow the minimum of $\{P_{Set}, P_{Ava}\}$.
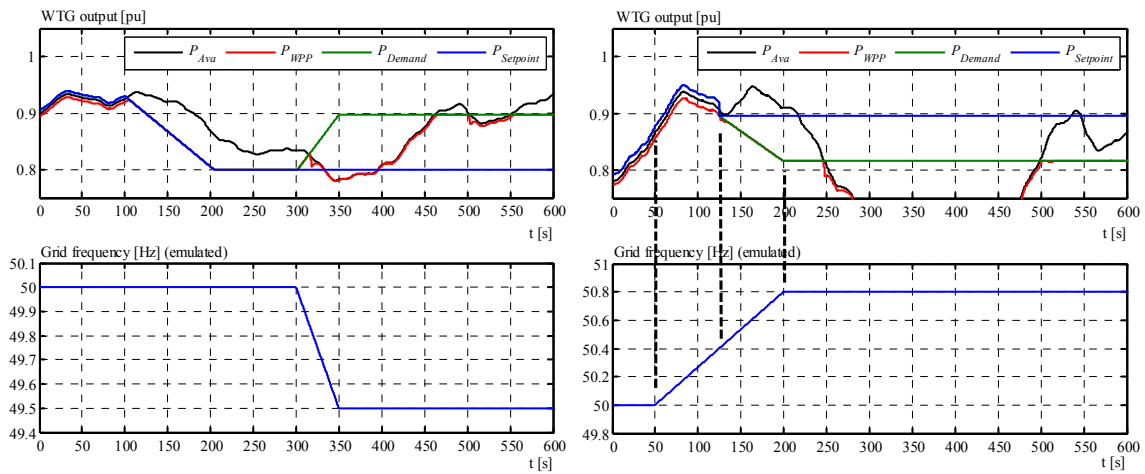

Figure 2-15: Simulation of WTG response with FSM (left) and LFSM (right). For a frequency controller at WPP level, similar response shall be expected.

Table 2-2: Frequency ranges in some European systems

System state		Frequency range [Hz]		
		EirGrid [3]	NGET [9]	Nordel [5]
A	Normal operating range	49.8 to 50.2	49.5 to 50.5	49.9 to 50.1
B	Transmission system disturbances	Low frequency: 48.0 to 49.8 High frequency: 50.2 to 52.0	Low frequency: 47.5 to 49.5 High frequency: 50.5 to 52.0	Low frequency: 49.5 to 49.9 High frequency: 50.1 to 52.0
C	Exceptional transmission system disturbances	Low frequency: 47.0 to 48.0	Low frequency: 47.0 to 47.5	Low frequency: 47.0 to 49.0

2.5 Measurements - Islanded power system with wind power

Extensive measurements in an isolated power system with large share of WPG were carried out as part of this work. This power system is situated in the Danish island of Bornholm [108]. The measurement results show the impact in the grid frequency produced by high wind power penetration. Following, the obtained results relevant in this study are presented in a condensed form.

2.5.1 System description

Only a brief description is presented here. The reader can find a more complete description of this power system in Appendix A.5 and [108]-[109]. This power system is referred as PS2 in this work. A computational model of this power system has been built for dynamic simulations with high wind power penetration and the developed control algorithms in this work were verified in this model.

Bornholm is a Danish Island situated in the Baltic Sea. Its surface can be fit in a square-shape area of approximately 20x30 km^2. Its power system consists mainly of a ring-shape transmission system of 60kV surrounding the island. Sixteen bus-bars spread over the island are connected to this transmission system, from where the voltage is reduced to 10 kV for each local distribution system. Loads are mainly homes and farms, but also few industries. Registered load consumption by 2008 was ~56 MW maximum and ~15 MW minimum [63] [108]. The Bornholm power system is normally connected to the Nordic Power System (NPS) [5] through a 60kV/70MVA submarine cable, thus feeding the whole island.

Local generation consists of one conventional generator –steam turbine – with a permanently engaged governor, named SG1 in this work; one Combined Heat and Power unit (CHP) – steam turbine– with a normally disabled governor, named SG2; other diesel generators operated normally at constant power, which can be lumped in SG3 and other minor generators not operated during these measurements. The operated generators are concentrated in a main bus-bar supplying power to the whole system. Additionally, two controllable wind power plants (WPP1 and WPP2) located at two different bus-bars in the system –in parallel with local load– which are approximately 20 km distant from each other. Each one of the WPPs is composed of three 2MW variable speed wind turbines, doubly-fed generator based, controlled remotely and centrally via SCADA system. The WPPs can be operated at optimal production as well as controlled by power limitation or curtailment. The wind turbines can be connected/disconnected individually by remote instruction. Other wind turbines of old design (fixed speed, not controllable), which were off during the measurements, can also be found in the island.
While the system is connected to the NPS the local generation is normally off, ready for start-up in case necessary, except for the CHP unit (attending the heat demand) and the wind turbines normally operating at available power. The installed capacity of SG1 is

about 0.45 pu of the system peak demand. The installed capacity of SG2 is about 0.68 pu of the system peak demand. The installed capacity of "controllable" wind power is about 0.2 pu of the system peak demand. The installed capacity of total WPG (controllable and not-controllable) is about 0.55 pu of system peak demand, which gives a large capacity penetration of $WP_C \approx 55\%$ and large share penetrations of $WP_{Sh} \approx 40\%$ when connected to the NPS. A large $WP_{Sh} \approx 200\%$ can be achieved during island operation.

2.5.2 Motivation for measurements

As the island is normally connected to the NPS, the wind power fluctuations in the island are absorbed by the system without any problem. But some cases where the island was disconnected from the NPS have shown that the wind power resources cannot be fully exploited during island operation. The relatively large amount of fluctuating wind power production causes troubles in the local system operation for power balance and frequency control. Therefore during island operations, the grid operator is forced to shut the non-controllable wind turbines down and operate at minimum power (constant minimum production) the controllable ones, if wind conditions are good.

This power system is able to show situations of high wind power penetration. Furthermore, these situations have shown that high wind power penetration cannot be handled by means of standard regulation mechanisms. It was therefore useful to take this case for learning and understanding what are the characteristics of the impact and limitations of wind power in such power systems. The knowledge was then used in this work for validation of the wind turbines and the power system models, and for developing suitable control methodologies for wind power production, focused on power balance and frequency control of the power system. These were the main motivations for performing measurements in this power system during island operation.

2.5.3 Measurements set-up

High performance measurement devices were installed at the terminals of the main power sources in the island to record –with high sampling rate , instantaneous values of voltages, currents, active and reactive powers and grid frequency; particularly at the regulating machine SG1, the CHP plant SG2 and all the controllable wind turbines in WPP1 and WPP2. At the wind turbines, additional measurements of the main variables such as wind, rotor and generator speeds and pitch angle were carried out. These measurements were used later also in models validation. Additional measurements and notes taken at the main control room during the tests complete the set of data.

The power system was in island operation in different opportunities. In some of those opportunities, the grid operator kindly accepted to increase and decrease the wind power production at different levels, by connecting/disconnecting wind turbines and by remote control of their power set points (power limitation). Different penetration levels were

achieved and the respective impact on the islanded grid was registered. The maximum possible wind power penetration allowed by the standard regulation mechanism was observed. The main results are summarized in the next subsection.

2.5.4 Main results

Main measurement results for characterizing the wind power impact in a power system with high wind power penetration are shown. The relevant data is grouped according to three different system conditions:

1- System connected to the NPS during three different days. Section 2.5.4.1.
2- System in island operation with no wind power during three different days. Section 2.5.4.2.
3- System in island operation with different wind power penetration levels during two different days. Section 2.5.4.3.

Figure 2-16 shows measurements from a wind turbine in this power system during island operation. This figure shows typical wind turbine behaviour in this island. **Figure 2-17** shows the active power output and electric frequency of SG1 during a planned transition to island operation by opening the sea cable breaker. No wind power was being generated during this transition. Observe the degradation of the grid frequency due to the reduction in system inertia when operating in islanded condition.

Figure 2-18 shows the wind power impact on the power system during island operation when increasing the wind power penetration. The wind power penetration was increased by gradual connection of wind turbines in WPP1 and WPP2 and releasing their power constraint. It is shown the total wind power production in the system and an example of the power output of an individual wind turbine. Observe the impact on SG1 power output and electric frequency when increasing the wind power production during island operation. There is a degradation of the conventional plant production and grid frequency due to the high fluctuation of wind power. The maximum penetration achieved was about 13.5% of system load, where the maximum allowed frequency variations of ±100 mHz were experienced, with an eventual minimum of 49.8 Hz.
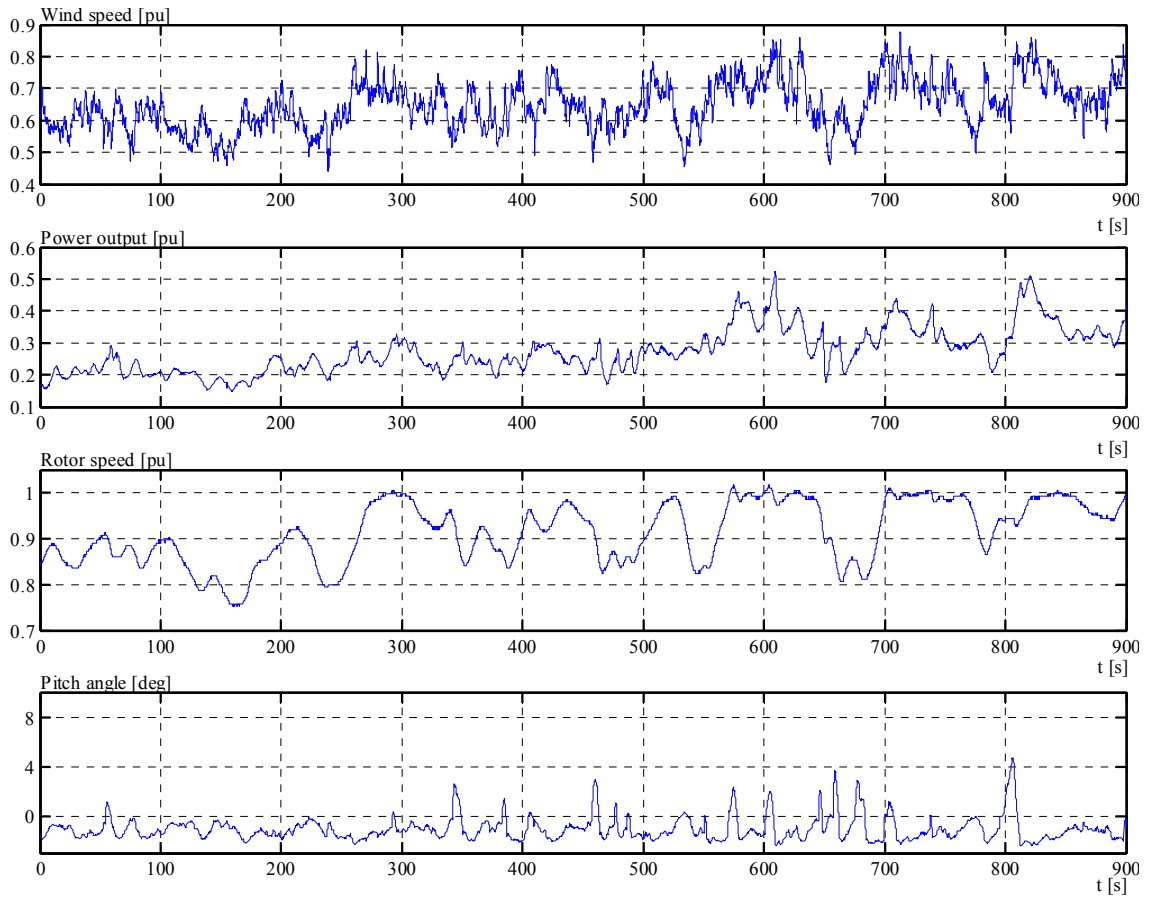
Figure 2-16: Wind turbine measurements during island operation at 10 Hz sampling. Wind speed passed through a 1st order filter with $\tau = 1$s.
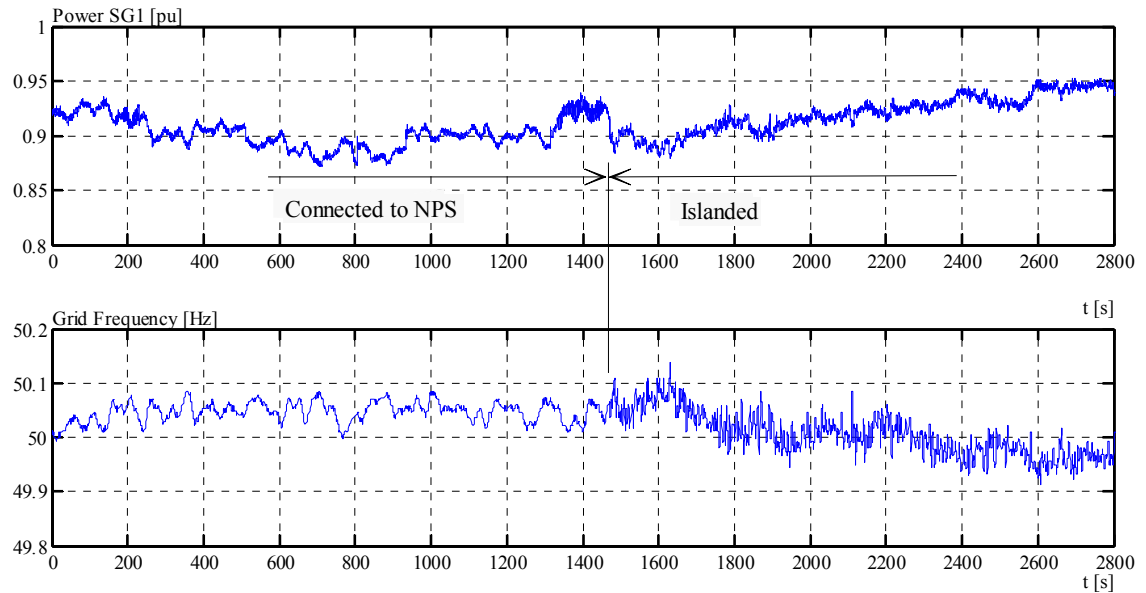

Figure 2-17: Grid frequency and SG1 power output during the transition connected/islanded. Measurement sampling at 10 Hz for power and at 1 Hz for frequency.
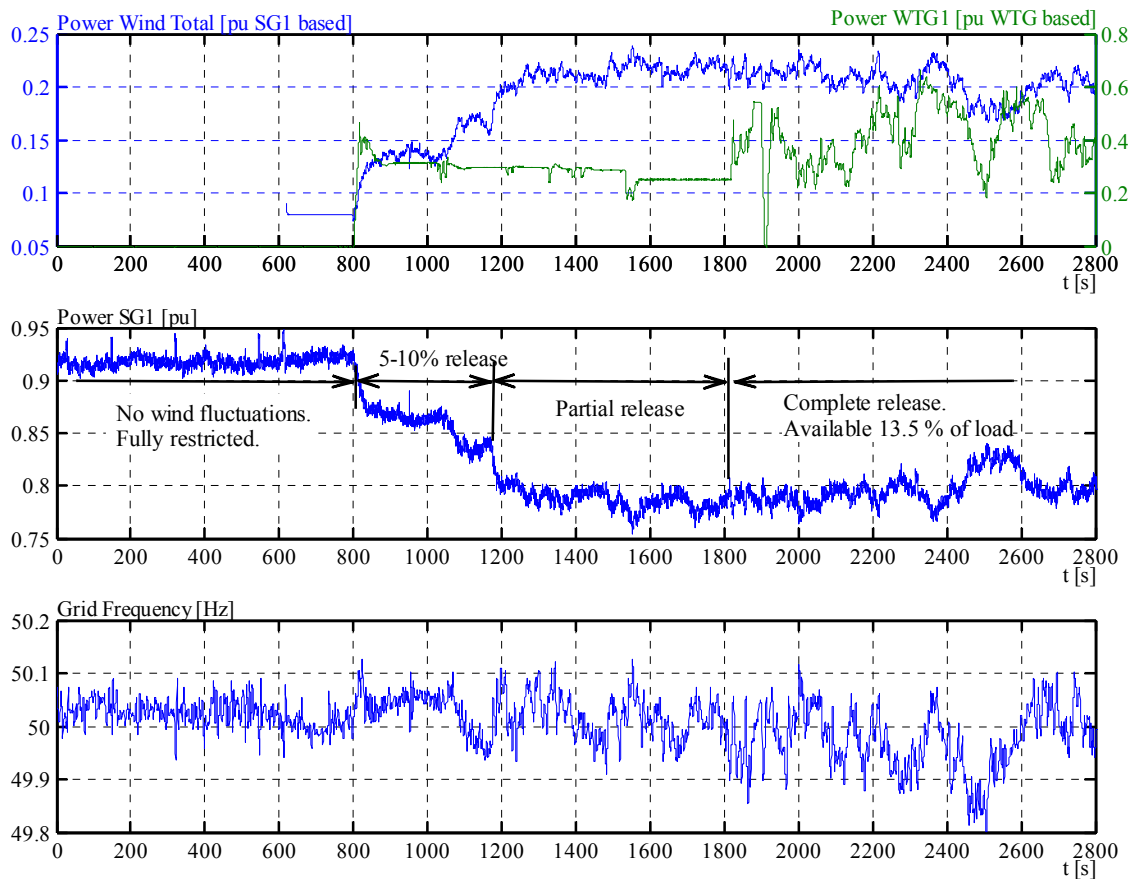
Figure 2-18: Measurements in island operation. Conventional power plant output and frequency when increasing the wind power. Wind turbines gradually connected to the grid until complete restriction removal. Limit on wind power penetration was reached. Measurement sampling at 10 Hz for power and at 1 Hz for frequency.

2.5.4.1 System connected to the NPS

During this operation, the grid frequency was dictated by the NPS and there was no measurable impact of wind power production on grid frequency and power balance.

Figure 2-19 shows the time series of measured grid frequency, power output of SG1 and the calculated ROCOF, for a period of 30 minutes during Day 1. Observe the normal frequency fluctuations, characteristic of the Nordic power system. The range of fluctuations is lower than ±0.10 Hz, which is according to the grid code [5] (**Table 2-2 A**). The power output of SG1 fluctuates opposed to the grid frequency variations, indicating the operation of the governor, i.e. PFC. The ROCOF was calculated from the measured frequency at 1 Hz sampling.

Figure 2-20 presents the statistical data of grid frequency and ROCOF for periods of 30 min during Days 1, 2 and 3.

Figure 2-21 shows the FFT spectra analysis of grid frequency and SG1 output for the three days. While the grid frequency spectrum is similar for the three days, the SG1

output spectra present different peaks. This may be due to different grid configurations. Additionally, the correlation between grid frequency and SG1 output is presented, which was used for determining the regulation constant (MW/Hz) of SG1 and for adjustment of the computational model (see Section 3.3.3 and Appendix A.5).
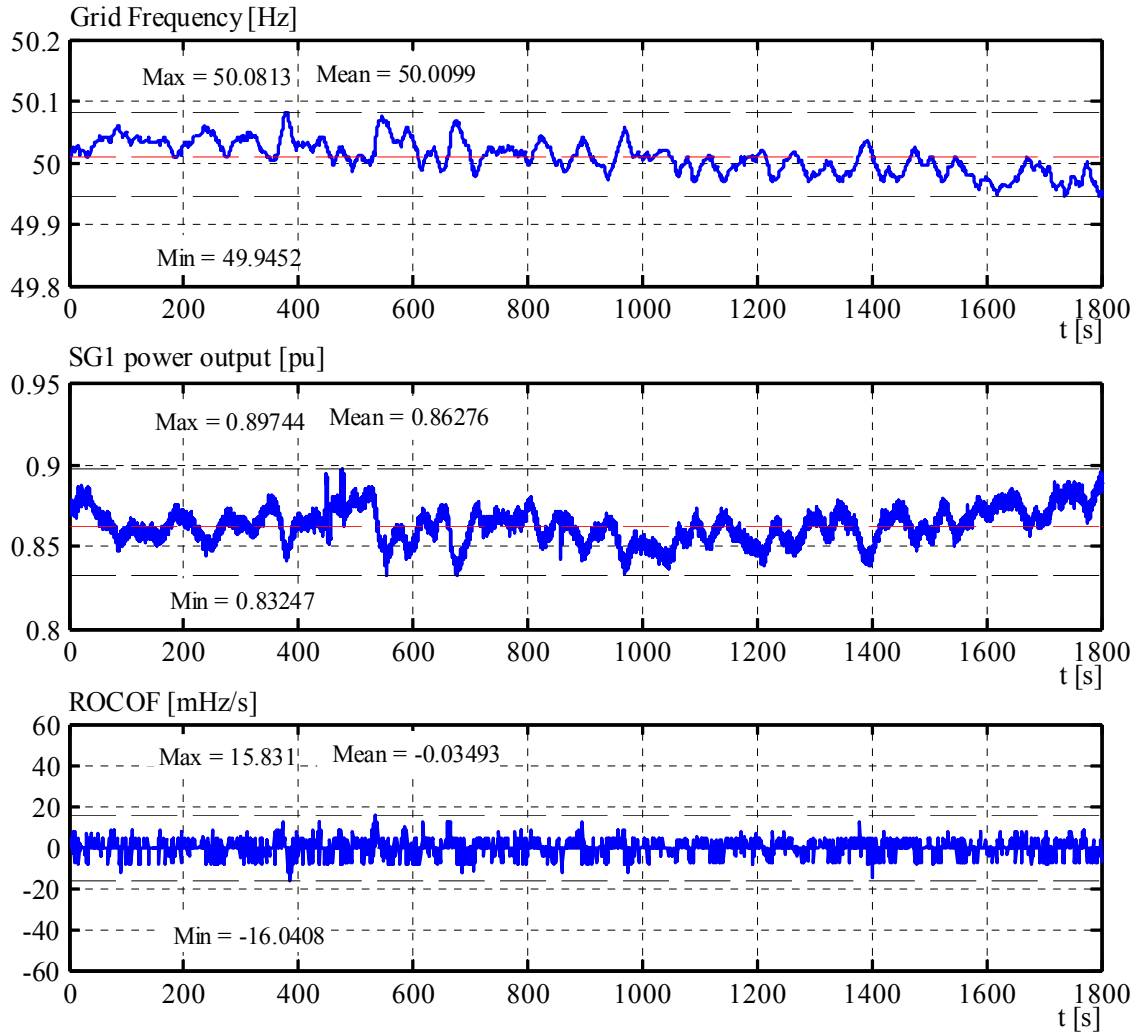

Figure 2-19: Measurements when connected to the NPS. Normal interconnected system operation and behaviour. No wind power impact can be observed. Calculated ROCOF based on measurements. 1 Hz sampling for frequency and 10 Hz sampling for power.
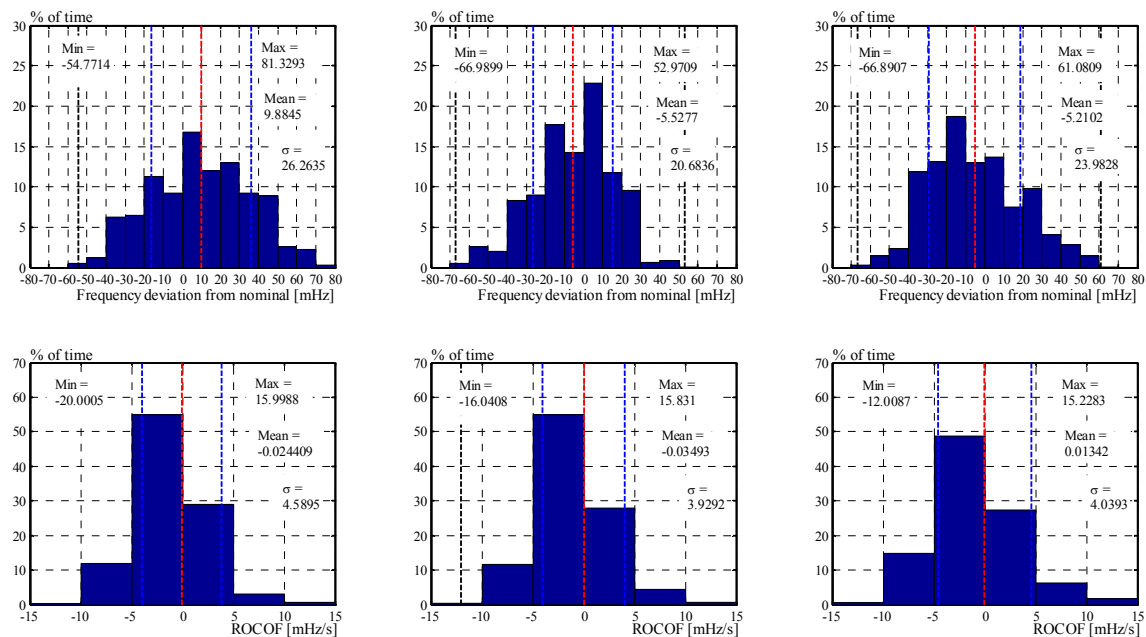
Figure 2-20: Statistical data of grid frequency for 30 min measurement during inter-connection to NPS, Day 1 (left), Day 2 (centre) and Day 3 (right). Normal values.
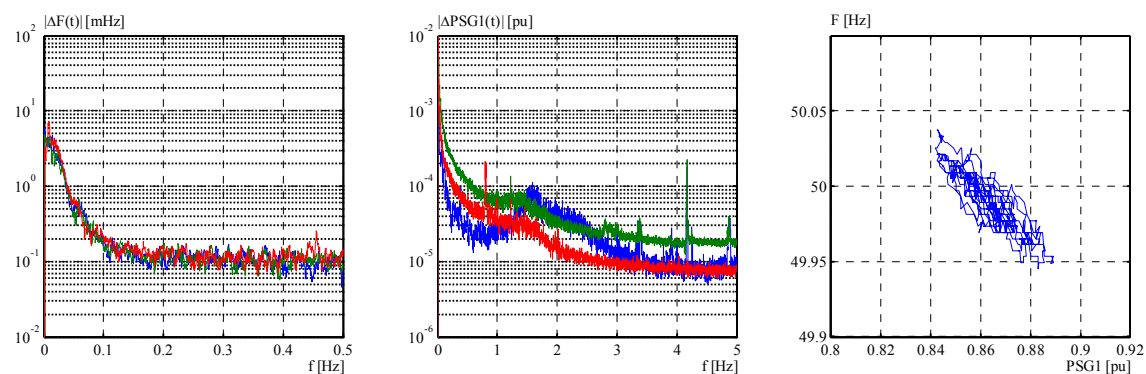

Figure 2-21: FFT spectra of grid frequency (left) and SG1 power output (centre) for the three days Correlation of frequency and SG1 output for Day 1 (right). Normal values.

2.5.4.2 System in island operation with no wind power

During this operation, the grid frequency was dictated by the speed of SG1 and controlled by its governor. No wind power plant was in operation. System load was supplied by SG1 during Days 1&3 and by SG1+SG2 during Day 2.

Figure 2-22 shows the time series of measured grid frequency, power output of SG1 and the calculated ROCOF, for a period of 30 minutes during Day 1. Compare the frequency characteristics with the previous case connected to the NPS. Grid frequency still remains inside boundaries specified by the grid code (**Table 2-2 A**). The power output of SG1 changes according to the consumers and the grid frequency is controlled by the governor of SG1. Higher values of ROCOF can be observed, putting in evidence the low system inertia.
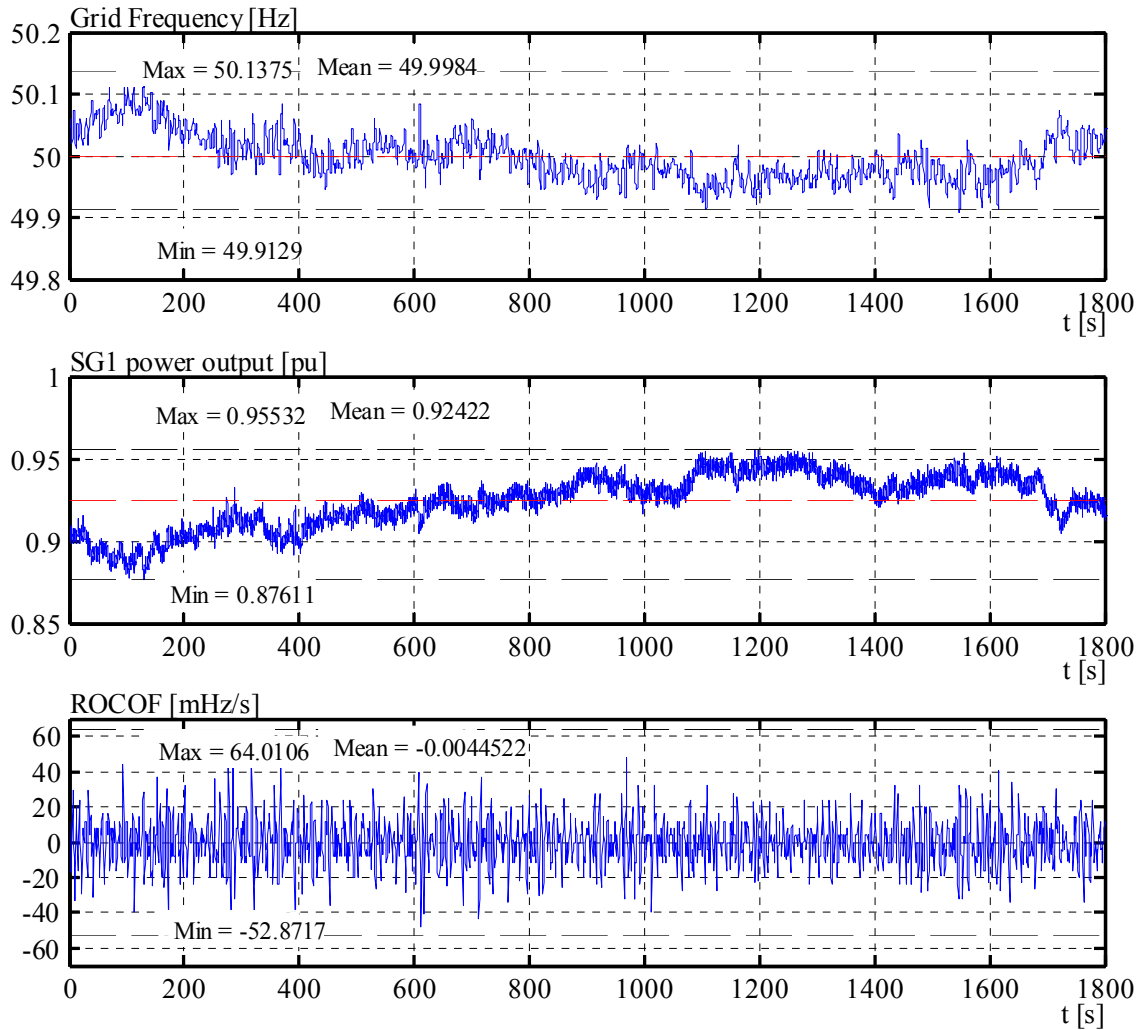
Figure 2-22: Measurements of grid frequency and SG1 power output in island operation, no wind power. 1 Hz sampling for frequency and 10 Hz sampling for power. ROCOF calculated from measured frequency.

Figure 2-23 presents statistical data of grid frequency and ROCOF for periods of 30 min in islanded operation but no wind power, Days 1, 2 and 3.

Figure 2-24 shows the FFT spectra analysis of grid frequency and SG1 power output for the three days. Comparing with the previous case (connected to the NPS), it can be seen how the grid frequency is deteriorated due to the low system inertia. The oscillations are lower for Day 2, where SG2 was in operation too (increased system inertia). Additionally, the correlation between grid frequency and SG1 output is presented.
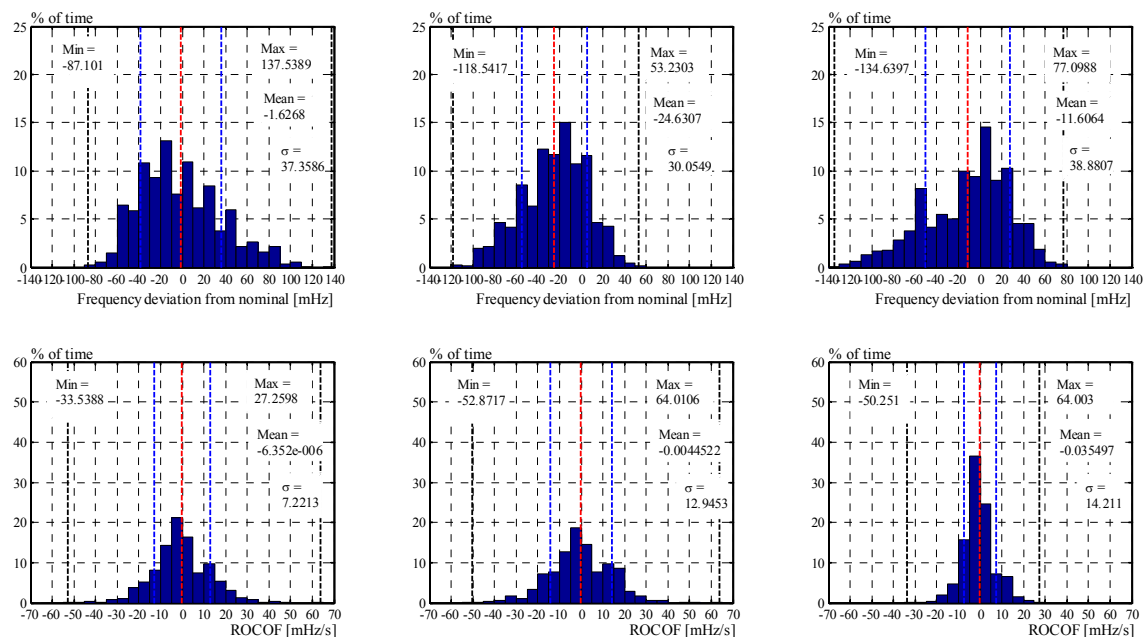
Figure 2-23: Statistical data of grid frequency for 30 min measurement in islanded operation, no wind power, Day 1 (left), Day 2 (centre) and Day 3 (right).
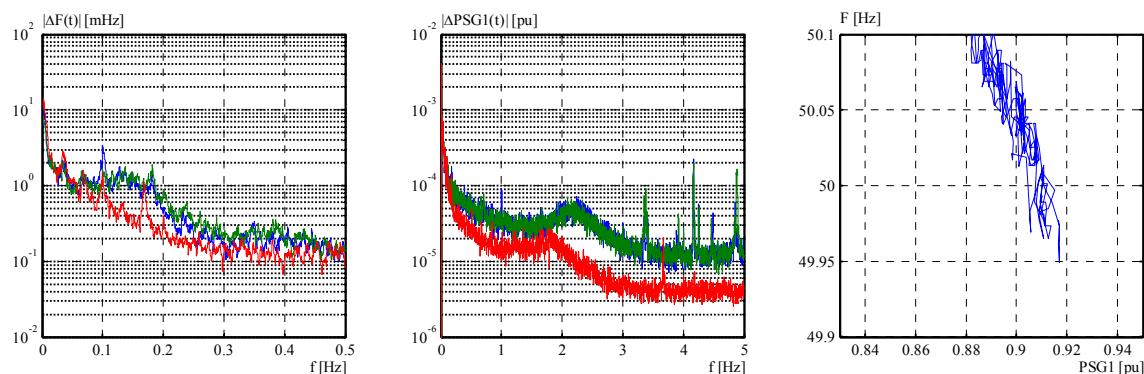

Figure 2-24: FFT spectra of grid frequency (left) and SG1 power output (centre) for the three days, island/no wind. Correlation of frequency and SG1 output for Day 1 (right).

2.5.4.3 System in island operation with different wind power penetration levels

Different instantaneous wind power penetration levels (WP$_I$) were achieved during the days of island operation. From those measurements, only representative ones are presented here, showing three different WP$_I$ levels. The highest penetration level was WP$_I$ ≈ 13.5 % achieved in Day 1 when only SG1 was in operation. The power system was operated only for 20 minutes in this condition due to large frequency fluctuations. After this period, wind turbines production was reduced by control action. This penetration value is taken as the maximum possible wind penetration in island operation, because the SG1 was the only machine normally dedicated to the frequency control in the system. The other penetration levels shown are 5.9 % and 2.7 %, for Day 2. Similar results were obtained in Day 3. **Figure 2-25** to **Figure 2-27** show time series of 20-30 min

measurement periods of grid frequency, total wind power production, SG1 power output and calculated ROCOF. These figures show the system behaviour for the three penetration levels. Observe the degradation of the grid frequency compared with the previous case. For the highest WP$_I$ (**Figure 2-25**), the grid frequency clearly exceeds the boundaries specified for normal operation (±0,1 Hz) reaching low values of ~49.8 Hz, which is considered as disturbance for the NPS. Same behaviour is observed for the other WP$_I$ levels, with reduced impact. **Figure 2-28** shows the statistical data of grid frequency for the respective periods. **Figure 2-29** shows the grid frequency vs. SG1 output and vs. wind power production. Observe the correlation between wind power and frequency fluctuations. A trend line was placed manually for better visualization. **Figure 2-30** shows the power spectra analysis of grid frequency, SG1 power output and wind power production for the three periods. For the figures, the base power is SG1's nominal power (regulating machine in the system). Measurements were carried out with 1 Hz sampling for frequency and 10 Hz sampling for power. ROCOF calculated from frequency.
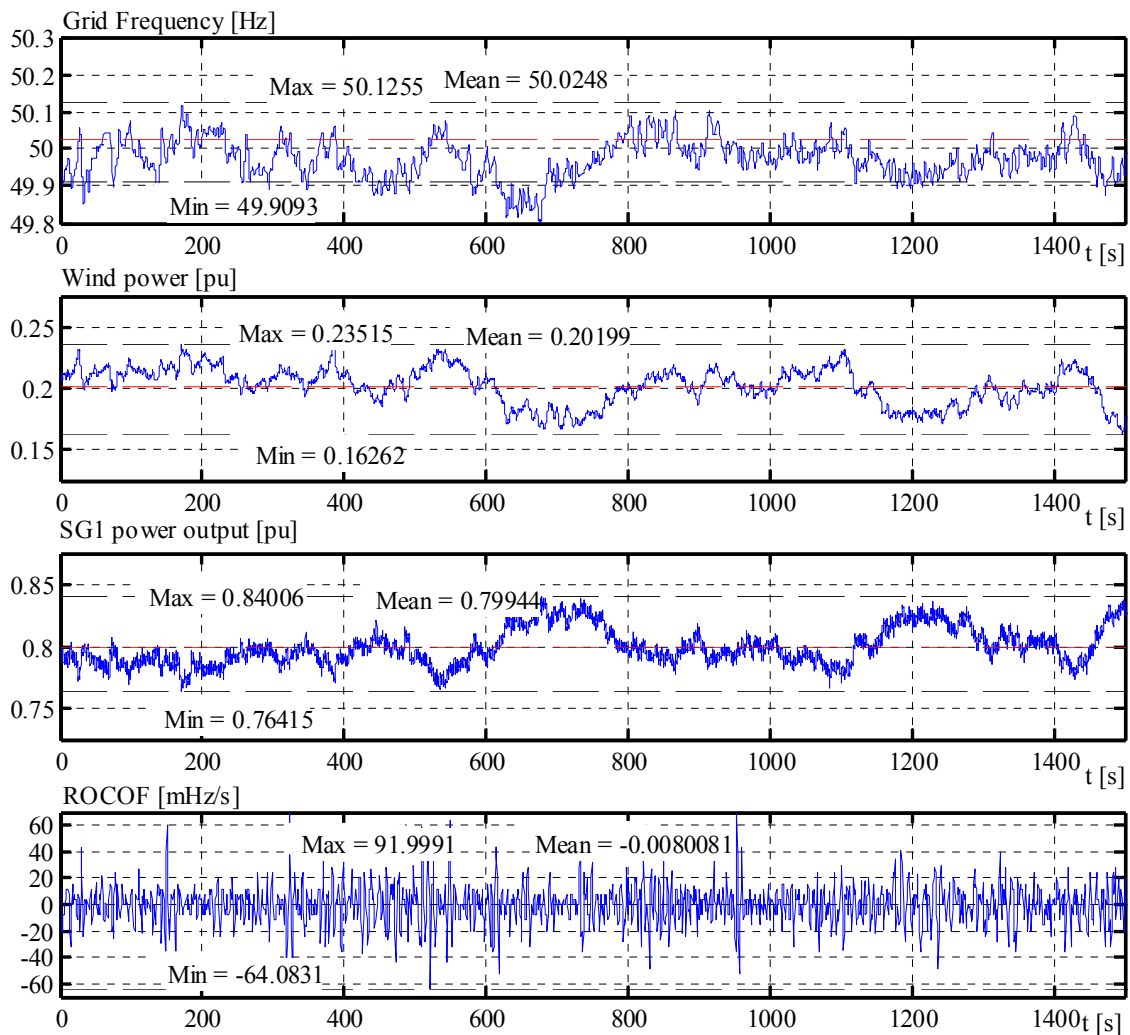
Figure 2-25: Measurements Day 1. 13.5% wind penetration. Load 1.48 pu.
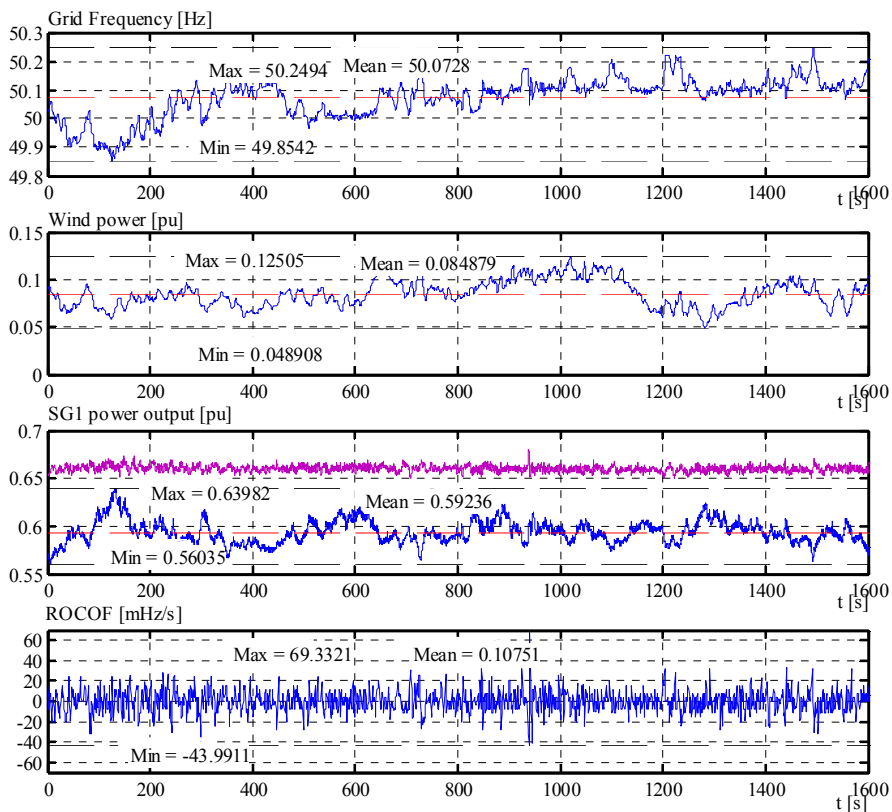
Figure 2-26: Measurements Day 2. 5.9% wind penetration. Load 1.44 pu
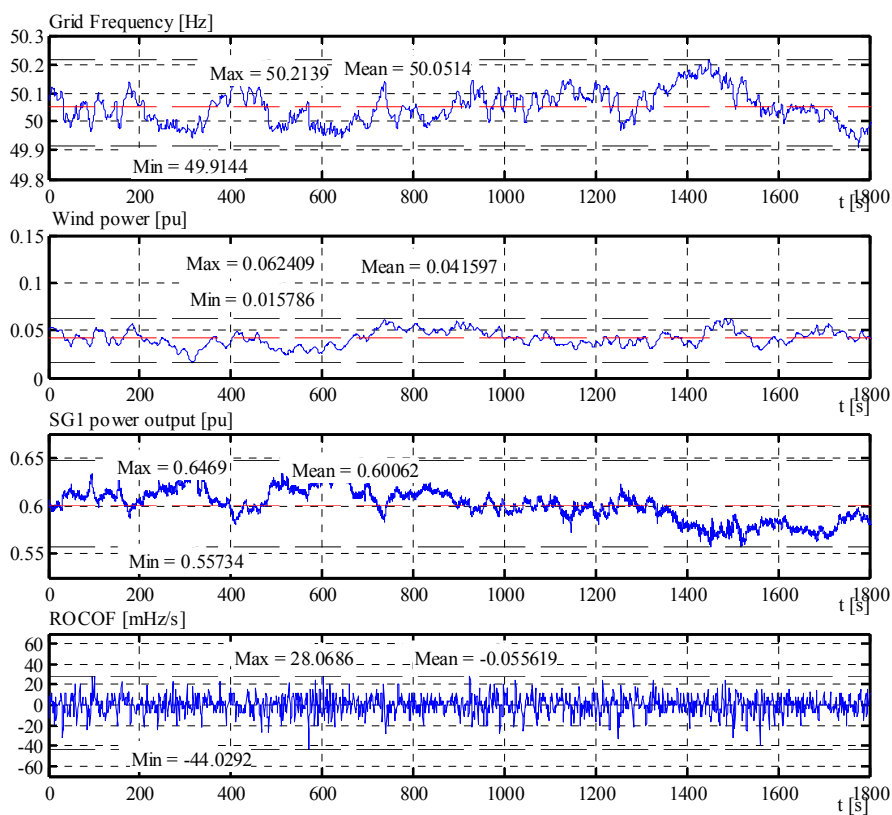
Figure 2-27: Measurements Day 2. 2.7% wind penetration. Load 1.46 pu.
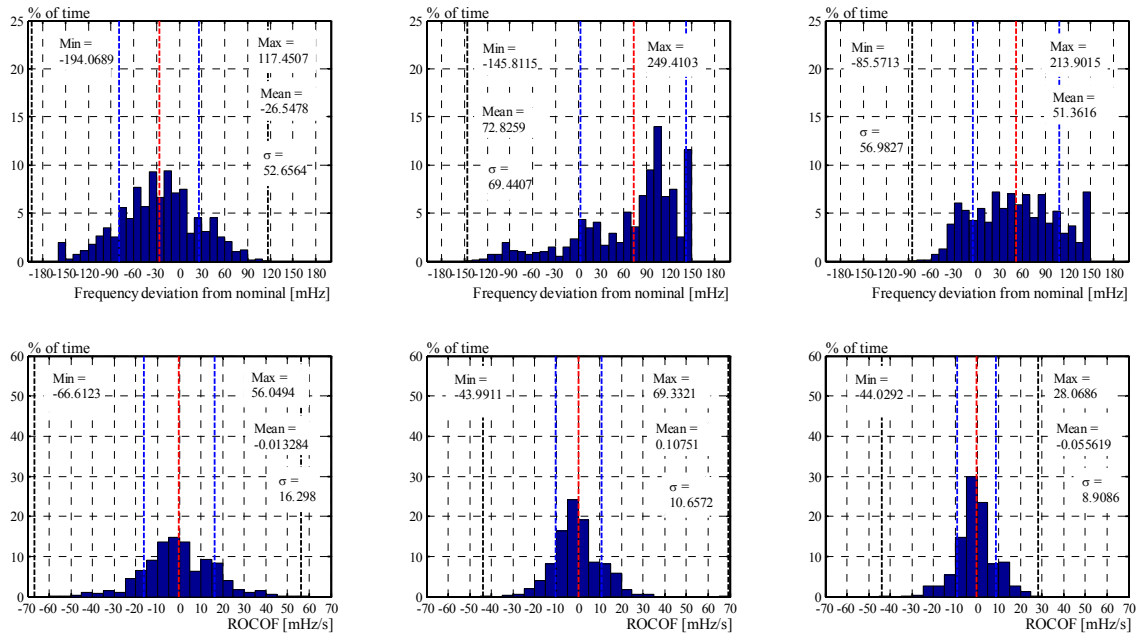
Figure 2-28: Statistical data of grid frequency for the penetration levels of 13.5 % (left), 5.9 % (center) and 2.7 % (right). Grid frequency (top row) and ROCOF (bottom row).
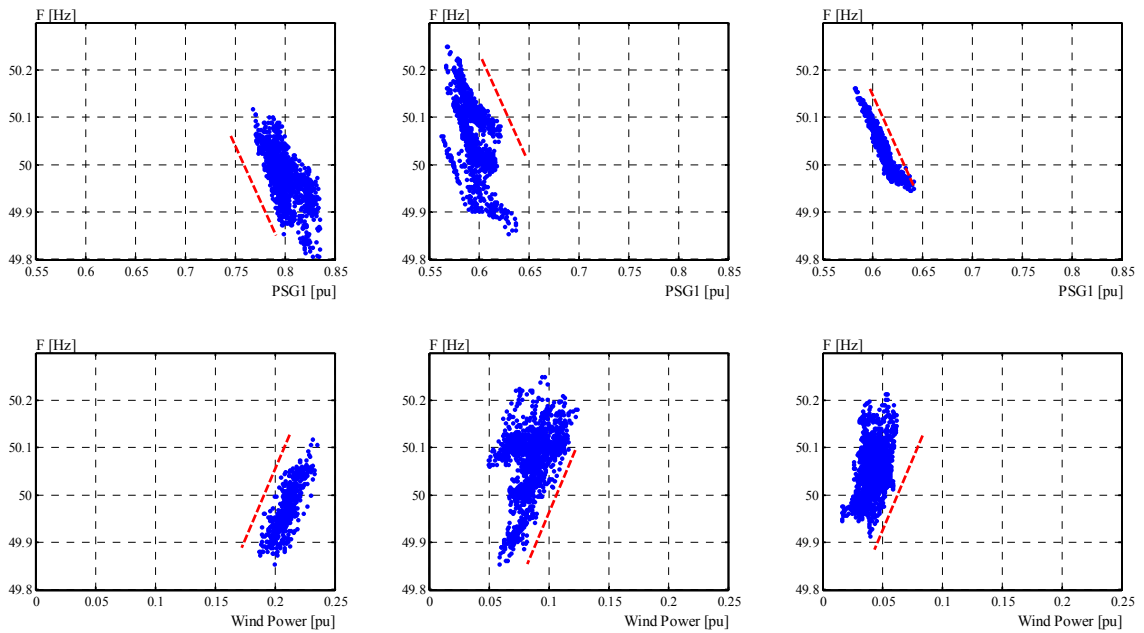
Figure 2-29: Measurements. Grid frequency vs. power output SG1 (top row) and grid frequency vs. wind power output (bottom row) for the wind penetration levels of 13.5 % (left column), 5.9 % (centre column) and 2.7 % (right column). Trend lines were manually placed for better indication.
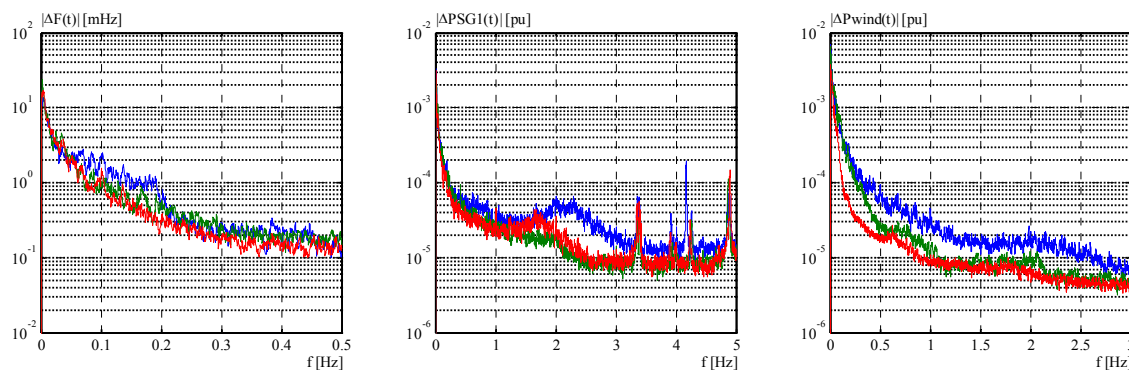
Figure 2-30: FFT spectra of grid frequency (right), SG1 output (centre) and wind power production (left) for the wind power penetration levels of 13.5 % (blue), 5.9 % (green) and 2.7 % (red). Blue is for Day 1 and green and red for Day 2.

2.5.5 Observations and characterization

2.5.5.1 System stiffness

The system stiffness K_{sys} was determined from the measurements during island operation. Neglecting the load-frequency dependency (being a small system and having small frequency deviations) the K_{sys} was determined by relating the grid frequency fluctuations and the SG1 power output for a time period where the grid operator did not modify the load reference of SG1, similarly to the data shown in **Figure 2-29**, top row. Therefore $K_{sys} \approx 0.4$ pu/Hz on SG1 rated power. From this, the system composite droop can be determined as $R_{sys} \approx 0.05$ pu.

In **Figure 2-29** it can be seen that the system stiffness during the measurements was not enough to absorb the wind power fluctuations. As the droop of SG1 was not possible to be changed (reduced), the feasible solution to reduce excessive frequency fluctuations was to start up more conventional generators to share the regulation burden therefore to increase the K_{sys}.

In [63] and [67] further studies were performed on this power system, with different R_{sys} provided by the other generators in the system and different levels of wind power penetration. These cited references show how the wind power penetration can be allowed in this power system by increasing the K_{sys} and what the impact in the conventional machines is.

2.5.5.2 Observed issues during island operation with wind

Some of the relevant observations on the system operation and behaviour, based on this field experience during island operation, are summarized below.

A- Limited regulation capacity: If the grid frequency should remain inside the range [49.9 - 50.1] Hz in continuous operation, according to the Nordic Grid Code [5], the maximum load imbalance that this system can absorb with SG1 as regulating

machine is about ±0.04 pu, considering that the frequency is initially at 50 Hz. Free wind power fluctuations can be ±0.05 pu for 13.5% penetration, as demonstrated in **Figure 2-29** bottom row. To increase the system stiffness in this case, more conventional generators with governors need to start up, which increases the operation cost. Observed maximum step change in consumption was no more than 0.012 pu.

B- Boiler low time constant: when regulating wind power fluctuations with SG1 and trying to follow with load set point adjustments, undesired boiler pressure fluctuations were generated. From the test experience it has been observed that grid power fluctuations of ±0.05 pu at ~0.0085 Hz may generate boiler pressure variations. Those are difficult to control due to the low time constant of the boiler system. Measured wind power fluctuations can be about the same frequency.

C- No AGC: the governor references are adjusted manually when the grid frequency mean value is normally beyond [49.9 – 50.1] Hz. During normal operation (no wind) and periods of maximum load gradient the governor adjustment is done approximately every 10 minutes. In summer season, load gradient can be about 0.005 pu/min, but some very short periods of 0.01pu/min has been observed. Thus normal island operation is smooth. If the wind conditions are good, wind turbines are constrained to approx. 0.25 pu (WTG based) to avoid introducing fluctuations. Free WPG demands more attention and activity from operator for adjusting governor references, besides introducing other operational issues. High activity in governor reference adjustment also affects boiler pressure.

D- Concentrated wind power production: controllable wind power is located practically in 2 points separated by a distance of approx. 18 km. One site has normally good wind conditions from the sea. The other site is more affected by land surroundings. Large wind power fluctuations can be expected from each site, which can be correlated or uncorrelated, depending on the wind direction.

E- Low system inertia: it is an inherent characteristic of the island. Short term-large grid frequency fluctuations have been observed when comparing island operation with interconnected operation, i.e. comparing the ROCOF of **Figure 2-20** with **Figure 2-23**. When introducing wind power during island operation, these short term frequency distortions are aggravated just a little, comparing **Figure 2-23** with **Figure 2-28**. Nevertheless in occasions of fast wind power changes the low inertia plays a fundamental stability role as the frequency variation is faster than SG1 steam turbine reaction.

It can be observed that the main issue in this system is not created by the amount of wind penetration level itself, but rather on the amount of *fluctuation* level, since this characteristic is interplaying with the regulation reserves. If the wind power fluctuations could be reduced just to an amount that does not create large frequency fluctuations, e.g. to a ±0.04 pu according to actual system capability, then wind power generation can be

allowed. One option to achieve this is by control actions on the wind plants production, aiming at reducing just the overall fluctuations at system level and allowing individual wind plants and turbines to generate as close to the optimal production as possible. Considering the **Figure 2-25**, the wind production would be allowed to fluctuate just between ~0.16 pu and ~0.2 pu. This obviously implicates a loss in wind energy compared to optimal production. But the other solution is to start up more conventional machines. If the power balance in the system is not sufficiently controlled, wind production cannot be allowed. If the wind power fluctuations at system level are constrained to a desired value, then different wind penetration levels could be achieved.

2.6 Requirements for wind power control

In Section 2.4 the present requirements from key grid codes for frequency control for wind power plants (and conventional plants) were described. Modern WPP are able to meet these requirements by implementing different control actions [62]. But these control actions are local (at single WPP) and limited to the actual grid codes.

The power balance in the system depends on the combination of the overall consumption and generation. To meet a suitable power balance with large amounts of wind power, a real time coordination[1] of the overall wind power production is necessary. Rather than implementing local (isolated) control functionalities on individual wind plants, these control functionalities can be moved up to the power system level in order to allow *multi plant* control architecture. Relevant information can be exchanged and the production of all wind plants can then be coordinated aiming at balancing the system, providing with coordinated regulation services and increasing the overall generation yield. This coordination should operate as an integrated part of the central control in the power system.

Measurements showed that additional requirements for the wind power production should be addressed, such as upward gradient limits, power output limitation, fast frequency response and fast dispatching of set-points. Recent works e.g. [46] provide an update on present wind power plants performance and identify the need of similar power quality requirements for system balance.

Thus, the following control requirements are *proposed* and *addressed* in this work:

- Constraint on the rate of change of wind power production at system level: Fast changes in wind power production at time scales less than 15 minutes are difficult to compensate by means of system secondary frequency control or market based control. During that period the only mechanism for power balance is normally pro-

---

[1] Coordination: To perform an action considering component characteristics and capabilities.

vided by governor's responses. Thus the rate of change of average wind power production *at system level* should not exceed a maximum in this period.

- Limitation on the amount of wind power fluctuations at system level: Large increase of WPG in the power system will displace conventional generation. With this, an increase in regulation capacity in MW/Hz provided from remaining conventional power plants becomes necessary. For both, compensating the displaced regulation services and for compensating the increase of power imbalances due to wind power fluctuations [63]. If the regulation margin in the power system is not enough (increasing operation costs) then wind power will need to limit its fluctuations to a given value and/or provide with regulation services.

- Power reserve and frequency response at system level: In order to maintain system security under generation or load loss, enough regulation capacity and spinning reserve need to be allocated. If remaining conventional plants are not able to provide more spinning reserve, then wind power should be able to contribute with reserves and respond for frequency deviations to high and low frequency events. Securing power reserve at system level permits individual WPP's or WTG's to fluctuate locally, taking advantage of the variability of power among wind plants.

- Inertial response: If synchronous machines are displaced by modern wind power generation, the inertia of the system is reduced. If excessive reduction of system inertia is experienced, the governor response of conventional prime movers may not be fast enough to keep the minimum allowed nadir upon large generation loss. Wind turbines can be programmed to provide with fast power support to stabilize the grid [60] [61]. But the limitations for this response and the combined action with the slower primary frequency response should be addressed.

A *multi plant* control architecture of wind power from a power system level may allow an increase of energy yield, as production from wind plants can be coordinated to meet the overall objectives. But some of these requirements may not be possible to be met from a power system control level due to the limitation in communication speeds and need for fast actuation, e.g. inertial response. A control system architecture needs to be elaborated. This control system should allow the implementation and coordination of specific functionalities to meet the requirements abovementioned. In the following chapters, the development of these functionalities is addressed.

2.7 Conclusions

In this chapter an overview of the main concepts regarding the classical mechanisms for frequency stability and control in power systems was carried out. Those mechanisms divide that process in several stages. Performed analysis of the dynamic performance of the average grid frequency has shown its strong dependence on the system inertia, the time constant of the prime movers and the amount of regulating capacity on-line (as primary frequency control).

The impact of wind power on power balance and frequency has been reviewed. Wind power generation can cause frequency fluctuations. The impact is most seen in the 15-minute balancing market for slower reserves. In some interconnected systems there is *still* room for regulation capacity, but this is limited in isolated systems. However, what is relevant for balancing the wind power is the collective behaviour of all wind power plants at system level. It was shown that the increase of wind power may produce a reduction in system inertia only if synchronous machines are disconnected and that the security of the grid under large load changes may be compromised. One solution to face this is to increase conventional regulation reserves. Other solutions need to be elaborated if want to avoid using conventional plants for dealing with these integration issues.

A grid code survey regarding actual requirements for wind power frequency response was carried out. Some grid codes require a variable characteristic for the frequency response of the wind plant, which depends on the available wind power, whereas other grid codes require a fixed characteristic similar to conventional plants.

Measurements in an isolated power system with large share of wind power generation were carried out as part of this work. Results have shown the impact in the grid frequency produced by high wind power penetration. The main issue observed in this system is the amount of wind power *fluctuation*, rather than the absolute power, since this characteristic is interplaying with the regulation reserves. The same data has been used in computational modelling for dynamic simulations with high wind power penetration and for controls development.

Wind power will have to assume responsibility in maintaining the system frequency stability. Modern wind turbines are indeed programmable power sources, and they present flexibility for very fast control of generated active and reactive powers, inside limits. Requirements for a *multi plant* wind power control architecture has been proposed here, which includes: i) constraint on the rate of change of wind power production at system level, ii) limitation on the amount of wind power fluctuations at system level, iii) power reserve and frequency response at system level and iv) inertial response for dynamic frequency support. Control system architecture needs to be elaborated, which allows the implementation and coordination of specific functionalities to meet these requirements. The development of these functionalities and architecture is addressed in the following chapters.

3
MODELLING FOR SIMULATIONS AND CONTROL

This chapter presents briefly the models used in this work. A description of the studies to perform and the requirements to models is done in first place. Depending on the analysis to carry out, different models were considered. The models used for power systems are: i) classical multimachine system with network, ii) classical lumped mass-prime mover-governor, iii) real islanded power system with large amount of wind power and iv) modified 9-bus power system which includes wind power generation. Additionally, a detailed model based around a particular manufacturer's wind turbine and a wind power plant lay out with individual wind turbines were developed in this work. The turbine's model includes detailed representation of the turbine's relevant components and control algorithms, allowing implementation of new control functionalities, such as inertial response and primary frequency control. The models of the wind turbine and the islanded power system were adjusted and verified against field measurements from the represented site. The wind power plant model is built with the modelled turbine, where the control system is also modelled and simulated realistic wind speeds are used with it. Only a brief description of it is presented.

3.1 Studies to perform

The type of studies performed in this work deal with active power imbalances in the power system and active power control of wind turbines and wind power plants. These power imbalances are produced from two different sources: i) wind power generation and ii) system load changes. Classical mechanisms for frequency stability and control in power systems, such as inertial response and primary frequency control, are involved. Additionally, the performance of control functionalities for wind power is analysed.

The studies to perform in this work are:
- Analysis of the speeds and inertial responses (powers) of synchronous machines in a multimachine system upon load change.
- Studies of the average performance of the system frequency upon load change, when varying different parameters of the system, such as inertia constant H, droop R, prime movers time constant T, etc.
- Study of the impact on drive train and tower of a WTG when performing synthetic inertial response.

- Study of the capability of VSWT for releasing kinetic energy, considering aero-dynamical power drops, shaft torque overloading, electrical power overloading, losses, rotational speed changes and control actions for curtailment.

- Implementation of new active power control algorithms in a standard WTG-DFIG control architecture, considering filtering, ramp rates, etc.

- Simulation of the operation of the WTG performing inertial response with constant and variable wind speeds, assuming a strong grid.

- Characterization of the wind power plant output when individual WTGs perform inertial response with variable (realistic) wind speeds.

- Impact of wind power generation in power systems with high wind power generation, including powers and frequency fluctuations. Several wind power plants should be represented, with independent wind speeds, power fluctuations and control systems.

- Impact on power system and synchronous machines when wind power plants perform frequency control and inertial response, including variable wind speeds and independent control systems. Synchronous machines should respond with primary and secondary frequency controls (PFC & SFC).

3.2 Requirements to models for simulations and control

The time scale of the dynamics involved in the type of events above mentioned ranges from tens of milliseconds to tens of minutes [43] [56] [58] [70] [71] [72]. For such time scale, fundamental frequency simulations (RMS) of electrical components are suitable. Dynamics of shorter time scales do not (practically) impact on the frequency stability mechanisms in the power system, therefore are not considered necessary to be "observed" in this work. Most of the dynamics inside the wind turbine that are interesting to observe in this work do not require simulations of shorter time scale either: E.g. current control loops in wind turbines are able to respond to set-point changes in the order of milliseconds, [77]-[81], therefore such dynamics do not impact in the grid frequency and are not necessary to be observed.

The modelling should be detailed enough to represent the impact of active power imbalances (and associated dynamics) on specific components in the power system in the time frame of 50 ms to 20 min. The main system components of interest are wind turbines, wind power plants and conventional power plants (with synchronous generators and governors). Therefore the modelling should represent the behaviour of wind turbines and conventional generation when having: i) wind power fluctuations caused by realistic wind speed fluctuations; ii) wind power output changes caused by active power control loop in wind turbines; iii) system load imbalances caused by sudden disconnection of generation or load. Moreover, the modelling should allow modifications to the wind turbine controllers in order to introduce new responses to such power imbalances.

Specifically, wind turbine model should represent:
- Components:
  - Rotor aerodynamics receiving wind speed input (among others).
  - Pitch actuation.
  - Drive train and tower (1st modes).
  - Generator RMS currents, voltages and torque. Can be merged with power electronic fundamentals.
- Controls:
  - P and Q control loops.
  - Speed control with limiters and nonlinearities.
  - P reference generator with limiters and nonlinearities. ($Q_{ref} = 0$)
  - Pitch control with limiters and nonlinearities.
  - Should receive external inputs such as power reference.
  - Should provide signal outputs to external controller, such as generated power, available wind power and signals indicating state machine.
  - Should permit introducing modifications in the P reference and control loop.
  - Should represent the delays and sampling times in the controller.

Wind power plant model should represent:
- Internal losses.
- Individual power production of wind turbines.
- Different (realistic) wind speed distribution among turbines.
- Realistic RMS voltages at each wind turbine.
- Realistic RMS voltages and currents at the PCC.

Power system model should represent:
- Conventional power plants active power response.
- Prime movers and governors (primary frequency control).
- Synchronous machines rotor oscillations.
- Grid frequency dynamics.
- Power balance impact.
- Simple loads.
- Wind power plants at transmission level.

During the simulations, conventional power plants are operated as: (i) Constant load reference, adjustable by the secondary frequency control when specified; (ii) governor response with no dead-band and (iii) governor response with large dead-band. Two simulation tools were used for the models building and simulations: (i) Matlab/Simulink and (ii) Power Factory DIgSILENT GmbH. Matlab was used for initial building and

development of models, controllers and algorithms for wind turbines and wind power plants, such as inertial response or frequency control. Power Factory was used later for RMS simulations of large electrical systems, containing wind power plants and conventional power plants with respective controllers. The developed *discrete* controllers in Matlab were later rebuilt in Power Factory, also discrete, in DSL language through dedicated functions especially developed.

3.3 Models used in this work

The models used for power systems are: i) classical multimachine system with network, ii) classical lumped mass-prime mover-governor, iii) real islanded power system with large amount of wind power and iv) modified 9-bus power system which includes wind power generation. Additionally, a detailed model based around a particular manufacturer's wind turbine and a wind power plant lay out with individual wind turbines were developed in this work. The turbine's model includes detailed representation of the turbine's relevant components and control algorithms, allowing implementation of new control functionalities. The wind power plant is built with the modelled turbine, where the control system is also modelled and simulated realistic wind speeds are used with it.

3.3.1 Classical power system

This representation was used for conceptual analysis of the speeds and inertial responses (powers) of synchronous machines in a multimachine power system when a load change is experienced [70] [71]. The application of detailed models for conceptual studies is difficult and many times unnecessary. Here the discussions are limited to the assumptions, yet, the observations are instructive and valid. The physical assumptions are:
- Negligible electromagnetic transients (RMS values).
- A small load change ΔP_L is applied at some bus L in the system.
- Load with negligible reactive component.
- Very high X/R ratio of the network with negligible conductances.
- Generators represented by the classical model of constant voltage behind transient reactance.

This model was used for analysis in Chapter 2. Complete description of this model is presented in Appendix A.1.

3.3.2 Simplified model for load-frequency response: PS1

This simple model (**Figure 3-1**) represents the collective performance of all generators in the system. Qualitative linear analysis of the mean frequency response and regulating characteristic of a power system due to a load change can be done with it [70]. In this work, this simple power system model is referred as PS1 and it was used for simulations and conceptual analysis in Chapter 2. Detailed description of this model can be found in Appendix A.3.
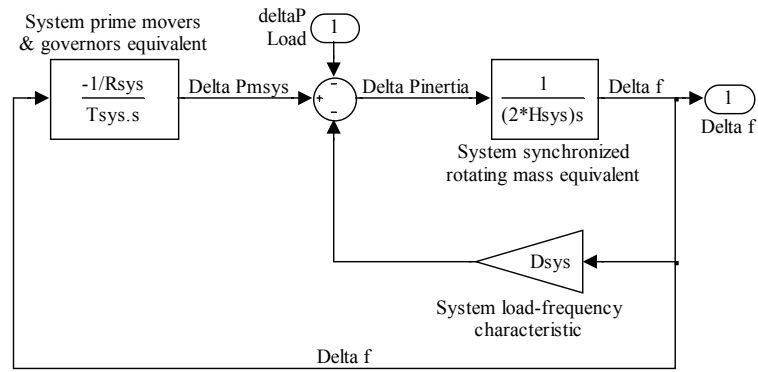
Figure 3-1: Power system linear equivalent for composite load-frequency response analysis.

Normalized Case

A normalized case was defined based on PS1, **Figure 3-2**, for carrying out general analysis of the mean grid frequency impact when varying different parameters of the model. By normalizing the variables, it is easier to observe the deviations from a known case when changes in parameters are performed. The analysis shows relevant impacts on the grid frequency performance. Detailed description of this case can be found in Appendix A.4.
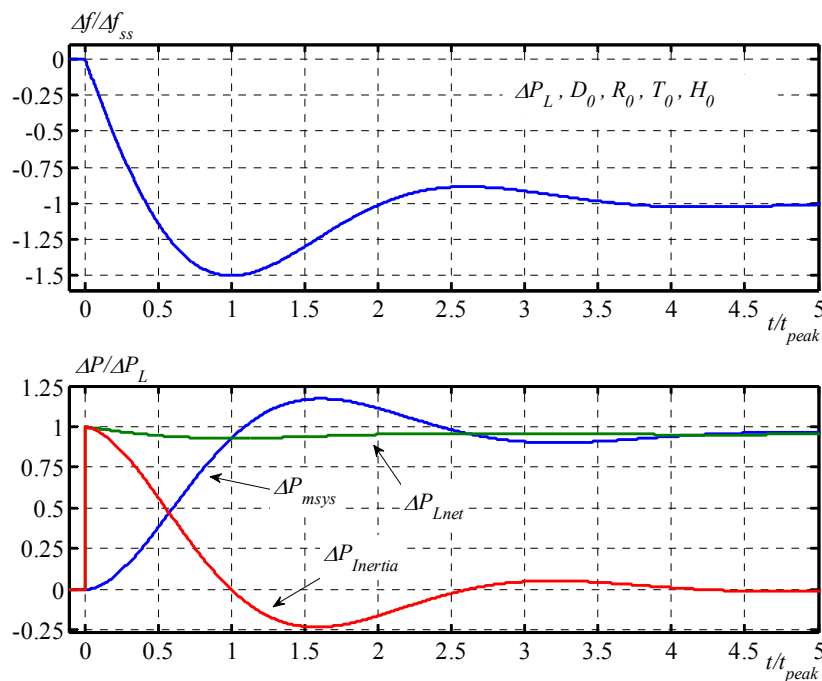

Figure 3-2: Normalized Case: composite system frequency response (Δf) and equivalent primary frequency control activation (ΔP_{msys}) due to a system load change (ΔP_L).

3.3.3 Islanded power system: PS2

This power system has been used for the control development and simulations in Chapter 5, and it is referred as PS2 in this work. It corresponds to the power system of the Danish island of Bornholm. **Figure 3-3** shows a simplified diagram of this system in islanding mode with the wind power plants. Each wind power plant is composed by three VSWT. More detailed description of this system can be found in Appendix A.5.
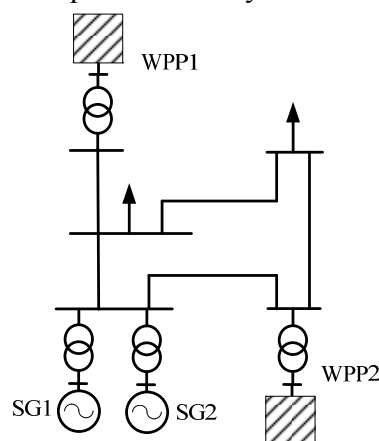

Figure 3-3: Simplified layout of Bornholm power system in island mode with wind power.

3.3.4 Modified nine-bus power system: PS3

This power system has been used for the performance simulations of coordinated frequency control in Chapter 6, and it is referred as PS3 in this work. It is a modification of the classical 9-bus power system model found in [71]. **Figure 3-4** shows the diagram of this power system with its synchronous machines, transmission lines and loads. More detailed description of this system can be found in Appendix A.6.
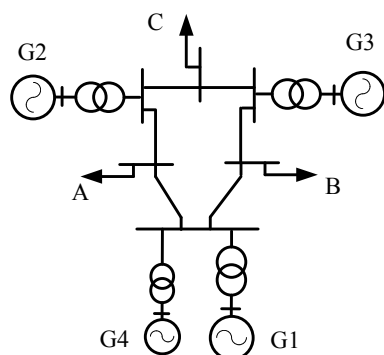

Figure 3-4: Modified nine-bus power system for load imbalances and wind power.

3.3.5 Wind turbine generator

The modelling of the wind turbine is based on a component approach, i.e. the modelling is built by representing the main components of the machine. No aggregated representa-

tion of the WTGs has been used in this work. This wind turbine is based on Doubly Fed Induction Generators technology (DFIG) [78] [80].

The main components modelled are:
- Rotor aerodynamics
- Drive train torsion 1st mode (two masses)
- Tower bending 1st mode (one mass), x & y directions
- DFIG
- Turbine transformer
- Power converters
- Converter controls
- Pitch actuator (same for the three blades)
- Main WTG control system

Figure 3-5 shows the VSWT model with all these components interacting. A complete description of the aerodynamical modelling used here can be found in Appendix B.1. Regarding the drive train and tower, a complete description of the respective modelling can be found in Appendix B.2. The modelling for DFIG is already known in the literature and it will not be described here. But description of inputs and outputs is provided when necessary. The reader can find details about DFIG modelling in e.g. [76]-[85]. In Power Factory, the DFIG was represented from the tool's library. The turbine transformer is represented in Power Factory from the tool's library as well. Regarding controls, in general, the control system of a wind turbine is divided in three main sets (**Figure 3-5**):

1- Generator and power converter controls, with inner (fast) currents control loops in the d-q axis and outer (slower) P and Q control loops.
2- Pitch angle control system, including pitch actuator.
3- Main controller, which determines mainly the references for P, Q and θ.

The power converters are modelled according to the respective simulation platform: i) in Simulink, the DC link was considered with constant voltage and the grid side converter was considered as current source, injecting the power generated/consumed in the rotor; ii) in Power Factory the DC link and grid side converter were modelled using the built in models from the tool. In both simulation tools, the rotor side converter together with current control (inner faster loop) and power controls (outer slower loop) were modelled following the basic structure shown in **Figure 3-6**. The pitch actuator also includes the pitch controller, which receives the reference θ_{ref} from the main controller.

The main controller is the "brain" of the WTG, and generates references $P_{conv-ref}$, Q_{ref} and θ_{ref} based on sensors inputs and specific algorithms. These algorithms are not described in this work. The main controller is modelled as a "digital" device, that is, with a computation cycle of $T_{sWTG} = 100ms$. This means that the outputs of the main controller occur after 100 ms of the inputs. Modern wind turbines can have faster computation

cycles for the main controller, but this value was chosen here as suitable for the studies. The main controller receives the external set point, $P_{ext-ref}$, from the operator or from the WPPC. It sends signals back to the WPPC such as actual production, available power, etc. (indicated in **Figure 3-5**). A power ramp rate limiter for external set points to the turbine, $P_{ext-ref}$ (or $P_{demandWTG}$), is located inside the main controller. This ramp limiter reduces the bandwidth of the WPPC for fast changes in turbine set point. In this work the focus is done in active power control. The reactive power is kept at fixed reference ($Q_{ref} = 0$). If the external power reference is larger than the power available from the wind, then the WTG will generate just what is possible, i.e. will generate optimal power given by P_{opt}. **Figure 3-7** shows a simplification of this power reference selector for the power converter including the ramp rate limiter. Notice that the converter receives a new set point, $P_{conv-ref}$, with a 100 ms period. The curtailed (deloaded) production is obtained by setting an external set point $P_{ext-ref}$ below available power. The rotational speed is limited by the pitch actuator.

Figure 3-8 and **Figure 3-9** show the characteristics of normal operation of the modelled turbine. Each point in the curves represents a steady state operation following the optimal production (no curtailment) for different wind speeds. **Table 3-1** presents the characteristic values for the points shown in the **Figure 3-8**.
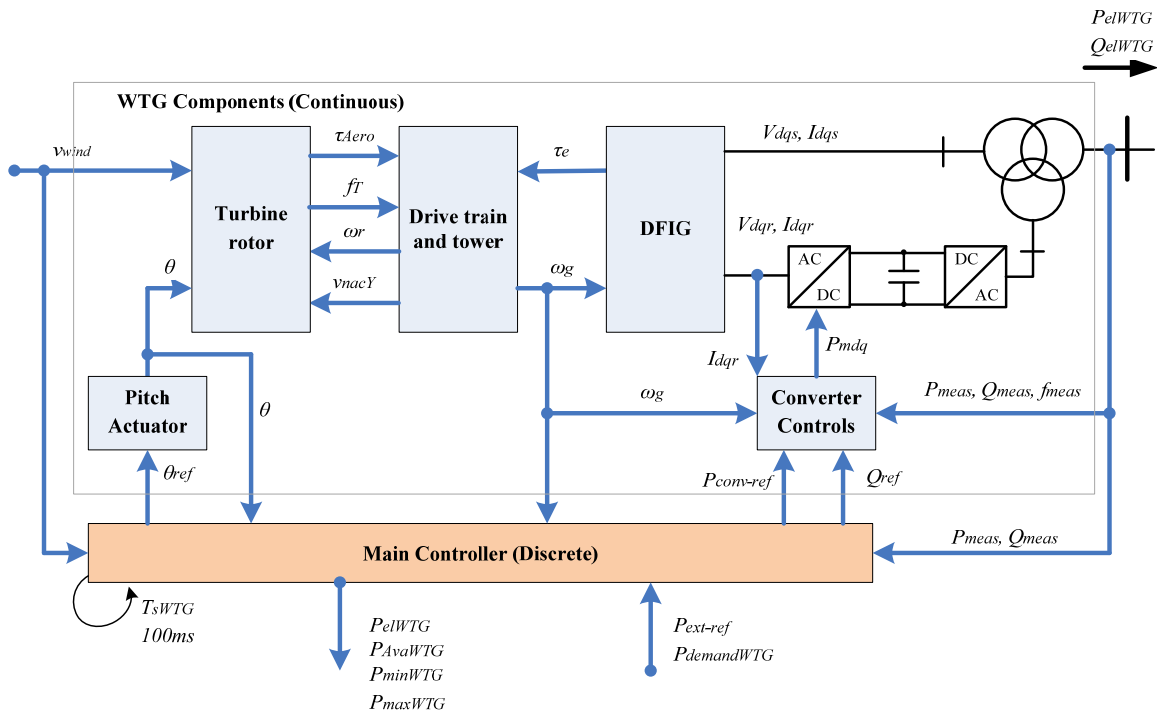
Figure 3-5: Simplified model structure of the WTG: components, controls, signals and electrical connections.
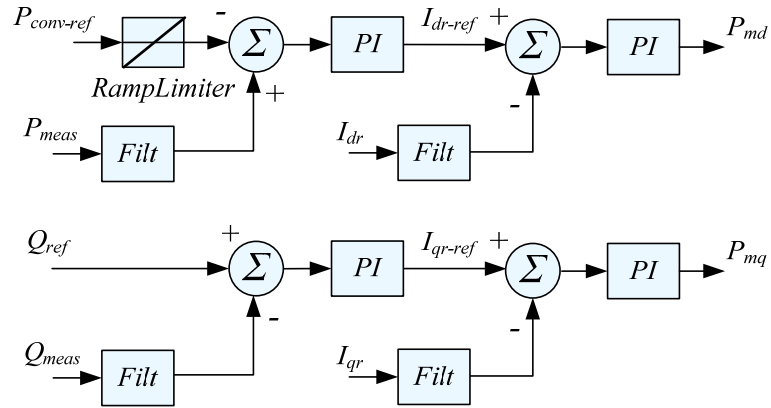
Figure 3-6: Simplified diagram of the modelled powers and currents controls in WTG.
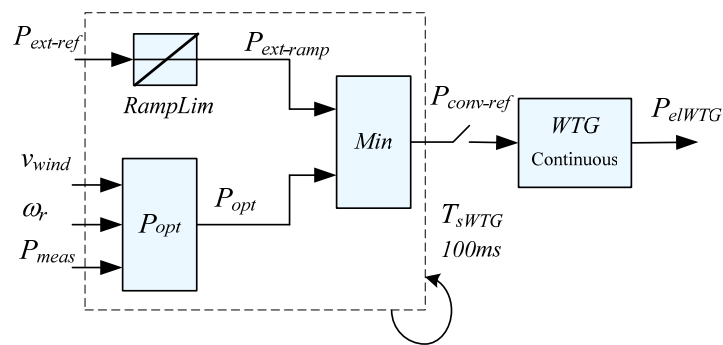
Figure 3-7: Simplified diagram of the power reference signals selector in the WTG.

Table 3-1: Characteristic values of the modelled wind turbine's operational points

Point in Figure 3-8	V_w [p.u.]	P_{WTG} [p.u.]	ω_r [p.u.]
1	0.3	0.025	0.6
2	0.4	0.07	0.6
3	0.66	0.33	1
4	1	1	1
5	2	1	1

Figure 3-8: Characteristics for normal operation for the modelled turbine WTG1.

Figure 3-9: Aerodynamic power vs. rotational speed for several wind speeds. The blue line is the WTG normal operation curve.

3.3.6 Wind power plants

The modelled Wind Power Plant (WPP) (or wind farm) represents an offshore plant. It was modelled as a complete set, including individual wind turbines with its transformers, cables, feeders and main transformer. Protection system was not modelled. It was implemented in Power Factory as shown in **Figure 3-10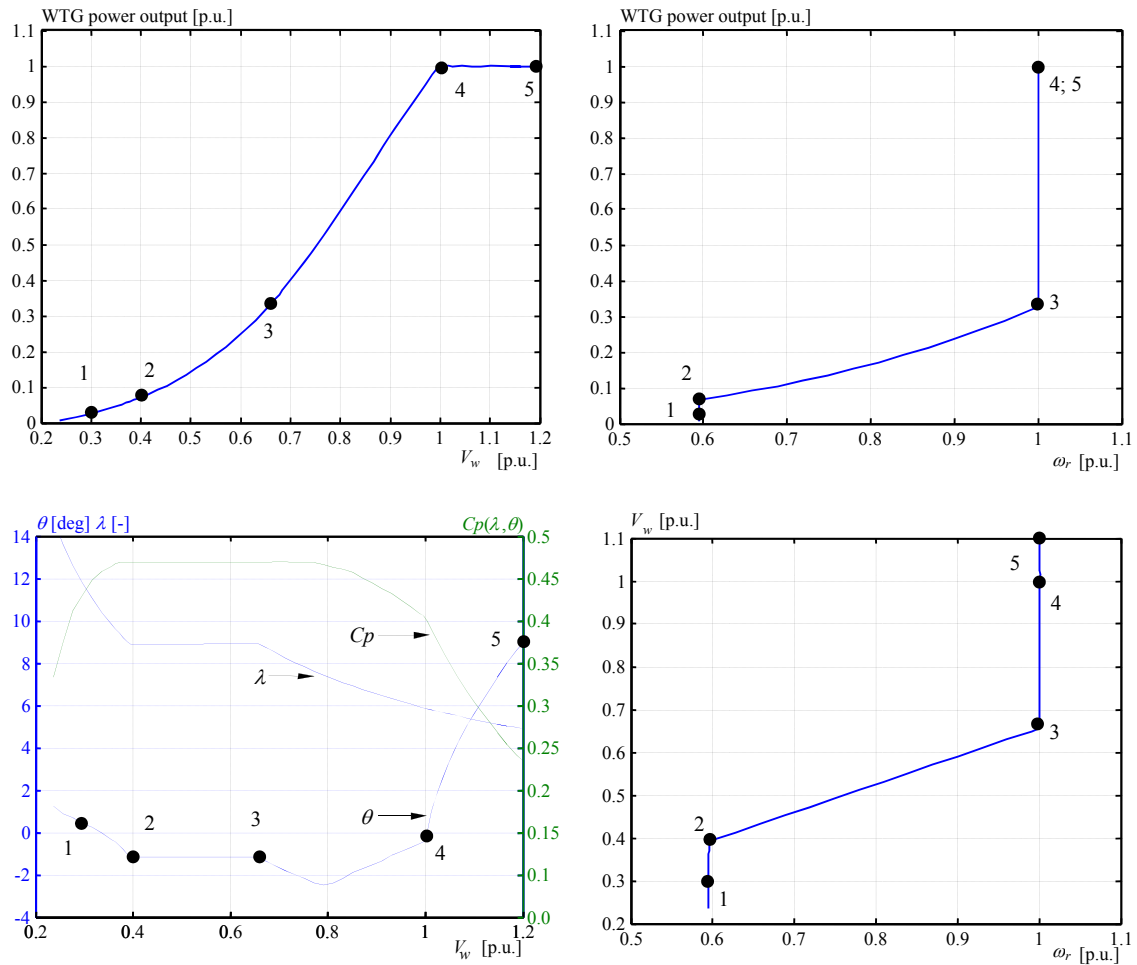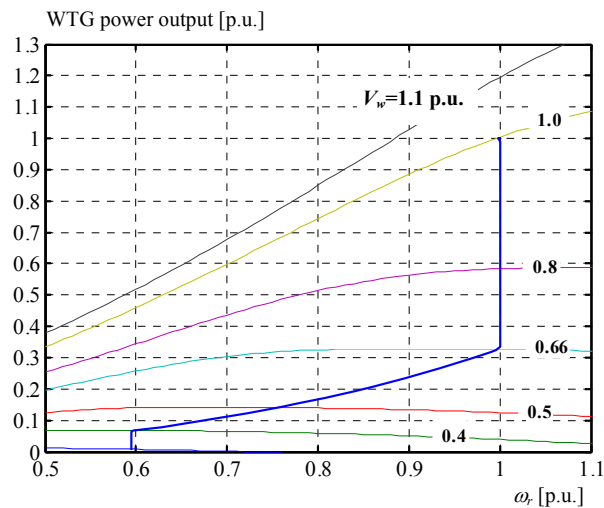**. Twenty five VSWT of 2MW are connected in a symmetrical arrangement giving a total capacity of 50 MW. Distance between turbines is ~560 m. The cables in the WPP are selected in order to obtain a nominal loss of 2% of rated power. With this, the voltage profile remains inside nominal range (±5%). The WTG's are modelled in Power Factory as described in the previous section.

The model of the WPP should provide not only the overall waveform of the injected power into the grid, but also the behaviour of individual wind turbines inside the plant, in order to: i) observe the turbines' performance during the inertial response and ii) be able to implement control strategies for the wind turbines and internal dispatching of set points. The internal distribution of the generated powers in the WPP is mainly influenced by the wake effect characteristic [89]-[93]. To consider the wake effect in a WPP, detailed modelling and computer processing is necessary. In this work, a detailed modelling of wake effect was *not* implemented. But, in order to be closer to a realistic wind distribution, a simplified approach was applied. A description of this approach can be found in Appendix B.3. **Figure 3-11** shows an example of the generated wind speed for one row in the WPP. Besides internal representation of winds, the WPP model should also represent the internal voltage drops and phase angle shifts in order to consider the electrical behaviour and control performance during inertial response.
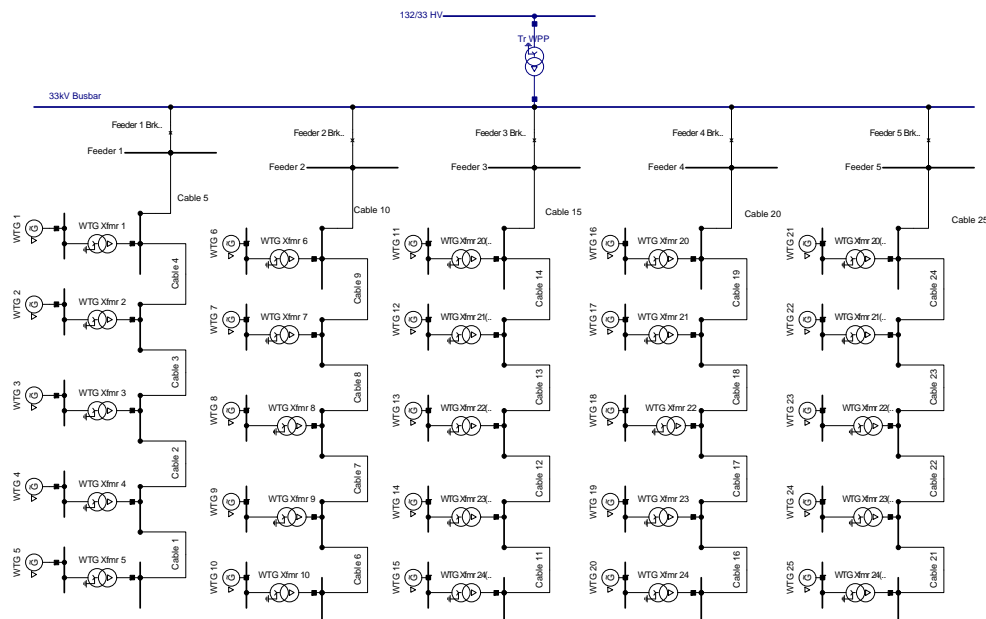

Figure 3-10: Wind power plant lay out. Implementation in Power Factory.
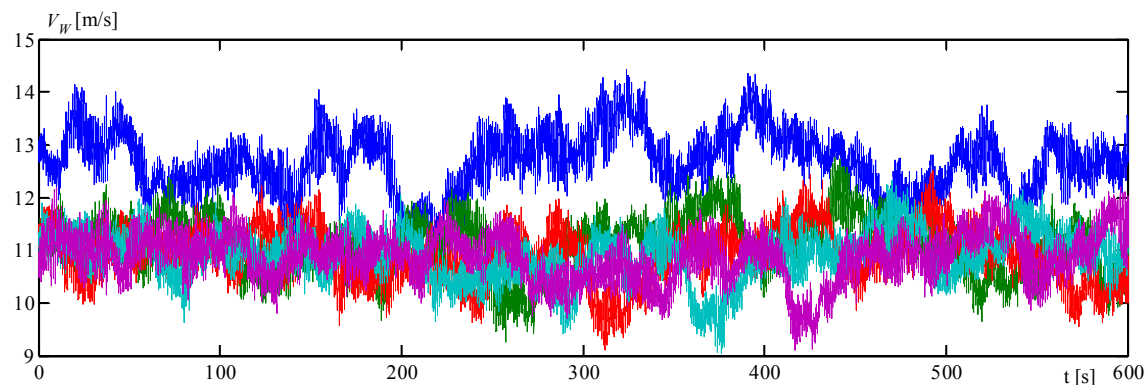
Figure 3-11: Generated wind speed for one row of the modelled WPP. Note the higher values for the first turbine in the row (blue).

Figure 3-12 shows the communication system of the different controllers involved in this study. The wind power plant controller (WPPC) is in charge of controlling the power output, P_{elWPP}, as close to the reference, $P_{demandWPP}$, as possible (other variables are controlled at the same time but not considered in this work). The WPPC sends set points $P_{demandWTG}$ to the WTGs and receives other variables (status) from them (shown in this figure but also in **Figure 3-5**). As the WPPC is a digital device, it was modelled with a computation cycle of T_{sWPP} = 100 ms, similar to the WTG. In this computation cycle, the measurement sampling and communication delays are merged. The functionalities inside the WPPC are studied in Chapter 5, and their execution time is T_{sWPP}.

The WPPC also communicates upstream with a central controller at power system level, WPSC, for multi plant control which is studied in Chapter 5. Here, this controller sends set points to the WPPs downstream and receives feedback from each WPP, as shown in the figure. The WPSC is also modelled with a computation cycle of T_{sWPSC} = 100 ms. By using the same computation period among controllers, it facilitates the analysis for different configurations.

In the previous section it was shown that the WTG has a power ramp rate limiter for the reference received from the WPPC. Thus, does not matter how fast the WPPC is, the WTG will follow the reference with that ramp rate limitation, or it will generate optimal power if the external reference is too high. Normally, in order to eliminate the error in the WPP output, a controller with integrator is placed in the WPPC, e.g. a PI controller (this is discussed in Chapter 5). This PI controller use to have a ramp rate limiter in the integrator too, to coordinate with the WTG limiters and avoid windup.
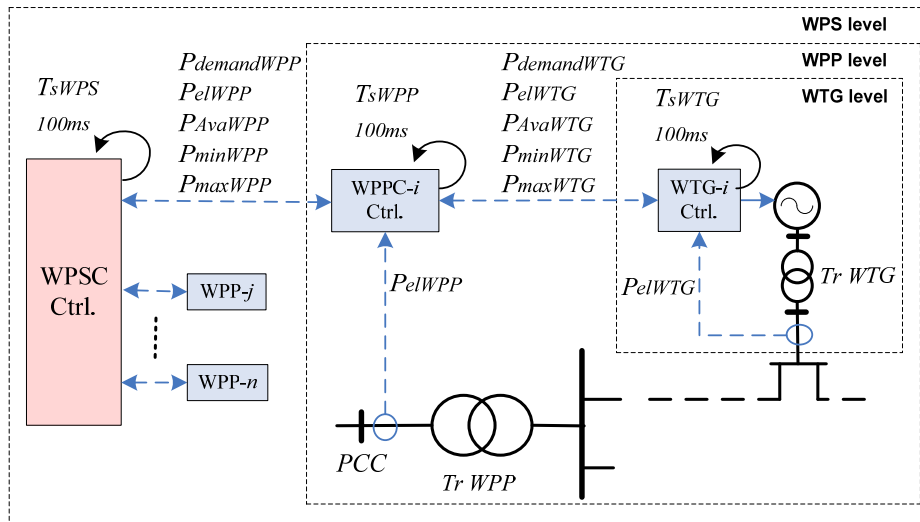
Figure 3-12: Block diagram showing measurements and communications at the different levels in the wind power system control architecture (WTG, WPP and WPGS)

3.4 Verification and applicability of the models

The models of the wind turbine WTG1 and the power system PS2 were verified and adjusted against measurements of the respective real system. Selected measured cases with high wind power penetration were reproduced by computational simulations. The simulation results were compared with the measurements, showing a good agreement in all cases.

3.4.1 Power system PS2 model verification
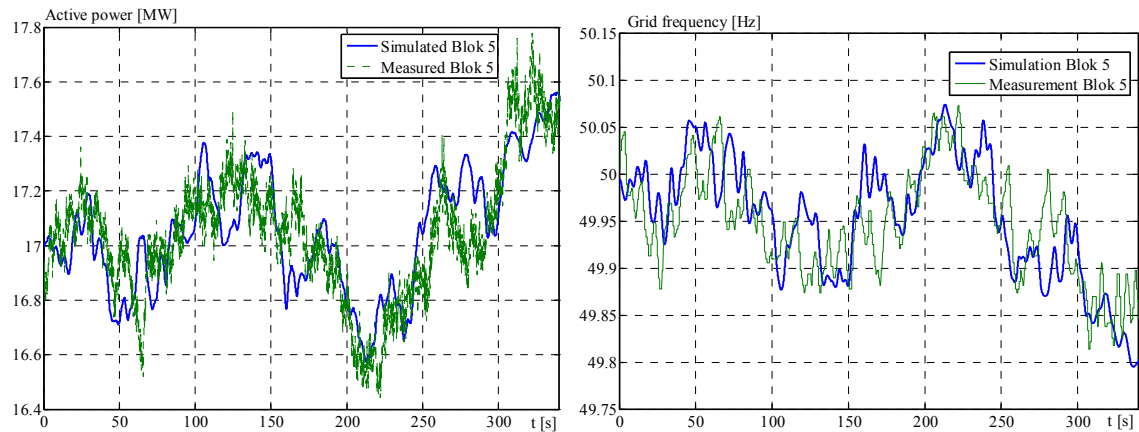
Figure 3-13: Comparison of measured and simulated power output and speed of SG1 in the SP2 system (Island operation, Bornholm 17th Aug. 2009, sample record from 11:50 to 11:56)

3.4.2 Wind turbine model verification
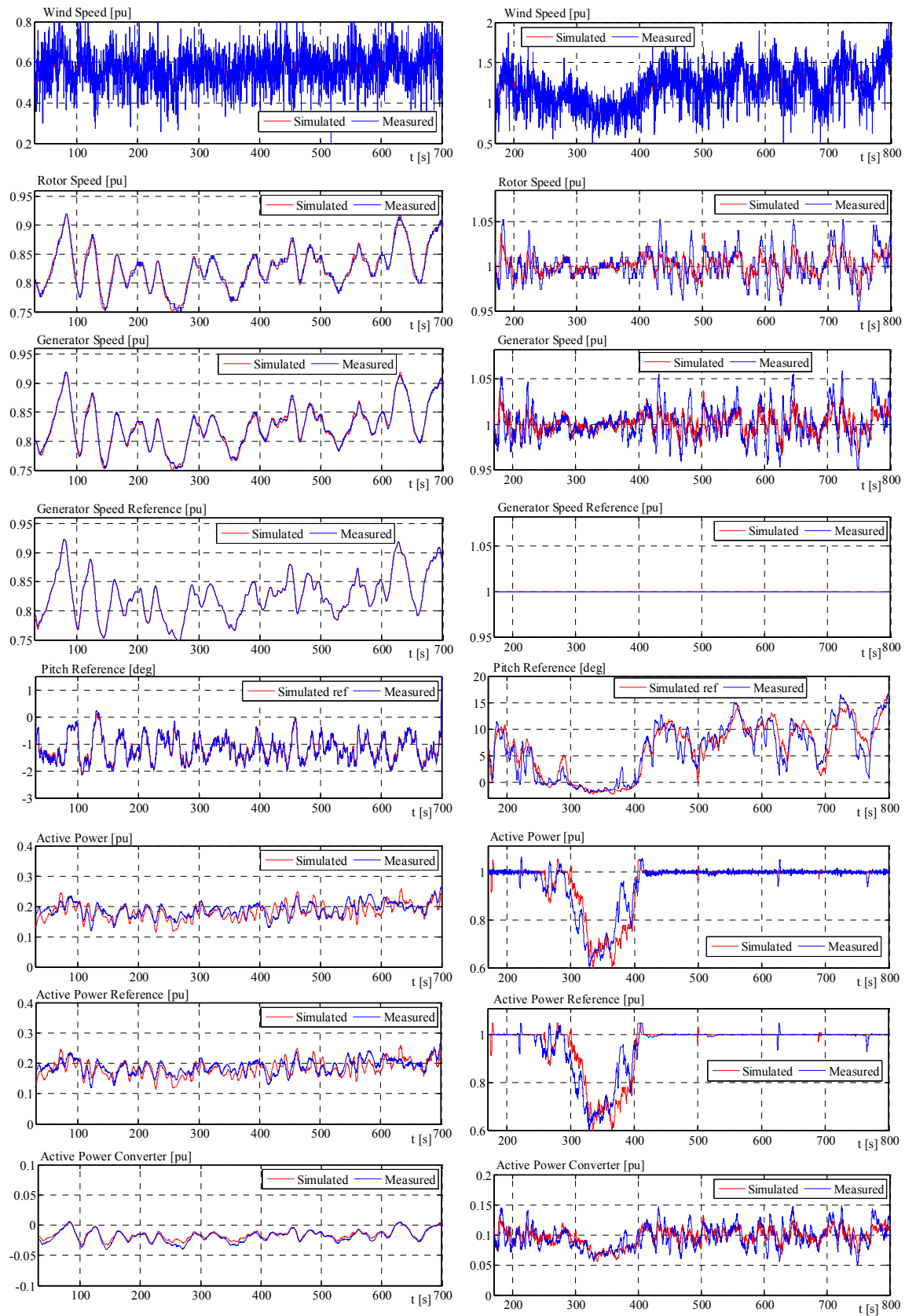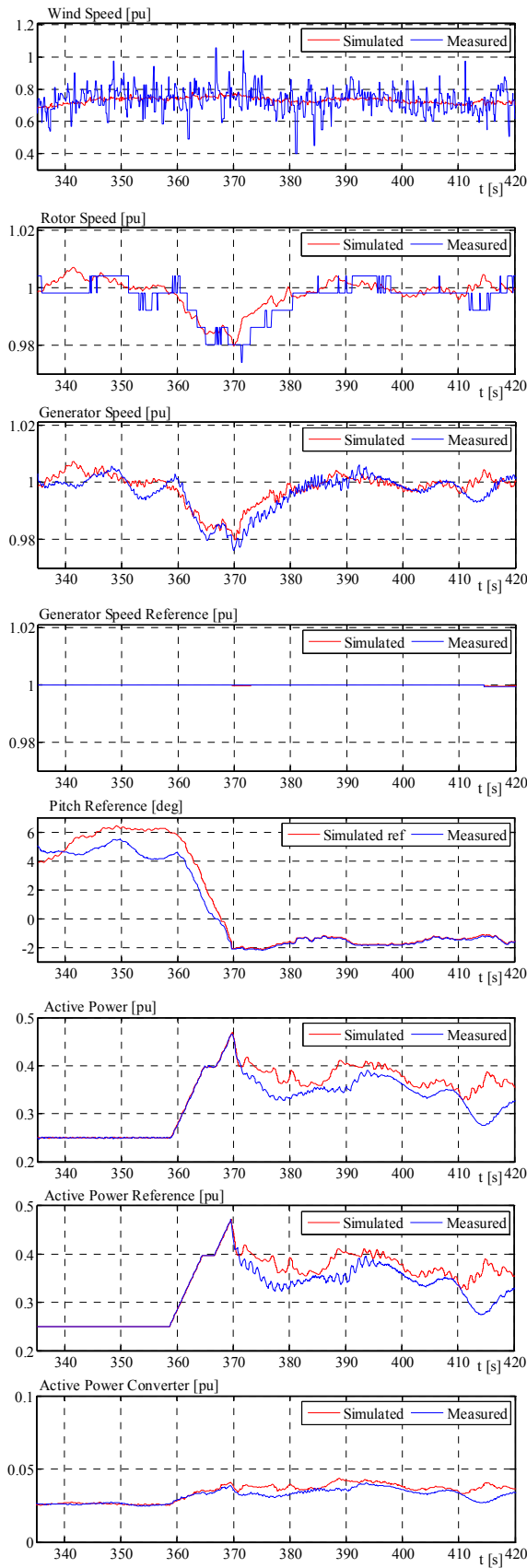
Figure 3-14: Comparison of measured with simulated values of wind turbine operation. The only inputs to the model were the measured wind speed and the power reference setpoint. Measured wind speed was taken from the wind turbine anemometer while operating the turbine and recording the main variables. This wind speed is from one single measurement point, however it can be noticed that it produces a very good matching by using it with the model.

Left-left: Low wind speed measured & simulated case

Left-middle: High wind speed measured & simulated case

Left-right: Power reference ramp up measured & simulated case.

3.4.3 Base case

Below, an application case of the two verified models is shown. It is a base case from the system PS2. It was simulated by using real wind speed, measured in the system. This base case is used in Chapter 5 for performance verification of developed controls. Compare with measurements in Section 2.5.4.3 to observe similar system performance.
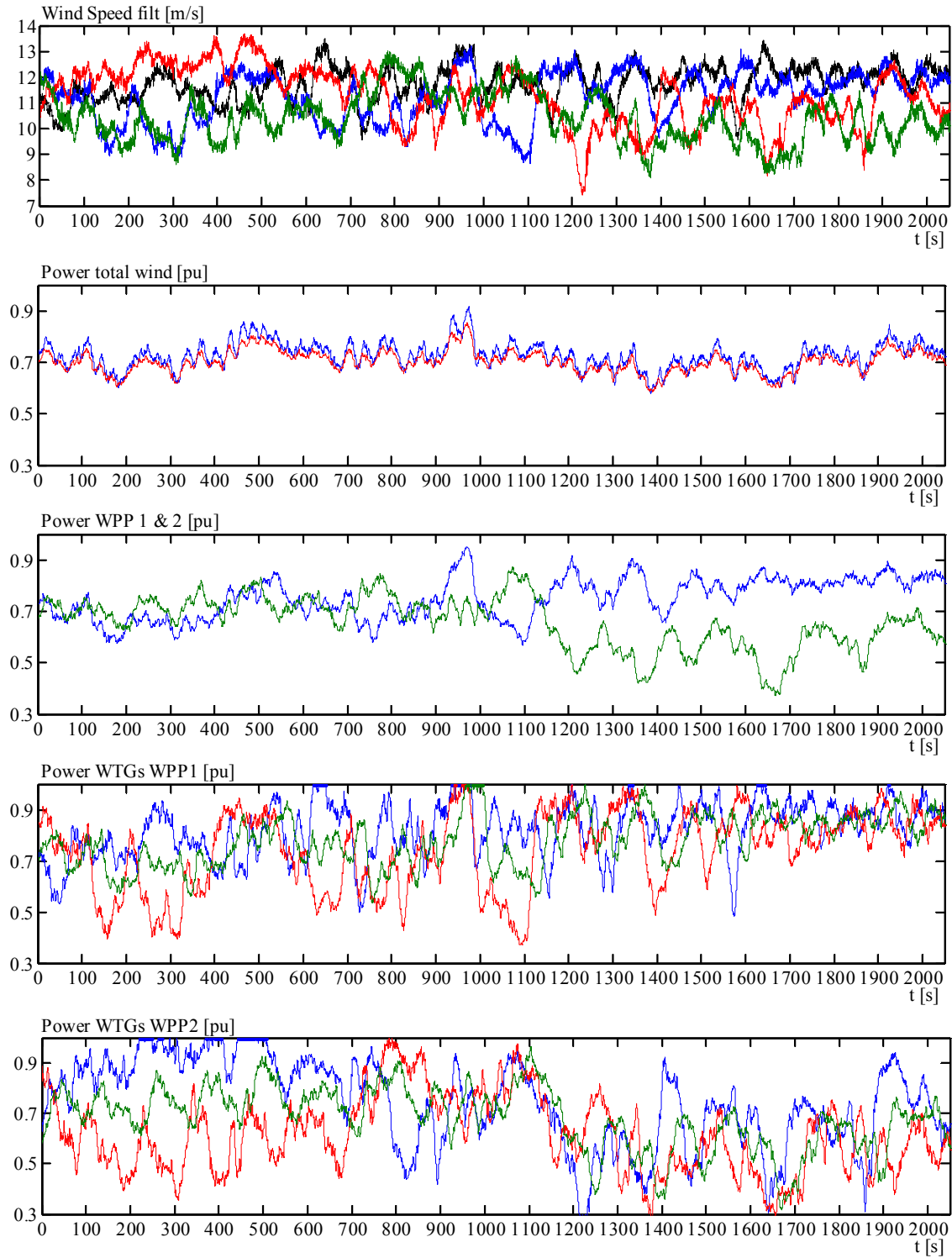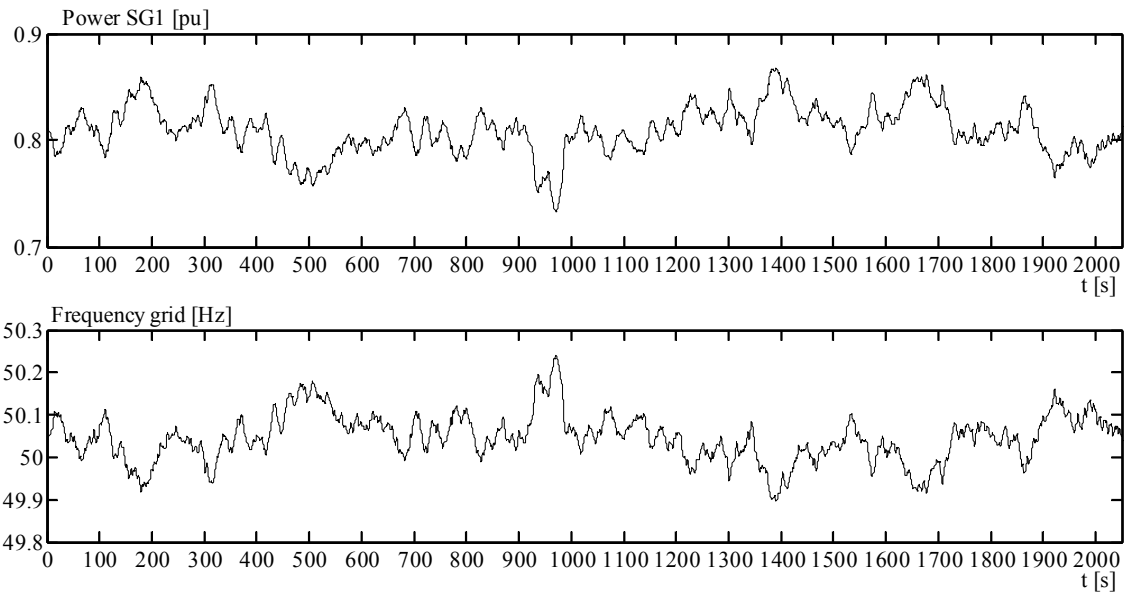
Figure 3-15: Base Case PS2 system with high wind power penetration.

3.5 Conclusions

In this chapter the different models used along this work were presented. The classical power system modelling with synchronous machines and network was used for conceptual analysis of generator's load impact and individual inertial responses under grid load changes. The simplified lumped mass-governor power system model was used for analysis of average grid frequency dynamics. The particular model of a real islanded power system with large amounts of installed wind capacity was used for analysis of wind power impact on system balance and for development of the wind power frequency control algorithms in this work. A modified 9-bus power system model was used for testing the developed control algorithms aiming at a larger scale system scenario with wind power. A turbine simulation model was developed, based around a particular manufacturer's turbine. This model includes detailed representation of the turbine's components and the original control algorithms. This model is suitable for introducing modifications to the original control structure in order to simulate the response with the new algorithms developed in this work. A wind power plant model based on individual wind turbines was developed. This model provides not only the overall waveform of the injected power into the grid, but also the behaviour of individual wind turbines inside the plant, in order to: i) observe the turbines' performance during the inertial response and ii) be able to implement control strategies for the wind turbines and internal dispatching of set points. The models of the wind turbine and the islanded power system were adjusted and verified against field measurements from the original site.

4
INERTIAL RESPONSE CONTROL

This chapter is dedicated to the study and development of inertial response control for wind turbines. Modern variable speed wind turbines can be considered as programmable power sources, with flexibility for very fast control of generated active and reactive powers inside design and operational limits. It is therefore possible to generate a stabilizing power from wind turbines following a large power imbalance in the grid, in order to provide a temporary support for the grid frequency stability.

The capability of variable speed wind turbines for inertial response is firstly analysed. This analysis covers issues such as measurement and detection of grid events; drive train and tower impact upon fast and large torque increase; amount of extra energy that can be obtained from a single turbine and injected into the grid; recovery period and power drop. It is found that this capability is strongly dependent on the wind and aerodynamical efficiency, which introduces an important limitation for the implementation of this functionality in wind turbines.

A control algorithm for wind turbine inertial response is developed. This control algorithm takes into account, not only the characteristics of the grid event for generating a suitable power waveform, but also the analysed capability of the wind turbine for delivering extra energy. The impact on the power drop and time during the recovery period as well as protection mechanisms for the wind turbine are considered.

The performance of the developed control algorithm is verified through simulations of a single wind turbine with several constant wind speed conditions and three representative grid frequency events. The simulation were repeated using real wind speed measurements obtained from a wind turbine equal to the modelled one, but operating in normal conditions. These simulation results are compared with the respective measurements from the turbine to observe how would be the behaviour change in the real turbine.

Finally, the capability of wind power plants (wind farms) for providing inertial response is assessed for the same grid events and different realistic wind speed scenarios. This analysis is important, as the contribution of inertial response from wind power cannot be assessed by just considering a single turbine. Simulated realistic wind speeds are utilised with the individual wind turbines in the modelled wind power plant.

4.1 Introduction

The reliability of the power system is based upon properties of synchronous machines in power plants. After stabilization of electromagnetic transients following a large power imbalance in the grid, the rate of change of the grid frequency is dependent on the total rotating inertia in the power system (Section 2.1.1). Such a grid disturbance can be mainly caused by load change, generation change or large changes in the grid power flow. Following this event, a dynamic grid frequency variation is experienced all over the system until it is stabilized, normally by action of governor system in conventional plants [56] [58].

The larger the total system rotating inertia, the slower the rate of change of frequency is. Hence, governor control in conventional power plants has time to react supplying the deficit in power, maintaining the frequency stability and power balance.

In modern variable-speed wind turbines, its rotational speed is normally decoupled from the grid frequency by the power electronic converter configuration. Therefore variations in grid frequency do –per default –not alter the turbine output power. With high wind power penetration there is a risk that the power system inertial effect decreases, thus aggravating the grid frequency stability under such events, as discussed in Section 2.3.2.

Grid codes add more requirements to wind power connections as they grow [6]. Requirements that tend to compensate the lack of inherent response to system events, which is a normal behaviour of synchronous machines. One of the more important and popular requirements for wind turbines is the Low Voltage Ride Through (LVRT) capability, which is the ability to remain connected to the grid and contribute with reactive current during severe low voltage events (such as short circuits) [15]. Following the same philosophy, it may be desirable that wind power offers a capability to contribute stabilizing the grid during the first stage of large active power imbalances, referred as Inertial Response (**IR**).

It is estimated that few, if any, power systems "today" with recognizable amounts of wind power installed have reached operational conditions where the inertial response potentially available from wind turbines is really needed. The actual wind power penetration in the vast majority of power systems, in despite of growing fast, has not created inertial effect problems because of the presence of large number of thermal and hydro power plants and interconnections with other power systems. Future grid codes may well include wind power inertial response requirements, and such functionality is possible for WPP solutions. Grid codes are still to quantify requirements to wind turbine inertial response.

Already today, WPP are provided with primary frequency response functionality, which decreases WPP output upon detected frequency increases. If WPP should increase its output upon frequency reductions, then there must be additional power available. This has so far only been achievable by operating the WPP curtailed (deloaded), and then releasing the withheld power when called upon. In contrast, by using the IR functionality for providing a stabilizing power for a relatively short period of time, the source of extra energy can involve the rotating masses of the rotor and drive train systems. But IR operation also implies that any power boost must be followed by a recovery period, i.e. a drop in power output from pre-event value.

The motivations for IR functionality are: i) *to reduce the lost energy*, which otherwise would have to be assumed if running the WPP constantly curtailed for power reserve and ii) *to provide a faster power response* for grid stability than the slower primary frequency response.

Figure 4-1 left shows a simplified block diagram of wind power inertia response functionality and at the right, simulation results of a wind turbine providing inertia response. At the first power swing the wind turbine is delivering a controlled power boosting to the grid while temporary supporting the power system and damping the system frequency change. Following, a recovery period with a power drop is experienced.

This chapter addresses the study, control development and performance of IR functionality in wind power plants.
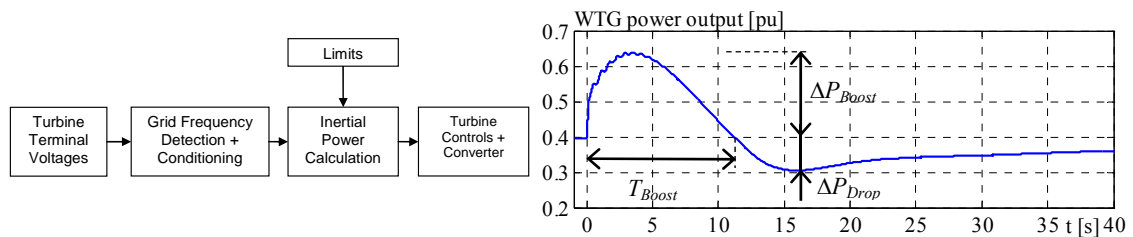
Figure 4-1: Simplified block diagram and waveform of wind turbine IR functionality

4.2 Capability of wind turbine generators for inertial response

In order to design a suitable IR control, first *it is necessary to know the capabilities* of a single wind turbine for providing power from stored kinetic energy. Issues such as grid event detection, drive train and tower impact, released amount of extra energy, power drop and recovery period impact need to be addressed. This is done in this section. Many variables are involved when investigating the capabilities for power boosting. The main are:

- Actual wind speed
- Power boosting magnitude

- Delivered energy
- Power drop during recovery period
- Turbine speed variation
- Pre-event curtailment
- Power overloading
- Torque overloading
- Speed acceleration during recovery period

4.2.1 Detection and actuation

Modern wind turbines are machines that perform different control actions while generating electricity from the wind. They are normally controlled by advanced and dedicated programmable logic controllers (PLC) which are digital devices that read the inputs, perform calculations and write the outputs to the actuators, with a specified sampling time. That is, the WTG's control is discrete. Some vital control actions in WTG's are uninterruptible e.g. generator currents control or blades angular position, whereas some others control actions can be enabled/disabled, e.g. *V/Q/cos φ* control from operator command or automatic frequency control activation beyond a threshold, etc., or can be interrupted in special situations by other functionalities, e.g. low voltage ride through (LVRT).

In the case of IR functionality, the control action is not developed here as a continuous control. That is, the WTG is not constantly manipulating its power output according to the grid condition for its stability. Instead, it will only actuate when it is necessary for the grid and, at the same time, the WTG conditions are suitable for enabling the inertial response action. The grid is constantly monitored but the *actuation* is upon grid event *detection*.

Two main questions arise at this point: i) what is a grid event? And ii) how to detect it?

Many publications about wind turbines inertial response try to simulate the behaviour of the WTG or the benefits for the system by doing a kind of inertial response action, e.g. [21]-[28], but very few publications that study the grid event detection or proposes a methodology for doing that were found, e.g. [24] [26]. Yet, they do not approach the issue with the necessary practical overview, which is important for assessing the viability of the methodology.

As discussed in Chapter 2, a grid event that involves inertial response from synchronous machines basically is when a power imbalance in the grid (ΔP_L), as described by (**2.20**), is produced. Relatively small imbalances in the grid occur all the time, thus inertial response from synchronous machines exists *all the time*, keeping the power system stable by absorbing or releasing that inertial power. As discussed in Chapter 2, it is important

to have it clear that changes in grid frequency occur *all the time* according to consumption changes and shifting of generation schedules. Power systems based on synchronous machines work in this way and it is normal. A measurement example characterizing the normal system frequency behaviour is shown in **Figure 2-19**.

The issue arises when the grid frequency tends to go *beyond* normal limits. Those limits are: i) absolute value and ii) rate of change [47] [58]. Considering this, in this work a grid event demanding inertial response from wind turbines exists when there is an active load change in the grid that can compromise these two frequency limits. If the system imbalance is small, then there is no need for activation of the IR functionality.

Regarding detection of the system load imbalance, several ways of doing it can be imagined. Two of them are:

1- Measuring the actual grid frequency f and use this value for suitable calculations and comparisons [24], such as calculation of rate of change, $\Delta f/\Delta t$, or comparison with thresholds. The larger the $\Delta f/\Delta t$ value, the larger the grid load imbalance is.

2- Measuring the voltage angle change and compare it with an internal voltage based on a synthetic reference frame [65]. The larger the voltage angle change, the larger the grid load imbalance is.

In this work, the first methodology is adopted, i.e. the grid frequency is measured as accurate as possible and used for suitable calculations (as described in Section 4.3.4).

The most common methodology for measuring frequency in a three phase voltages system is by means of a phase-locked loop (PLL). Several types of PLL can be found in the literature [122] [123]. In this work a 2nd order PLL is adopted for carrying out the grid frequency observations. **Figure 4-2** shows its block structure.
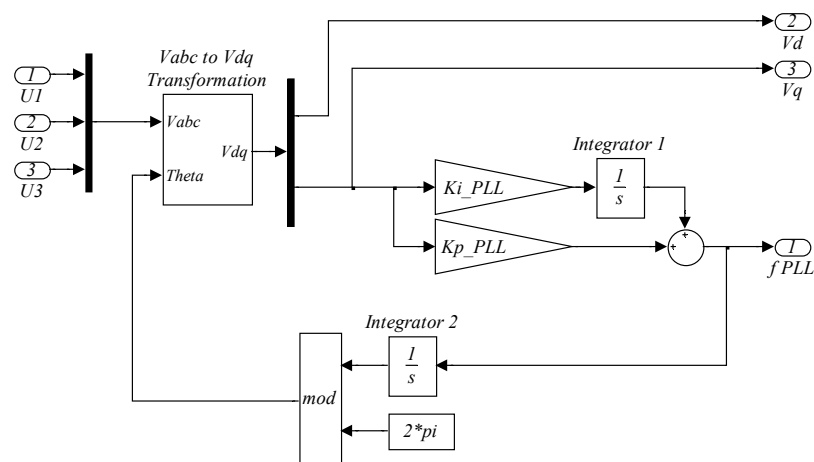

Figure 4-2: PLL block structure

The performance of the PLL should be such that accurate value of grid frequency f_{PLL} should be provided with proper timing (for large system events, there would be initial transients in the PLL output that may not be an information about the system, but proper of the PLL performance). As discussed in Section 2.6, large power systems do not require an instantaneous (sharp) inertial response from wind turbines, but rather a *waiting time* before initial response of conventional governors. Therefore the requirements for this PLL performance are not as demanding as for PLL dedicated to power electronics currents control [122]. **Table 4-1** presents the chosen PLL parameters for IR functionality. The observed grid frequency f_{PLL} is used in the IR algorithm as described in Section 4.3.4.

Table 4-1: PLL chosen parameters for IR functionality

Gain	Value
K_{p_PLL}	450 rad/s/pu
K_{i_PLL}	2226 rad/s^2/pu

4.2.2 Drive train & tower

It is important to know if wind turbine components are subjected to abnormal stress when a particular IR methodology is implemented. The detailed study of those components under such operating conditions is out of scope of this work. Nevertheless, it is possible to observe some of the main variables based on the modelling presented in Section 3.3.5, for having an idea of the response and magnitudes during IR. The modelling can show an estimation of deflections and oscillations of tower top and drive train under several operational conditions. A more detailed mechanical modelling can show other components responses.

In order to assess the mechanical feasibility for providing IR, a comparison with a LVRT response has been done. Standard (modern) wind turbines are normally provided with LVRT capabilities. During LVRT operation, the mechanical and electrical stresses are considerably large, but the standard wind turbine is designed, at least, for facing those stresses, fulfilling the requirements. If a new functionality (such as IR) demands equal or less stress on all its components (verified through proper procedure), we can say that the wind turbine components basically do not need to be re-designed for maintaining the requirements with this new functionality, which enables its implementation.

Figure 4-3 left shows measured and simulated WTG responses during LVRT. The WTG is equipped with Gear Box and Low/High Speed shafts. The measured and simulated variables show good matching; therefore those simulated variables that are not contrasted with measurements are yet considered good estimations of the real magni-

tudes. In **Figure 4-3** the variables of interest are the generators' rotor swings (plotted as the difference between hub speed and generator speed, $\omega_g - \omega_r$, with proper gear ratio transformation) and tower top deflections (plotted as axial deflection –aligned with main shaft direction- and transversal deflection).

Figure 4-3 right shows the simulated WTG response during a severe IR operation. The wind turbine was simulated operating at constant rated wind and rated power output when an overload of 20% in power output was applied (independently of the power system conditions). The IR control algorithm is as described in Section 4.3.4. The wind turbine power output first increased with a speed of 1 pu/s up to 120% of rated, delivering kinetic energy to the grid (no more power was available from the wind), then reducing it later to 70% of rated during the recovery period. That power output increase and later reduction produced the generator rotor swings and tower top deflections as shown in **Figure 4-3** right. This particular simulated case is considered as a severe IR operation, as studied in Section 4.4 with more simulated cases.

By comparing **Figure 4-3** left and right it can be seen that the magnitudes of the observed mechanical variables during IR operation are much lower than their counterparts in LVRT operation. *During LVRT, shaft swings can be expected to be at least 10 times larger than during IR.* The average changes in rotational speed have been seen inside design limits.

An observation should be done on the tower axial deflection during IR operation. In **Figure 4-3** right, the axial deflection from $t = 0$s to $t \approx 6$s decreases much more than during LVRT (actually, it oscillates during LVRT). This can be explained considering that the rotor speed was reduced during IR, which in turn produced a reduction in the thrust (as no more power could be captured from the wind by pitching). Thus, the tower top tends towards its no-load position when the thrust is reduced. Nevertheless, the reduction in axial deflection means a reduction in tower stress and no oscillation can be evidenced here.

Figure 4-4 left shows the XY plot of the previous two tower deflection cases, "seen from above the tower", giving an understanding of the physical displacement. The wind speed reaches from the left of the figure.
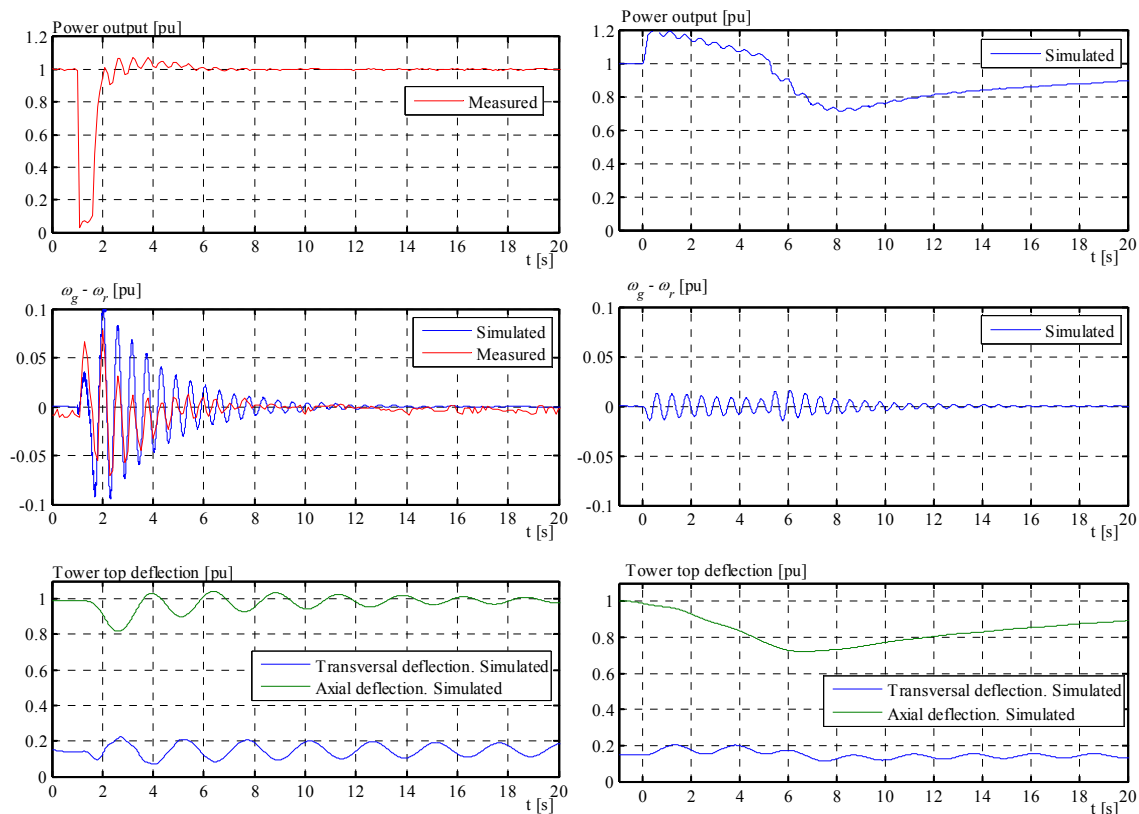
Figure 4-3: Comparison of drive train oscillations during LVRT with measurements (left) and large inertial response (right).

Figure 4-4 right shows the tower deflections during inertial response for 5 different constant wind speeds and 2 different delivered energies, ΔE_{Boost}, at each wind speed. The inertial power boost was 10% of rated in all cases. Arrows indicate the direction of the movement: first moving to the left, then moving to the right. It can be seen how the tower deflection is different for different wind speeds. Also, the higher the delivered energy, the larger the axial tower deflection. The largest tower deflection is seen for rated wind speed case. This can be explained considering that the reduction in aerodynamical efficiency (and thrust) is larger at rated wind speed, as demonstrated in Section 4.2.3.

For high wind speed conditions, the tower deflection is the opposite, as seen in the green line in **Figure 4-4** right, for $V_w = 1.2$ pu. That is, the pitching during high wind IR captures more power but also increases the thrust. However, the steady state tower deflection during high winds is lower than the rated deflection (for $V_w = 1$ pu).

Transversal tower deflections depends more on the magnitude of the generator torque increase, thus in the IR power boost magnitude. The simulation results presented here suggest that the overall tower deflections during IR can be expected to remain inside design boundaries.

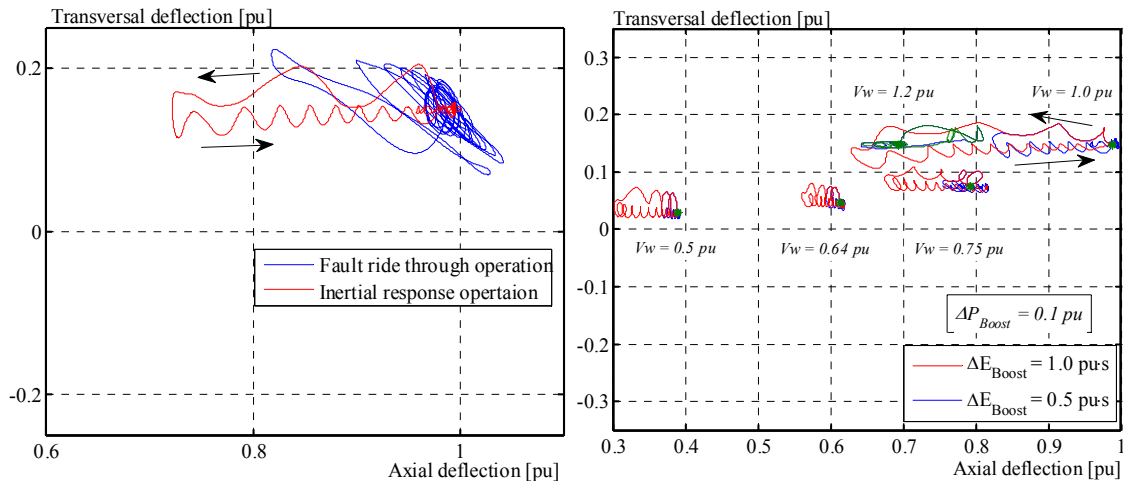**Figure 4-4:** Left: Tower deflection comparison between fault ride through and inertial response operation. Right: Simulated displacement of tower top on the horizontal plane when the wind turbine is performing inertial response. Each green point is a different wind speed steady state initial condition. The nominal tower deflection (at rated power) was taken as base deflection.

Based on the observations above, we can estimate that standard wind turbines with capability for LVRT operation are also mechanically able to perform IR operation within the magnitudes used in this work, without need of main components re-design. Obviously, the whole integrity of the installation should be investigated through specific tools, developed for such purpose. The analysis made here should be taken only as estimation.

4.2.3 Released energy

The amount of released extra energy during inertial response is one of the most important issues to analyse for assessing the WTG capability. This is due to the impact that can cause to both, the WTG and the power system if too much extra energy is released during IR operation.

By *released* energy it is understood here as the extra energy ΔE_{Boost} delivered to the grid for stabilizing the grid frequency during the first period of IR. This energy would not be delivered by other means if the IR is not activated at that time. It is important to clarify here that the ΔE_{Boost} can be obtained either from the kinetic energy in the WTG's rotating masses or from the available wind power by blades' pitching if wind speed is higher than rated or if the WTG was running curtailed (deloaded). Another important point to consider is the *direction* of the released energy. That is, for positive grid load imbalances (causing positive frequency changes), the IR power output is negative.

Here, some key questions should be elaborated, such as:
1- How much extra energy (ΔE_{Boost}) can be injected in the grid by a single WTG?
2- How much time (T_{Boost}) can be spent for delivering that energy?
3- How large is the power output drop (ΔP_{Drop}) and speed change ($\Delta\omega_t$) after delivering that energy?
4- How much time ($T_{Recovery}$) does it take to recover the WTG to normal operation after releasing that energy?
5- How are the previous being affected with different WTG curtailment levels?

For approaching the problem, a theoretical analysis has been done first. This analysis shows the relationship between ΔE_{Boost}, T_{Boost}, ΔP_{Drop} and $\Delta\omega_t$.

Considering the power flow inside the machine, as represented in **Figure 4-5**, we can write:

$$P_{Aero} - P_{Electric} - P_{Losses} - P_{Kinetic} = 0 \qquad \textbf{(4.28)}$$
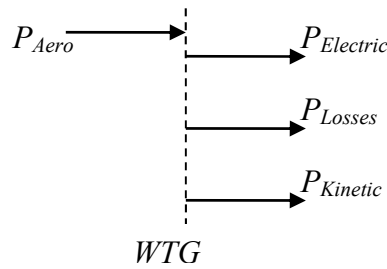
Figure 4-5: Power conversion flow inside the wind turbine

where P_{Aero} is the power being captured from the wind, $P_{Electric}$ is the power being injected into the grid, P_{Losses} is the power being lost in the WTG (mechanical + electrical) and $P_{Kinetic}$ is the power that is being stored in (or released from) rotating masses.
The first important assumption is the consideration of constant wind speed. If no other changes are applied, the WTG operates in steady state where no variations in kinetic energy are experienced, thus $P_{Kinetic} = 0$. The steady state energy balance in a time period is then:

$$E_{Aero0} - E_{Electric0} - E_{Losses0} = 0 \qquad \textbf{(4.29)}$$

But if during a period of time denoted by T_{Boost}, where the wind speed does not change, the electrical output $P_{Electric}$ is modified by control actions, there will be a variation in the machine energies balance, which can be expressed as:

$$\Delta E_{Aero} - \Delta E_{Electric} - \Delta E_{Losses} - \Delta E_{Kinetic} = 0 \tag{4.30}$$

In the last expression, the Δ represent changes from the steady state equilibrium. Those changes would not occur if $\Delta E_{Electric} = \Delta E_{Aero} = 0$, that is, if $P_{Electric}$ is not modified and wind is kept constant. The (**4.30**) can represent an inertial response situation, where the variation of electric output $\Delta E_{Electric}$ is the IR energy (ΔE_{Boost}) delivered to the grid and controlled by the WTG's power controller.

The individual expressions for ΔE_{Aero}, $\Delta E_{Electric}$, ΔE_{Losses} and $\Delta E_{Kinetic}$, with ΔE_{Boost}, T_{Boost} and $\Delta \omega_t$ as main independent variables, were found and substituted in (**4.30**). The main assumptions for the deductions were: i) constant wind speed V_w (pu) equal or below rated; ii) optimal value of C_P for the actual V_w and actual rotor speed ω_t, i.e. the pitch angle is adjusted for the optimal $C_P(\lambda, \theta_{opt})$; iii) constant rotor speed deceleration, $d\omega_t/dt = C$; iv) approximation of functions by the first two terms of Taylor's series (i.e. linear + quadratic terms) and v) constant self-consumption and generator losses during T_{Boost}. The complete deduction can be found in Appendix C. The expressions are as follows:

Aerodynamical energy variation, ΔE_{Aero}:
The aerodynamical energy variation (pu), for a rotational speed variation $\Delta \omega_t$ over a period T_{Boost} at constant wind speed V_w, can be approximated as:

$$\Delta E_{Aero} \approx \frac{1}{2} K_{Aero} V_w^3 \frac{R_t}{V_w} \frac{\partial C_P}{\partial \lambda}\bigg|_{t=0} T_{Boost} \ \Delta \omega_t + \frac{1}{6} K_{Aero} V_w^3 \left(\frac{R_t}{V_w}\right)^2 \frac{\partial^2 C_P}{\partial \lambda^2}\bigg|_{t=0} T_{Boost} \ \Delta \omega_t^2 \tag{4.31}$$

Where

$$K_{Aero} = \frac{P_{AeroN}}{V_{wN}^3 \cdot C_{PN}} \ [pu]$$

Electrical energy variation, $\Delta E_{Electric}$:
This is the manipulated variable through the inertial response control and can be represented generically as (pu):

$$\Delta E_{Electric} = \Delta E_{Boost} \tag{4.32}$$

Losses energy variation, ΔE_{Losses}:
Energy losses (pu) are given by three main components: mechanical losses, electrical losses and WTG self-consumption (auxiliary elements). Therefore:

$$E_{Losses} = E_{Losses-Mech} + E_{Losses-Gen} + E_{Self} \tag{4.33}$$

Combining them as described in Appendix C and finding the variation Δ, we can approximate it as:

$$\Delta E_{Losses} \approx \left(1 - \eta_{DT}\right)\Delta E_{Aero} + \eta_{DT}\, F_{DT}\, \omega_t(0)\, T_{Boost}\, \Delta\omega_t + \frac{1}{6}\eta_{DT}\, F_{DT}\, T_{Boost}\, \Delta\omega_t^2 \tag{4.34}$$

Kinetic energy variation, $\Delta E_{Kinetic}$:

Here is where the total moment of inertia J_t of the wind turbine is included. The kinetic energy variation (pu) is a variation from a pre-event speed $\omega_t(0)$:

$$\Delta E_{Kinetic} = J_t\, \omega(0)\, \Delta\omega + \frac{1}{2}J_t\, \Delta\omega^2 \tag{4.35}$$

Finally, combining (**4.31**), (**4.32**), (**4.34**) and (**4.35**) in (**4.30**) we obtain a quadratic equation in which the rotational speed *deviation* $\Delta\omega_t$ can be taken as unknown:

$$\left[\frac{\eta_{DT}\, K_{Aero}\, R_t^2\, V_w\, T_{Boost}\, \left.\dfrac{\partial^2 C_P}{\partial\lambda^2}\right|_{t=0}}{6} - \frac{\eta_{DT}\, F_{DT}\, T_{Boost}}{6} - \frac{J_t}{2} \right]\Delta\omega_t^2$$

$$+ \left[\frac{\eta_{DT}\, K_{Aero}\, R_t\, V_w^2\, T_{Boost}\, \left.\dfrac{\partial C_P}{\partial\lambda}\right|_{t=0}}{2} - \eta_{DT}\, F_{DT}\, T_{Boost}\, \omega_t(0) - J_t\, \omega_t(0) \right]\Delta\omega_t \tag{4.36}$$

$$- \Delta E_{Boost} = 0$$

Interesting observations can be made on (**4.36**), despite of having it obtained with some simplifications and assumptions. At a given wind speed V_w, variation of rotational speed $\Delta\omega_t$ depends not only on the amount of extra energy ΔE_{Boost} injected into the grid, but also *on the amount of time T_{Boost} spent for injecting this energy*. It can be demonstrated, as shown later, that the higher the ΔE_{Boost} the larger the $\Delta\omega_t$ will be, but the shorter the T_{Boost}, the smaller the $\Delta\omega_t$ is for the same ΔE_{Boost}.

The (**4.36**) can be used for calculating, for example, the maximum energy $\Delta E_{BoostMax}$ that can be injected into the grid at a given wind V_w having a limitation in the maximum

allowed speed deviation $\Delta\omega_{tMax}$. Other limitation can be the maximum allowable power drop $\Delta P_{DropMax}$ due to reduction in aerodynamical efficiency (ΔP_{Aero}).

For using (**4.36**) it is necessary to know the partial derivatives of $C_P(\lambda,\theta_{opt})$ with respect to the tip speed ratio λ (this derivative can also be obtained as function of the turbine speed ω_t, as the wind is considered constant). These derivatives can be numerically determined if the characteristic $C_P(\lambda,\theta)$ is known, as shown in Appendix D, **Figure D-1** for the turbine WTG1: The optimal C_P and its respective θ_{opt} can be determined at each λ, giving $C_P(\lambda,\theta_{opt})$ as shown in **Figure D-2**; then calculate numerically the partial derivatives at each point for each wind, resulting in **Figure 4-6**. These curves were obtained for the turbine WTG1 described in Appendix D.

Paying attention to **Figure 4-6** left, it can be noticed how steep is the curve $\partial C_{Popt}/\partial\omega_t$ around nominal wind speed and how flat it is below medium wind speeds. This means that the developed mechanical power (given by the C_P) is very sensitive to rotational speed changes (reflected in λ) when wind speed is around nominal. The developed mechanical power is more stable for medium and low wind speeds. As shown in simulations later, this particular characteristic of wind turbines is the responsible of large power drops during recovery period when performing IR around rated wind speed. But smaller mechanical power drops are experienced when the turbine is operating at medium or low wind speeds.

Figure 4-7 shows how is the variation of the $C_{Popt}t(\omega_t)$ for different pre-event power levels (and corresponding constant wind speed) for the turbine WTG1. For winds > 0.66 pu, the C_P variation is positive with $\Delta\omega_t$ and for winds between 0.66 pu and 0.4 pu the C_P practically does not change for limited $\Delta\omega_t$.
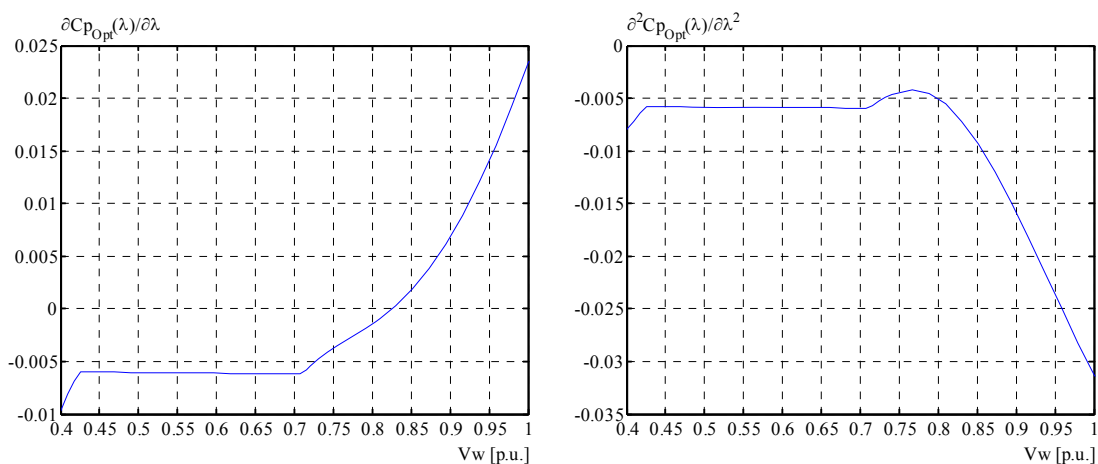

Figure 4-6: First derivative (left) and second derivative (right) of $C_{Popt}(\lambda)$ with respect to λ at each wind speed, for turbine WTG1.
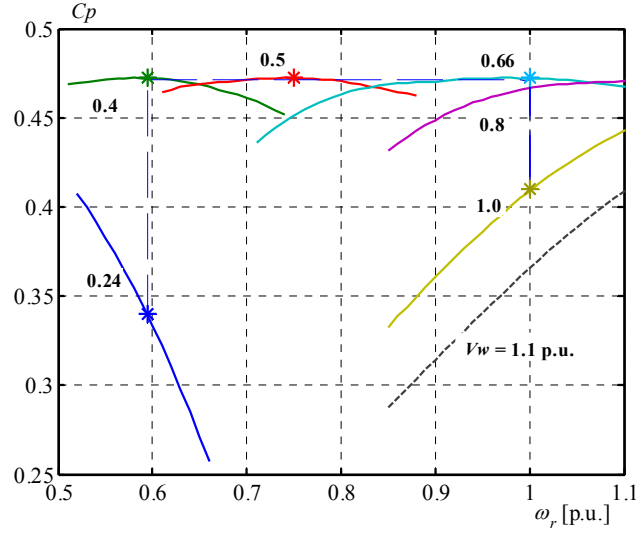
Figure 4-7: C_P vs. rotational speed at different constant wind speed. Each mark corresponds to the normal turbine operation at the given wind speed.

Further simplifications can be done in (**4.36**). Neglecting drive train losses ($\eta_{DT} = 1$ & $F_{DT} = 0$) and higher order derivatives of C_P we have:

$$-\frac{J}{2}\Delta\omega_t^2 + \left[\frac{K_{Aero}R_t\,V_w^2\,T_{Boost}\left.\frac{\partial C_P}{\partial\lambda}\right|_{t=0}}{2} - J_t\,\omega_t(0)\right]\Delta\omega_t - \Delta E_{Boost} = 0 \qquad (4.37)$$

Assuming no variation in aerodynamical efficiency ($\partial C_P/\partial\lambda = 0$) we have:

$$-\frac{J_t}{2}\Delta\omega_t^2 - J_t\,\omega_t(0)\,\Delta\omega_t - \Delta E_{Boost} = 0 \qquad (4.38)$$

The last expression is the simplest, assuming the mechanical input does not change with $\Delta\omega_t$. It says that the variation of stored kinetic energy in J_t is used solely for supplying the delivered IR energy, ΔE_{Boost}. This is not true when the mechanical power drops, because, in fact, the stored energy in J_t is taken also for compensating that mechanical power drop. It is clear then that it is not correct to use the (**4.38**) for calculating rotor speed deviations in wind turbines, as it does not consider the (important) reduction in mechanical input, thus giving erroneous $\Delta\omega_t$ values.

4.2.3.1 Power drop and recovery period

After injection of ΔE_{Boost}, the aerodynamical efficiency is reduced if the rotor speed is reduced. The electrical output must then be reduced to a level equal or below actual mechanical power, so to stop the turbine deceleration or to create rotor acceleration.

For determining the amount of power reduction ΔP_{Drop}, taking as reference the pre-event mechanical power, we can write:

$$\Delta P_{Drop}\big|_{\Delta\omega_t} = P_{Aero}(\omega_{t2}) - P_{Aero}(\omega_{t1})$$

$$= K_{Aero}\, V_w^3 \left(C_P(\omega_{t2}) - C_P(\omega_{t1}) \right) \qquad \textbf{(4.39)}$$

$$= K_{Aero}\, V_w^3\, \Delta C_P\big|_{\Delta\omega_t}$$

Here the power drop after speed deviation is proportional to the drop in aerodynamical efficiency $\Delta C_P(\Delta\omega_t)$, which can be visualized in **Figure 4-7**. By approximating the ΔC_P with the first two terms of Taylor's series, as described in Appendix C, we have:

$$\Delta P_{Drop}\big|_{\Delta\omega_t} = K_{Aero}\, V_w^3 \left(\frac{R_t}{V_w}\frac{\partial C_P}{\partial\lambda}\Delta\omega_t + \frac{1}{2}\frac{R_t^2}{V_w^2}\frac{\partial^2 C_P}{\partial\lambda^2}\Delta\omega_t^2 \right) \qquad \textbf{(4.40)}$$

The expressions (**4.36**) and (**4.40**) establish the searched relationship between ΔE_{Boost}, T_{Boost}, ΔP_{Drop} and $\Delta\omega_t$ for a given wind speed V_w. They are two equations with four unknowns. Therefore, by specifying two, for example maximum desired power drop $\Delta P_{DropMax}$ and maximum acceptable speed deviation $\Delta\omega_{tMax}$ for the given wind, the maximum energy that can be injected into the grid $\Delta E_{BoostMax}$ can be estimated for different T_{Boost} (different T_{Boost} determine different ΔP_{Boost}). Finally, the value of T_{Boost} might be specified depending on the severity of the grid event, e.g. if the measured $\Delta f/\Delta t$ is large, it determines the need of a short T_{Boost}, and vice versa.

4.2.3.2 Wind turbine operational constraints for inertial response

A complete analysis of the WTG capabilities for inertial response must include all the physical limitations. In this work, the WTG capability for inertial response has been determined considering the following constraints:

1- Minimum rotational speed: ω_{tMin}
2- Maximum power overload: P_{MaxOL}
3- Maximum torque overload: T_{MaxTOL}
4- Minimum power output: P_{Min}
5- Maximum dynamic rotational speed: $\omega_{tDynMax}$
6- Maximum rate of change of power reference: max dP_{Ref}/dt
7- Maximum power drop: $\Delta P_{DropMax}$
8- Minimum available wind power: P_{AvaMin}
9- DFIG's rotor voltage/current/power limitation (modelled technology)

In IR operations during low frequency events, the WTG's power output increases and the rotational speed decreases, transiently. This can generate a high torque in the drive train beyond the nominal value when the machine is operating around the nominal wind. Therefore the wind turbine power output should be limited to a P_{MaxTOL} in order to restrict the torque to a specified overload T_{MaxTOL}. These limitations can be expressed as:

$$P_{MaxTOL}(\omega_t) = T_{MaxTOL} \cdot \omega_t$$

$$T_{MaxTOL} = \left(1 + \frac{TOL\%}{100}\right) \cdot \frac{P_{tN}}{\omega_{tN}}$$

(4.41)

where $TOL\%$ is the acceptable torque overload in per cent of nominal.

Figure 4-8 shows the boundaries in powers and speeds in the P-ω and P-V_w charts. Three different torque levels (Nominal, 110% and 120%) are shown, indicating where the turbine power should be limited in order to restrict the specified torque overload value in the drive train (certainly, due to rotational speed oscillations, this torque limitation represents the average).
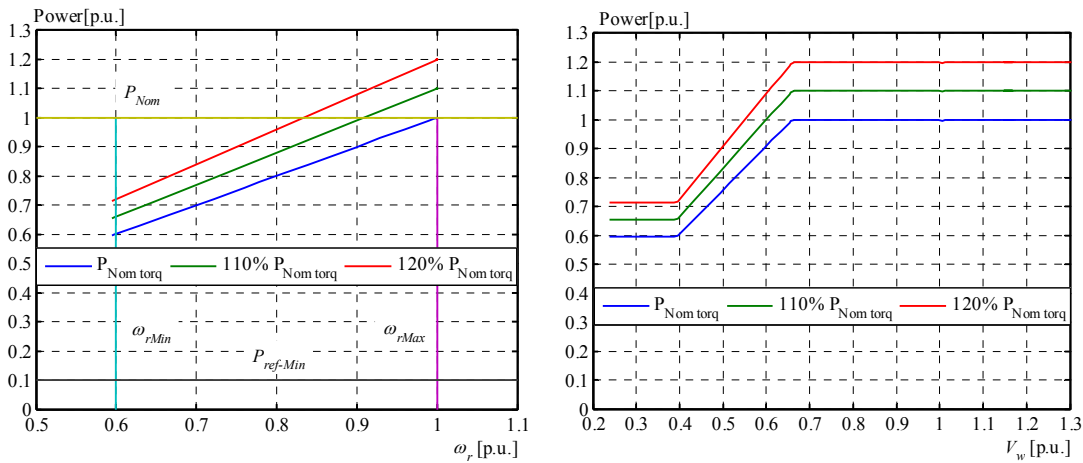
Figure 4-8: Limitations on power and speed in the P-ω (left) and P-V_w (right) charts.

4.2.3.3 Dynamical simulations

As stated in the previous paragraph, all the constraints must be considered for assessing the WTG capability for inertial response. The expressions (**4.36**) and (**4.40**) are very useful for understanding the problem. They can be used, for example, in an optimization algorithm together with all the constraints previously mentioned and, thus, to determine the capability for delivering IR energy at different wind speeds. Instead, by using an accurate dynamic model of the wind turbine, a more accurate response can be obtained, because the further simplifications in the C_P characteristics, generator losses, etc., are avoided, besides including other time dependent constraints such as ramp rate limitations and controls. Furthermore, real wind speed time series can be included if wished.

In this work, dynamical simulations were carried out to determine more accurately the WTG's capability for inertial response. The simulation methodology developed in this work is presented in [60] and it consists in manipulating the WTG power set point for delivering more power to the grid than the income, independently of the power system response and impact. Therefore, the independent simulation variables were:

- V_w
- ΔP_{Boost}
- ΔE_{Boost}

Figure 4-9 shows examples of IR dynamical simulations in the P-ω chart for 5 different constant wind speeds. Here, from the normal operational point, the IR was a step of $\Delta P_{Boost} = 10\%$ and the delivered energy was $\Delta E_{Boost} = 1.0$ pu·s. It can be seen in the figure how the limitation for torque overload, P_{MaxTOL}, works for wind conditions close to nominal. Also, large power drop, ΔP_{Drop}, is experienced at rated wind. Key time domain results are shown in **Figure 4-11** and **Figure 4-12**. Four different wind speed cases (low, medium, rated and high) with 2 different ΔP_{Boost} (5% and 10%) in each wind case are presented. The delivered energy ΔE_{Boost} is constant = 1.0 pu·s. Observe the characteristic power drop ΔP_{Drop} below available power, P_{Ava}, after injection of $\Delta E_{Boost.}$

Excessive ΔP_{Drop} is undesirable from the power system stability point of view. Solutions to this can be: i) to reduce the amount of delivered energy at wind speeds close to nominal or ii) to curtail (deload) the WTG production close to nominal wind, thus the developed mechanical power can be increased by pitching.
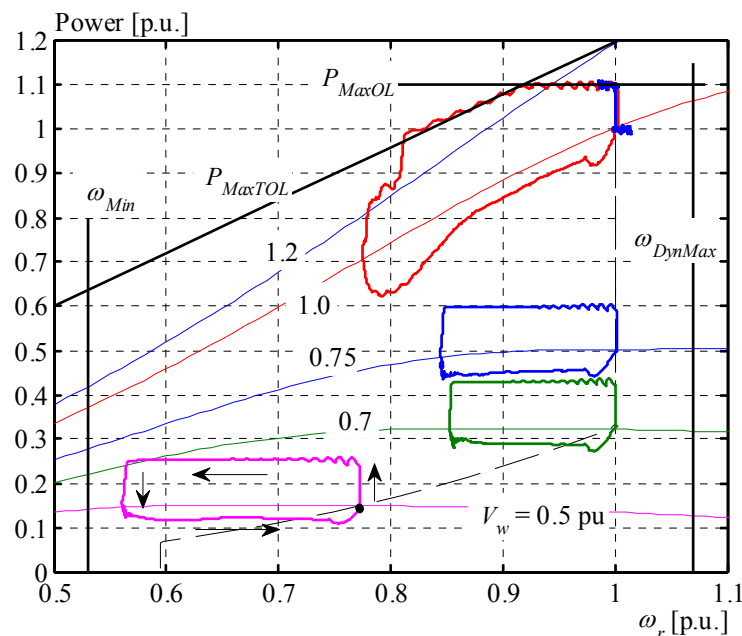

Figure 4-9: Dynamical simulations for IR functionality. Power output variation vs. rotational speed for 5 different constant wind speeds. Large ΔP_{Drop} at rated wind.

With the methodology shown in e.g. **Figure 4-11**, a series of dynamical simulations by changing the V_w, ΔP_{Boost} and the ΔE_{Boost} were carried out over a wide range of values. In the simulations, the operation of the wind turbine was constrained to the following values:

- Minimum rotational speed: $\omega_{Min} = 0.53$ pu
- Maximum power overload: $P_{MaxOL} = 110\%$
- Maximum torque overload: $T_{MaxTOL} = 120\%$
- Minimum power output: $P_{Min} = 0$ pu
- Maximum dynamic rotational speed: $\omega_{DynMax} = 1.1$ pu
- Maximum rate of change of power reference: max $dP_{Ref}/dt = 1.0$ pu/s
- Maximum power drop during recovery period: $\Delta P_{DropMax} = 10\%$
- Minimum available wind power: $P_{AvaMin} = 5\%$

A more detailed explanation of the procedure and results can be found in [60]. In order to characterize the capabilities for delivering energy, the simulation results were analysed. **Figure 4-10** summarizes the dynamical simulations results, characterizing the WTG capability for ΔE_{Boost} delivery at each wind speed. The maximum deliverable energy, $\Delta E_{BoostMax}$, *that fulfils the previous constraints* is plotted vs. wind speed. At each wind speed different maximum energies can be obtained *depending on how much time T_{Boost} was spent*. This time is inversely proportional to ΔP_{Boost}. Observe that the maximum energy at a given wind increases with a high ΔP_{Boost} and vice versa.

*Characterization like **Figure 4-10** can be useful for elaborating a gain scheduling for the IR controller, as described in Section 4.3.4.*
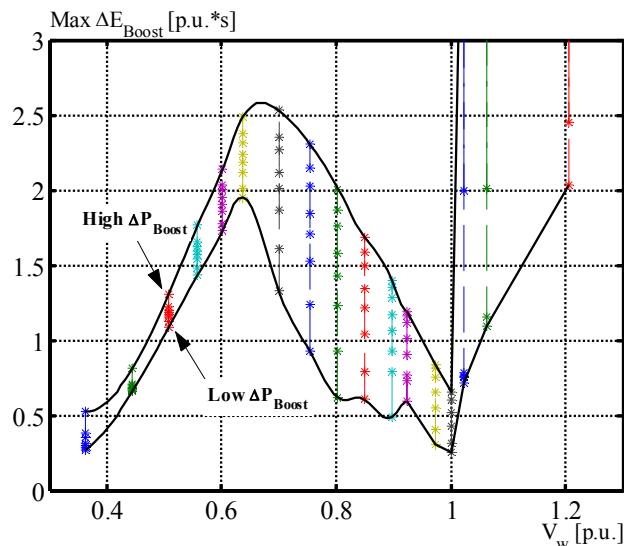
Figure 4-10: Maximum energy able to be injected into the grid fulfilling WTG constraints, for different wind speed conditions and no curtailment.
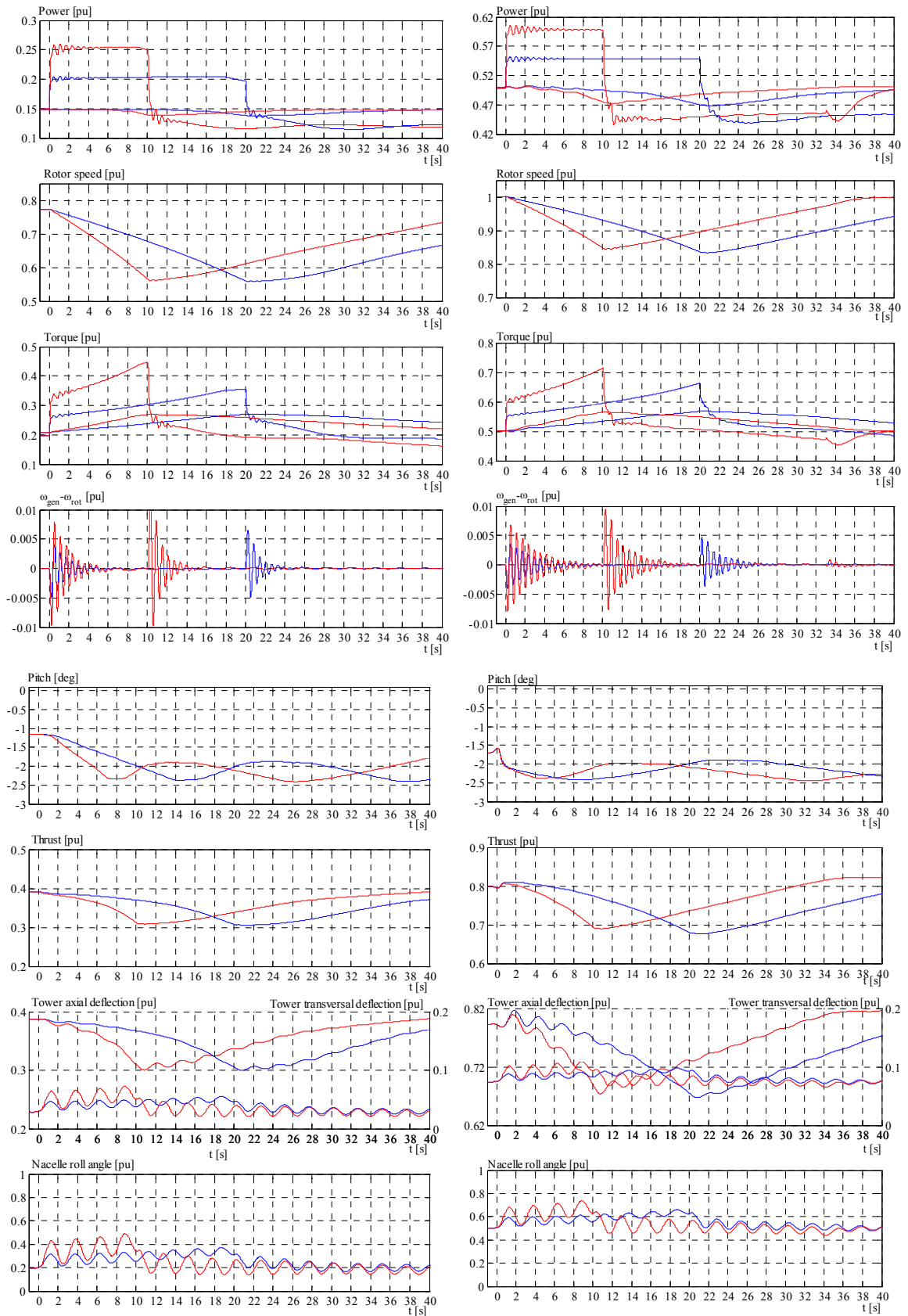
Figure 4-11: Over-production operation. Low wind (left) and medium wind (right). ΔP_{Boost} = 5% (blue) and 10% (red). ΔE_{Boost} = 1 pu·s. Electrical and mechanical P (top).
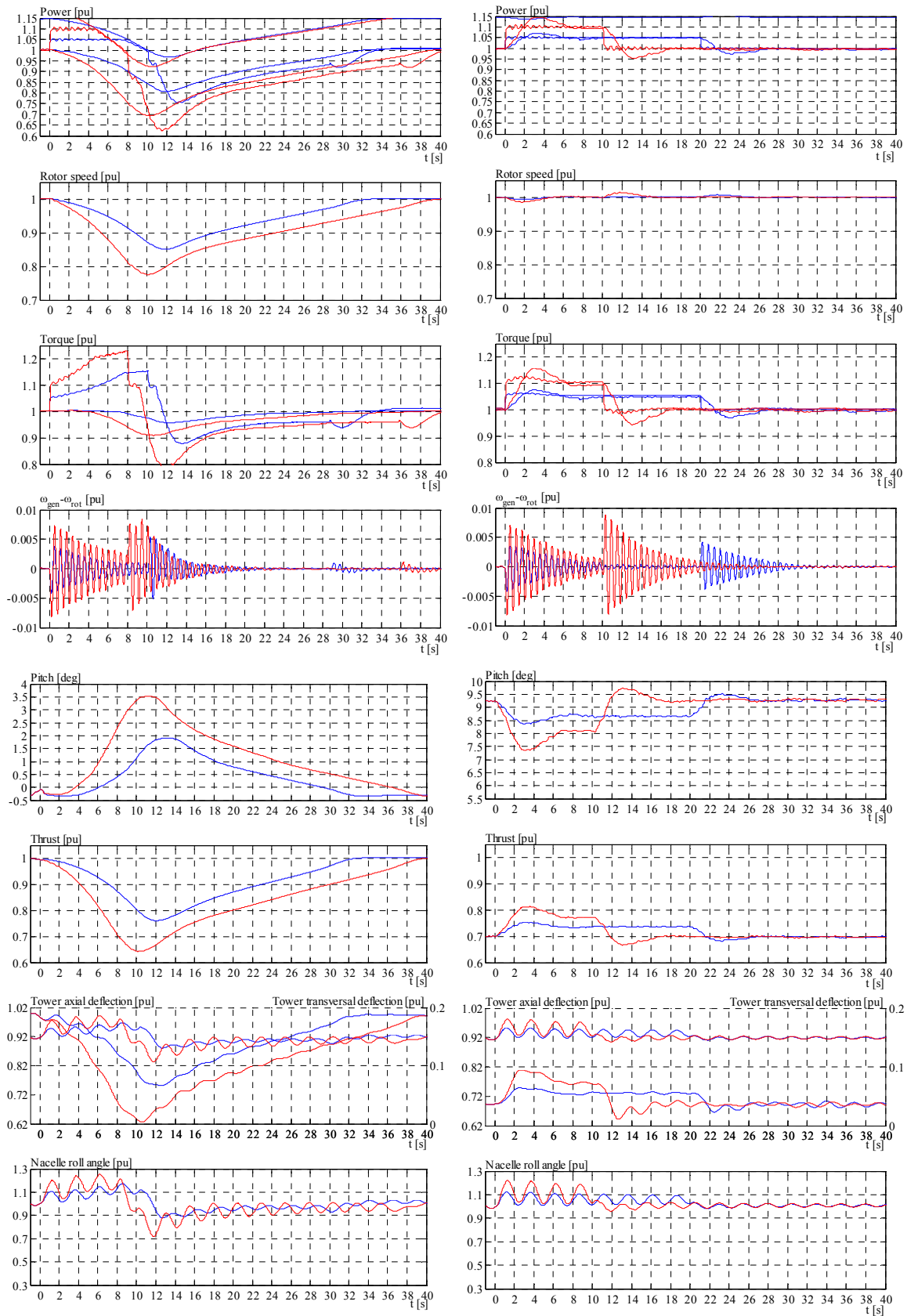
Figure 4-12: Over-production operation. Rated wind (left) and high wind (right). ΔP_{Boost} = 5% (blue) and 10% (red). ΔE_{Boost} = 1 pu·s. Electrical and mechanical P (top).

4.3 Control algorithm for inertial response of wind turbine generators

In this section, a control algorithm for wind turbine inertial response (IR) is developed. The state machine is presented and the states and events are described in detail.

4.3.1 State machine for inertial response

As discussed in Section 4.2.1 the IR is activated upon grid event detection. In this investigation, a state machine composed of three basic states, characterizing the IR functionality for wind turbines, was developed. **Figure 4-13** shows this basic state machine structure; **Table 4-2** describes each state and transition and **Figure 4-14** shows an overview of the active power and rotor speed at each state. This technique is presented in [64]. In the following sub-sections each State and Transition is described.
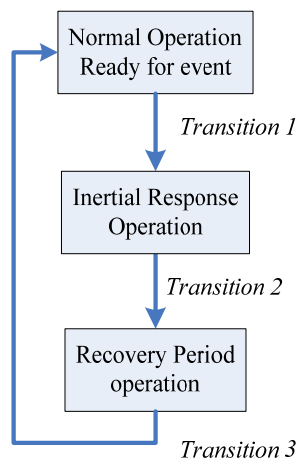
Figure 4-13: Basic state machine for wind turbine IR functionality

Table 4-2: Description of state machine for IR functionality

State or Transition	Descriptions of State Actions or Transition Conditions
State 1: Normal Operation	The wind turbine or wind power plant is operating normally in partial or full load or according to other control functionalities. No need for inertial support for the grid. No detectable grid event.
Transition 1: Grid event.	Grid event detection requiring inertial response from wind turbines.
State 2: Power boosting	An appropriate wind turbine active power variation for grid frequency stabilization is applied on top of the pre-event active power output. The characteristics of the grid event are considered, i.e. need for positive or negative power variation.
Transition 2:	The previous active power boosting is finalized or interrupted if, re-

End of power boost-ing.	spectively, the grid frequency is judged stable or the turbine protection system is activated.
State 3: Recovery Period	In case of large extracted kinetic energy, the rotational speed is re-stored back to normal for the actual wind speed but minimizing the grid impact, i.e. minimizing the active power drop from pre-event value (ΔP_{Drop}).
Transition 3: Wind plant stable	The recovery period is finalized. Rotational speed and actual power output close to normal operation for the actual wind speed.
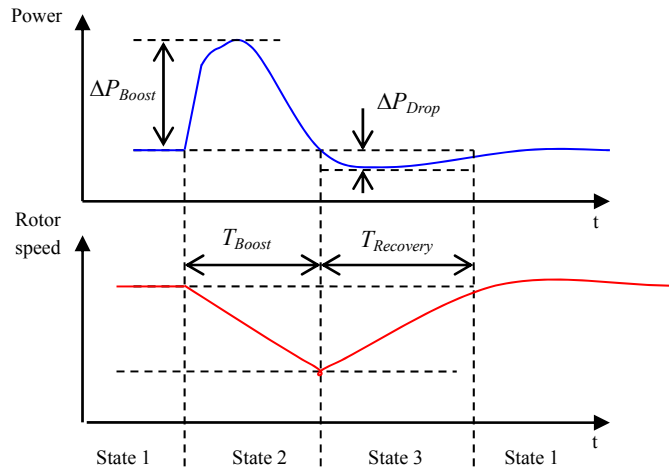
Figure 4-14: Overview of wind turbine response at each IR state.

4.3.2 Enabling IR functionality

It should be possible to automatically enable or disable the IR functionality at any time due to higher priority reasons, e.g. action from machine protection system or other control actions. The following enabling conditions for the IR functionality were adopted in this work:

$$
if \begin{cases} IR\,externalEnable = 1 \\ \& \\ P_{Ava} >= P_{AvaMinIR} \\ \& \\ \omega_t > \omega_{MinIR} \\ \& \\ IRreco\,very = 0 \\ \& \\ IR\,elapsedTime = 0 \end{cases} \Rightarrow IR\,enabled = 1, \text{otherwise } IR\,enabled = 0. \quad \textbf{(4.42)}
$$

Where *IRexternalEnable* is an enabling signal from the wind plant operator, $P_{AvaMinIR}$ is the minimum available wind power for allowing IR operation, ω_{MinIR} is the minimum turbine speed for allowing IR operation, *IRrecovery* is the signal indicating the machine is in recovery period state (state 3), *IRelapsedTime* is the signal indicating the machine has been in state 2 (power boosting) for more than the permitted time (this time may be an indication of other components stress, e.g. overheating). Other enabling conditions can be added to (**4.42**), e.g. fault ride through state, etc. For different conditions than in (**4.42**), the *IRenabled* = 0.

4.3.3 Transition 1: Grid event detection

The detection of the grid event that requires IR support from WPG is a critical step. The IR should be activated only to stabilize large grid frequency deviations caused by large load imbalances. The IR should not be activated for minor grid events that can be normally taken over by conventional generation regulation. By avoiding activating the IR functionality when not necessary, the impact in machine life time is minimized, which is reflected in the wind power *cost of energy*.

The characteristics of the grid event should also be considered for IR support, i.e. if the load imbalance in the grid is positive or negative, therefore requiring respectively a negative or positive IR power variation.

From measurements shown in **Figure 2-19** to **Figure 2-30** it can be concluded that there is a dead band on grid frequency values where it is *not* necessary to activate the IR functionality. Different power systems may have different frequency dead bands.

Additionally, it is necessary to specify a dead band for the ROCOF, where the IR should *not* be activated, also exemplified with measurements shown in **Figure 2-19** to **Figure 2-30**. Different power systems may require different ROCOF dead band for IR activation. This dead band is necessary due to, at least, two reasons:

1- As studied in Section 4.2.3 and shown in simulation results in Section 4.4, the wind turbine power drop during recovery period depends also on the *amount of time* spent during State 2 of IR. A small ROCOF value would mean a large amount of time T_{Boost} until reaching the minimum grid frequency (nadir) in case the grid frequency does not recover on time. If the IR is activated in this situation, the drop on turbine power output during recovery period would be unacceptable for the power system, independently of the values of ΔE_{Boost} or ΔP_{Boost}.

2- A small ROCOF does not represent a critical situation for the power system. There would be enough time after a detectable grid frequency deviation for other frequency control mechanisms to take over the load imbalance, such as frequency activated reserves (normal or disturbance) [39] or secondary (supplementary)

frequency control [70]. In fact, small ROCOFs are necessary for proper power system operation, as described in Section 2.1.2.

In this work, a grid event requiring IR from wind power plants is detected when three conditions are met simultaneously:

1- The demanded inertial response power $\Delta P_{IRdemand}$ given by the calculation algorithm is positive (or negative, respectively).

2- The measured grid frequency f_{meas} is lower (or higher, respectively) than a threshold value.

3- The measured grid frequency rate of change $\Delta f_{meas}/\Delta t$ (ROCOF) is lower (or higher, respectively) than a threshold value.

An extra condition is that *IRenabled* = 1, as described below. Expressions (**4.43**) and (**4.44**) summarize the conditions for IR activation for low-frequencies and high-frequencies events respectively. For any other combination in (**4.43**) or (**4.44**), the IR functionality is not activated.

Low-frequency event conditions for IR activation:

$$
if \quad \begin{cases} \Delta P_{IRdemand} > 0 \\ \& \\ f_{meas} <= Thf_{Lo} \\ \& \\ \Delta f_{meas}/\Delta t <= Thdf_{Lo} \\ \& \\ IR\,enabled \end{cases} \Rightarrow Set \begin{cases} IRactive = 1 \\ \& \\ IRboostLoF = 1 \end{cases}, \qquad (4.43)
$$

High-frequency event conditions for IR activation:

$$
if \quad \begin{cases} \Delta P_{IRdemand} < 0 \\ \& \\ f_{meas} >= Thf_{Hi} \\ \& \\ \Delta f_{meas}/\Delta t >= Thdf_{Hi} \\ \& \\ IR\,enabled \end{cases} \Rightarrow Set \begin{cases} IRactive = 1 \\ \& \\ IRboostHiF = 1 \end{cases}, \qquad (4.44)
$$

where Thf_{Lo} and Thf_{Hi} are *Th*reshold values for measured low and high grid frequency f_{meas} respectively, and $Thdf_{Lo}$ and $Thdf_{Hi}$ are *Th*reshold values for measured low and high grid frequency rate of change $\Delta f_{meas}/\Delta t$. The function *Set*{.} indicates that the signals remain activated (true) even if conditions in left side of (4.43) or (4.44) are no longer

fulfilled. When *IRboost = 1* (*LoF* or *HiF*), the value $\Delta P_{IRdemand}$ is used for determining the IR reference ΔP_{IRref} for the electronic power converter, as described in Section 4.3.4.

The performance and effectiveness of the IR support to the grid depends on the instant of activation of the IR. If it takes too long to activate it after the grid event, the obtained IR power support can be little. If, in the other hand, it is activated too early, conventional governors and prime movers may not be activated yet, and then most of the temporary power support to the grid will come from wind turbines only. This early IR actuation can create undesired effects, such as turbine overload or large turbine power drops during recovery period, which is bad for the grid. **Figure 4-15** shows the detection of a grid event requiring IR activation for a generation loss event. It can be seen that, according to the IR controller settings and to the characteristics of the simulated power system and power imbalance, the activation of IR functionality takes place after ~1.3 seconds. If the grid event (power imbalance) is different, the activation instant is also different.
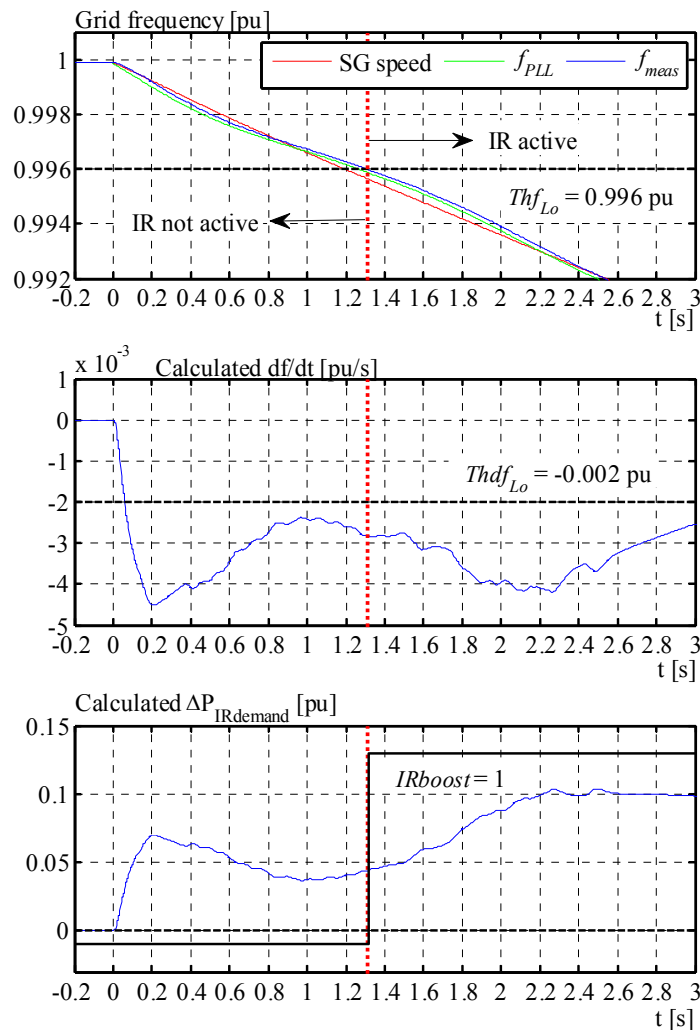

Figure 4-15: Grid event detection for activating the IR functionality

4.3.4 State2: Power boosting

In this state, the wind turbine active power production is modified temporarily for grid frequency dynamic stabilization. This power modification is carried out by controlling the wind turbine active power production through manipulation of the power converter set point with a suitable IR reference component. The power control loop of modern wind turbine power electronic converters can be designed with bandwidth of at least 100 Hz. Additionally, it is adopted a ramp rate restriction of 1.0 pu/s for the converter reference, as used in the dynamical simulations in Section 4.2.3.3. Thus, the power control loop of the power electronic converter is fast enough for controlling the IR power injection without need of modifying or manipulating the inner current control loops of the power electronic converter.

Upon grid event detection, the actual $\Delta P_{IRdemand}$ (as shown in **Figure 4-15**, bottom) is used for generating the power reference component ΔP_{IRref} for the converter. As shown in Figure 4-16, at the moment that $IRboost = 1$ the ΔP_{IRref} is increased with a ramp rate from zero up to the actual value $\Delta P_{Rdemand}$ while it is added to the actual power reference of the converter, $P_{prod-ref}$. The ramp rate limiter is necessary for: i) lowering the impact on the drive train due to fast increase of electromechanical torque (as e.g. in **Figure 4-3**, left) and ii) adapting the set point speed variation to the power controller bandwidth thus power overshoots due to control loop performance are eliminated.

During state 2, the $P_{prod-ref}$ may be kept fixed and equal to the pre-event value, or it may be manipulated by a parallel control action in order to obtain a combined response from the wind turbine. Such parallel control actions can be a primary frequency control together with inertial response, as studied in Chapter 6. Primary frequency control simultaneously to inertial response during low-frequency events are only possible if the wind turbine is running curtailed (deloaded). But for a high frequency event, the only restriction for performing both actions at the same time are the power ramp rate limitations for power references and the minimum power that the machine can generate for the actual wind speed. The ramp rate limitation is also normally imposed to the external signal driving $P_{prod-ref}$.

Because the turbine speed decreases while the power output increases during IR operation (for low frequency events), the torque in the drive train increases beyond the nominal value when the machine is previously operating around the nominal. In order to limit the torque to a certain overload value and to protect the machine, a maximum torque power reference limiter is added as shown in Figure 4-16, and described in the following pages. A further limitation is given by the maximum power overload during IR when the turbine is operating around the nominal. This maximum power limitation is achieved by a saturation limiter as shown in Figure 4-16. **Figure 4-8** and **Figure 4-9** show the boundaries for IR operation created by these limitations.
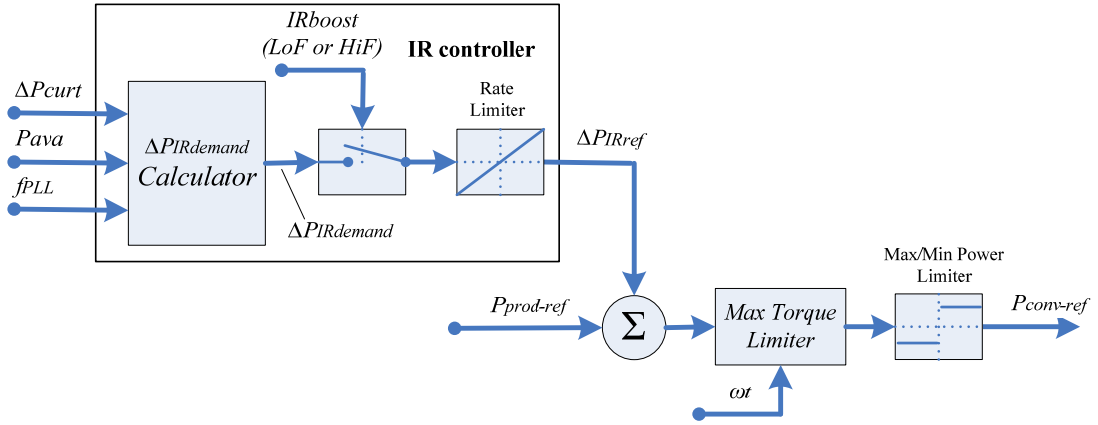
Figure 4-16: Block diagram of the IR reference added to the power converter reference.

The $\Delta P_{IRdemand}$ is calculated according to the following expressions:

$$\Delta P_{IRdemand} = G_{EIR} \cdot \left(\Delta P_{Derivative} + \Delta P_{Transient} \right)$$

$$\Delta P_{Derivative} = -K_{DIR} \cdot \frac{\Delta f_{meas}}{\Delta t}$$

$$\Delta P_{Transient} = -K_{TIR} \cdot \left(\Delta f_{meas} - \frac{\Delta f_{meas}}{T_{TIR} \cdot s + 1} \right)$$

$$\Delta f_{meas} = \begin{cases} f_{meas} - Thf_{Lo}, & if \quad f_{meas} <= Thf_{Lo} \\[2mm] f_{meas} - Thf_{Hi}, & if \quad f_{meas} >= Thf_{Hi} \\[2mm] 0, & if \quad Thf_{Lo} < f_{meas} < Thf_{Hi} \end{cases}$$

$$G_{EIR} = F_1(V_w, \Delta P_{curt}) = F_2(P_{Ava}, \Delta P_{curt})$$

(4.45)

where $\Delta P_{IRdemand}$ is the calculated inertial response value in pu, $\Delta P_{Derivative}$ is a power component based on the ROCOF, $\Delta P_{Transient}$ is a power component based on a "transient" value of Δf_{meas}, G_{EIR} is a scheduled gain based on actual available power P_{Ava} and curtailed power ΔP_{Curt} as described later, Δf_{meas} is the delta of actual measured grid frequency f_{meas} bounded by the thresholds Thf_{Lo} and Thf_{Hi}, K_{DIR} and K_{TIR} are proportionality constants for the derivative and transient components respectively and T_{TIR} is a time constant for the transient component.

The selection of the algorithm given in (**4.45**) was based on the following criteria:

1- It is better to deliver the IR power after conventional plant governors are reacting due to grid frequency deviation. In this way the wind power IR is acting together with system governors and not before. The proper activation time is obtained implicitly by suitable setting of the thresholds Thf_{Lo} and Thf_{Hi}.

2- The IR waveform should be dependent on grid frequency dynamic variations. That is, the IR output should be according to the magnitude of the event, but zero for steady state frequency deviation.

3- In order to reduce the risk of a double-dip in grid frequency deviations [66], the recovery period of IR (with associated ΔP_{Drop}) should start after the grid frequency has reached the nadir, i.e. the wind power IR is injecting power to the grid even when the frequency has overcame the nadir.

4- The amount of energy delivered by IR should be adaptable to the present wind and operational conditions by a gain scheduling.

The use of the component $\Delta P_{Derivative}$ based on grid frequency rate of change, for generating a synthetic inertial response, has been suggested and studied in several works, e.g. [21]-[27]. The intention in those works of using a derivative component is to *emulate* the response of a conventional synchronous generator by representing it with a *virtual* inertia constant H that multiplies a *df/dt* term. In theory, this approach is mathematically representative of such desired behaviour, nevertheless it is impossible to obtain it in practice, for several reasons. Some of these reasons are: i) the physical implementation of a pure differentiator is impossible [75]; ii) even if the implementation were possible, the gain of a derivative transfer function ($F(s) = K \cdot s$) increases with frequency, therefore this system is extremely sensitive to high frequency noise, making necessary to implement filters for reducing the bandwidth; iii) the rate of change of the power system grid frequency, *df/dt*, is a *consequence* of the system powers imbalance and not a *cause*, as discussed in Section 2.1. Therefore, emulating artificially synchronous machine inertial response by taking the *consequence* (*df/dt*) to generate the *cause* (ΔP_{ei}) introduces lags and oscillations in the closed loop power response.

In this work, synchronous machines are not emulated. The use of the term $\Delta P_{Derivative}$ based on $\Delta f_{meas}/\Delta t$ (in (**4.45**)) is not for emulating a synchronous machine, but just for generating an *anticipatory* response when the IR is activated, just for complementing the $\Delta P_{Transient}$ component. Therefore the $\Delta P_{Derivative}$ may be tuned with a reduced K_{DIR} if necessary, depending on the characteristics of the particular power system. However in practice, as stated above, the implementation of a derivative action is done by introducing a pole in the transfer function, for limiting its high frequency gain. The respective transfer function for $\Delta P_{Derivative}$ is then:

$$\frac{\Delta f_{meas}}{\Delta t} = \frac{s}{T_{DIR} \cdot s + 1} \cdot f_{meas}$$

$$\Delta P_{Derivative} = -K_{DIR} \cdot \frac{s}{T_{DIR} \cdot s + 1} \cdot f_{meas}$$

(4.46)

where T_{DIR} is the time constant of the derivative filter. The IR performance is not necessary to be as fast (instantaneous and sharp) as in conventional synchronous machines. Therefore the time constant in (4.46) can be moderated, giving room for proper noise filtering design.

The component $\Delta P_{Transient}$ based on Δf_{meas} provides the largest contribution of IR. The use of a transient Δf_{meas} gives stability to the calculation algorithm and ensures that the IR is injecting power even after the grid frequency has passed the nadir. The combination of $\Delta P_{Derivative}$ and $\Delta P_{Transient}$ provides flexibility for tuning the controller in order to optimize the IR functionality for a particular power system and improve the grid support performance as a whole. The $\Delta P_{Derivative}$ component supports the grid at the beginning of IR operation, when Δf_{meas} is still small.

Figure 4-17 shows the block structure of the algorithm given by (4.45) and (4.46). The measured grid frequency f_{meas} can be an output signal from e.g. a PLL or similar, as described in Section 4.2.1. It normally requires passing through a filter before using it for calculations. A first order filter with time constant T_{filt} has shown to be acceptable, which is also shown in **Figure 4-17**.
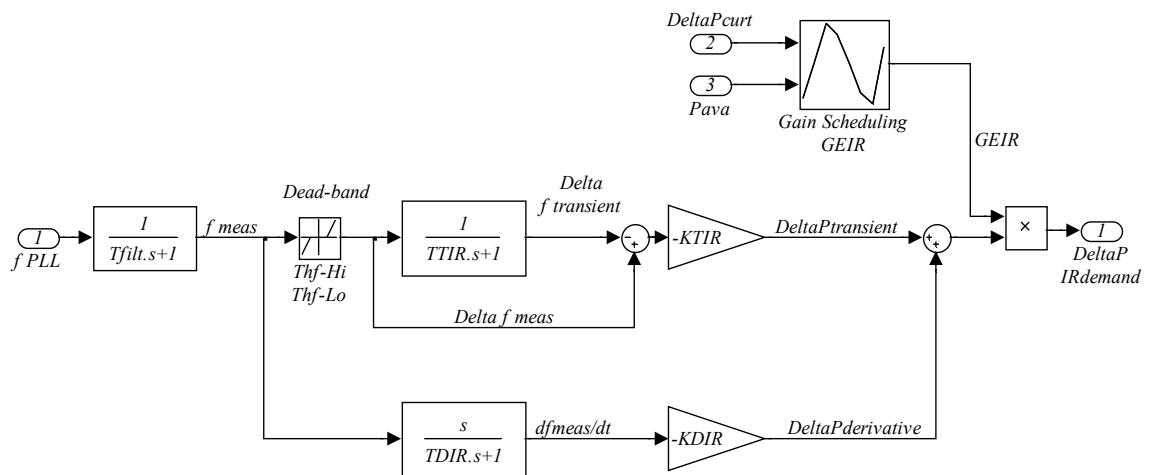

Figure 4-17: IR controller. Calculation of $\Delta P_{IRdemand}$.

4.3.4.1 Tuning the IR controller

Finding the right values for K_{DIR}, K_{TIR}, T_{DIR}, T_{TIR}, and T_{filt} is not trivial. In this work, these parameters were adjusted by simulations in an iterative procedure. For that, the wind turbine had to deliver $\Delta E_{BoostMax}$ even for the worst grid frequency case and worst wind condition. Thus, one option for the tuning procedure is:

1- Define the worst grid frequency case (profile): the one which demands more ΔE_{Boost} from the wind turbine. As the ΔE_{Boost} is also time dependent, the worst frequency case is normally given by *large* and *slow* frequency deviations, as demonstrated later with simulations.

2- Define the worst wind condition: the one which provides the lowest $\Delta E_{BoostMax}$. From **Figure 4-10**, the worst wind condition is $V_w = 1$ pu, with $\Delta E_{BoostMax} \approx 0.2$ pu·s for a $\Delta P_{Drop} = 10\%$.

3- Define $G_{EIR} = 1$.

4- Tune the IR controller parameters (**Figure 4-17**) for delivering the $\Delta E_{BoostMax}$ using the frequency profile from 1). The $\Delta E_{BoostMax}$ should be delivered during a suitable time period, i.e. the ΔP_{IRref} reaching zero a time after the nadir. The impact on the recovery period is implicit in the amount of ΔE_{Boost}.

For other grid frequency cases the delivered energy would be lower for the same G_{EIR}, and for other wind conditions the available energy will be higher (except for very low winds). The gain G_{EIR} should then be scheduled properly, as described later.

The values for Thf_{Hi}, Thf_{Lo}, $Thdf_{Hi}$ and $Thdf_{Lo}$ were defined based on the measurements of the islanded system with high wind power penetration, carried out during this work. By analysing the data from **Figure 2-25** to **Figure 2-29**, it was found that values of ±200 mHz for Thf_{Hi} and Thf_{Lo}, and ±100 mHz/s for $Thdf_{Hi}$ and $Thdf_{Lo}$ are safe enough to avoid false detection. It has to be considered that these measurements show cases of continuous operation of the system, where no need for IR was registered.

The worst grid frequency case (base case) was chosen for 1 Hz maximum deviation and time to minimum frequency $t_{fmin} = 10$ s. **Table 4-3** contains the parameters adjusted with this frequency case. These parameters were used for the IR performance simulations in this thesis. **Figure 4-18** shows the response performance of the IR controller tuned according to the previous procedure. The figure is shown for another grid case though (same parameters), for better visualization. Observe that the output ΔP_{IRref} is activated only when the detection conditions are met, ramping up with 1.0 pu/s to the value of $\Delta P_{IRdemand}$. The $\Delta P_{Derivative}$ and $\Delta P_{Transient}$ are tuned in such a way that the ΔP_{IRref} reaches zero ~1 s after the nadir (for the base case), while providing the desired $\Delta E_{Boost\text{Max}}$ (consider that this is not the base case, therefore the area below ΔP_{IRref} in **Figure 4-18** is

smaller). The detection conditions introduce a small delay between the time of event and the IR activation. This implicit delay is different for different grid events.

Table 4-3: IR parameters.

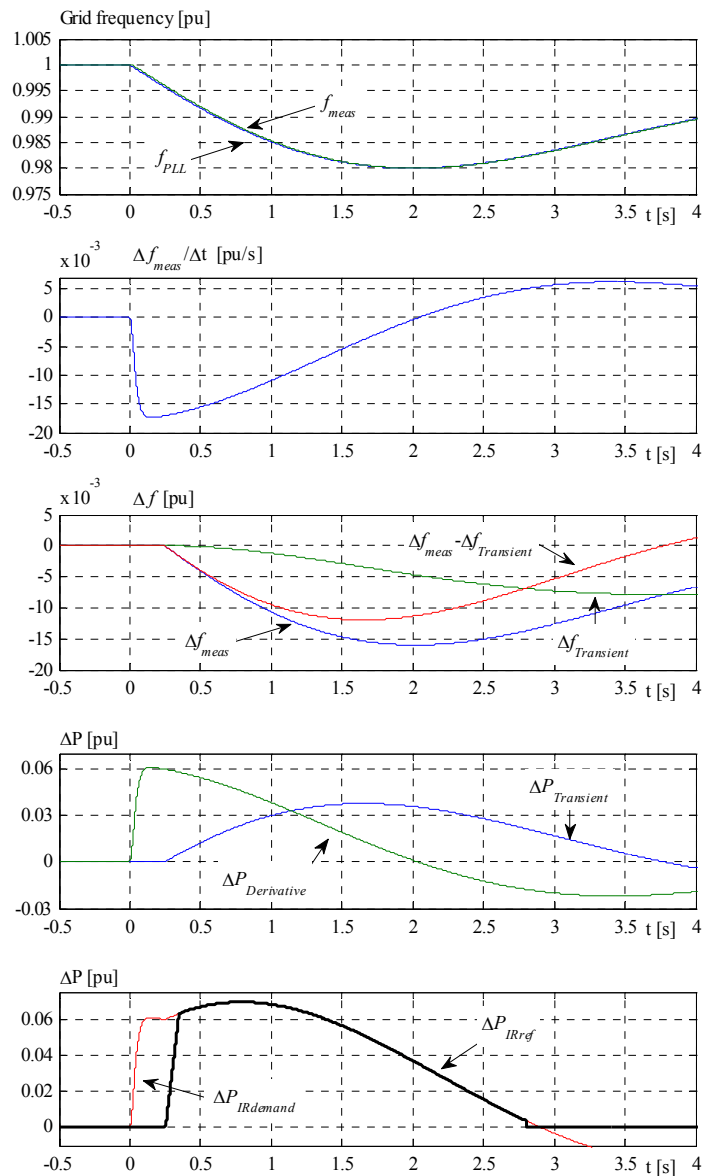| Parameter	Tfilt	TTIR	TDIR	KTIR	KDIR	Thf-Hi	Thf-Lo	Thdf-Hi	Thdf-Lo	G_{EIR}
Value	0.05 s	3.30 s	0.05 s	3.15	3.50	1.004 pu	0.996 pu	0.002 pu/s	-0.002 pu/s	1.0 (look up table)

*) Base frequency = 50 Hz.

Figure 4-18: Performance of the IR calculation algorithm. The ΔP_{IRref} is added to the converter reference $P_{conv-ref}$ for injecting into the grid. Base frequency 50 Hz

4.3.4.2 Scheduling of gain G_{EIR}

As studied in Section 4.2.3, the capability of the wind turbine for delivering extra energy to the grid during IR operation is variable with wind speed conditions and with the amount of curtailed power, ΔP_{Curt}. This capability of $\Delta E_{BoostMmax}(V_w, \Delta P_{Curt})$ was represented in **Figure 4-10**, which was built based on the wind turbine WTG1.

If the algorithm in (**4.45**) is tuned for $G_{EIR} = 1$ and delivering the lowest $\Delta E_{BoostMmax}$ (as described in the previous subsection), then for other wind conditions and curtailments it is possible to make $G_{EIR} > 1$. The variation of G_{EIR} should be linear with $\Delta E_{BoostMax}$. Therefore, based in **Figure 4-10**, the lowest $\Delta E_{BoostMax}$ is taken as base value and the G_{EIR} is given by:

$$G_{EIR}(V_W, \Delta P_{Curt}) = \frac{\Delta E_{BoostMax}(V_w, \Delta P_{Curt})}{\Delta E_{BoostMax}(1,0)}, \qquad (4.47)$$

which is shown in **Figure 4-19**. This is the scheduling curve for G_{EIR} for an individual wind turbine and particularly the turbine WTG1. In the figure, the main limitations in delivering $\Delta E_{BoostMax}$ are also indicated.
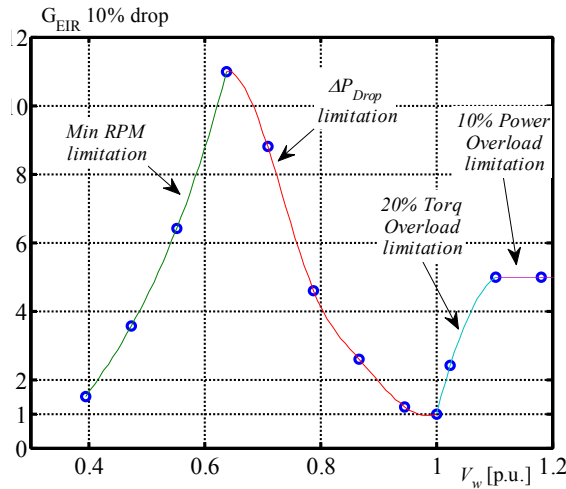
Figure 4-19: Example of G_{EIR} scheduling, determined for turbine WTG1 for a power drop $\Delta P_{Drop} = 10\%$ of rated and curtailment $\Delta P_{Curt} = 0\%$. The parameters imposing the limitations at the respective wind speed are also indicated.

4.3.4.3 Maximum torque overload limitation

As mentioned previously, during IR operation for low frequency cases the torque in the drive train increases beyond the nominal value when the machine is operating around the nominal. The wind turbine power output should be limited to a specified torque overload. In **Figure 4-8** it was shown how the turbine power should be limited according to turbine speed reduction in order to maintain a specified torque value in the drive

train (certainly, due to generator's shaft oscillations, this torque represents the average). Therefore, the limitation in the converter power reference for keeping the torque below an overload value is given by the following:

$$P_{conv-ref} = \min\left\{\left(P_{prod-ref} + \Delta P_{IRref}\right), P_{MaxTorq}(\omega_t)\right\}$$

$$P_{MaxTorq}(\omega_t) = K_{MaxTorq} \cdot \omega_t \qquad\qquad ,$$

(4.48)

$$K_{MaxTorq} = \left(1 + \frac{TOL\%}{100}\right) \cdot \frac{P_{tN}}{\omega_{tN}}$$

where $P_{MaxTorq}$ in pu is the power that produces the torque overload, *TOL,* in % of the nominal for the actual turbine speed ω_t in pu, $K_{MaxTorq}$ is relationship between $P_{MaxTorq}$ and ω_t, P_{tN} is the nominal power in pu and ω_{tN} is the nominal turbine speed in pu. **Figure 4-20** shows the block diagram of (**4.48**), which complements **Figure 4-16**.
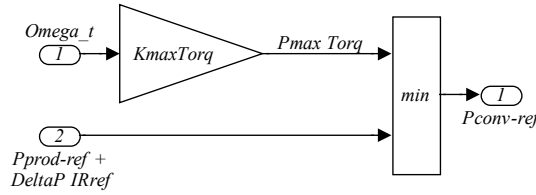
Figure 4-20: Maximum Torque Limiter.

4.3.5 Transition 2: End of power boosting state

The period of power injection for stabilizing the grid ends when the following conditions are met:

For a low-frequency event:

$$if \quad \begin{cases} \Delta P_{IRdemand} <= 0 \\ \& \\ IRboostLoF = 1 \\ \& \\ IR\,enabled = 0 \end{cases} OR \begin{cases} P_{WTG} < P_{pre-event} \\ \& \\ IRboostLoF = 1 \\ \& \\ IR\,enabled = 0 \end{cases} OR \begin{cases} IR\,enabled = 0 \\ \& \\ IRboostLoF = 1 \\ \& \\ IR\,enabled = 0 \end{cases}$$

(4.49)

$$\Rightarrow \quad Reset\{IRboostLoF = 0\}$$

For a high-frequency event:

$$if \left\{ \begin{array}{l} \Delta P_{IRdemand} >= 0 \\ \& \\ IRboostHiF = 1 \\ \& \\ IR\,enabled = 0 \end{array} \right\} OR \left\{ \begin{array}{l} P_{WTG} > P_{pre-event} \\ \& \\ IRboostHiF = 1 \\ \& \\ IR\,enabled = 0 \end{array} \right\} OR \left\{ \begin{array}{l} IR\,enabled = 0 \\ \& \\ IRboostHiF = 1 \\ \& \\ IR\,enabled = 0 \end{array} \right\} \quad (4.50)$$

,

$$\Rightarrow \ Reset\{IRboostHiF = 0\}$$

where $P_{pre\text{-}event}$ is the wind plant production previous to the grid event detection.

The (**4.49**) and (**4.50**) reset the respective signals in (**4.43**) and (**4.44**), which in turns, deactivate the ΔP_{IRref} as shown in **Figure 4-16**.

4.3.6 State 3: Recovery period

After State 2 of IR operation, the turbine speed may be different from optimal for the actual wind speed, therefore the developed aerodynamical power may be lower than the pre-event power [61] (Section 4.2.3). To recover the normal operation, the turbine speed must be restored to the optimal by means of an accelerating power on the drive train. This can be achieved by controlling the turbine power output to an appropriate value given the actual wind speed conditions. However, this new power output variation ΔP_{Drop} (power output reduction in low frequency events) may create a new impact on the power system if it is too large.

To reduce the negative impact on the power system made by the power drop, and to restore the normal operational condition of the wind turbine, a controlled recovery period is necessary.

Recovery period operation makes sense for low-frequency events where kinetic energy from the rotor is extracted. For high frequency events, the IR functionality may produce and acceleration of turbine's speed, which can be limited automatically by the speed controller, by pitching the blades out of the wind.

Different types of control actions can be performed for recovery period [64]. Three of them are:

1- Based on speed reference ramp variation: When State 3 starts, the turbine speed reference is equal to the actual speed, then it increases with a ramp rate to the value corresponding to the actual wind (optimal), where this ramp is finally disabled. A desired ramp rate can be set, which is reflected as rotor acceleration.

2- Based on accelerating power control: the acceleration of the turbine is controlled by measuring turbine's rotor acceleration and manipulating the power reference. When reaching the speed close to the optimal, the optimal control takes over. Desired turbine acceleration can be set.

3- Based on estimation of the mechanical power (actual propelling power): The actual aerodynamical power can be estimated (depending on actual turbine speed, pitch and wind) and used for driving the power set point of the turbine, affected by a desired accelerating power.

All of the previous recovery options produce more or less the same impact in the power system and on the wind turbine. In this work, the first type was adopted for simplicity (recovery based on speed reference ramp variation).

The conditions for activating the recovery period are:

$$
if \quad \begin{cases} \left| \omega_t - \omega_{normal} \right| \; > \; Tol_{\Delta\omega} \\ \& \\ IRactive = 1 \\ \& \\ IRboost = 0 \end{cases} \quad \Rightarrow \quad IRrec\,overy = 1, \tag{4.51}
$$

where ω_t is the actual turbine speed, ω_{normal} is the normal turbine speed for the given wind conditions, $Tol_{\Delta\omega}$ is the tolerance on turbine speed deviation from normal for activating a controlled recovery period.

The speed reference during recovery period is represented by the block structure in **Figure 4-21**. In this figure, the ramp rate limiter is enabled with *IRrecovery*, with ω_{normal} as input and actual ω_t as initial condition.
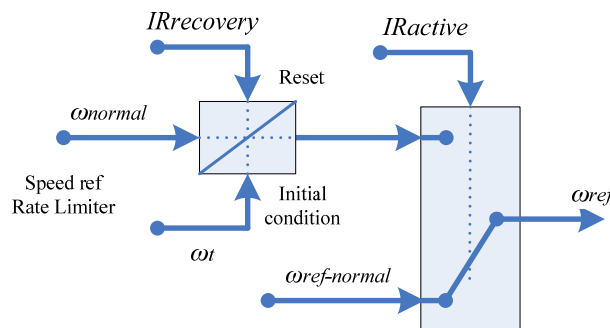

Figure 4-21: Turbine speed reference during recovery period.

4.3.7 Transition 3: wind turbine stable

The IR functionality ends when the following conditions are met:

$$
if \quad \begin{Bmatrix} IRboost = 0 \\ \& \\ IRrecovery = 0 \end{Bmatrix} \quad \Rightarrow \quad Reset\{IRactive = 0\} \tag{4.52}
$$

The wind turbine is then ready for a new IR operation.

4.4 Open loop simulated performance of inertial response

Only the performance of the wind turbine output is analysed here, without considering the power system impact. It is interesting to know the behaviour of the wind turbine and the developed IR control when performing inertial response in different wind speed conditions, grid events and gains G_{EIR}. As a first attempt, and in order to facilitate the observations, purely constant wind speeds were applied to the full wind turbine model in Section 4.4.2. In Section 4.4.3 similar simulations were carried out but utilizing real wind speed measurements as model input and compared with measured WTG variables in normal operation.

4.4.1 Simulations set up

An individual wind turbine is simulated connected to a large power system. The power of the wind turbine is very small compared to the power of the power system. Therefore any change in turbine's output will not impact in the power system frequency and voltages. A very large load imbalance is produced in the system, which changes the grid frequency with a desired profile. The wind turbine reacts to this frequency deviation. Cases combining three different grid frequencies and five different wind speeds were simulated.

Grid frequency events
- Base case: 1 Hz maximum frequency deviation and 10s to f_{min}
- Case B: 1 Hz maximum frequency deviation and 5s to f_{min}
- Case C: 1 Hz maximum frequency deviation and 2s to f_{min}

Wind speed conditions
- Very high wind: The wind range where the available wind power is higher than any desirable power output from the turbine, i.e. more than the overload limit, P_{MaxOL}. Therefore there will always be a surplus of power which can be captured by a suitable pitching if necessary.
- High wind: The available wind power is higher than the rated but lower than P_{MaxOL}, therefore the wind turbine is normally operating at rated power production if it is not

curtailed by external set point. More mechanical power can be captured by pitching if necessary, but the turbine power output during IR can be higher than the available.

- Rated wind: wind turbine can only operate permanently at optimal or curtailed. This is the worst wind condition for IR functionality.
- Medium wind: The wind speed where the scheduled G_{EIR} can be a maximum.
- Low wind: The wind where the minimum rotor speed can be reached if the scheduled G_{EIR} is excessive.

IR controller settings

The IR controller was tuned as described in Section 4.3.4.1. The maximum power overload has been specified as 10% and the torque overload as 20%. The IR functionality is activated when the grid frequency is below 49.8 Hz and the *df/dt* (ROCOF) larger than 0.1 Hz/s (**Table 4-3**). The impact on the grid is not observed in these simulations, but due to the threshold values, the activation of IR is at different times in each grid case. For each wind speed, the grid frequency base case is simulated at first with different values of G_{EIR} to see the impact on the recovery period power drop. The suitable value of G_{EIR} that creates a power drop less than 10% is used later with the other grid frequency cases. A comparison with the G_{EIR} of **Figure 4-19** demonstrates the effectiveness of the scheduling technique described in Section 4.3.4.2.

4.4.2 Constant wind speed simulation results

Purely constant wind speed has been used in these simulations. The 3p effect was also neglected for better visualization of the source of power and mechanical oscillations. Drive train oscillations are excited as described in 4.2.2. Those oscillations are damped and reflected as power output oscillations, as seen in all simulations results from the time of IR activation.

For a better visualization and interpretation, the WTG power output is shown as a variation around pre event power: $\Delta P_{IR} = P_{elWTG} - P_{elWTG-0}$. The same applies for the available power P_{Ava}.

Very high wind speed

Figure 4-22 shows the simulation results for the base case grid event and constant wind speed of 1.15 pu, which corresponds to $P_{Ava} \approx 1.2$ pu for the turbine WTG1. Values of G_{EIR} were increased with 1, 2, 4 and 5. Observe that for any value of G_{EIR} the wind turbine does not create a power drop during the recovery period. Upon IR actuation, the turbine speed reduction activates the pitch actuation, capturing more power from the wind and balancing the extra power delivered to the grid. The oscillations in rotational speed are coupled to the pitch actuation.

Due to the power overload limitation, no matter which value of G_{EIR}, the maximum effective inertial response is 0.1 pu. A gain $G_{EIR} = 5$ has been taken as practical value for this wind condition, which is in accordance with the gain scheduling in **Figure 4-19** for $V_w = 1.15$ pu. The torque overload protection also actuates, which can be noticed by the straight trajectory from $t = 8$ s to $t = 12$ s. Higher values than this will not improve the inertial response due to the maximum turbine overload limitation. Observe that for G_{EIR} values lower than 5 the impact is seen on the turbine speed and pitch actuation.

This particular wind speed situation provides a secure inertial response from an individual wind turbine with no power drop in recovery period, mainly because the extra energy is obtained from the wind by pitching and not from kinetic energy of rotating masses. This is valid as long as the available power is higher than the overload limit: $P_{Ava} > P_{MaxOL}$.

Higher power overload than 10% has not been investigated in this work, as this value would go beyond practical turbine limitations and model reliability. In the future, modern wind turbines may well be designed for larger overloads, and those new known limitations and associated behaviours would be updated in the dedicated models.

Figure 4-23 shows the results for the Case B and Case C, together with Base Case. The IR is simulated for the chosen $G_{EIR} = 5$. As expected, there is no recovery period for Case B and Case C too. Due to the overload limitation, the power output do not increase beyond 10% no matter how high the *df/dt* is, therefore the $P_{conv-ref}$ in Figure 4-16 is saturated. If the G_{EIR} was chosen for creating this saturation with the lowest (defined) *df/dt* case, as shown in **Figure 4-22**, then it is obvious that saturation will exist for any faster grid event, as seen in **Figure 4-23**.

If the maximum delivered power is a constant, then the energy delivered during IR operation is *reduced* for *higher df/dt*, as it can be deduced looking at the areas below the ΔP_{IR} curves for each case in **Figure 4-23**. This means that, at very high wind speed, the inertial response contribution (energy) from wind power is different for different *df/dt*: lower IR energy contribution for larger *df/dt* and vice versa.

This behaviour can be different if the G_{EIR} is reduced. That is, to first tune it for reaching the overload capability with the fastest possible *df/dt*, therefore for slower *df/dt* events the IR power contribution would be proportional. This different tuning was not simulated for this wind case, but the IR power would be qualitatively similar to the ΔP_{IR} shown in **Figure 4-27**, with the difference of not having a recovery period at all.

High wind speed

For light grid frequency events, the turbine IR output may be lower than the available wind power, and for severe grid frequency events the turbine IR output may be higher than the available wind power. Obviously, it will depend also on the scheduled G_{EIR} for the actual wind speed.

Figure 4-24 shows simulation results for the Base Case event and constant wind speed of 1.06 pu, which corresponds to $P_{Ava} \approx 1.05$ pu for the turbine WTG1.

Upon IR actuation, the turbine power output increases based on actual grid frequency, and the rotational speed decreases according to the difference between electrical power output and mechanical power input. Once the boosting period finishes (after $t \approx 12.5$s), the turbine power output drops below actual mechanical power if it is necessary to recover the turbine rotational speed. Observe how the ΔP_{IR} varies with G_{EIR}. For low values of G_{EIR}, there is no recovery period, because the power output during State 2 does not exceed the actual available power while the pitching action captures more aerodynamical power, balancing the electrical output. Thus no kinetic energy is actually extracted. For larger G_{EIR}, the turbine output during Stage 2 exceeds the available power for $G_{EIR} = 2.7$ and $G_{EIR} = 3$. It has to be considered that the grid event here is the base case, as in **Figure 4-22**, therefore the ΔP_{IR} waveform is *similar*, with the difference of injecting a different *quantity* of inertial response energy, ΔE_{Boost}.
It is interesting to notice that above certain G_{EIR} value, part of the ΔE_{Boost} has to come from the rotor kinetic energy, therefore a reduction on rotational speed is experienced.

As described in Section 4.2.3, the ΔP_{Drop} for wind speeds around nominal is large. The reason is that the developed aerodynamical power is *very* sensitive to rotational speed reductions. E.g. with a small change in G_{EIR} from 2.7 to 3, a large rotational speed reduction and a large power drop during recovery period are experienced. Thus, as G_{EIR} depends on actual wind, its value may vary during IR actuation and it is expected to experience either large or small ΔP_{Drop} around this average wind condition. This behaviour is shown in Section 4.4.3 by using real wind speed data.

The value of G_{EIR} can be chosen in order to generate a desired % of power drop during recovery period. For this wind of 1.05 pu and this Base Case grid event, a ~10% power drop is obtained with a $G_{EIR} \approx 2.7$, which is matching with the gain scheduling in **Figure 4-19**. Values of G_{EIR} lower than 2 will not generate (significant) drops in speed and power output during state 3, as seen in **Figure 4-24**.

Figure 4-25 shows the results for the Case B and Case C, together with Base Case. The IR operation is simulated for the chosen $G_{EIR} = 2.7$.

For the grid Case C, the ΔP_{IR} is larger, but the turbine power output is saturated by the 10% overload limit. Therefore, the delivered ΔE_{Boost} decreases for fast df/dt grid events. It can be noticed that the largest drops in power and speed are for the slower grid event (Base Case). This is in part due to the larger amount of delivered ΔE_{Boost} but also due to the larger actuation time during state 2. As it was demonstrated in Section 4.2.3, the aerodynamical drop depends not only on the ΔE_{Boost} but also on the *time period of actuation*.

Rated wind speed

This is a special condition where the wind speed, the available power and the power output are 1 pu. Unless the turbine is curtailed by external set point, the available power is not higher than the normal production; therefore the ΔE_{Boost} comes totally from the rotor kinetic energy, meaning a speed reduction and a power drop during IR actuation.

Figure 4-26 shows the results for the grid Base Case and $G_{EIR} = 1$ and $G_{EIR} = 2$. As the IR controller has been tuned for the combination of rated wind, grid base case and $G_{EIR} = 1$, the power drop is 10% by default. The delivered ΔE_{Boost} is the lowest (area below ΔP_{IR}) compared to all the other wind speed conditions. If required for grid support, higher ΔE_{Boost} can be extracted by increasing the G_{EIR} proportionally. Increasing the G_{EIR} by a factor of 2 (hence the ΔE_{Boost}), the power drop becomes ~3 times larger.

To avoid large power drops, the WTG can be operated curtailed (*Curt.* –or deloaded). The effect of curtailment was also studied. Keeping the $G_{EIR} = 2$, three different curtailments were investigated: $\Delta P_{Curt} = 0\%$, $\Delta P_{Curt} = 1\%$ and $\Delta P_{Curt} = 2.5\%$ of rated power. Different reductions on power drop were obtained, as seen in **Figure 4-26**.

With a $\Delta P_{Curt} = 2.5\%$, a power drop of 10% is achieved with a $G_{EIR} = 2$ (doted green line), i.e. same power drop but the double of delivered IR energy compared to the default gain. This characteristic is very important to consider when studying the impact on the power system: *if the delivered ΔP_{IR} and ΔE_{Boost} are not enough for supporting the system, then an increase in G_{EIR} would be necessary. But in order to maintain the same power drop during recovery, the turbine must be run with a small % curtailment. This curtailment is only needed around this wind speed condition because it is characterized by the lowest G_{EIR}, i.e. the lowest IR capability, as described in Section 4.2.3.*

Figure 4-27 shows the results for the Case B and Case C, together with Base Case. The IR operation is simulated with the default $G_{EIR} = 1$.

There is no saturation for $G_{EIR} = 1$. But for higher G_{EIR} values, saturation for Case C can be expected. However, as discussed previously, if G_{EIR} is set with higher values than

default, a curtailment must be applied (for keeping the same ΔP_{Drop}), which reduces the pre-event power output, averting the saturation and giving room for ΔP_{IR} increase.

Similarly to high wind case, the largest drops in power and speed are for the slower grid frequency event (Base Case).

Medium wind speed

It is the wind range where large amounts of ΔE_{Boost} can be extracted, with no turbine overload and low values of ΔP_{Drop}. Similarly to the previous case, unless the turbine is curtailed by external set point, the ΔE_{Boost} comes totally from the rotor kinetic energy, meaning a speed reduction and a power drop during IR actuation. Simulations were carried out for wind speed of 0.66 pu, which corresponds to a pre-event power of ~0.33 pu.

Figure 4-28 shows results for the grid frequency Base Case and G_{EIR} = [1, 2, 9, 10]. Looking at the power drop during recovery period, the G_{EIR} can be increased up to ~9 for a 10% power drop. This is in agreement with the gain scheduling presented in **Figure 4-19** for the wind turbine WTG1. With this wind speed the increase in WTG capability for IR operation is enormous, if we compare with the previous cases. This is due to the more stable aerodynamical power, as was studied in Section 4.2.3.

Compared to the rated wind speed case, there is no need to curtail the WTG production to avoid large ΔP_{Drop} and obtain large amounts of ΔE_{Boost}. However, the rotational speed deviation is larger and the recovery period takes more time. These issues can be eliminated with a reduction in G_{EIR}, e.g. by setting it to 2 or 3 (It has to be considered that the simulations were done with extreme G_{EIR} values, meaning a large support to the grid).

Figure 4-29 shows the results for the Case B and Case C, together with Base Case. The IR operation is simulated with the chosen G_{EIR} = 9.

There is no turbine overload for G_{EIR} = 9. Notice how large the IR power output can be for faster grid frequency changes: up to 60% ΔP_{IR} increase for grid Case C. Due to this large value variation, the ramp rate limitation can be identified in this plot. Similarly to rated wind case, the largest drops in power and speed are for the slower grid event (Base Case).

Low wind speed

It is the wind range where the minimum rotational speed can be hit when delivering certain amount of ΔE_{Boost}. Thus, the limitations are not ΔP_{Drop} or ΔP_{MaxOL} but the minimum rotational speed ω_{min}.

Similarly to the previous cases, unless the turbine is curtailed by external set point, the ΔE_{Boost} comes totally from the rotor kinetic energy. Simulations were carried out for wind speed of 0.4 pu, which corresponds to a power output of ~0.07 pu.

Figure 4-30 shows results for the grid Base Case and G_{EIR} = [1, 1.5, 2]. For all the cases the ΔP_{Drop} < 2% of rated, meaning that this variable is not relevant for low wind speeds. However, for G_{EIR} = 2 it can be seen how the ΔP_{IR} is *interrupted* by the minimum speed protection (as described in Section 4.3.2).

The maximum of G_{EIR} for low wind conditions should be scheduled in order to avoid this kind of *interruptions*, because it impacts negatively in the power system. Instead, the maximum G_{EIR} must assure a continuous ΔP_{IR} waveform. For the analysed wind turbine, this value is $G_{EIR} \approx 1.5$ for wind of 0.4 pu, in agreement with the gain scheduling of **Figure 4-19**. Thus, the minimum rotational speed is achieved but no interruption is experienced.

If higher value of G_{EIR} is needed, the WTG could be tempted to be curtailed. However, with low wind speed conditions, curtailment is almost impossible due to the requirement of minimum generated power for turbine proper control and operation. Nevertheless, with low wind speed conditions, the number of synchronous machines in the system may be higher, reducing the overall need for wind power inertial support.

Figure 4-31 shows the results for the Case B and Case C, together with Base Case. The IR operation is simulated with the chosen G_{EIR} = 1.5. The IR power output increases up to 10% of rated; low ΔP_{Drop} are observed and rotational speeds are higher than the minimum.
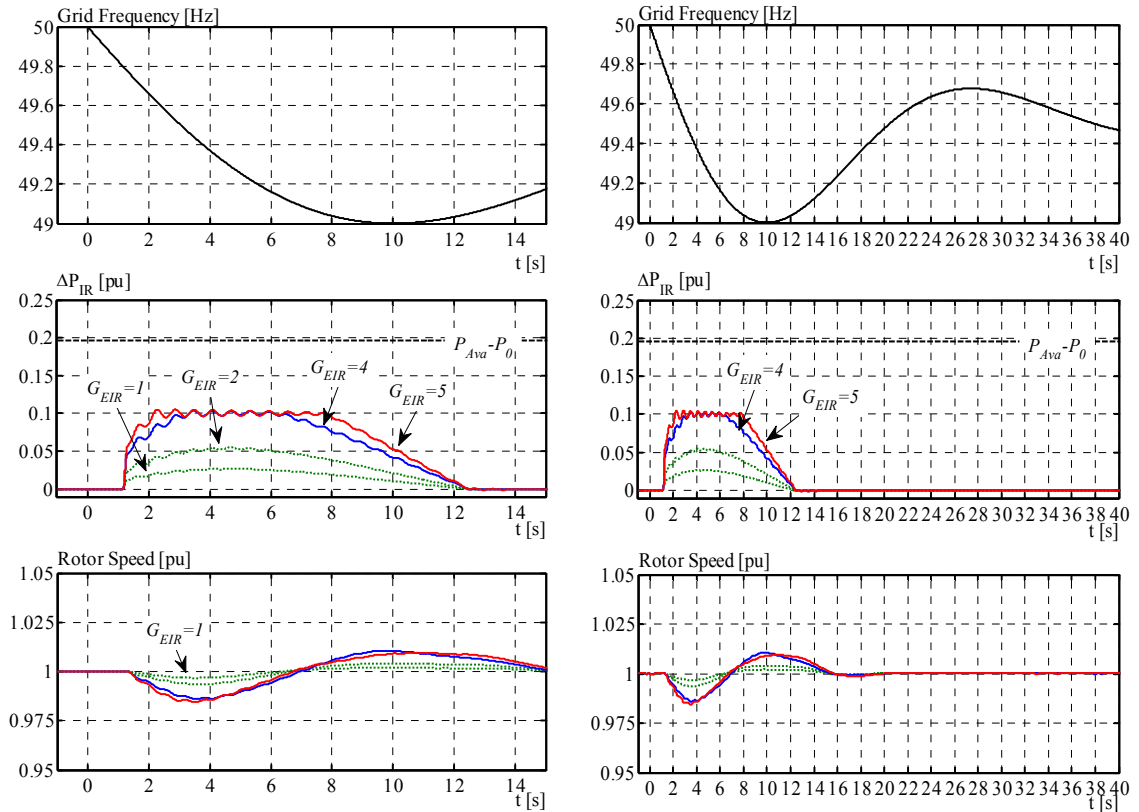
Very high wind speed (V_w = 1.15 pu)

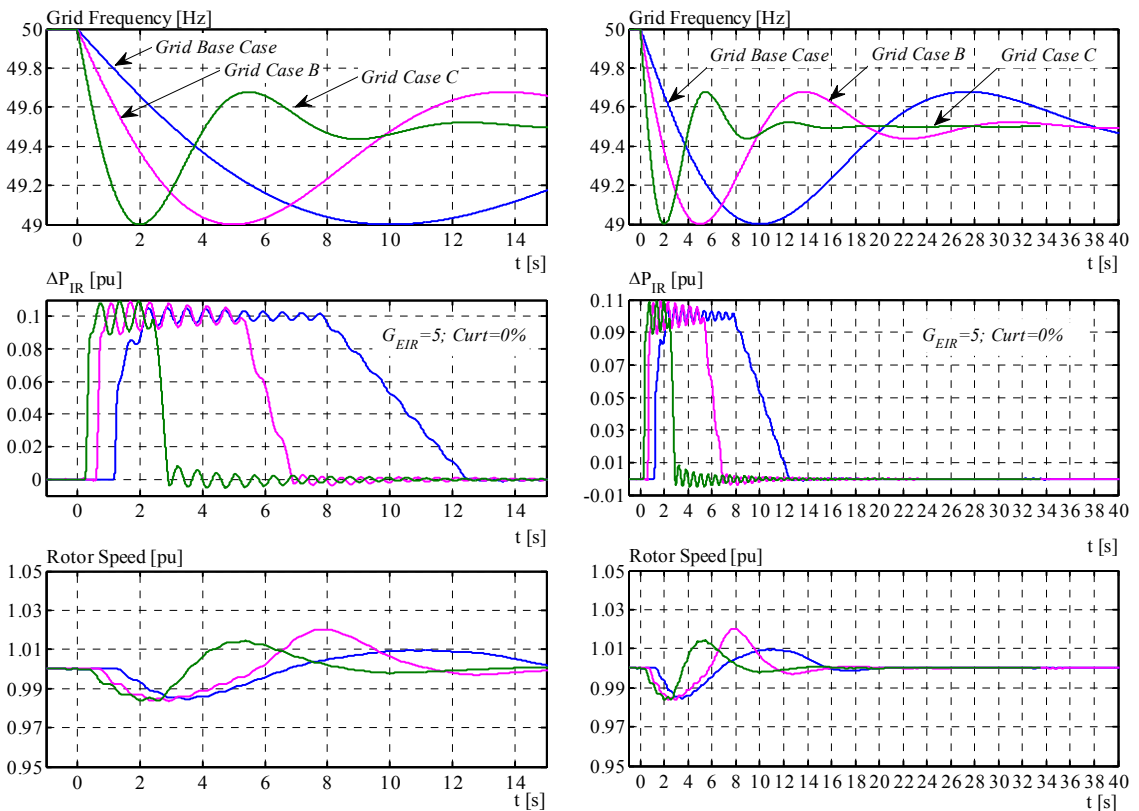**Figure 4-22:** IR very high wind speed, base grid case. Powers as variations around P_0.

Figure 4-23: IR very high wind, other grid cases. Powers as variations around P_0.
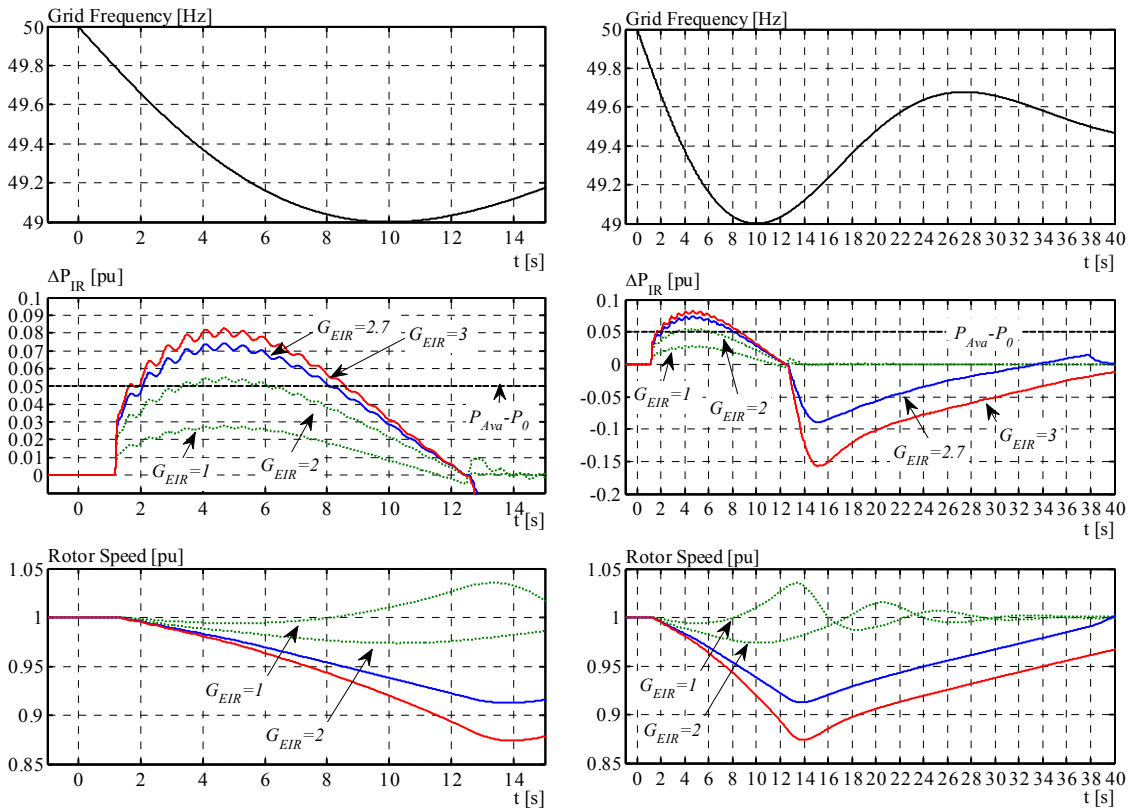
High wind speed (V_w = 1.05 pu)

Figure 4-24: IR high wind speed, base grid case. Powers as variations around P_0.
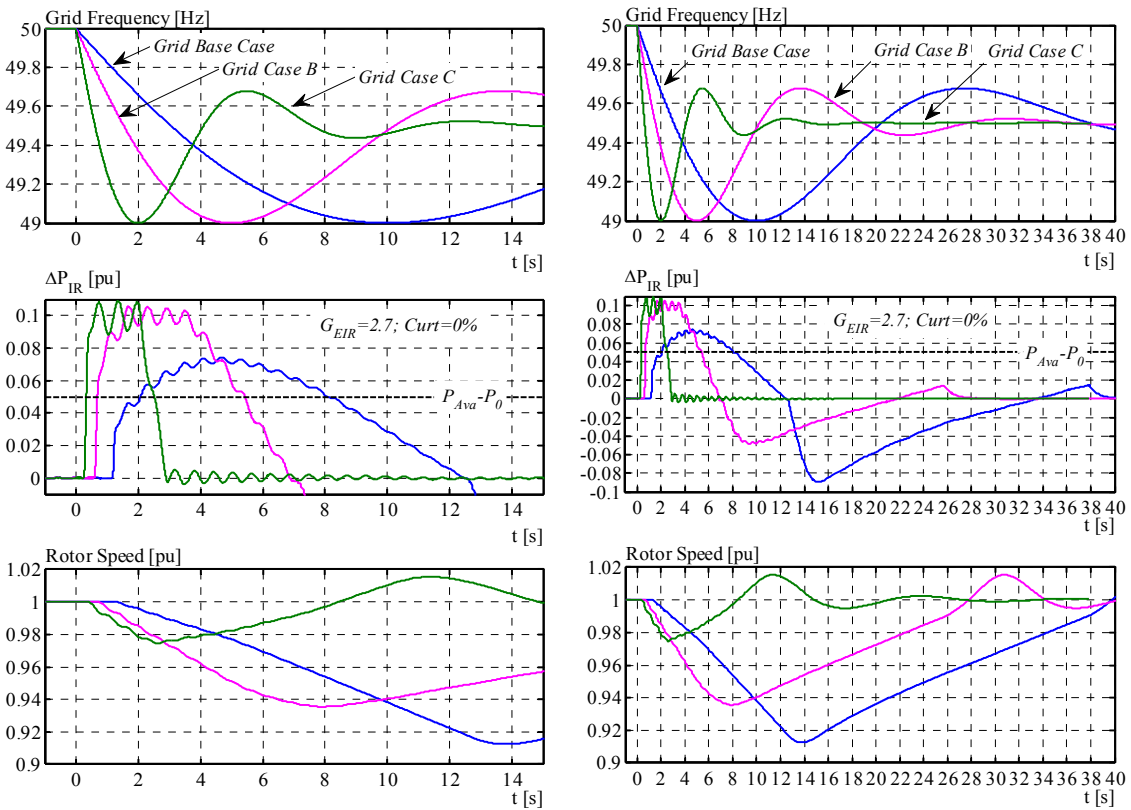

Figure 4-25: IR high wind speed, other grid cases.. Powers as variations around P_0.

Rated wind speed (V_w = 1.0 pu)

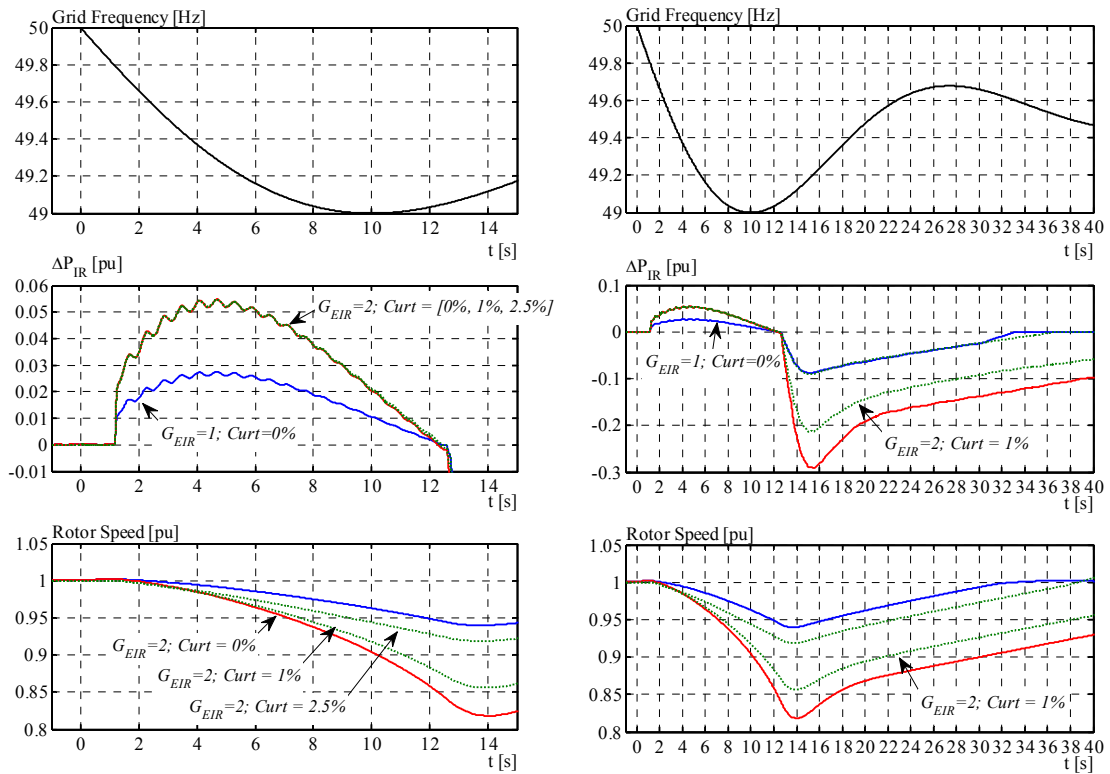**Figure 4-26:** IR rated wind speed, base grid case. Powers as variations around P_0.

Figure 4-27: IR rated wind speed, other grid cases.. Powers as variations around P_0.

Medium wind speed (V_w = 0.66 pu)

Figure 4-28: IR medium wind speed, base grid case. Powers as variations around P_0.

Figure 4-29: IR medium wind speed, other grid cases.. Powers as variations around P_0.

Low wind speed (V_w = 0.4 pu)

Figure 4-30: IR low wind speed, base grid case. Powers as variations around P_0.
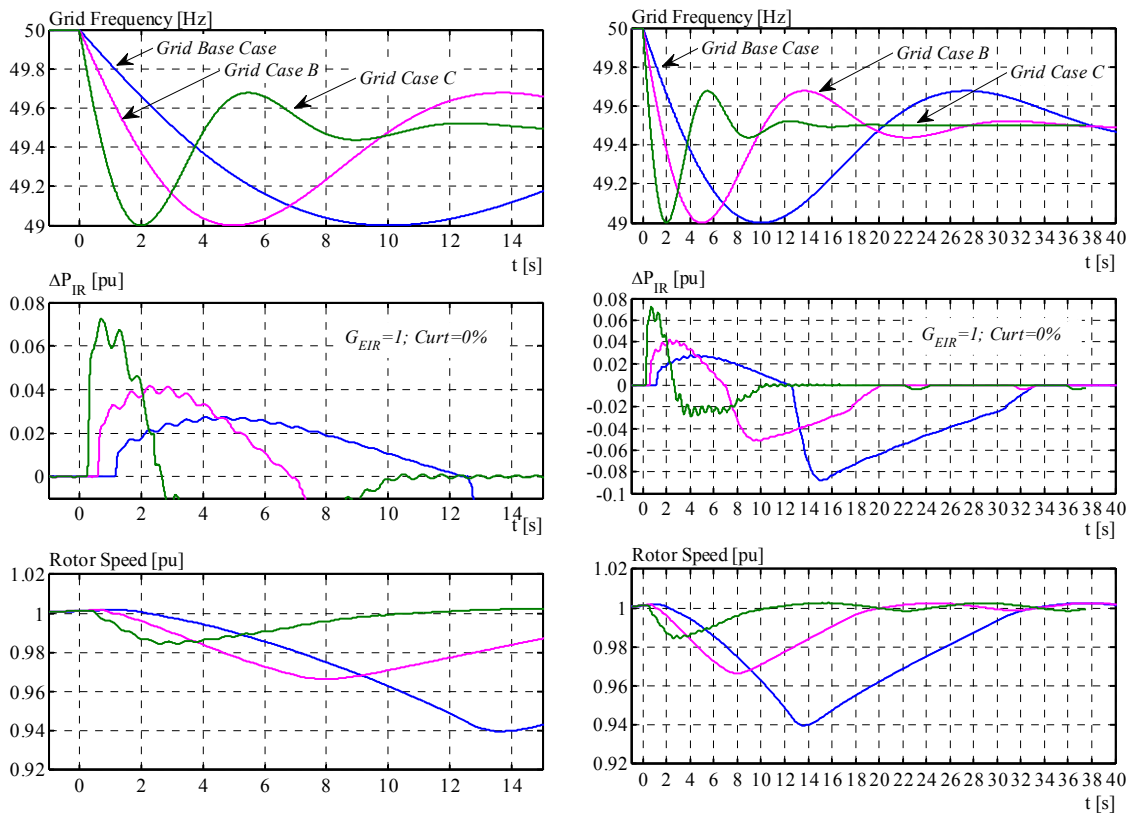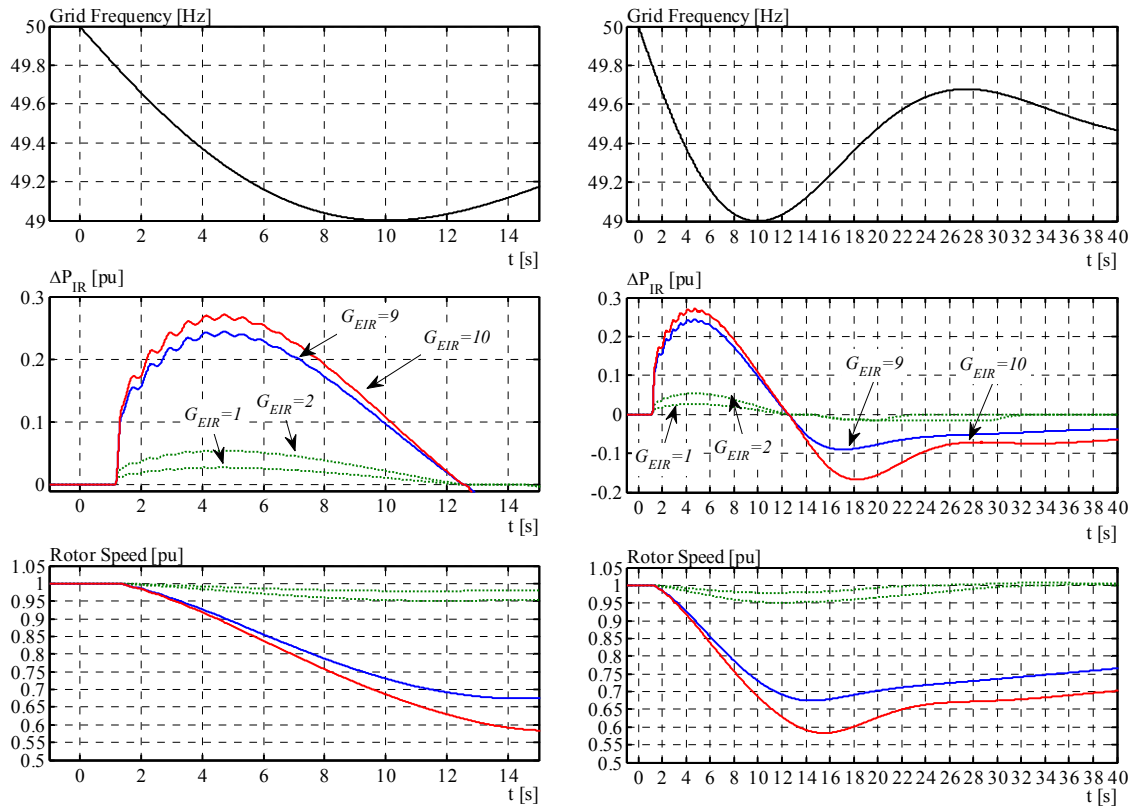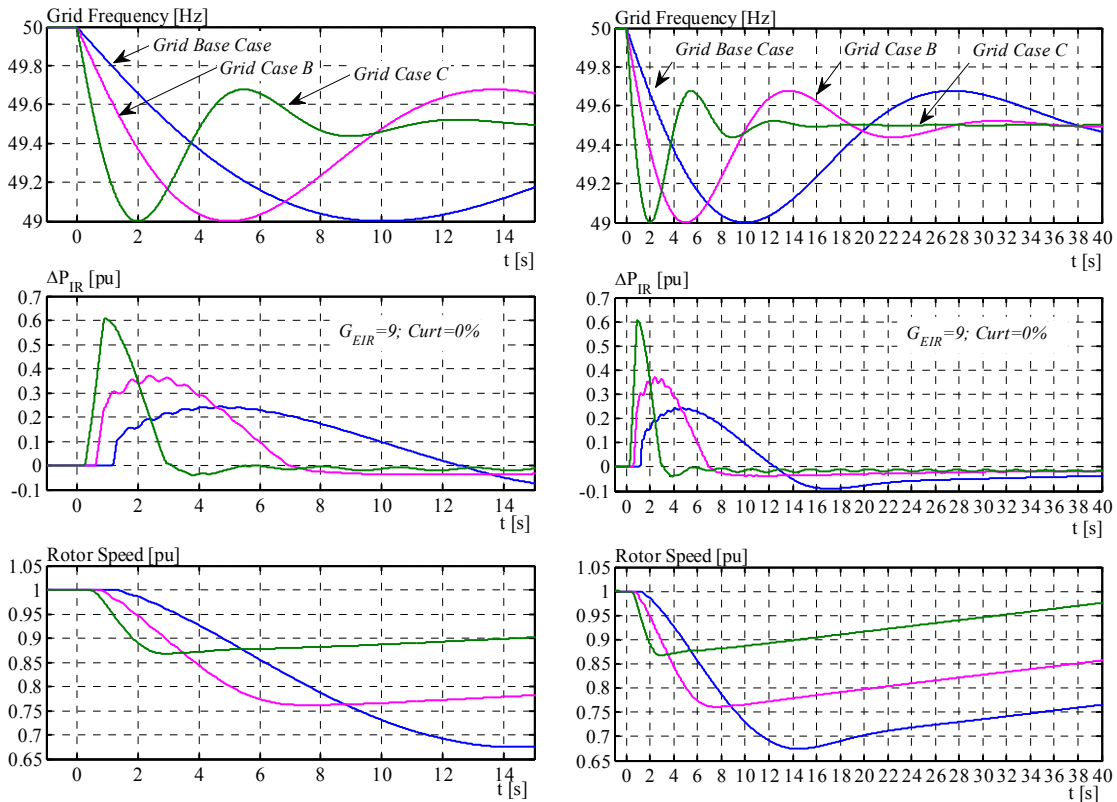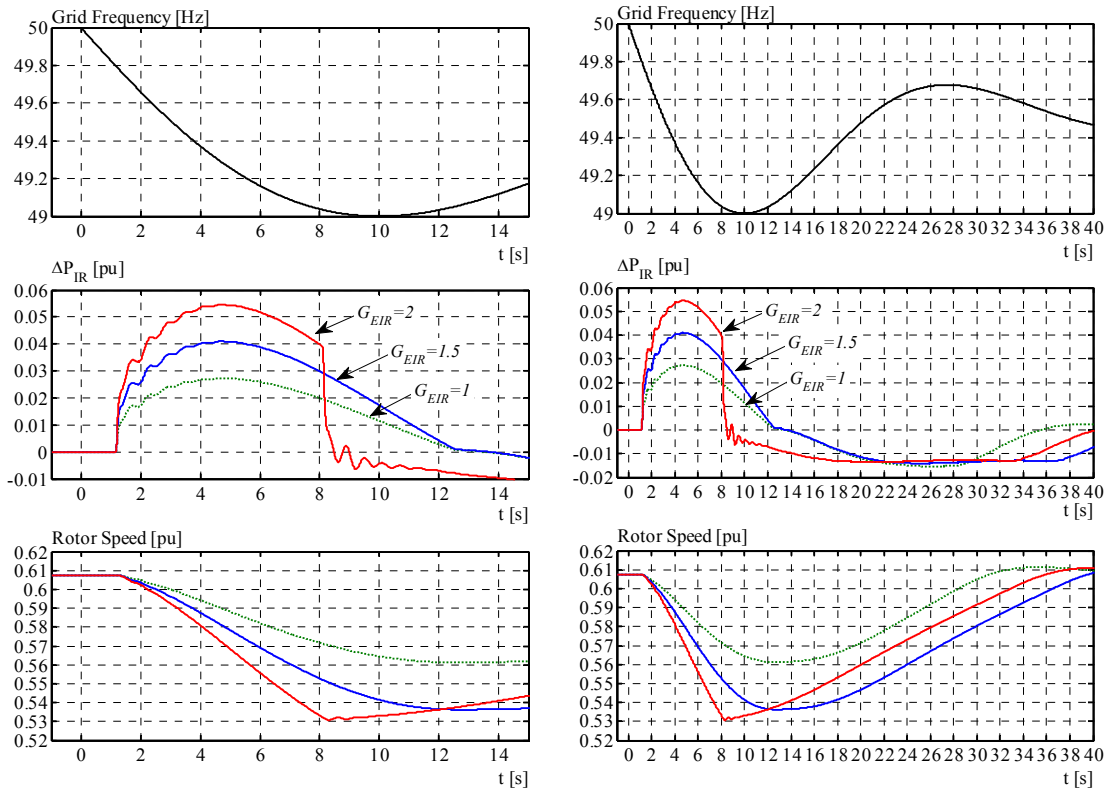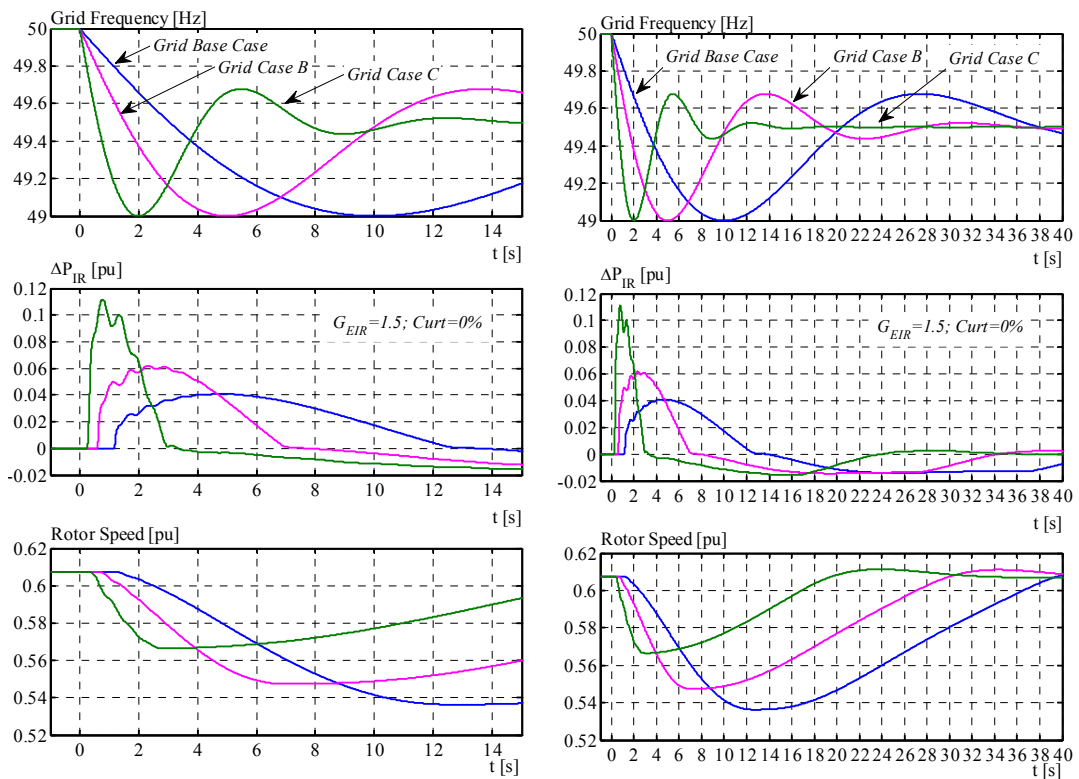

Figure 4-31: IR low wind speed, other grid cases. Powers as variations around P_0.

4.4.3 Real wind speed simulation results

The same kind of simulations done in Section 4.4.2 was performed again but using real wind speed data. Thus the performance of the calibrated IR controller is assessed for real wind speed conditions. The effectiveness of the gain scheduling was demonstrated in the previous section. Therefore, in this section, the gain scheduling G_{EIR} is given by the actual wind conditions and by the **Figure 4-19**. A look up table was built from this and incorporated as shown in **Figure 4-17.**

Real wind speed measurements from the anemometer of the modelled wind turbine have been used here. The same type of wind was used for model validation, obtaining a very good matching with the measured variables (see Section 3.4.2). The simulation results, such as power, rotational speed and pitch angle are compared with the respective measurements from the turbine, showing a good matching for the similar operating conditions. While the measured turbine was operating normally, the simulated turbine was performing inertial response.

The 3p effect is also enabled in the model. Therefore all the oscillations are seen in the results as well as in the measurements.

Very high wind speed

Figure 4-32 shows the simulation results for the 3 grid frequency cases using the measured wind speed as input to the turbine model. The wind oscillates between 1.1 pu and 1.3 pu. Values of G_{EIR} depends on wind speed, but it remains most of the time = 5 due to high wind.

The rotational speed and pitch angle are constantly changing due to wind speed, independently of IR actuation. It is difficult to say whether the change in rotational speed was caused by the wind or by the IR actuation.

Nevertheless, this wind speed situation provides a secure inertial response from an individual wind turbine, as long as the available power is higher than the overload limit: $P_{Ava} > P_{MaxOL}$.

Similarly to the observations in Section 4.4.2, the energy delivered during IR operation is *reduced* for *faster df/dt*, as can be deduced looking at the areas below the ΔP_{IR} curves for each grid frequency case.

High wind speed

Figure 4-33 shows the simulation results for the 3 grid frequency cases using the measured wind speed as input to the turbine model. The wind oscillates between 0.9 pu and

1.1 pu. Value of G_{EIR} depends on wind speed, changing considerably with the wind around this average.

The inertial power response is hidden among the normal wind power fluctuations. This is a very important observation, where we can see that *the inertial response of a single wind turbine is not meaningful for the power system.*

By looking at the rotational speeds, the impact of IR actuation becomes more evident compared with the previous wind case. There is no evident impact in pitch angle compared with the measurements in normal operation.

Rated wind speed

Figure 4-34 shows the simulation results for the 3 grid frequency cases using the measured wind speed as input to the turbine model. Exactly the same measured wind speed series used in the previous case has been used here, which oscillates between 0.9 pu and 1.1 pu. The value of G_{EIR} also changes equally.

In this case the grid event is taking place 7 seconds after the previous case. The intention is to show: i) how sensitive is the turbine response to wind changes when wind is around nominal and ii) how fluctuating the normal wind speed can be. Just few seconds time shift can change the turbine response. Observe the large power drop for the Base Case. Despite of having calibrated the gain scheduling for constant wind speed, the calibration effectiveness is reduced with real wind speed.

Similarly to the previous case, the inertial power response is hidden among the normal power fluctuations. This is a very important observation, where we can see that the IR actuation of a single wind turbine is not meaningful for the power system.

Rotor speed variations and power drop can be larger or smaller, depending on the wind.

Medium wind speed

Figure 4-35 shows the simulation results for the 3 grid frequency cases using the measured wind speed as input to the turbine model. The wind oscillates very little, between 0.8 pu and 0.9 pu. Value of G_{EIR} depends on wind speed.

The IR actuation is more evident in the active power and rotational speed. The pitch angle was already in optimal position. It can be noticed that at $t > 15$ s the simulated pitch angle remains in optimal position while the measured angle increases. This is because in the simulated case the turbine is performing recovery period (based on the algorithm described in Section 4.3.6), while the measured turbine experienced an increase in speed beyond the maximum, thus the pitch system is limiting maximum speed.

Low wind speed

Figure 4-36 shows the simulation results for the 3 grid frequency cases using the measured wind speed as input to the turbine model. The wind oscillates between 0.0.49 pu and 0.56 pu. Value of G_{EIR} are larger than in previous cases.

For all the cases, the $\Delta P_{Drop} < 2\%$ of rated (very small). The ΔP_{IR} is not *interrupted*, thanks to a suitable scheduling of G_{EIR}. Rotational speeds are higher than the minimum (0.53 pu). The IR power is larger than in the previous wind cases, only comparable with the case of very high wind.

Figure 4-32: Very high wind conditions. Measured wind speed as input. Comparison of simulated IR against turbine measurements under same wind, normal production.

Figure 4-33: High wind conditions. Measured wind speed as input. Comparison of simulated IR against turbine measurements under same wind, normal production.

Figure 4-34: Rated wind conditions. Measured wind speed as input. Comparison of simulated IR against turbine measurements under same wind, normal production.

Figure 4-35: Medium wind conditions. Measured wind speed as input. Comparison of simulated IR against turbine measurements under same wind, normal production.

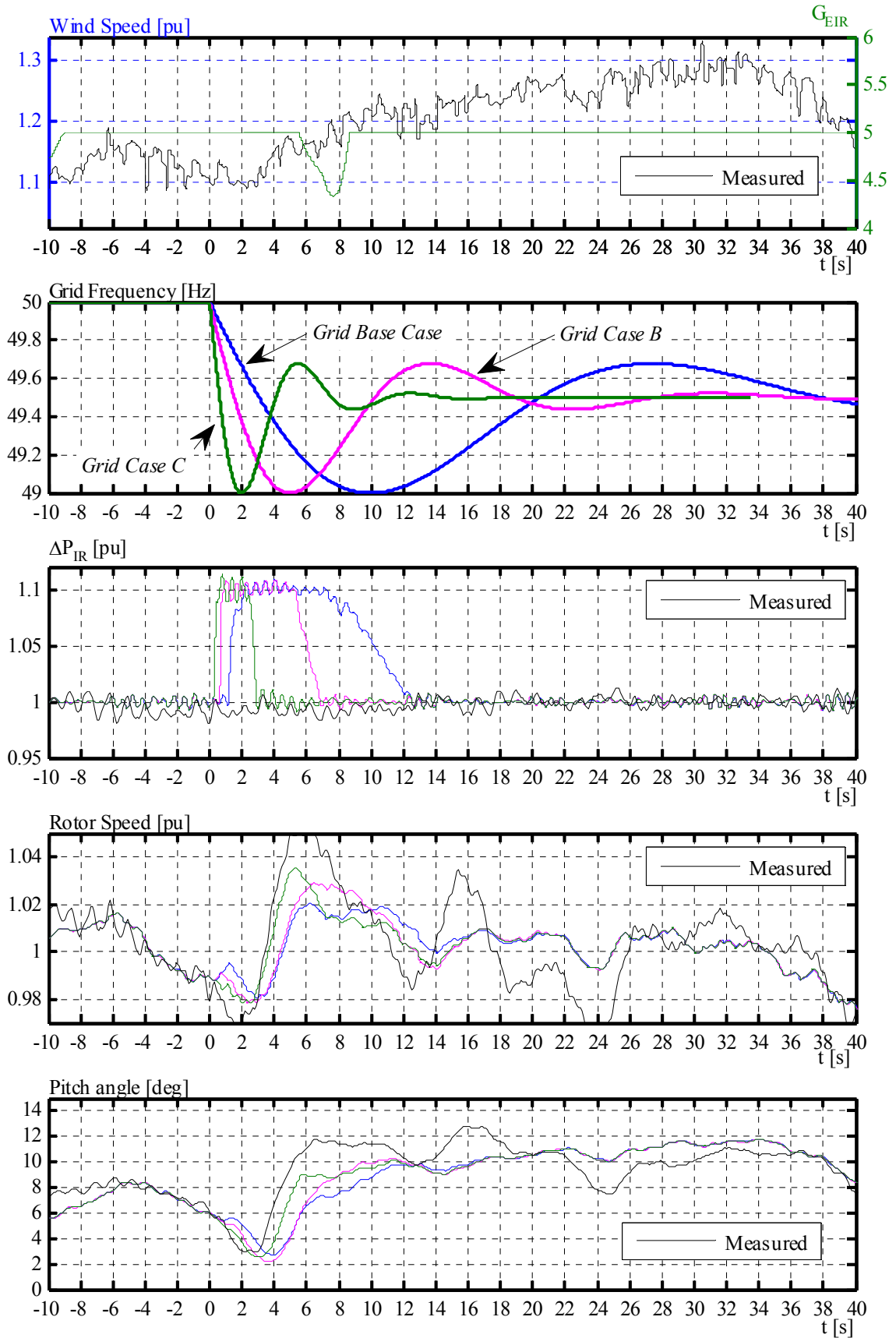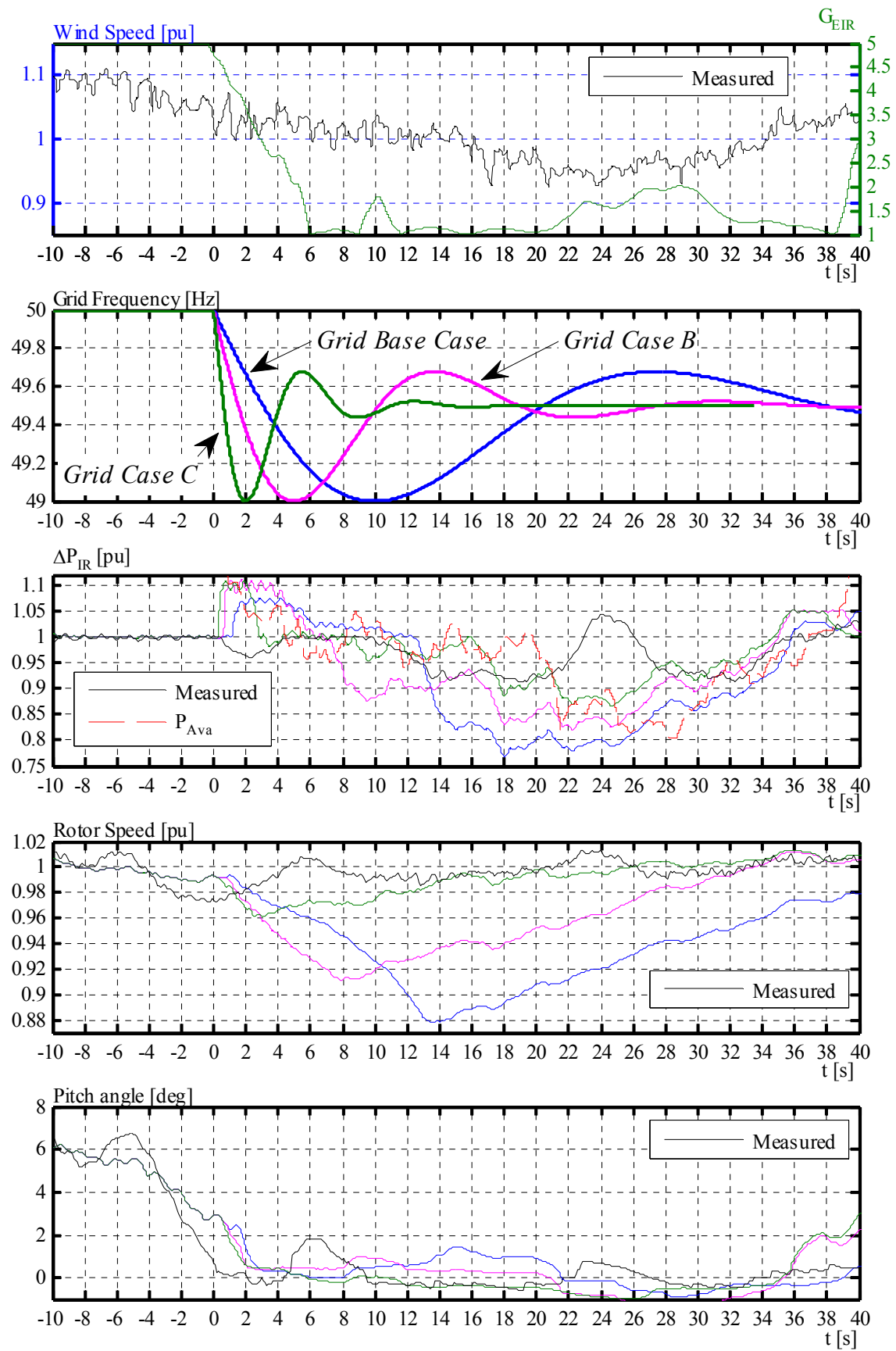**Figure 4-36:** Low wind conditions. Measured wind speed as input. Comparison of simulated IR against turbine measurements under same wind, normal production.
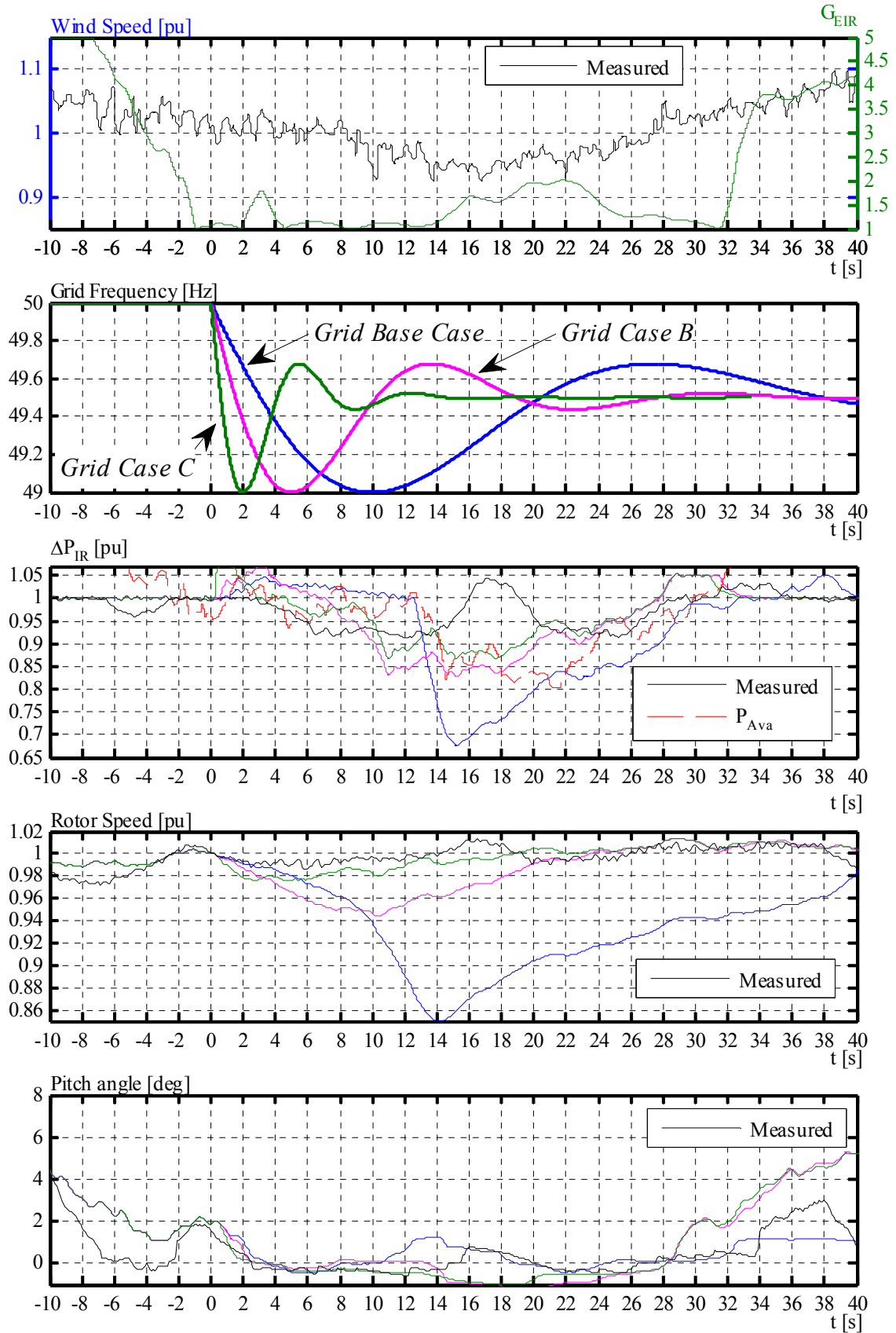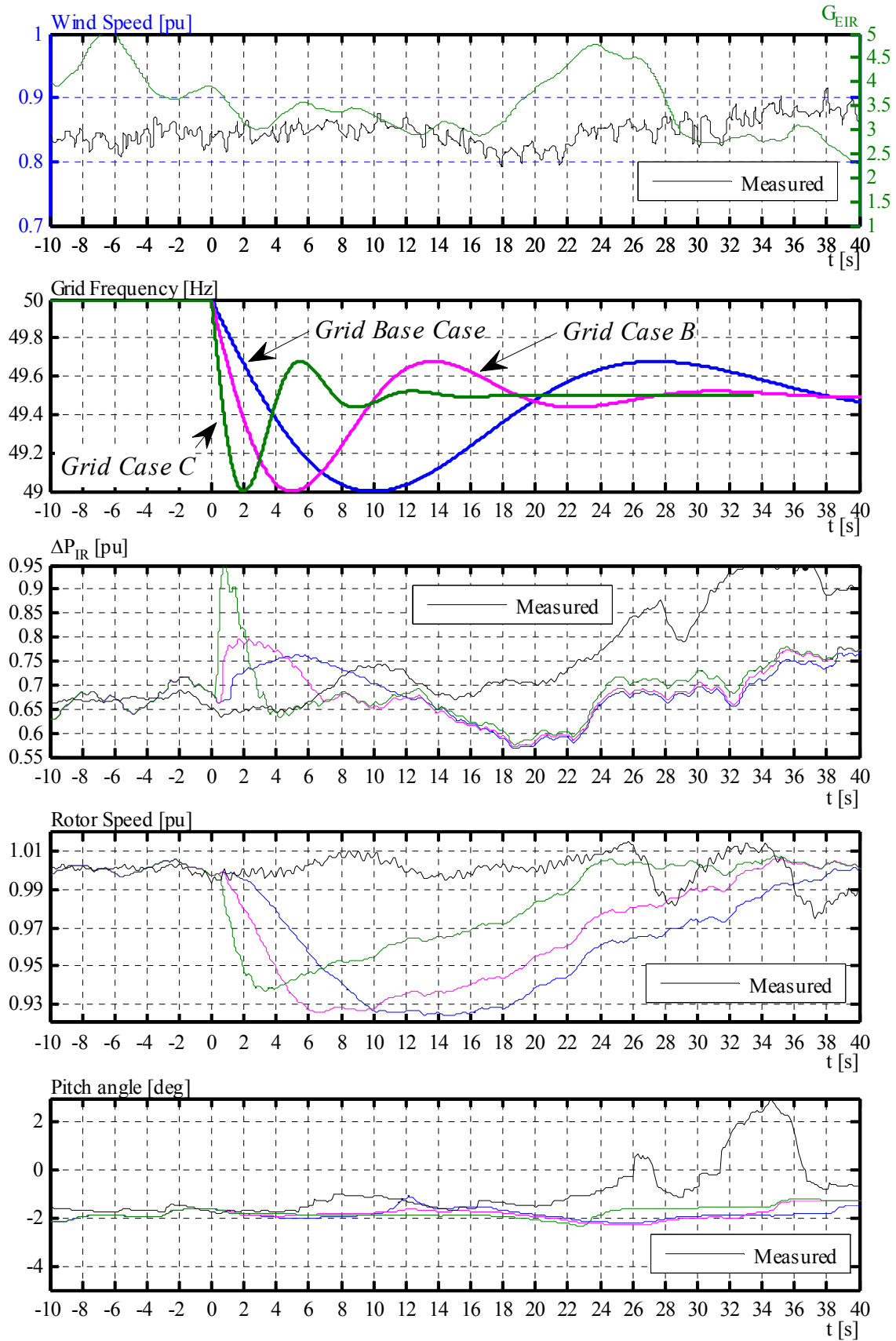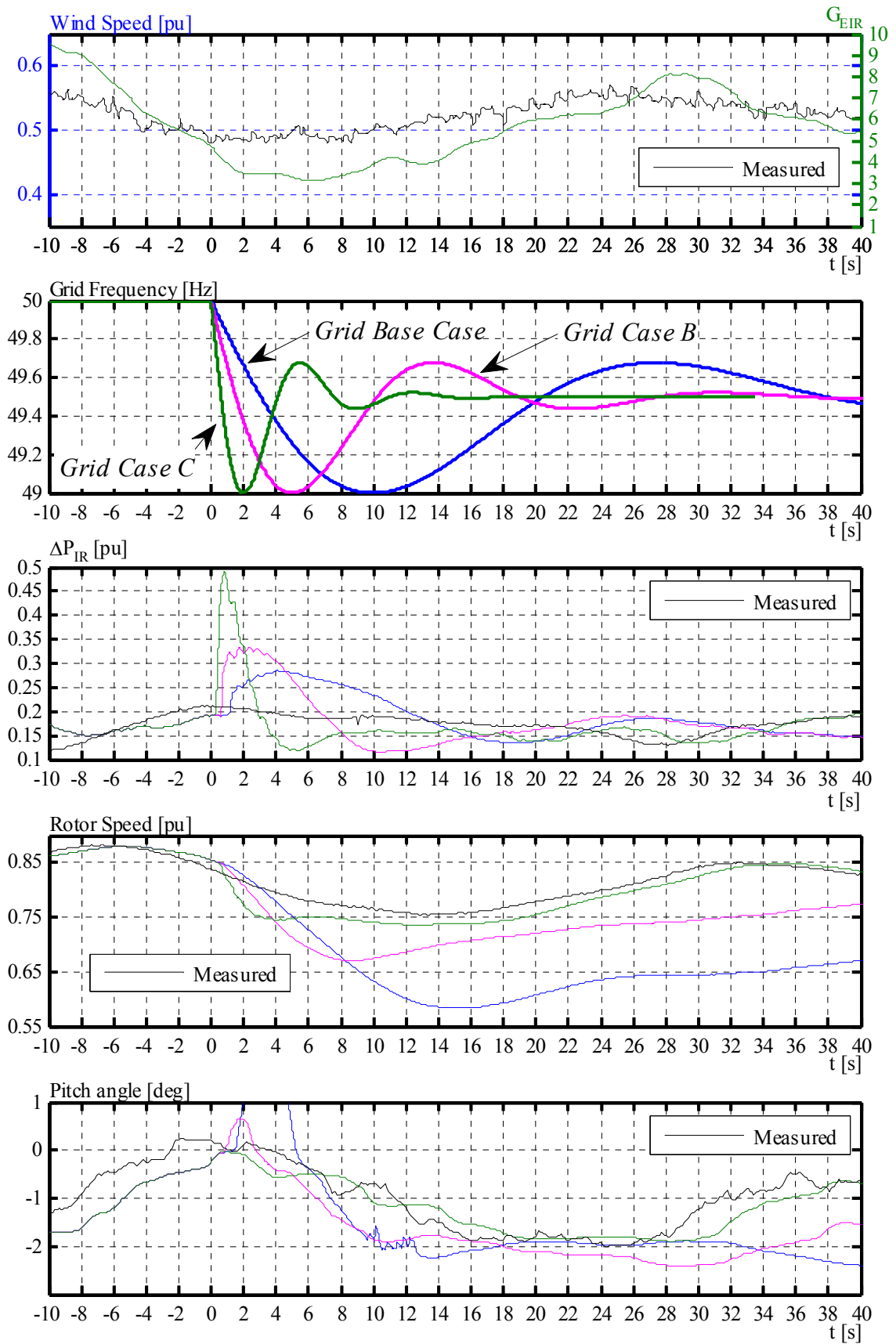
4.5 Capability of wind power plants for inertial response

Only the performance of the WPP and individual wind turbines outputs are analysed here, without considering the power system impact. It is interesting to know the behaviour of the WPP when its wind turbines perform IR with different (realistic) wind speed conditions and severe grid event.

The inertial response from wind power cannot be assessed just by considering the response of a single wind turbine. Inertial response from the WPP is the summation of individual responses from wind turbines. But individual responses are very different from each other, depending on local wind conditions. This was demonstrated in the previous section with real wind speed simulations. It was observed also that the worst grid event for inertial response is the one with a large and slow frequency deviation, i.e. the Base Case. This generates the largest power drop during recovery period.

Here, the capability of a WPP is assessed by accurate computational simulations. The Base Case grid event from Section 4.4.1, as worst case for WTGs inertial response, is repeated for different realistic wind speed scenarios. Simulated realistic wind speeds were utilized, which include also an approximation of wake effect in the wind plant.

4.5.1 Simulations set up

Complete wind farm with 25 wind turbines represented in detail, wind turbines controllers, transformers, cables, feeders, main plant transformer and transmission line was simulated. Individual realistic wind speeds, properly correlated, were used as input at each wind turbine. In order to get one step closer to the reality, this wind speed includes an approximation of wake effect. The modelling is described in Section 3.3.6.

The power of the WPP is very small compared to the power system; therefore any change in the WPP output will not impact in the system frequency and plant bus bar voltage. The internal voltages in the WPP vary. A very large load imbalance is produced in the system, which changes the grid frequency. Only the Base Case grid event from Section 4.4 was simulated.

Each wind turbine is equipped with individual IR controllers, with individual G_{EIR} scheduling based on **Figure 4-19**. Each wind turbine responds according to the locally measured grid frequency, based on the PLL described in 4.2.1.

Wind speed conditions

Wind speed conditions for the wind plant here are referred to the *free wind*. That is, the wind speed that would exist on place if no wind plant would exist. It has to be considered that due to the approximated wake effect, the effective wind speed reaching the inner wind turbines in the plant is lower. This is important to have in mind when analysing simulation results. When specifying e.g. a high wind condition, it is referred to the

free wind, but in fact, the wind turbines behind the first row will receive a lower wind reduced by a factor of ~1.17 (according to the modelling), therefore those wind turbines will be operating with an effective medium speed. Simulated wind conditions were:

- Very high wind
- High wind
- Rated wind
- Medium
- Low wind
- Very low wind

WTG fixed settings

Same settings than in Section 4.4.1. The reactive power set point in each WTG was Q_{ref} = 0. The total reactive power of the WPP was observed during the IR simulations.

4.5.2 Realistic wind speed simulation results. Open loop simulation

Figure 4-37 present results for very high wind conditions. Free wind of 1.6 pu. It can be seen how all the wind turbines respond equally and similarly to the single turbine case shown in **Figure 4-22**. The WPP output is limited to 10% overload.

Figure 4-38 present results for high wind conditions. Free wind of 1.26 pu. Due to the simulated wake effect, wind turbines in last row receive wind speed of ~1.05 pu. Different responses from the turbines are observed, each one in agreement with results shown in **Figure 4-32** to **Figure 4-34**. Some of the turbines experience a recovery period and large power drop, and other behaves just like in the previous wind case. However, the overall WPP response is better defined than individual turbines, with maximum and minimum of 10%.

Figure 4-39 present results for rated wind conditions. Free wind of 1.1 pu. Many wind turbines receive a wind of ~0.93 pu. The wind speed is fluctuating, therefore all the wind turbines experience a recovery period in different degrees. They behave in agreement with results shown in **Figure 4-33** to **Figure 4-35**. However, the overall WPP response is better defined than individual turbines, with maximum and minimum of 10%.

Figure 4-40 present results for medium wind conditions. Free wind of 1.0 pu. Most of the wind turbines receive a wind of ~0.85 pu. Turbines in first row receives wind fluctuating around rated value as shown in **Figure 4-26** and **Figure 4-34**, therefore they experience a larger power drop due to low aerodynamical efficiency. Nevertheless, these power drops are hidden in the overall WPP output. The total WPP output presents a power drop of ~12%, larger than previous cases. This indicates the need for curtailment

around rated wind speed if power drop during recovery period need to be reduced; or a better adjustment of the gain G_{EIR}, which would produce a lower IR output.

Figure 4-41 present results for low wind conditions. Free wind of 0.65 pu. Most of the wind turbines receive a wind of ~0.55 pu. Therefore they are running with maximum efficiency, meaning low power drops during inertial response. The responses of the wind turbines are similar to each other, in agreement with the results shown in **Figure 4-28**. The total WPP output presents a much better defined shape, with +15% power increase and -5% power drop.

Figure 4-42 present results for very low wind conditions. A very low wind speed situation was simulated. Simulation shows that even at very low wind speed in the WPP, some of the turbines may still be able to provide inertial response. Simulated free wind was 0.4 pu average, with most of the turbines receiving a mean wind of 0.35 pu, which is very close to the cut in value (0.3 pu). Observe that many wind turbines do not activate the IR functionality (which is according to the developed algorithm and respective settings). Only the turbines in the first row perform inertial response, as they receive enough wind speed. Observe also that some of the wind turbines *interrupt* the IR functionality due to minimum rotational speed. This is due to a sudden decrease in local wind speed, reducing the mechanical power. The interruptions, as they are few, are hidden in the total WPP output. Here we have to remember the kind of modelling of the WPP with an approximation of wake effect. In the reality, more wind turbines may receive enough wind speed (which depends also on the wind direction). Nevertheless, the simulated response here is believed to be representative.
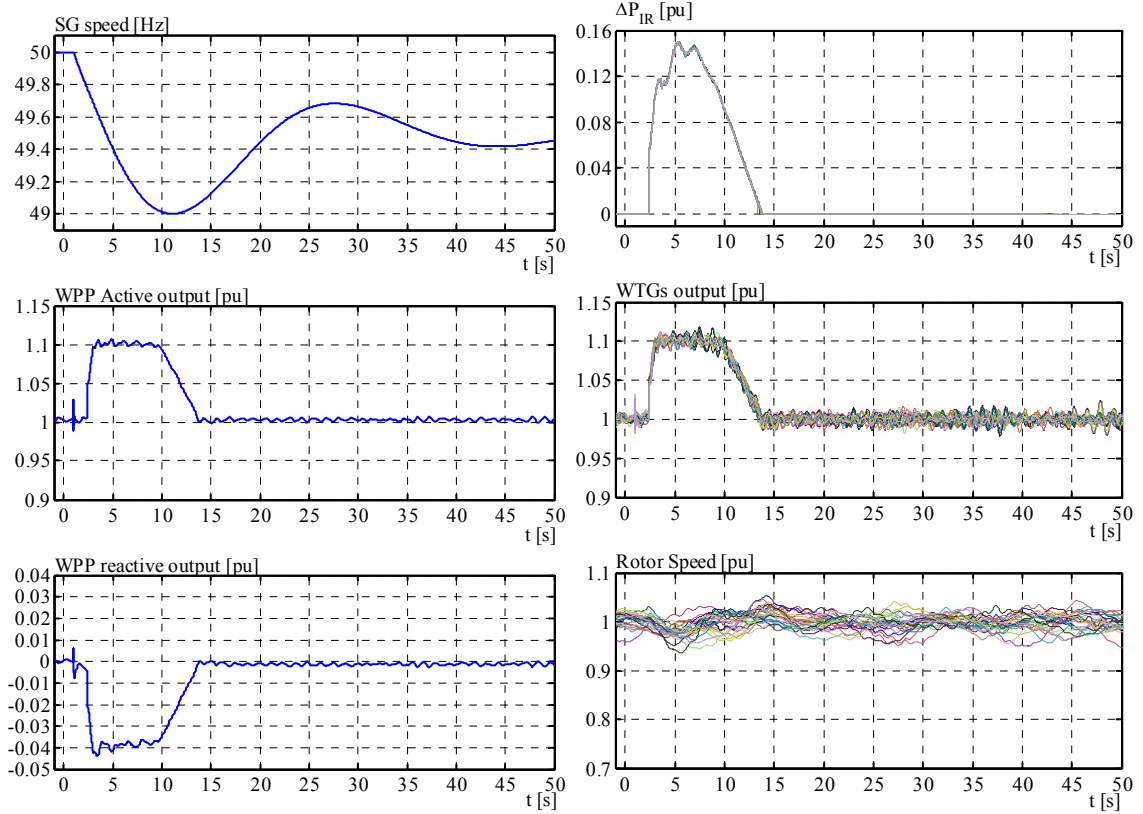
Figure 4-37: Very high, realistic wind. IR in a wind power plant. Frequency base case.
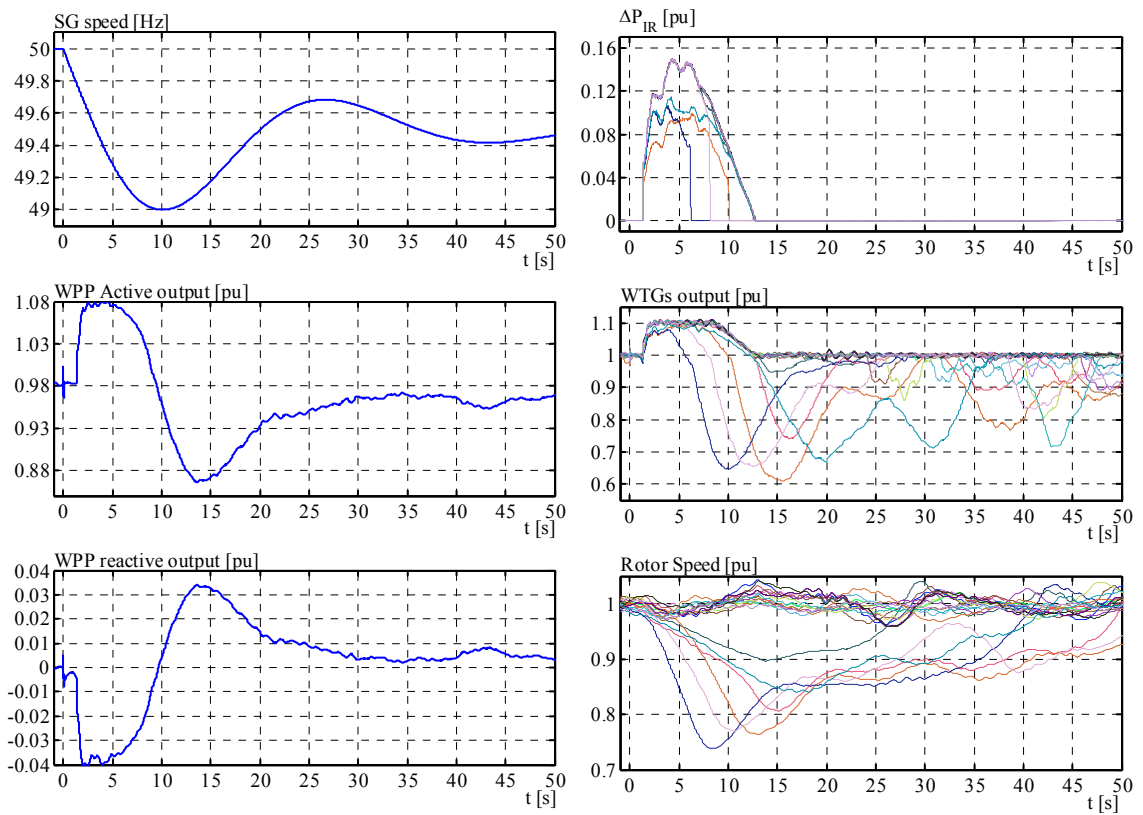
Figure 4-38: High, realistic wind. IR in a wind power plant. Frequency base case.
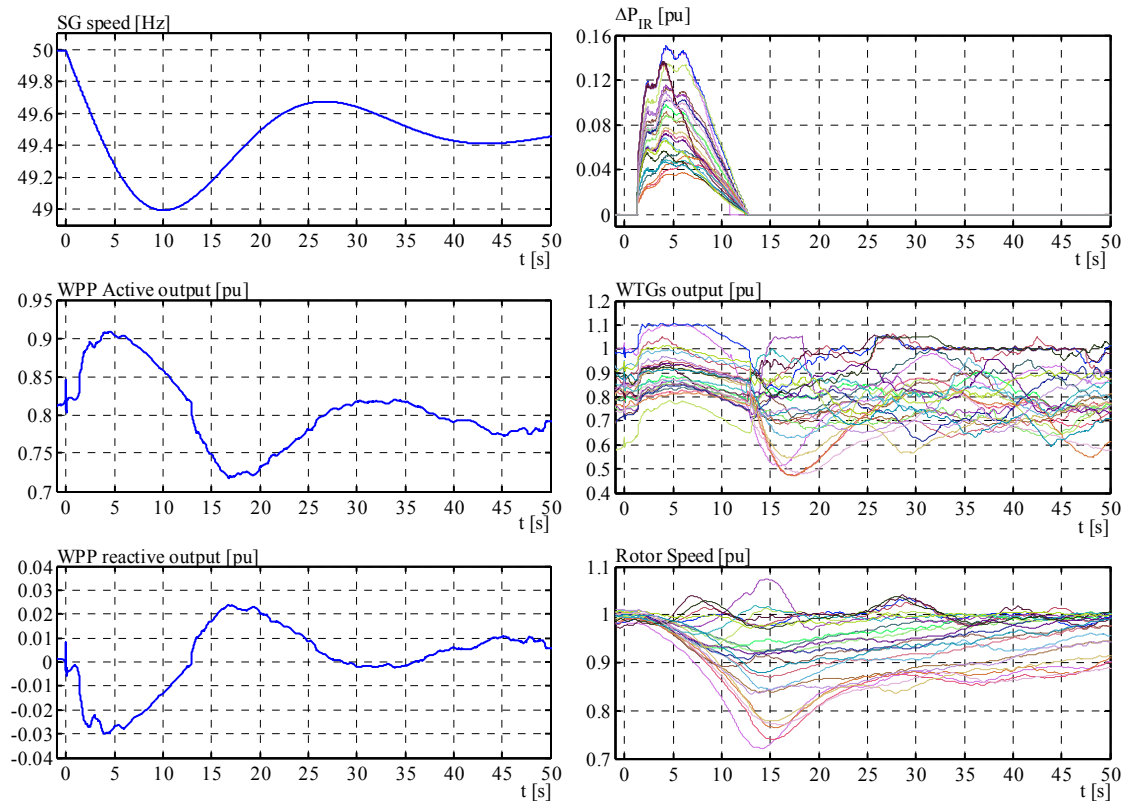
Figure 4-39: Rated, realistic wind. IR in a wind power plant. Frequency base case.
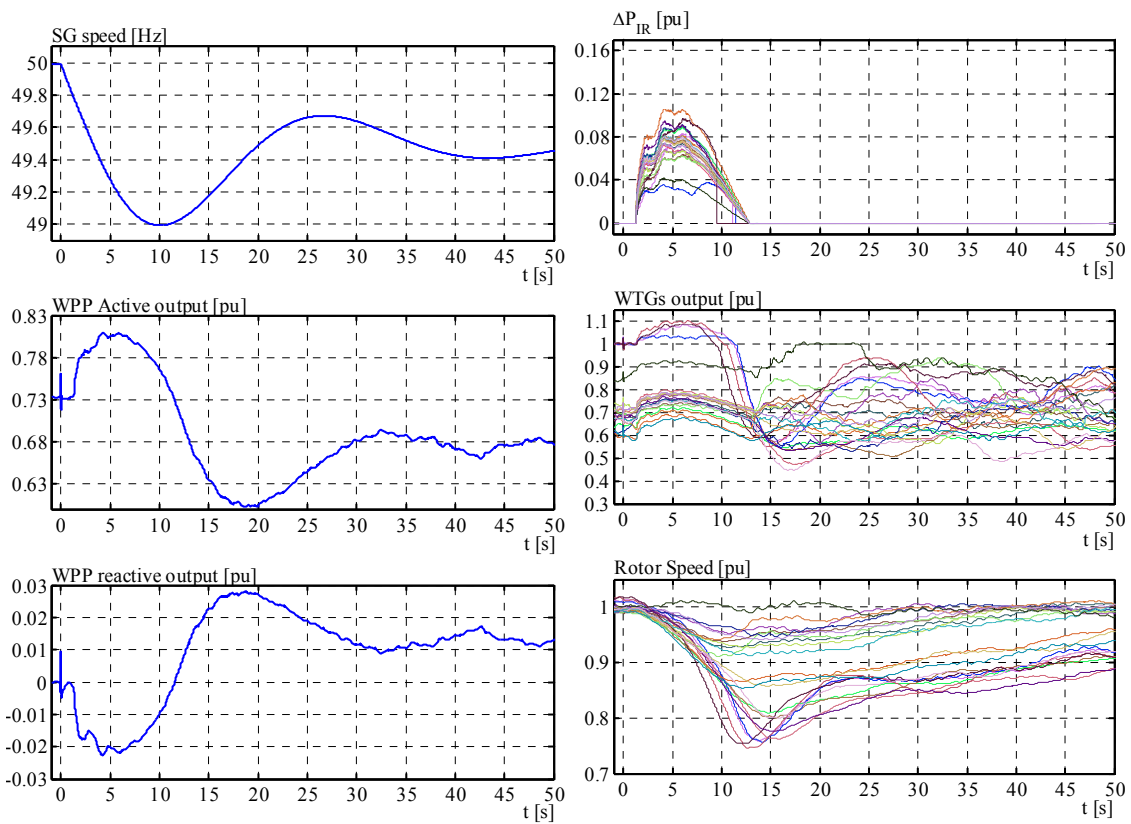
Figure 4-40: Medium, realistic wind. IR in a wind power plant. Frequency base case.
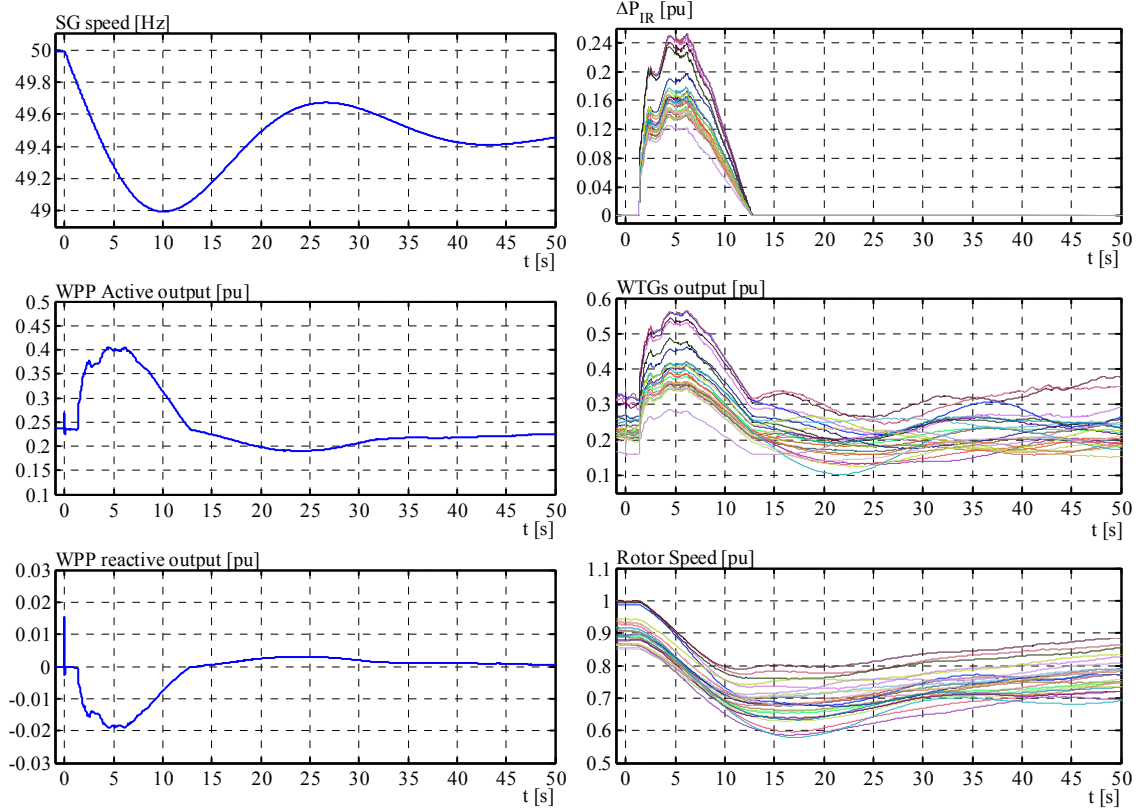
Figure 4-41: Low, realistic wind. IR in a wind power plant. Frequency base case.
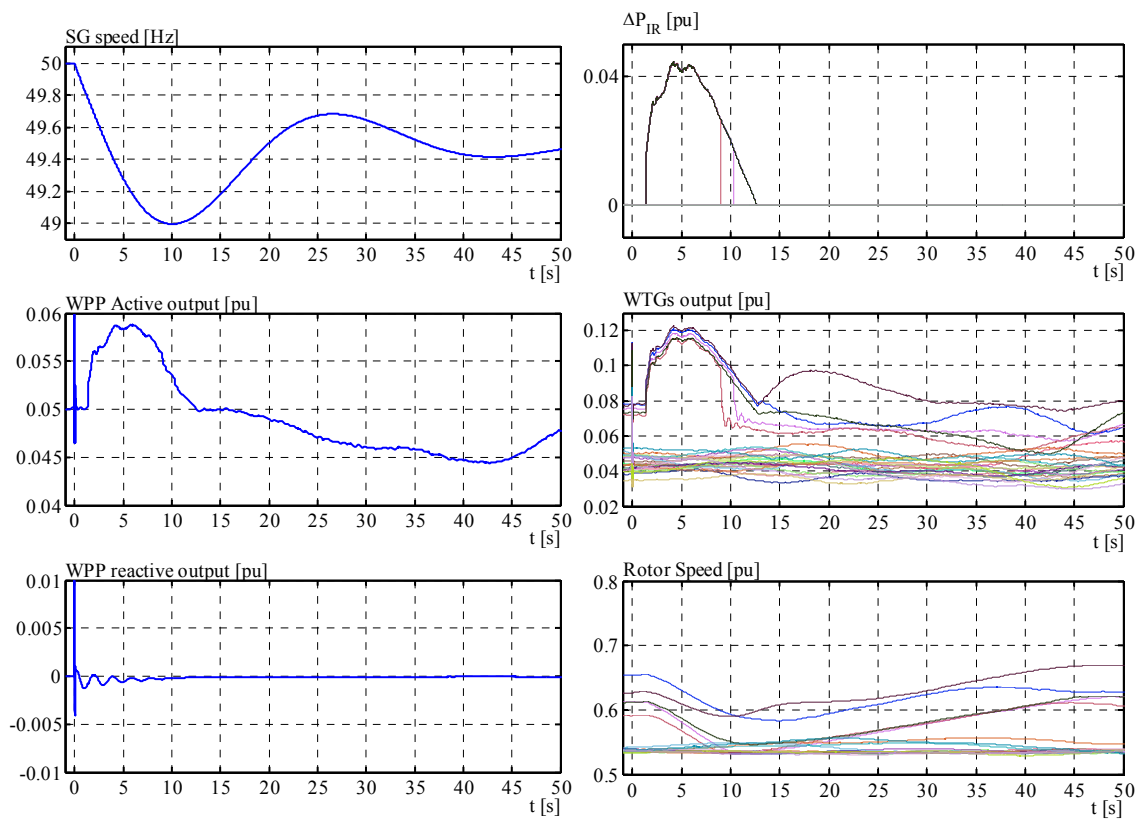
Figure 4-42: Very low, realistic wind. IR in a wind power plant. Frequency base case.

4.5.3 Results comparisons

The results of simulated cases in Section 4.5.2 are summarized here. **Figure 4-43** shows the values of G_{EIR} in each wind turbine for each wind speed case. Figure 4-44 left shows the WPP inertial response for each simulated case, and Figure 4-44 the variations in active and reactive power around the pre event value (the pre event reactive power was $Q_{ref} = 0$).
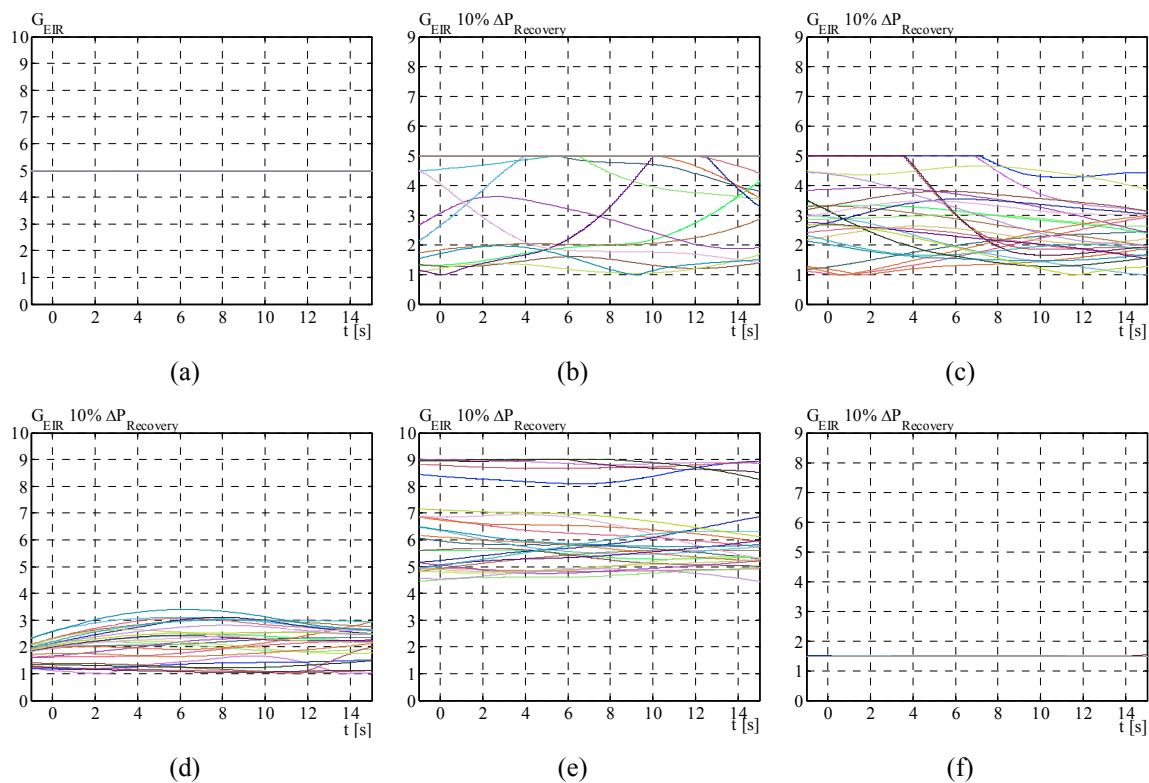
Figure 4-43: Variation of individual IR gains, G_{EIR}, for different wind speed conditions in the WPP: (a) very high wind speed, (b) high wind speed, (c) around rated wind speed, (d) medium wind speed, (e) low wind speed and (f) very low wind speed.
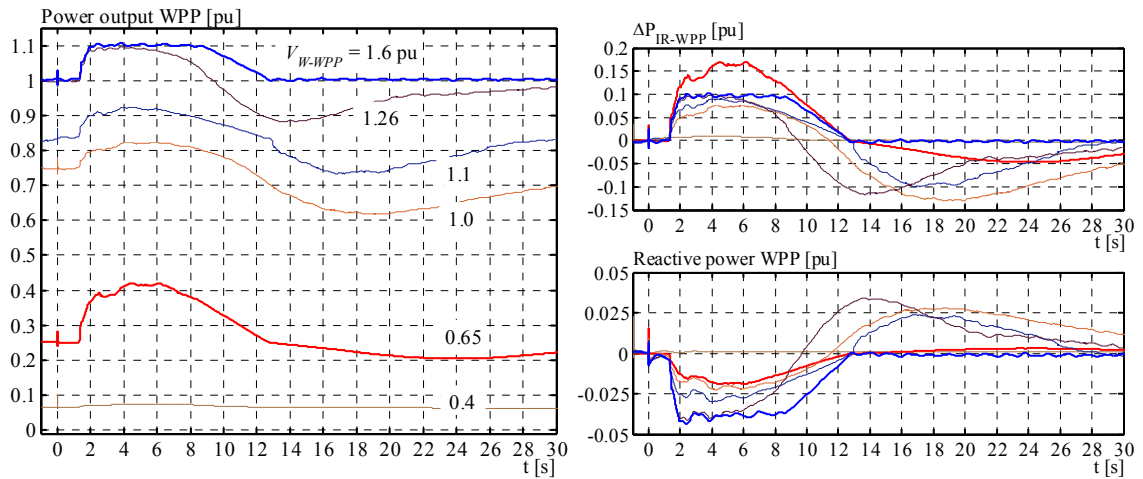
Figure 4-44: Response outputs of inertial response in a wind power plant for different wind speed conditions.

4.6 Conclusions

Inertial response from wind turbines, or wind power plants, is an option for providing dynamic support to the system in high wind power penetration scenarios. This chapter has studied the capability of variable speed wind turbines and wind power plants for providing inertial response. A suitable control algorithm has also been developed.

The study has considered most of the technical limitations in wind turbines. Results have shown that wind turbines are not abnormally stressed during this operation if suitable overloading limitations are imposed. The capability for providing extra energy for grid stabilization is strongly dependent on wind speed and curtailment (deloading) conditions. The capability is largely reduced for wind speeds around nominal and close to the cut in speed. At rated wind speed, large power drop is experienced during recovery period due to the drop in aerodynamical efficiency. This is a drawback for the power system in terms of frequency stability, but it can be largely improved when at least 2.5% to 3% curtailment is applied around rated wind speed. For medium or very high wind speeds, the capability increases without need of curtailment.

A control algorithm for wind turbines for providing inertial response has been developed. Such algorithm not only generates a suitable stabilizing power waveform but also minimizes the impact on the gird during recovery period. The developed control algorithm takes into account the previously studied capability of the wind turbine, which is done through a gain scheduling based on operational conditions. This gain scheduling provides the largest amount of energy considering limitations such as power drop during recovery, power overload, torque overload and minimum rotor speed. A state machine has been implemented which controls the operational periods.

Simulations using accurate wind turbine model, fed with real wind speed data, have shown that single turbine inertial response output is in the same order of magnitude than normal variations due to wind speed fluctuations. Thus, inertial response from wind power cannot be assessed just by observing a single wind turbine.

Simulations of inertial response from a wind power plant, composed of several individual wind turbines, have shown a more "clean" output waveform as all the wind turbines boost the power simultaneously. Due to the differences in local wind speed, there is a diversification of inertial responses inside the wind plant, during the boosting period as well as during the recovery period, with different values of power drop. Nevertheless, the total power output of the wind plant is more "homogeneous" and, to some degree, less dependent on wind speed, compared to an individual wind turbine.

Wind power is able to provide valuable inertial response when combining a large number of wind turbines in a wind plant. This functionality needs to be coordinated with the primary frequency response, which is developed in Chapter 5 and coordinated in Chapter 6.

5
ACTIVE POWER AND FREQUENCY CONTROL

This chapter is dedicated to the development of control architecture for wind power generation systems. The main objective of this architecture is to manage the variability of the generated wind power in the power system in order to reduce the impact on the grid frequency and to provide with suitable frequency regulation service when required.

Firstly, the control objectives are defined, and then the control architecture is proposed based on that. The proposed architecture contains different "functionalities", which are developed along the chapter. These functionalities are: Wind Power Fluctuations Limitation, Wind Power Tracking, Frequency Control, Active Power Control and Dispatching of Power References.

The proposed architecture is designed for implementation at either power system level or lower levels, i.e. cluster level, wind power plant level or wind turbine level. The implementation at different levels presents different performances.

The performance of the developed control architecture and the interaction between controlled wind power generation and conventional power plants are proven through accurate computational simulations of a small real power system. The simulation results are compared with the measurements carried out on this power system under un-controlled operation of wind power, which was presented in Section 2.5.

5.1 Introduction

As discussed in Chapter 2, standard frequency control mechanisms in power systems can accommodate fluctuating wind power only to a certain level. The maximum wind penetration depends on each power system and its specific operation, but many studies have estimated, in general terms, a maximum instantaneous penetration of WP_I ~25% [69] without need of changing the basic methods of system operation.
If the wind penetration level goes beyond the present limitations, different ways of managing the wind power production are necessary. Additional requirements for the wind power production should be addressed, such as upward gradient limits, power output limitation, fast frequency response and fast dispatching of set-points.

As the impact of the power balance in the system depends on the combination of the overall consumption and generation, a *coordination* of the overall wind power production in the system may improve the regulation services from wind power. At the same time, that coordination will allow to maintain the overall wind generation yield to an optimal. This coordination should operate as an integrated part of the central control in the power system.

In the previous Section 2.6, requirements for the overall wind power generation in the power system were elaborated for this work. Those requirements are: i) constraint on the rate of change of wind power production at system level; ii) Limitation on the amount of wind power fluctuations at system level; iii) Power reserve and frequency response at system level.

Taking advantage of the controllability of modern wind power plant, suitable control architecture is developed and studied in this chapter.

5.2 Control objectives and basic architecture

In this section, the control objectives for active power and frequency control of wind power, and the control architecture for their achievement are presented.

5.2.1 Control objectives

Based on the requirements for wind power generation proposed for this work in Section 2.6, the following control objectives are established:

1. Constraint on the amount of wind power fluctuations at system level: Such constraint magnitude shall be *based* on at least the actual system stiffness, K_{sys} (MW/Hz). By doing this, the grid frequency fluctuations caused by wind power fluctuations at system level remain constrained to a limited band. Thus, as the wind power fluctuations at system level remain constrained, the impact on the normal regulation reserves, RR, can be reduced, or the RR can be better determined for the market (as part of the SRM, Section 2.1.5).

2. Constraint on the rate of change of average wind power production at system level: This allows the standard load balancing mechanisms, such as Secondary Frequency Control or Regulating Market, to adjust conventional generation in proper time, maintaining the average grid frequency around the nominal. This is applicable only to production increases, since decreases in wind power income cannot be controlled.

3. Frequency response at system level to high-frequency events: As conventional plants are displaced, wind power should contribute to the SRM (i.e. RR + DR, Section 2.1.5). Additionally, as high-frequencies can also be produced by the wind power variation itself, the wind power response to high-frequencies provides a self-regulating mechanism.

4. Frequency response at system level to low-frequency events: Similarly to the previous. Low-frequencies can also be produced by the wind power variation itself; therefore the wind power response to low-frequencies caused by wind provides a self-regulating mechanism. Obviously, the WPG should be operated with an amount of power *reserve*.

5. Wind power production as close to the optimal as possible: It is considering the objectives above. Individual set points to wind turbines and wind plants in the system should be manipulated accordingly.

6. Standard control features should not be affected: Wind plant operator should be allowed to control individual active powers from wind turbines or wind plants.

The objective 1 above could also consider constraints on power flows in transmission lines, e.g. tie-lines between areas, but these issues were not covered in this work.

Here, the controllability of the wind power system is largely influenced by the following factors:

- Available power (availability of wind).
- Ratings of components.
- Maximum and minimum external set point for wind turbines.
- Maximum and minimum ramp rates for power set point.
- External constraint (e.g. individual command from the operator to the wind turbine or wind plant).
- Communication delay (between turbines and higher level controllers).

Other factors that could be considered as limiters for controllability, but not covered in this work are:

- Noise reduction.
- Derating due to machine protection.

5.2.2 Control architecture

Based on the control objectives established above, three main control functionalities are identified, interacting as shown in **Figure 5-1** and described as follows:

1. Fluctuations Limitation and Power Reference (FL & PR): Performs control objectives 1 & 2. I.e. determines the limitation in total wind power fluctuations and limits the rate of change of total power. It also allocates the power reserve for frequency response functionality.

2. Frequency Response (FR): Performs control objectives 3 & 4. I.e. provides suitable frequency response to frequency deviations.

3. Power Control Loop and Dispatching (PCtrl & D): Performs control objectives 5 & 6. I.e. controls the power production at a measurement point (if any) and distributes set points to lower level actuators (which may be wind turbines, wind

plants or wind clusters as explained later) according to local availability and variability of wind power. It also provides individual control to dispatched actuators.
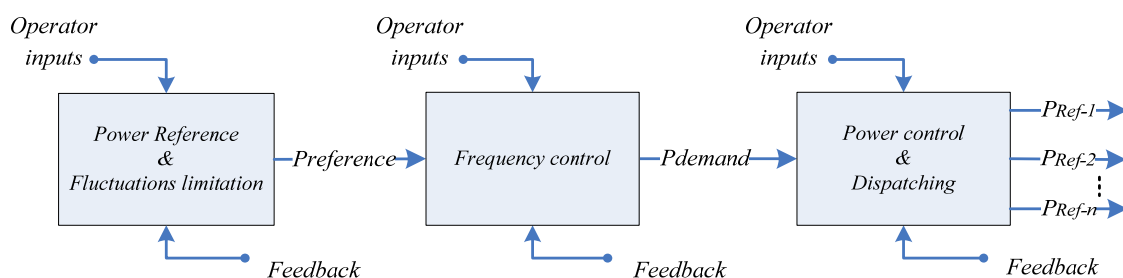
Figure 5-1: Main control functionalities for wind power production

These three control functionalities may be implemented at four different architectural levels in the power system, depending on the desired degree of controllability of wind power production in the power system. These levels are:

1. Wind turbine level: Individual WTG application, where the Dispatcher is not necessary. See
2. **Figure 5-2**.
3. Wind power plant level: Individual WPP application, where the power is controlled at the PCC and the Dispatcher is sending references to each WTG inside the wind plant. See **Figure 5-3**.
4. Cluster level: A group of WPPs in a geographical zone being controlled, where there is no PCC (no physical point for a single PCtrl.) and the Dispatcher is sending references to each WPP in the cluster. At the same time, each WPP contains PCtrl & D functionalities. See **Figure 5-4**.
5. Power system level: Centralized application, where the Dispatcher is sending references to each cluster or to all wind power plants in the power system. See **Figure 5-4**. Each sub-level containing respective dispatchers.

Observe that the FL & PR and the FR functionalities are always located in the upper level of the implementation (except for WTG level). There is a Dispatcher functionality for levels 2, 3 & 4. The PCtrl. Functionality is only used for WPP output control.

In the next section each one of these three control functionalities is developed independently of the architectural level application. Later, the performance when applying in different architectural levels will be simulated, analysed and compared.
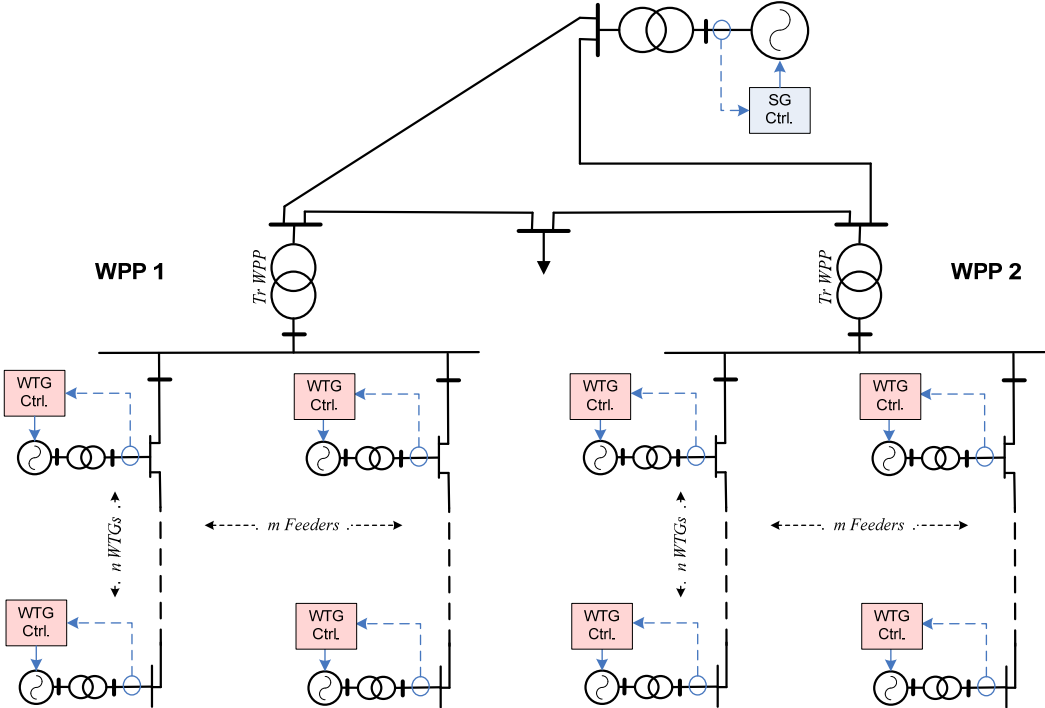
Figure 5-2: Wind turbine control level. Example of two wind power plants in a simplified power system representation.
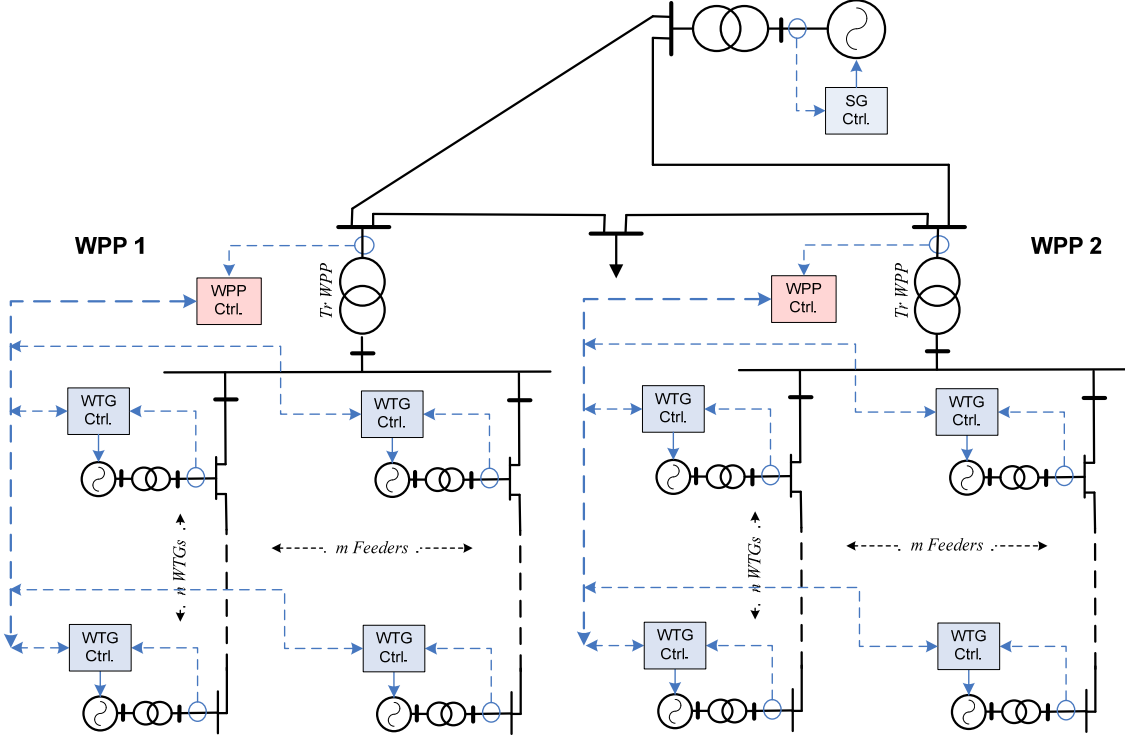
Figure 5-3: Wind power plant control level. Example of two wind power plants in a simplified power system representation.
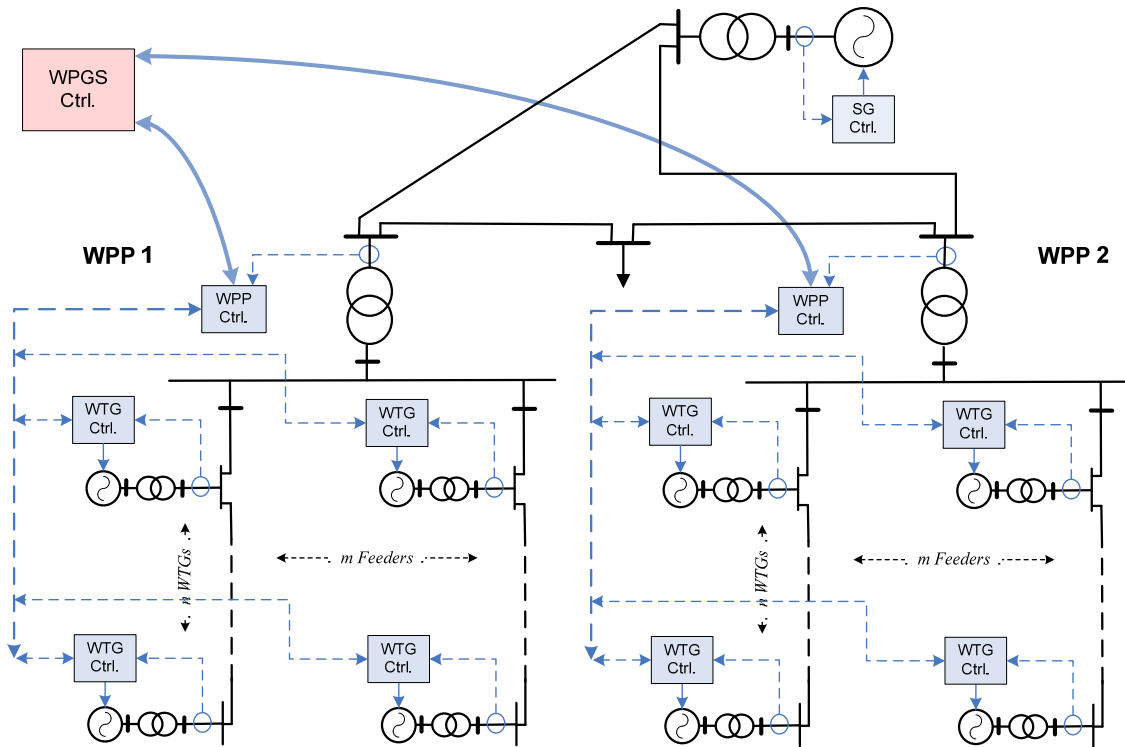
Figure 5-4: Cluster or Power system control level. Example of two wind power plants in a simplified power system representation.

5.3 Control development

In this section, the four control functionalities, interacting as indicated in **Figure 5-5**, are developed. These functionalities can be implemented at different levels, as studied later.
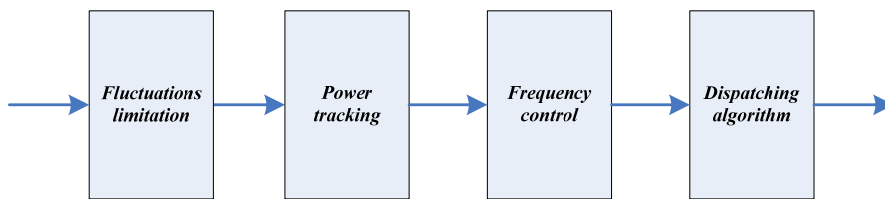
Figure 5-5: Developed functionalities

5.3.1 Fluctuations limitation

As discussed in Sections 2.3 and 2.6, in systems with high wind power penetration, the overall wind power fluctuations at system level would need to be *limited* in order to reduce RR requirements and to maintain grid frequency fluctuations inside a limited band. To reach this through control actions, the amount of *allowed* wind power fluctuation at *system* level, $\Delta P_{WindFluct}$, must be known.

To determine $\Delta P_{WindFluct}$, an "acceptable" grid *frequency fluctuation* produced by wind power at system level, $\Delta F_{WindFluct}$, must be *specified*. For simplification in the study, $\Delta F_{WindFluct}$ is firstly considered as a deviation from the nominal f_0. Therefore:

$$\Delta P_{WindFluct} = K_{sys} \cdot \Delta F_{WindFluct} \text{,} \qquad\qquad (5.1)$$

where $\Delta P_{WindFluct}$ is the *allowed* wind power fluctuation at system level in MW, K_{sys} is the system *stiffness* (or system regulation capacity) in MW/Hz and $\Delta F_{WindFluct}$ is in Hz. In (5.1) only the grid frequency is used to determine the limitation of wind power fluctuations. But other restrictions could be added to the right side of (5.1), such as power flow constraints, voltage limits, etc.

If at a given time the wind power production at system level is P_{Wind0} and the frequency is f_0, then the allowed maximum instantaneous wind power in the system, $P_{WindMax}$ –as a consequence of fluctuation– is:

$$P_{WindMax} = P_{Wind\,0} + \Delta P_{WindFluct} = P_{Wind\,0} + K_{sys} \cdot \Delta F_{WindFluct} \qquad\qquad (5.2)$$

By knowing or estimating the K_{sys} it is possible to *limit* the overall wind power fluctuations for the actual system regulation characteristics. It is important to notice that the K_{sys} is continuously varying due to changes in generation and demand [72]. The K_{sys} is largely influenced by the amount of RR and DR, which in many systems are managed by the regulation market. In this work it is considered a known and constant K_{sys} for a limited period of time.

Figure 5-6 left shows simulation results comparing the effect of overall $P_{WindMax}$ limitation on the grid frequency. The power system PS2 described in Section 3.3.3 was used (islanded system with a low $K_{sys} \approx 0.4$ pu/Hz, based on SG1 nominal power). The wind turbines productions were controlled in order to achieve this power limitation at system level. The control for this will be described later in this chapter. A value of $\Delta F_{WindFluct} = 0.1$ Hz was chosen for this example, which determines a $\Delta P_{WindFluct} = 0.04$ pu. Due to its low K_{sys}, this wind power limitation effect is easily visualized in the PS2.

The eq. (5.2) and **Figure 5-6** left describe the limitation on *positive* wind power variations. What happen when the wind power suddenly *decreases* below P_{Wind0} by an amount larger than $\Delta P_{WindFluct}$? In this case, if the K_{sys} does not increase, the grid frequency falls below f_0 by an amount larger than $\Delta F_{WindFluct}$ (as seen in the measurements in Section 2.5.5.2). Obviously we cannot impose a *lower* limitation for natural wind power decreases, thus the grid frequency fluctuations cannot be kept inside limits solely by (5.2).
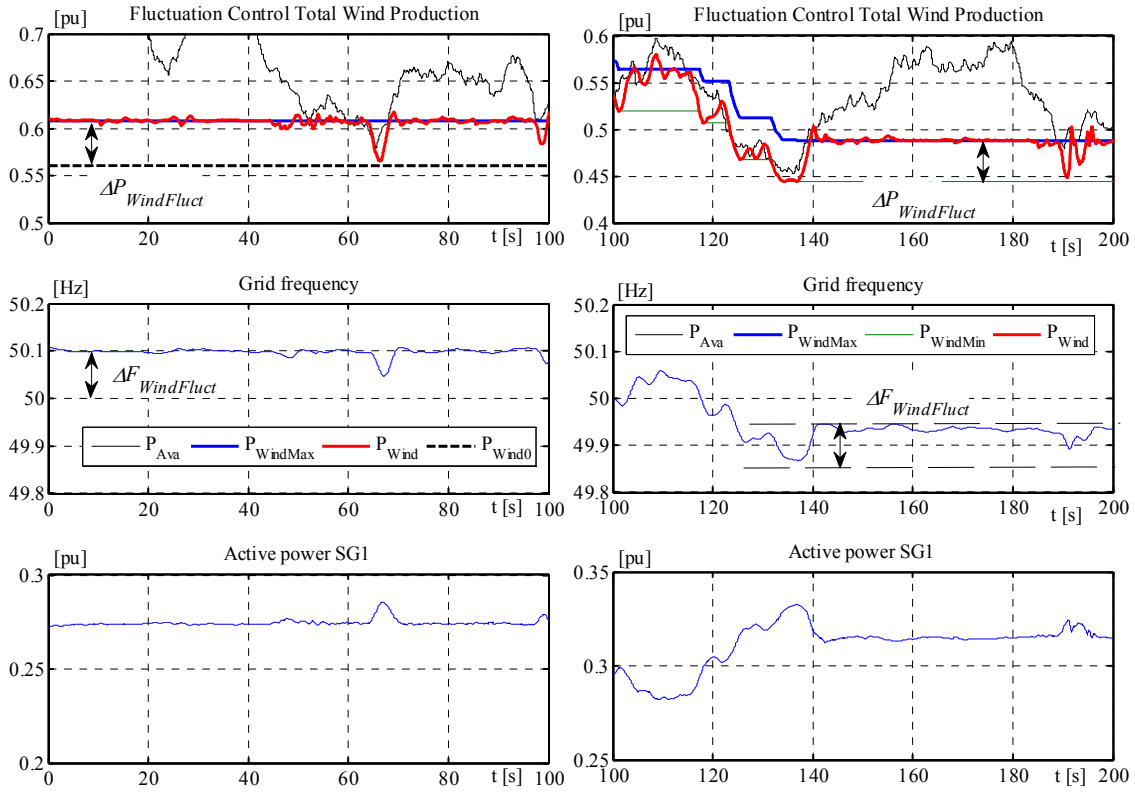
Figure 5-6: Fluctuations limitation of wind power and its effect on the grid frequency. Simple limitation (left) and considering the minimum generated power (right).

If, during normal wind power generation, we observe in real-time the minimum overall generated wind power, P_{elWPS}, and take this as the minimum possible power to be generated for the next period of time, $P_{WindMin}$, then we can allow wind power fluctuations on top of it. Thus, P_{Wind0} is substituted by $P_{WindMin}$ and:

$$P_{WindMax} = P_{WindMin} + \Delta P_{WindFluct} = P_{WindMin} + K_{sys} \cdot \Delta F_{WindFluct} \qquad (5.3)$$

Figure 5-6 right shows simulation results with the same system (PS2) having wind power fluctuations limited according to (**5.3**): While $P_{WindMin}$ is the minimum generated power, the $P_{WindMax}$ is an upper limitation for the wind power *at system level*. It can be seen in the figure that, despite of creating a permanent negative frequency deviation below $f_0 = 50$ Hz, the frequency *fluctuations* are kept inside limits for the time that $P_{WindMin}$ is unchanged. This limitation in frequency fluctuations facilitates the operation of the secondary frequency control (SFC) or AGC mechanism that will *restore* the mean frequency value on f_0 (Sections 2.1.3 and 2.1.4); especially useful in small islanded power systems with large amounts of wind (Section 2.5). With a proper SFC mechanism on the power system (manual or automatic), the average frequency deviation in **Figure 5-6** right will be only "temporary", as long as the SFC works properly.

The fluctuations limitation functionality (FL) given by (**5.3**) is intended to operate optimally only during the PFC period (up to 10-15 min), i.e. the period of continuous and normal operation of the power system where no adjustments of load set points are done in power plants (Sections 2.1.3, 2.1.4 and 2.4).

The system operator may choose not to have frequency fluctuations created by wind. In that case $\Delta F_{WindFluct} = 0$ and $P_{WindMax} = P_{WindMin}$ at system level. On the other hand, if not introducing a limitation $\Delta P_{WindFluct}$ at system level, it may end in a situation where excessive wind power fluctuations would require larger amounts of RR, or make the SFC operation difficult, or create other impacts in conventional prime movers, as discussed in Sections 2.5 and 2.6.

Obviously, the magnitude of the wind power impact depends not only on the amount of wind but also on the characteristics of the system (small systems vs. large, interconnected, systems). In large power systems the K_{sys} is large. This allows larger wind power fluctuations. Additionally, the increase and geographical dispersion of wind power sources over the system "smoothes out" the natural power fluctuations [42] [69]. However, the concept above described is still applicable; only the values of K_{sys}, $\Delta P_{WindFluct}$ and time scales of fluctuations may be different from system to system. The key is to determine the right $\Delta P_{WindFluct}$.

The basic algorithm for this FL functionality is described by (**5.4**) as a discrete time function. **Figure 5-7** shows the respective block diagram, with $\Delta P_{WindFluct}$ as parameter. The P^*_{ExtWPS} value is an external absolute constraint for the generated power. The *Enable* signal allows the operator to activate the functionality or to simply impose the P^*_{ExtWPS} constraint.

$$P_{WindMin}(k+1) = \begin{cases} \min\{ P_{WindMin}(k),\ P_{elWPS}(k)\},\ if\ Enable = 1 \\ \\ P^*_{ExtWPS}(k) - \Delta P_{WindFluct}\ ,\ if\ Enable = 0 \end{cases}$$

$$\text{(5.4)}$$

$$P^*_{WindMax}(k) = P_{WindMin}(k) + \Delta P_{WindFluct}$$

$$P^*_{refWPS}(k) = \min\{ P^*_{extWPS}(k)\ ,\ P^*_{WindMax}(k) \}$$
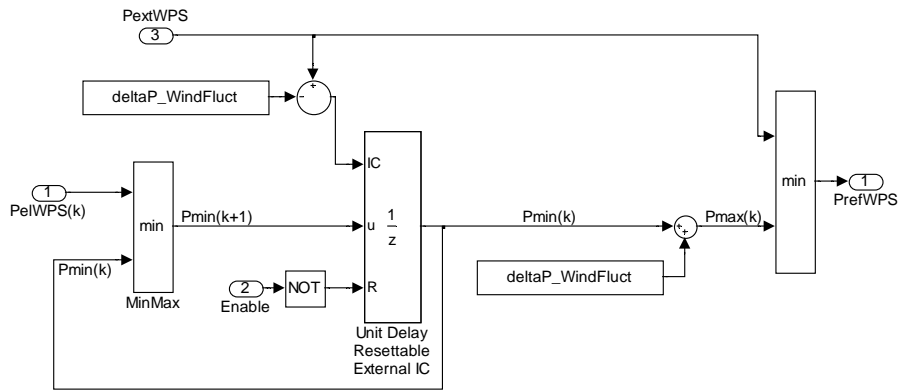
Figure 5-7: Pseudo algorithm for limitation of wind power fluctuations (FL)

5.3.1.1 Determination of $\Delta P_{WindFluct}$ for different implementation levels and comparison of energy yield

The previous concept may be implemented at power system level –that is, a restriction on the overall wind power production. It would require a centralized supervisory system and a reliable IT structure communicating all the wind power sources (WPS), sending set points and receiving information of actual local available power and power production for its processing. It would also require some additional algorithm for distributing (dispatching) appropriate set points to the different Clusters or WPPs (this is described later in Section 5.3.4). But if the (**5.4**) were implemented decentralized, at each WPP or WTG, then the limitation on overall $\Delta P_{WindFluct}$ at system level should be ensured somehow.

The FL functionality may be implemented at one of the levels previously described in Section 5.2.2, and repeated below:

1- Wind turbines level (WTG), where each *WTG-i* is a FL controlled point.
2- Wind power plants level (WPP), where each *WPP-i* is a FL controlled point.
3- Cluster level (Cl), where each *Cl-i* is a FL controlled point.
4- Power system level (PS), with just one FL control for the whole system.

Figure 5-8 shows a schematic of these levels and their dependencies: i) each WTG generate its own (controllable) power, ii) a group of WTGs concentrate their powers at one WPP point, characterizing its own power fluctuations, iii) a group of WPPs concentrate their powers at one Cluster point, characterizing its own power fluctuations and iv) all the Clusters inject their powers into the PS. The power produced at each level is characterized by a fluctuation component ΔP_{NN-x} (the PS is assumed with no interconnections).

In a decentralized control implementation, each of these controlled points *i* would require a $\Delta P_{WindFluct-i}$ as parameter. As result, the combination of the total produced wind

power fluctuations (open-loop controlled scheme) should not exceed the allowed $\Delta P_{WindFluct}$ at system level. This generates the following question: How can the $\Delta P_{WindFluct-i}$ be determined for each controlled point i so the total wind fluctuations at system level will not exceed $\Delta P_{WindFluct}$ given by (5.1)? An analysis can be made by considering the different implementation levels as lumped power sources.

Many works have studied the characteristics of power output fluctuations at a given point in the system when increasing the amount of WTGs or WPPs, e.g. [48]-[51]. One of the main conclusions in those studies is that there is a "smoothening" effect on the overall fluctuations. Additionally, the fluctuating wind power component tends to be constant upon a certain installed capacity and, most of all, upon a "suitable" distribution of the WTGs and WPPs over the system. Furthermore, this kind of studies has elaborated methodologies for estimating the combined power fluctuations based on the fluctuations observed at one or few lower level points (e.g. at WTG or at WPP levels) [42] [50]. But those methodologies were elaborated on the fact that wind power fluctuations can be approximated by a normal distribution function *if the wind power fluctuates as the wind blows*.

The difference with our case is that our power output fluctuations are "trimmed" by the controller in a decentralized FL application. So these fluctuations cannot be represented by a normal distribution any more, as deducted by e.g. looking at the electrical powers in **Figure 5-6**. This characteristic makes difficult to determine the resulting amount of limited wind power fluctuations at system level, when applying the FL methodologies above mentioned at controlled points i.
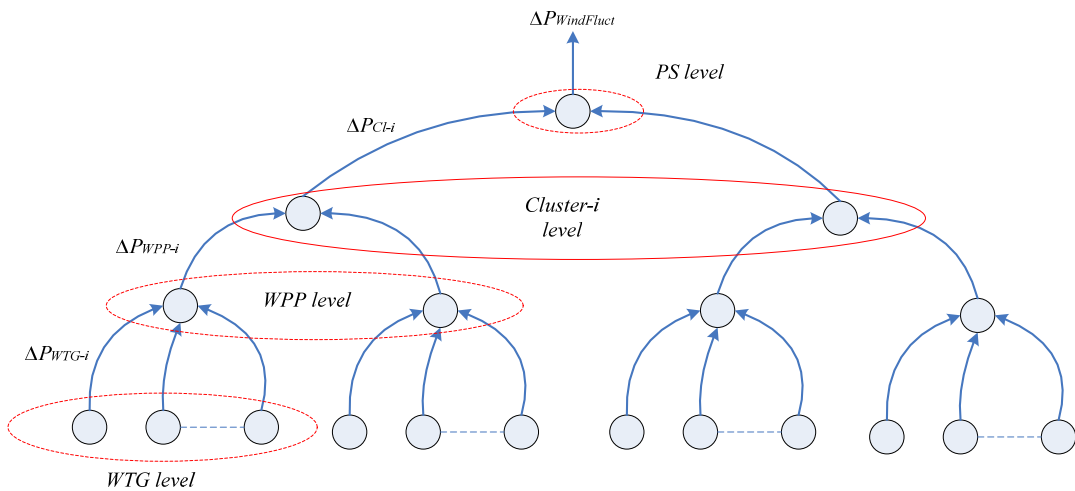

Figure 5-8: Controllability levels of wind power production in a power system. Wind turbines level (*WTG-i*), wind power plants level (*WPP-i*), clusters level (*Cl-i*) or power system level (*PS*).

In this work, a different approach has been used. Measurements of normal wind power production, $P_{measured-i}$, at each level and each lumped source i can be used for characterization of the necessary $\Delta P_{WindFluct-i}$, in order to obtain an amount of (resulting) $\Delta P_{WindFluct}$ at system level. By taking those measurements and "rebuilding" the power output, implementing the (**5.4**) with different $\Delta P_{WindFluct-i}$, a FL action can be emulated where $P_{elWPS-i}(k) = min\{ P_{WindMax-i}(k) , P_{measured-i}(k)\}$. It is possible to obtain a "characterization" for resulting $\Delta P_{WindFluct}$ vs. controlled $\Delta P_{WindFluct-i}$ when the FL control of fluctuations i is implemented at: i) WTG level, ii) WPP level or iii) PS level. Obviously, this characterization can be assured to be valid –most likely– only for the measured site under such wind conditions. Nevertheless, this approach is the closest to the reality and it was utilized with simulation studies of the power system PS2 with measured wind power from the wind turbines at the same site. Other systems or wind conditions will have different characterization, but the principle is still applicable.

Figure 5-9 shows an example of this approach applied to the measurements described in Section 2.5. Using the measured WTG's powers during normal operation, the FL operation was *emulated* at WTG level for different $\Delta P_{WindFluct-i}$ (on all the WTGs at the same time; only two WTGs are shown at the top/middle of the figure), *resulting* in a $\Delta P_{WindFluct}$ at system level (bottom, obtained). This process was repeated applying the FL at different levels too. The imposed value of $\Delta P_{WindFluct-i}$ was the same –in pu– for each i point.

Figure 5-10 (left) presents the obtained $\Delta P_{WindFluct}$ vs. imposed $\Delta P_{WindFluct-i}$. Values are based on the installed capacity of the respective power source (WTG, WPP or PS). This figure can be used to estimate the necessary setting $\Delta P_{WindFluct-i}$ depending at which level the FL functionality is implemented, and how much is the allowed $\Delta P_{WindFluct}$ for the system. **Figure 5-10** (right) shows the overall produced energy for each implementation level. This figure shows that, for a given allowed $\Delta P_{WindFluct}$ (system level), *the produced wind energy is higher when the FL is implemented at system level.*
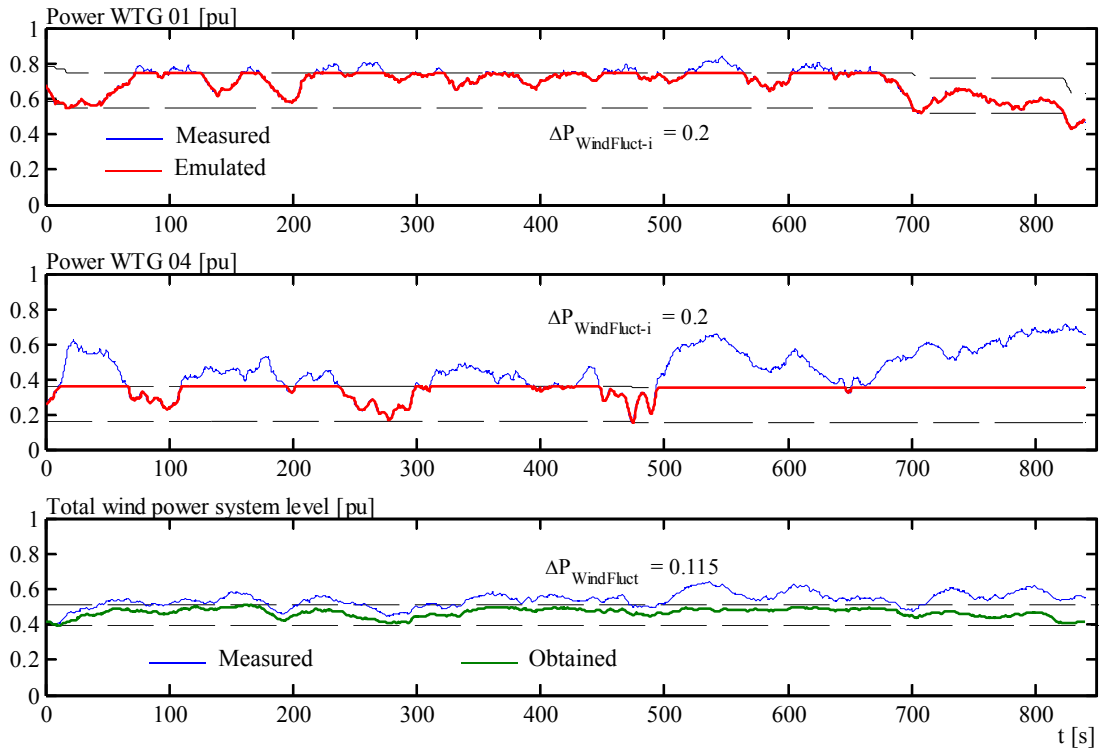
Figure 5-9: Measured wind power at WTG level and emulated $\Delta P_{WindFluct-i}$ (Two WTGs shown at the top/middle). Impact on the overall system fluctuations (bottom).
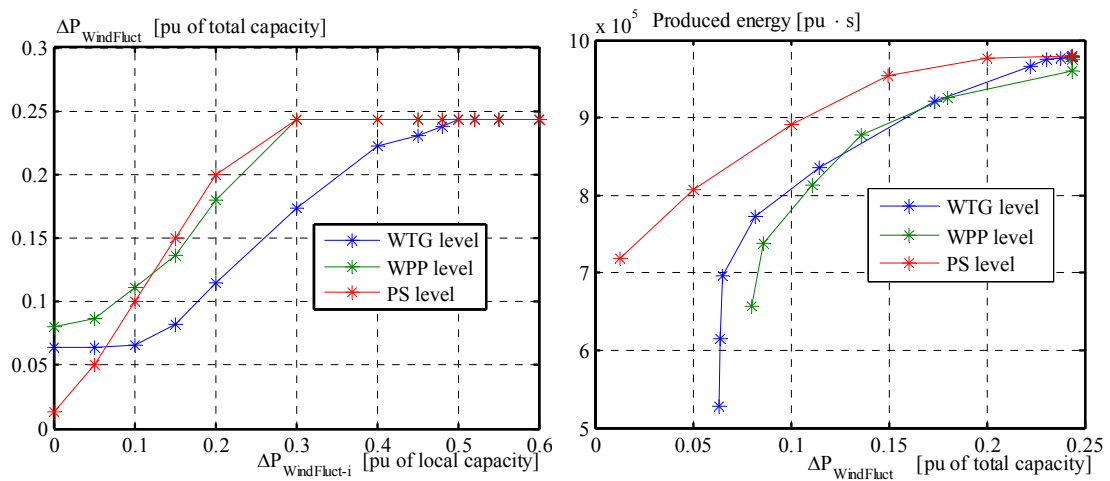
Figure 5-10: (left) Resulting overall power fluctuations by controlling $\Delta P_{WindFluct-i}$ at different levels and (right) produced energy for each.

5.3.2 Wind power tracking

If the algorithm in (**5.4**) is implemented as it is, then the limitation $P_{WindMax}$ will be kept reduced along the time and it will not increase, even if available wind power increases. The overall power production would remain limited to an unchanged $P_{WindMax}$ for long periods, as seen in **Figure 5-6** (right). There will be an unnecessary energy loss when, in fact, more wind power might be possible to be generated without introducing excessive

fluctuations into the system. Except if the operator applies an *Enable = 0* in (**5.4**) with a new P_{ExtWPS} value, to increase $P_{WindMax}$ every time it is wanted.

In order to automatically follow the available wind power, attending the control objective #2 stated in Section 5.2.1, the algorithm in (**5.4**) should be modified. But this power tracking should not introduce further wind power fluctuations than the specified $\Delta P_{WindFluct}$ at system level and it should permit a proper operation of the SFC in the system. A simple mechanism for smooth limitation of the increase in produced power is the so called "ramp limiter" or "rate control", which effect is shown in **Figure 5-11** (chosen ramp rate 0.25 pu/10 min.). This "limited power tracking" mechanism is a requirement in some grid codes [6] [7] [9]. Additionally, some works have studied the smoothening effect of this ramp limiter and the impact on requirements for reserves and ramping rates from conventional plants in the system [52] [53]. Basically, if the average wind power production increases over a period, the load references in conventional plants will have to ramp down at the same rate to balance it, normally driven by the SFC or AGC mechanism. Therefore the maximum ramp rates of WPPs need to be chosen according to the time constant of slow regulation mechanisms in the system. Additionally, the change in wind power production has to be compensated by system reserves, so the volume of the reserve has to consider the wind power change in that period [41]-[47]. A particular challenge exists when wind speed drops, as the wind power output in this situation cannot be controlled, if a good wind power forecast is not used.

Here, three different –simple– solutions for power reference tracking are studied, named Power Tracking Type 1, Type 2 and Type 3. They are based on the basic ramp limiter of **Figure 5-11** (considered in this Section as the base case), but combined with the Fluctuations Limiter described in the previous section. A comparison of produced energy and necessary system RR, with the basic ramp limiter (**Figure 5-11**) and with no limitation at all, is done at the end of this section.
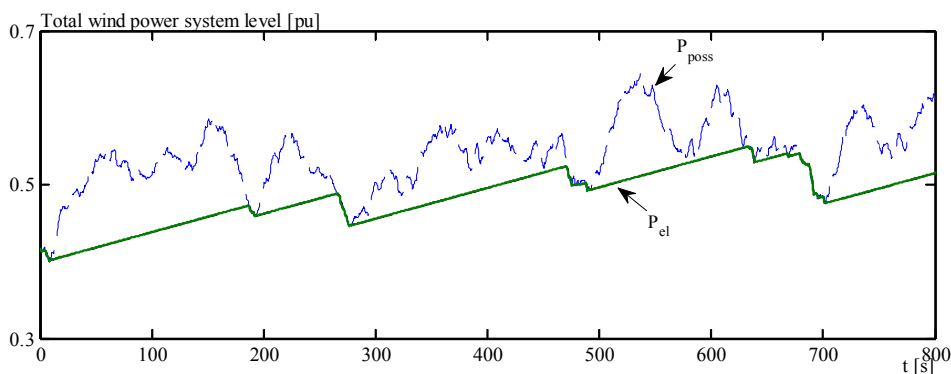
Figure 5-11: Standard requirement for ramp limitation [6] applied to measurements; basic ramp limiter; base case.

5.3.2.1 Power tracking type 1

Based on (**5.4**), the value $P_{WindMin}$ is constantly increased with a given *RampRate* if actual power production is equal or higher than the upper limit, i.e. $P_{elWPS} \geq P_{WindMax}$.

In this way the upper limit $P_{WindMax}$ increases with an appropriate ramp rate while electrical wind power is allowed to fluctuate with a $\Delta P_{WindFluct}$. This kind of power tracking benefits conventional power plants, giving time for proper SFC actuation if a suitable *RampRate* is defined. The difference with ramp limiters presented in e.g. [6] [52] [53] is that they do not implement a $\Delta P_{WindFluct}$ where the wind power production can freely fluctuate over a period and between boundaries.

The discrete time algorithm with time step T_s can be described as:

$$P_{WindMin}(k+1) = \begin{cases} \min\{P_{WindMin}(k) \; ; \; P_{elWPS}(k)\} & if \; P_{elWPS} < P_{WindMax} \\ \min\{P_{WindMin}(k) + RampRate \cdot T_s \; ; \; P_{elWPS}(k)\} & if \; P_{elWPS} \geq P_{WindMax} \\ P^*_{ExtWPS}(k) - \Delta P_{WindFluct} & if \; Enable = 0 \end{cases} \quad \textbf{(5.5)}$$

$$P^*_{WindMax}(k) = P_{WindMin}(k) + \Delta P_{WindFluct} \; , \quad\quad\quad\quad\quad\quad \textbf{(5.6)}$$

$$P^*_{refWPS}(k) = \min\{ P^*_{extWPS}(k) \; , \; P^*_{WindMax}(k) \}. \quad\quad\quad\quad \textbf{(5.7)}$$

where $P^*_{refWind}$ is the active power reference for the wind power system (which can be applicable at levels of PS, Cluster, WPP or WTG) and $\Delta P_{WindFluct}$ is given by (**5.1**) or by a characterization like **Figure 5-10** left (depending on the implementation level).

Figure 5-12 shows the block diagram of (**5.5**)-(**5.7**) and **Figure 5-13** shows the wind power production when implementing it on measurements at system level. Ramp rate was chosen 0.25 pu/10 min. Note the difference with **Figure 5-11**.
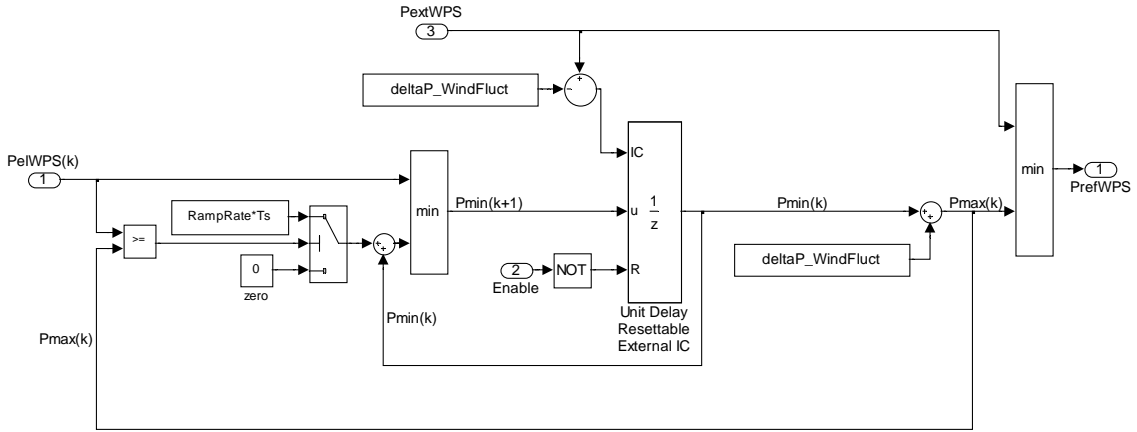
Figure 5-12: Algorithm for power tracking Type 1.
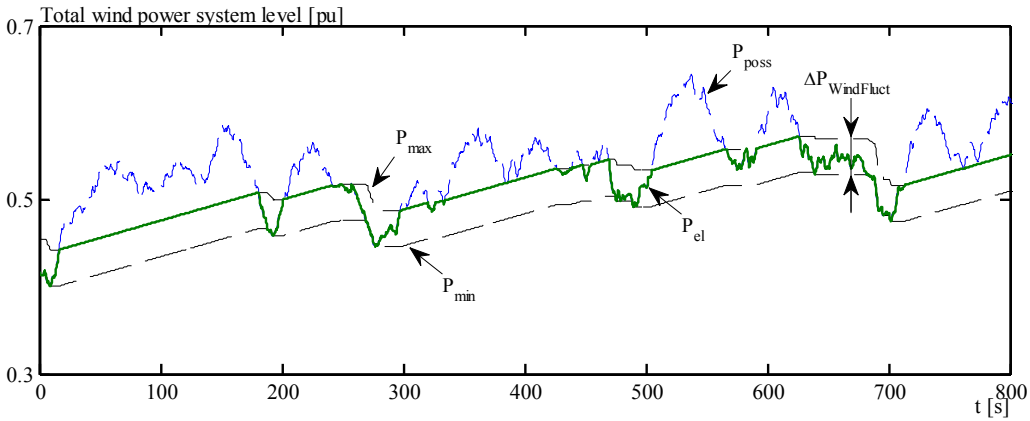
Figure 5-13: Wind power production with power tracking Type 1.

5.3.2.2 Power tracking Type 2

This is a variant of Type 1. Based on **(5.6)**, the $P_{WindMax}$ is affected by a component of the available power P_{AvaWPS} at the controlled level. The $P_{WindMin}$ is as **(5.5)**.

Thus the difference with Type 1 is:

$$P_{WindMax}(k) = \min \begin{cases} P_{WindMin}(k) + \Delta P_{WindFluct} \\[2ex] P_{WindMin}(k) + \dfrac{\Delta P_{WindFluct}}{2} + K \cdot \left(P_{AvaWPS}(k) - P_{WindMin}(k) - \dfrac{\Delta P_{WindFluct}}{2} \right) \end{cases} \qquad \textbf{(5.8)}$$

Where *K* can be any suitable value, for example $K = 0.3$. **Figure 5-14** shows the discrete block diagram of Type 2 and **Figure 5-15** shows the wind power production when implementing this algorithm. Note the difference with Type 1.
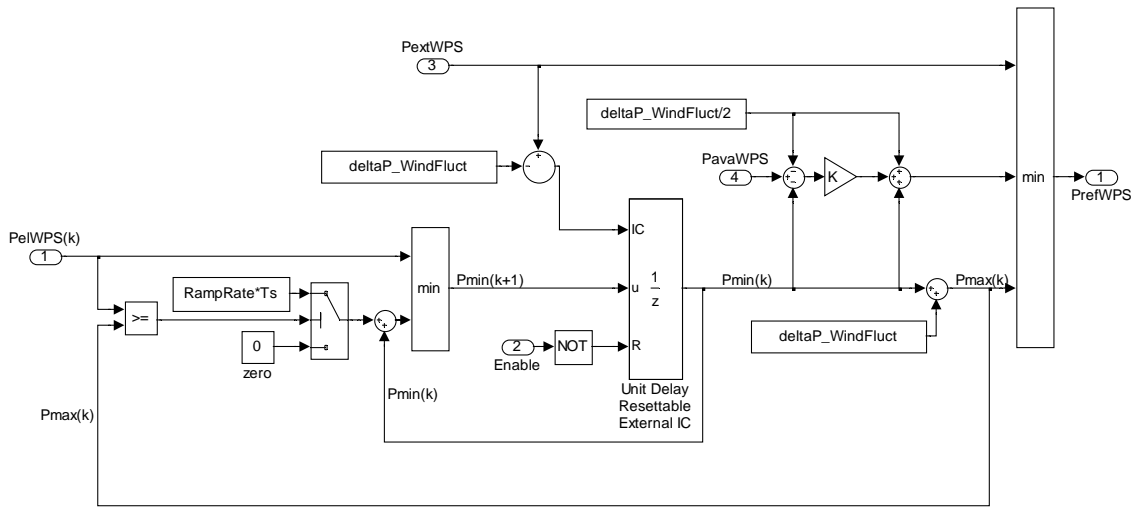
Figure 5-14: Algorithm for power tracking Type 2.
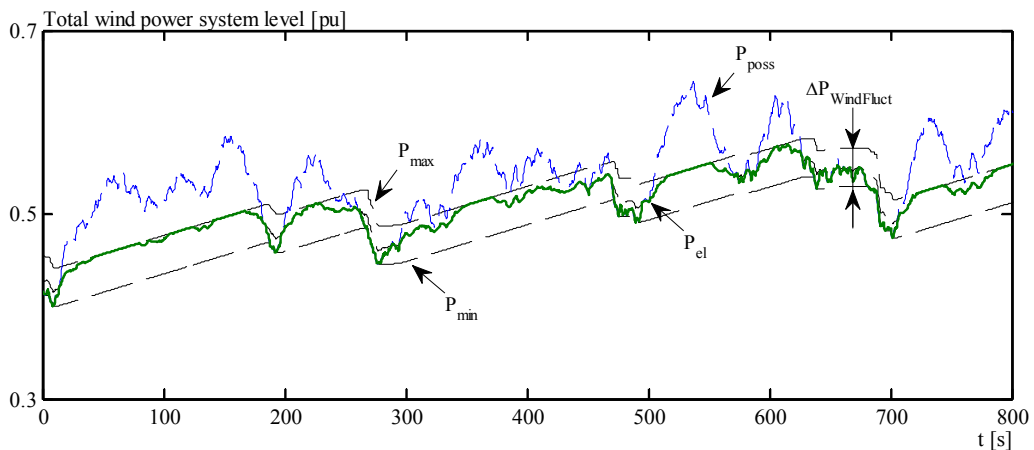
Figure 5-15: Wind power production with power tracking Type 2.

5.3.2.3 Power tracking Type 3

This is another variant of Type 1, with the difference of limiting the fluctuating power based on the moving average of the available power, P_{AvaAve}. Based on **(5.5)**, the $P_{WindMin}$ is chosen by comparison of: an offset of the P_{AvaAve}, the actual P_{elWPS} and the actual $P_{WindMin}$. The $P_{WindMax}$ is as **(5.6)**.

Thus the difference with Type 1 is:

$$P_{WindMin}(k+1) = \begin{cases} \min\{P_{WindMin}(k); P_{elWPS}(k) ; P_{PossAve}(k) - K \cdot \Delta P_{Fluct}\} \\ if\ P_{elWPSs}(k) < P_{WindMax}(k) \\[1em] \min\{P_{WindMin}(k) + RampRate \cdot T_s ; P_{elWPS}(k) ; P_{AvaAve}(k) - K \cdot \Delta P_{Fluct}\} \\ if\ P_{elWPS}(k) \geq P_{WindMax}(k) \\[1em] P_{ExtWPS}^{*}(k) - \Delta P_{WindFluct}\quad if\ Enable = 0 \end{cases} \textbf{(5.9)}$$

where K can be any suitable value, for example $K = 1.5$. For this type of power tracking, the calculation of the moving average P_{AvaAve} with a suitable time window need to be specified. This will depend on the application level (PS, Cluster, WPP or WTG level) because of the different fluctuation degrees.

Figure 5-16 shows the discrete time block diagram and **Figure 5-17** shows the wind power production when implementing this algorithm.
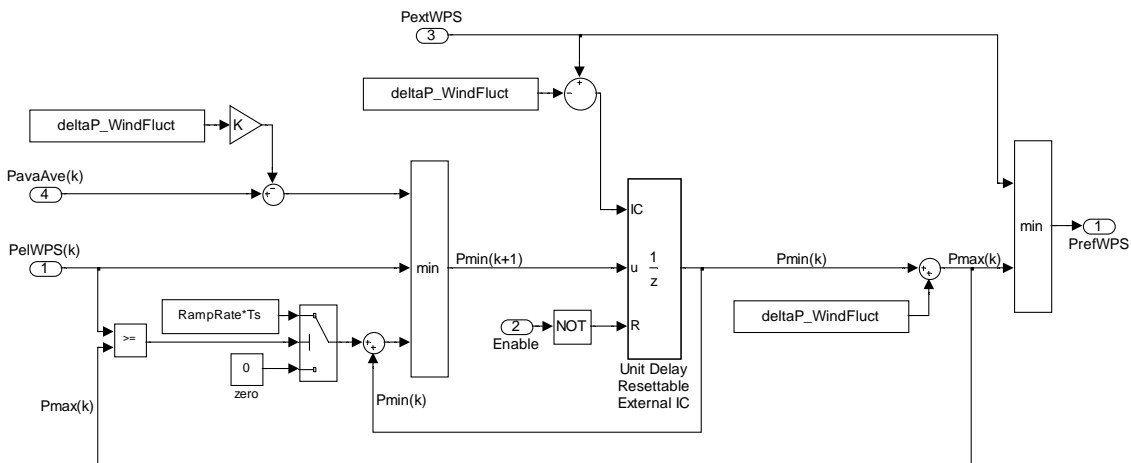
Figure 5-16: Algorithm for power tracking Type 3.
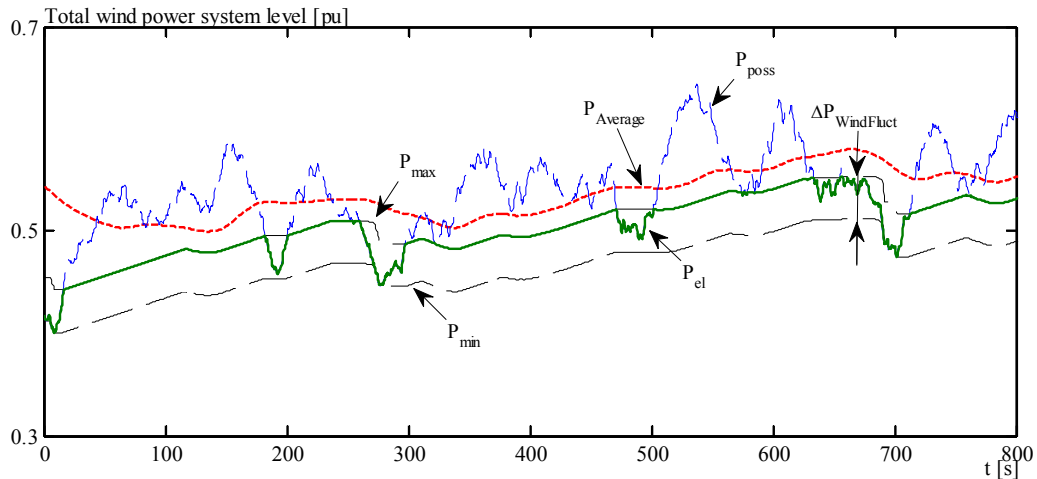
Figure 5-17: Wind power production with power tracking Type 3.

5.3.2.4 Comparison of power tracking types

Figure 5-18 shows the block diagram of each Type, with its inputs and outputs. For comparison, the same $\Delta P_{WindFluct}$ (0.04 pu) and *RampRate* (0.25 pu/10 min) were applied to Types 1, 2 and 3 over the same measured wind power at system level (**Figure 5-13**, **Figure 5-15** and **Figure 5-17**). **Figure 5-19** left shows the energy generated with each Type compared with the energy generated with the basic ramp limiter (**Figure 5-11**) and with no limiter at all. **Figure 5-19** right shows the amount of necessary system RR compared with the standard ramp limiter and with no limiter at all.

It is evident that Type 1 is the most efficient, with a modest gain of ~2% of energy over Type 3. Type 2 is in between with and improvement of ~1.5% of energy over Type 3. The Type 1 generates ~5.2% more energy than the basic ramp limiter, which is significant. Regarding the RR, the Types 1 and 2 need a little more reserves than the basic case, mainly due to the addition of the $\Delta P_{WindFluct}$ characteristic. Nevertheless, the needs for power reserves in the power system are much less compared with a no-limitation case, and the lost energy is reduced a ~50% compared with the basic ramp limiter.

Obviously, the absolute values shown in Figure 5-19 are specific of the measured case (site) and the selected parameters. Nevertheless, the relative differences between Types are more important to be noticed.
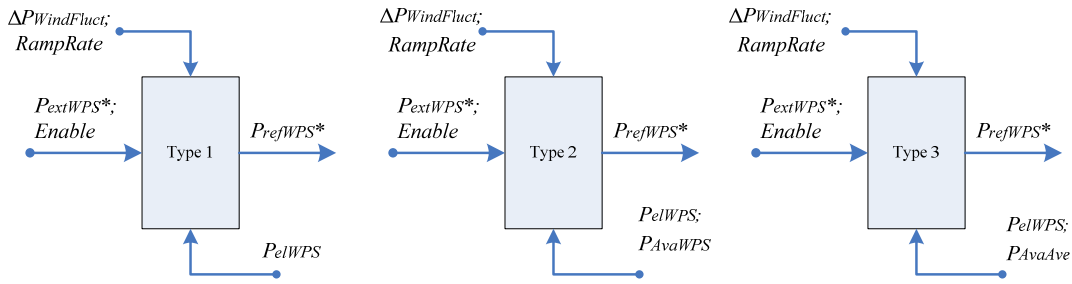
Figure 5-18: Inputs/Outputs for Types 1, 2 and 3.
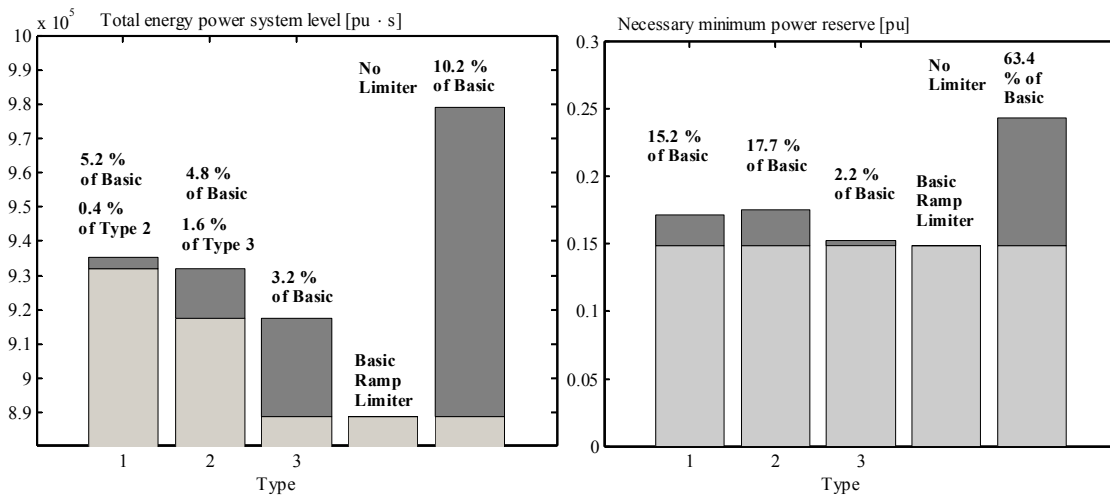
Figure 5-19: Produced energy (left) and minimum need for reserves (right) for each Type of power tracking applied to the same measured wind power and with the same setting for $\Delta P_{WindFluct}$. Type 1 produced ~2 % more energy than Type 3 and reduced ~50% the lost energy.

5.3.3 Frequency control and power reserve

Different grid codes (GC) may specify different requirements for frequency response from wind power (Section 2.4), which depends on the characteristics and needs of the respective power system. But implementation of requirements similar to the e.g. Irish or British GC will certainly generate different responses from wind power generation.

As demonstrated with measurements in Section 2.5 and e.g. [106] [107], in isolated power systems high wind power penetration causes a large impact on system frequency. Two main causes of frequency deviations are identified:

1- Frequency deviations caused by grid events (normal operation or disturbances), independently of the controlled wind power production, e.g. load changes, generation changes or fluctuations from "uncontrolled" wind power sources in the PS.

2- Frequency deviations caused by controllable wind power fluctuations (as studied in Section 5.3.1).

By implementing the Irish requirements on wind frequency control (Section 2.4.1, **Figure 2-15**) in a power system with large amounts of wind power, some issues might be generated during particular grid-wind situations. By analysing the requirements summarized in **Figure 2-13** one can deduce the following:

- Situations of high-frequency events followed by an increase in P_{Ava}: The increase in P_{Ava} produces an increase in generated power, even if the generated power was automatically reduced by the high-frequency event. As result, the high grid frequency may increase even further. This behaviour is avoided with the British GC.

- Situations of low-frequency events followed by a reduction in P_{Ava}: The reduction in P_{Ava} produces a reduction in generated power, even if the generated power was automatically increased by the low-frequency event and enough deload (reserve) was previously applied. As result, the low grid frequency may decrease even further. This behaviour is avoided with the British GC as long as enough deload is previously allocated.

By implementing the British requirements on wind frequency control (Section 2.4.2) in a power system with large amounts of wind power, no critical issues were identified but some characteristics to be considered, such as:

- Situations of high-frequency events followed by a reduction in P_{Ava}: If it is in FSM, the reduction in P_{Ava} will not reduce the generated power even if the generated power was automatically reduced by the high-frequency event, unless the P_{Ava} decreases below the deloaded value plus the generation reduction. Therefore the grid frequency will not be further benefitted by this P_{Ava} reduction. This behaviour is different with the Irish GC.

- Situations of low-frequency events and increase in P_{Ava}: If in FSM, the increase in P_{Ava} will not increase the generated power even if the generated power was automatically increased by the low-frequency event. Therefore the grid frequency will not be further benefitted by this P_{Ava} increase. This behaviour is different with the Irish GC.

- Situations of low-frequency events and decrease in P_{Ava}: If in FSM, an amount of deload needs to be applied in advance. The further reduction of P_{Ava} will reduce the margin of power reserve, therefore in low-frequency events the wind plant (or wind power system) may run out of reserve for frequency response. This behaviour is not possible in the Irish GC as it always consider the available power for allocating reserves (deloading).

In this work, a particular frequency response for wind power has been identified as suitable for power systems with high wind power penetration, especially for isolated/small systems. This functionality is part of the block structure described in Section 5.2.2 and in **Figure 5-1**. A frequency control mixing both the British and the Irish methodologies,

taking the beneficial part from each other, was elaborated. Its response depends on the characteristics of the frequency deviation, i.e. high-frequency events or low-frequency events and it is described as follows:

- High-frequency events: The new output of wind power production will be the *minimum* value of the following:
    - P_{RefA}: Wind power demand will decrease an amount ΔP_{FC} below the pre-event electrical output and proportionally to the grid frequency deviation.
    - P_{RefB}: Wind power demand will decrease an amount ΔP_{FC} below the pre-event deloaded power (related to P_{Ava}) proportionally to the grid frequency deviation.
- Low-frequency events: The new output of wind power production will be the *maximum* value of the following
    - P_{RefA}: Wind power demand will increase an amount ΔP_{FC} above the pre-event electrical output and proportionally to the grid frequency deviation.
    - P_{RefB}: Wind power demand will increase an amount ΔP_{FC} above the pre-event deloaded power (related to P_{Ava}) proportionally to the grid frequency deviation.

In order to respond to low frequency events with wind power, an amount of power *reserve* has to be allocated. Following the discussion in 5.2.2, depending on the control implementation level, this power reserve can be allocated by a central controller at system level, or can be *split* among decentralized controllers such as clusters, WPPs or WTGs level. Nevertheless, the wind frequency response described in this section can work independently of the implementation level, but parameters should be adjusted accordingly. Thus, for simplification in the analysis we assume here that it is implemented at system level. The reserve of wind power is achieved by deloading the generation an amount $P_{ReserveWPS}$ below the available power (many times referred as *Delta Control* [6]). **Figure 5-20** (a) shows the introduction of $P_{ReserveWPS}$ which requires modification of the structure in **Figure 5-12** and similar. **Figure 5-20** (b) shows how the coexistence of $P_{ReserveWPS}$ with the FL functionality ($\Delta P_{WindFLuct}$) is. Both functionalities are ensured by the controller, i.e. there are always a $P_{ReserveWPS}$ and a limitation $\Delta P_{WindFLuct}$.

(a)   (b)
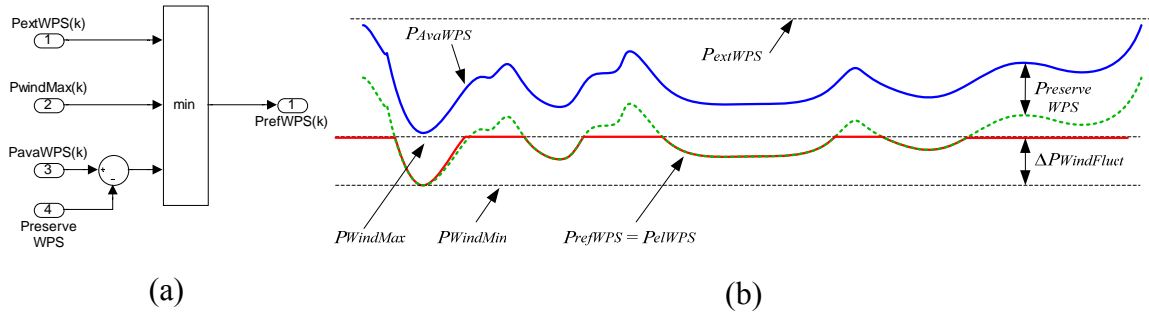
Figure 5-20: (a) Introduction of power reserve. (b) Example of coexistence of power reserve and fluctuations limitation (system level).

The value ΔP_{FC} in pu is calculated independently of the available power as follows:

$$\Delta P_{FC} = \begin{cases} \dfrac{1}{R_{HF}} \dfrac{\left(\Delta f - Thr_{HF}\right)}{f_0} & , \quad \forall \ \Delta f > Thr_{HF} \\[2em] \dfrac{1}{R_{LF}} \dfrac{\left(\Delta f - Thr_{LF}\right)}{f_0} & , \quad \forall \ \Delta f < Thr_{LF} \\[2em] 0 & , \quad \forall \ Thr_{LF} < \Delta f < Thr_{HF} \end{cases} \tag{5.10}$$

where R_{HF} and R_{LF} are proportionality constants (droop) respectively for high-frequencies and low-frequencies, Thr_{HF} and Thr_{LF} are threshold values respectively for high-frequencies and low-frequencies. **Figure 5-21** (a) shows the wind power regulation characteristic and (b) the block diagram for its calculation.

(a)

(b)
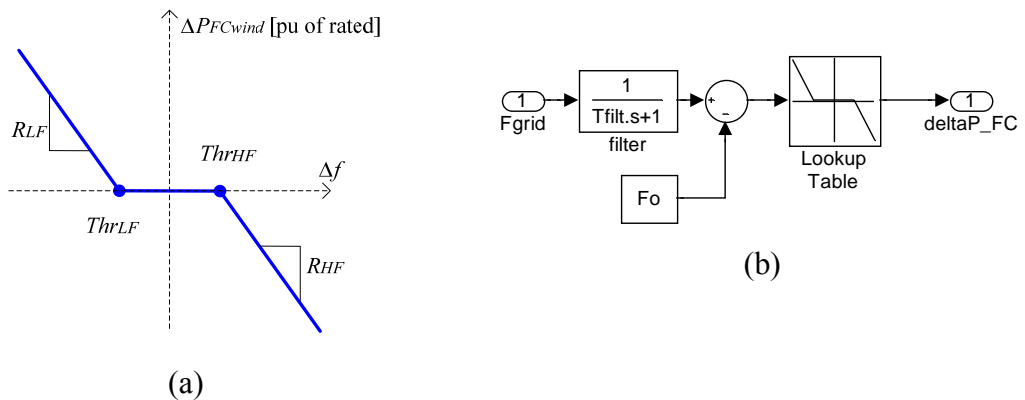
Figure 5-21: (a) Frequency response characteristic. (b) Calculation.

When the grid frequency deviation goes beyond the thresholds, the frequency control is activated, the actual electrical production is memorized as P_{elWPS0} and the actual available power is memorized as $P_{AvaWSP0}$. The pre-event deloaded power is given by:

$$P_{DeloadWPS0} = P_{AvaWPS} - P_{ResserveWPS0} = P_{AvaWPS} - \left(P_{AvaWPS0} - P_{elWPS0} \right) \tag{5.11}$$

The ΔP_{FC} is then applied to the P_{elWPS0} to get P_{RefA} and to the $P_{DeloadWPS0}$ to get the P_{RefB}. Then the demand on wind power production is chosen according to (**5.12**):

$$P_{DemandWPS} = \begin{cases} P_{refWPS}, \textit{for normal frequencies} \\ \\ \min\left\{ \left(P_{DeloadWPS0} + \Delta P_{FC} \right), \left(P_{el0} + \Delta P_{FC} \right) \right\}, \textit{for high-frequencies} \\ \\ \max\left\{ \left(P_{DeloadWPS0} + \Delta P_{FC} \right), \left(P_{el0} + \Delta P_{FC} \right) \right\}, \textit{for low-frequencies} \end{cases} \tag{5.12}$$

Figure 5-22 (a) shows the block diagrams for the memory functions and (b) the calculation of the demand for the wind power production. **Figure 5-23** presents the block diagram of the frequency controller with the inputs and outputs. **Figure 5-24** (a) exemplifies the generation response to a fictitious high-frequency event and (b) to a low-frequency event. In **Figure 5-24** (a) if the P_{Ava} increases, the generation can never be higher than P_{RefA}; but if P_{Ava} decreases, the generation can follow it with P_{RefB} and eventually bring the grid frequency down. In **Figure 5-24** (b) if the P_{Ava} decreases, the generation is not lower than P_{RefA} (as long as enough reserve is available); but if P_{Ava} increases, the generation can follow it with P_{RefB} and eventually bring the grid frequency up. As grid frequency fluctuations are also generated by wind power fluctuations, a frequency controller of these characteristics for wind power production introduces a self-stabilizing mechanism.

(a)   (b)
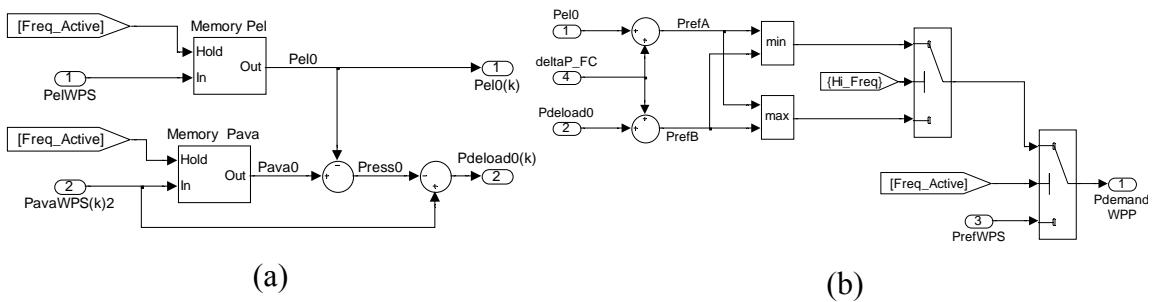
Figure 5-22: (a) Pre-event values and (b) calculation of wind power demand for frequency response.
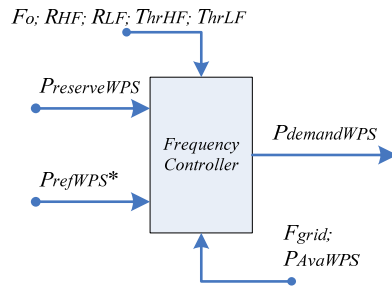
Figure 5-23: Block for frequency control with inputs/outputs.

(a)   (b)
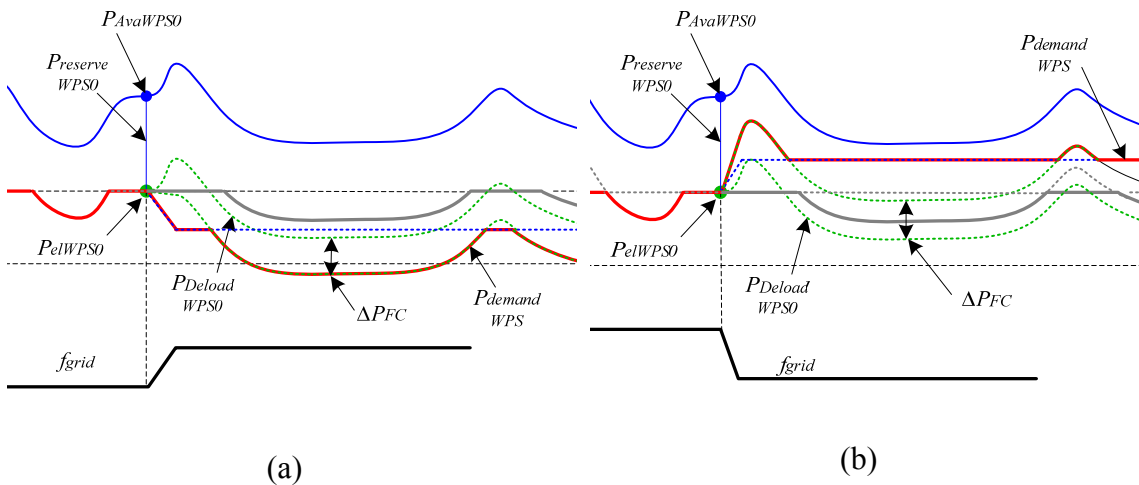
Figure 5-24: Frequency response characteristics. (a) High-frequency event and (b) low-frequency event.

Figure 5-25 shows simulation results with the islanded power system PS2 and artificial sinusoidal wind speed, where events of low frequency (left) and high frequency (right) were simulated. The wind power production is equipped with a frequency controller as described in (**5.10**)-(**5.12**) and running with a *reserve* of 6% of available power. Note how the wind frequency response acts towards grid frequency restoration.

Depending on the implementation level, the point for measurement of the grid frequency may be different. If implemented at WTG level, the measurement is at the WTG terminals. If implemented at WPP level, the measurement point is the PoC (point of the WPP connection to the grid, or PCC). If it is implemented at system level, it should be considered a practical and reliable measurement point for the grid frequency.
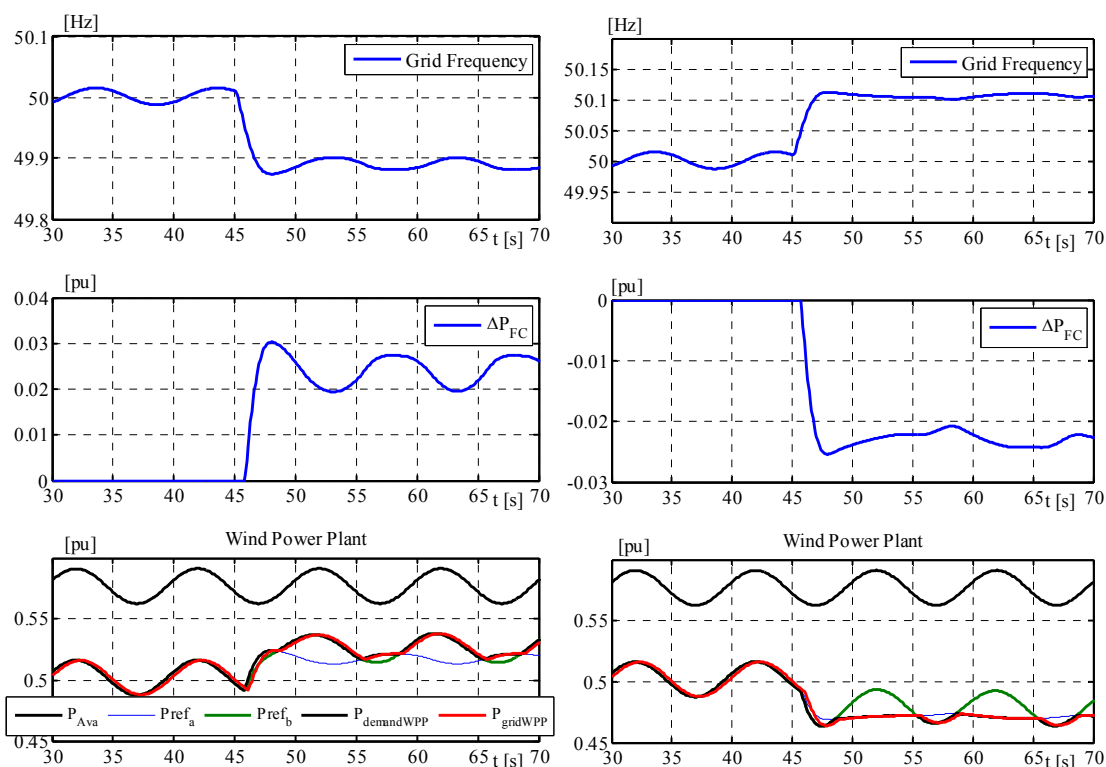
Figure 5-25: Frequency control of wind power in an islanded system for low-frequency (left) and high-frequency (right) according to the described algorithm. Wind power is also introducing frequency variations (Simulations).

5.3.4 Dispatching algorithms and active power control

In the previous sections, mechanisms for setting the overall wind power that should be generated in the power system were addressed. As the active power impact affects the whole power system, it is desirable to control the overall wind power production from higher levels. The overall wind power production in the power system will then be the composition of individual wind power sources (WPS) outputs. Therefore, to determine their individual set points and distribute them, a suitable *dispatcher* is necessary. In this Section, two dispatcher controllers for proper distribution of those set points in a wind power generation system (WPGS) are studied. These dispatchers distribute set points acting as *algebraic controllers*: each WPS in the WPGS receives a set point from the dispatcher aiming at maintaining a combined overall output.

Due to the high degree of freedom for setting individual set points to each WPS, different dispatching algorithms are possible. Selecting one or another dispatching algorithm may depend on different objectives, e.g. optimization of overall energy production; increase of stored kinetic energy in turbines rotors for the same produced power; simplification of control signals for practical implementation, and others. Nevertheless, the main objective for a dispatcher is to generate a combined power production according to a total power demand.

Whatever dispatching algorithm is used, it is important to identify or understand the different variables that characterize the "possible" power to be generated from a group of controllable WPS. From a generic interpretation, a WPS can be a single WTG inside a WPP, or a WPP inside a Cluster, or a Cluster in a power system. The total available power (or possible power) existing over a group of controllable WPS can be characterized by three components (shown in **Figure 5-26**):

1. Fluctuating power, P_{Fluct}, which is the amount of wind power that is produced by a set of WPS with no power constraint on their productions, i.e. power generated according actual local wind speed.
2. Regulated power, P_{Reg}, which is the amount of wind power that is produced by a set of WPS that follow a power constraint on their productions, i.e. power generated according to an external set point.
3. Curtailed power, P_{Curt}, which is the amount of wind power that is not generated due to the constraints on WPS production, i.e. the amount of possible overall wind power that is not exploited.

Therefore, the available wind power, P_{Ava}, over a group of controllable WPS is always given by:

$$P_{AvaWPGS} = P_{Reg} + P_{Fluct} + P_{Curt},$$ **(5.13)**

and the total electrical production from the WPGS is:

$$P_{WPGS} = P_{Reg} + P_{Fluct}$$ **(5.14)**

In the following sub-sections, only two types of dispatching algorithms are studied, named **Dispatcher 1** and **Dispatcher 2**.
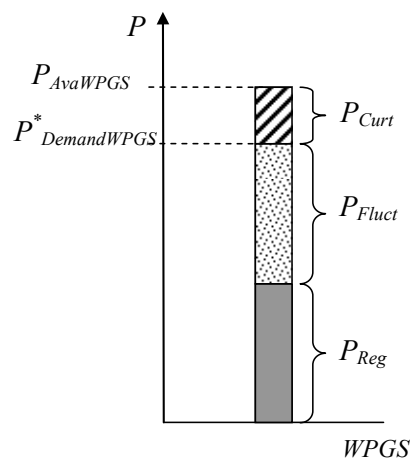
Figure 5-26: Generic representation of the wind power components in a WPGS.

5.3.4.1 Dispatcher 1

The objective of this dispatcher is to use the surplus of available power from a sub-group of WPS inside a WPGS to compensate the lack of power in others WPS, thus regulating the total WPGS power output to a desired value.

This dispatching for a WPGS works as follows:

- WPS receiving lower wind speeds are allowed to generate power without constraint. That is, the electrical power from this sub-group is generated according to actual wind speed.

- WPS with higher wind speeds generate regulated (constrained) power. That is, the electrical power from this sub-group is generated according to a set point sent from the dispatcher.

- Power fluctuations from low wind speed WPS group are compensated by changing the set points of high wind speed WPS group accordingly. Therefore the total wind power production in the WPGS remains regulated to a desired value by the dispatcher, as long as the regulated WPS inside the WPGS receive surplus of wind power.

- Inside the WPGS, the power generated from each fluctuating WPS is always lower than the power generated from each regulated WPS. Therefore all the WPS in the WPGS can receive the same *common* set point value from a central controller. Thus WPS with low wind speed will generate just what is possible locally while WPS with surplus of wind will follow the common set point value.

- The *common* set point value may be restricted locally at each WPS depending on local constraints, e.g. maximum/minimum powers, individual deloading, etc. In such case, the dispatcher will take this individual WPS as a non-controllable power source (i.e. fluctuating).

Figure 5-27 shows the principle of Dispatcher 1 for a given WPGS, and **Figure 5-31** shows simulation results of this dispatcher in a given WPGS containing three WPS.
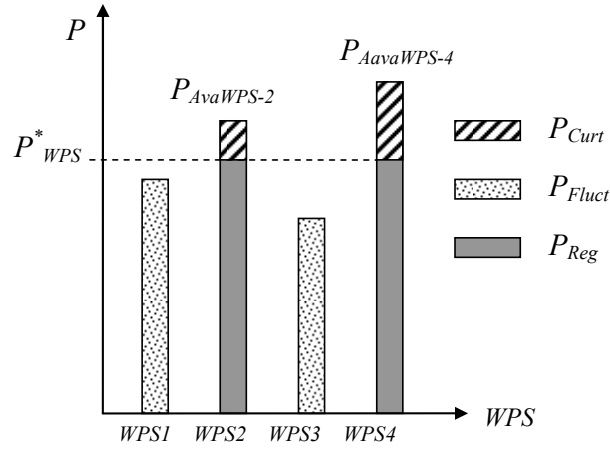
Figure 5-27: Dispatcher 1 principle. Group of WPS generating available power and group of WPS compensating internal power fluctuations by following the set point P^*_{WPS} sent from a central controller.

The following equations describe this dispatcher algorithm:

- Demand power reference for the entire WPGS, $P^*_{DemandWPGS}$:

$$P^*_{DemandWPGS} = P_{Reg} + P_{Fluct} \tag{5.15}$$

- Total amount of regulated power in the WPGS:

$$P_{Reg} = NWPS_{Reg} \cdot P^*_{WPS} , \tag{5.16}$$

where $NWPS_{Reg}$ is the number of WPS that are constrained by the common set point, P^*_{WPS}.

- Total electrical power that is not constrained (i.e. is fluctuating):

$$P_{Fluct} = \sum P_{WPS-i} \; ; \; \forall \left\{ i \in NWPS_{Fluct} \right\} \tag{5.17}$$

where $NWPS_{Fluct}$ is the number of WPS that are not constrained by the set point P_{WPS}^* and P_{WPS-i} is the actual electrical power produced by the WPS-i belonging to the $NWPS_{Fluct}$ set.

Therefore:

$$P^*_{DemandWPGS} = NWPS_{Reg} \cdot P^*_{WPS} + P_{Fluct} \tag{5.18}$$

From (5.18) the common set point, P^*_{WPS}, equal for all the WPS in the WPGS is:

$$P^*_{WPS} = \frac{P^*_{DemandWPGS} - P_{Fluct}}{NWPS_{Reg}} \; ; \; \forall \left\{ NWPS_{Reg} >= 1 \right\} \tag{5.19}$$

The (**5.19**) is the basic dispatching rule. To determine in practice the $NWPS_{Reg}$ and the P_{Fluct} it is necessary to know the WPS states at each instant by means of feedback signals to the central controller.

As example, two different ways for determining the $NWPS_{Reg}$ and the P_{Fluct}, based on WPS feedback, are presented as follows:

1. By reading the actual electrical power from each WPS, P_{WPS-i}, and comparing it with the *common* reference P^*_{WPS}, thus:

$$P_{Fluct} = \sum P_{WPS-i} \; ; \; \forall \left\{ P_{WPS-i} < P^*_{WPS} \right\} \tag{5.20}$$

$$NWPS_{Reg} = \sum i \; ; \; \forall \left\{ P_{WPS-i} >= P^*_{WPS} \right\} \tag{5.21}$$

2. By knowing the status of the internal flag *External_Ref* in each WPS that indicates the source of the power reference being adopted inside the WPS local control. Thus:

$$P_{Fluct} = \sum P_{WPS-i} \; ; \; \forall \left\{ External\_Ref_i = 0 \right\} \tag{5.22}$$

$$NWPS_{Reg} = \sum i \; ; \; \forall \left\{ External\_Ref_i = 1 \right\} \tag{5.23}$$

The maximum $P_{MaxWPS-i}$ and the minimum $P_{MinWPS-i}$ allowed set points are also necessary to know in order to determine whether the WPS-*i* is regulated or not by the Dispatcher, because if $P^*_{WPS} > P_{MaxWPS-i}$, or $P^*_{WPS} < P_{MinWPS-i}$, the WPS-*i* cannot be regulated by the dispatcher, hence it should not be part of the $NWPS_{Reg}$.

For a further development of this dispatching algorithm, particular operational conditions must be considered. For example (**5.19**) only works when $NWPS_{Reg} >= 1$, i.e. when at least one WPS inside the WPGS is being regulated, having power surplus from wind. Another condition to consider is when the operator of the WPGS needs –for some reason– to reduce the production of only one WPS. A further analysis of these operational conditions is done as follows.

When $NWPS_{Reg} = 0$ all the WPS in the WPGS produce fluctuating power, therefore they do not follow an external set point P^*_{WPS} and the total wind power production, P_{WPGS}, is not regulated in this case. This particular situation can generate two different states, on which particular power references can be applied as follows:

1. Case $NWPS_{Reg} = 0$ and $P^*_{DemandWPGS} > P_{WPGS}$: In this case the total WPGS production is lower than the demanded power, therefore WPS should receive a set point that allows an increase in production when later wind increases locally.

The value of this particular (not individual) set point should be of course higher than the actual electrical power of each WPS. An extreme case is by setting this set point equal to the rated WPS power, for all the WPS. Thus:

$$P^*_{WPS} = P_{RatedWPS} \; ; \; \forall \left\{ NWPS_{Reg} = 0 \; \& \; P_{WPGS} < P^*_{DemandWPGS} \right\} \qquad \textbf{(5.24)}$$

2. Case $NWPS_{Reg} = 0$ and $P_{WPGS} > P^*_{DemandWPGS}$: Here the total WPGS production is higher than the demanded power but no WPS is counted as regulated. This situation is generated when wind speed increases, or WPGS demand is reduced, while WPS set points are given by (**5.24**). Therefore WPS set point should be reduced to a value that allows the regulation of the WPGS according to $P^*_{DemandWPGS}$. An option for determining the set point in this case is to constraint only the WPS having actual production equal or higher than a *mean* set point value, $P^*_{MeanWPS}$:

$$P^*_{MeanWPS} = \frac{P^*_{DemandWPGS}}{NWPS} \; ; \; \forall \left\{ NWPS >= 1 \right\} \qquad \textbf{(5.25)}$$

Therefore the group of WPS with actual $P_{WPS} < P^*_{MeanWPS}$ will not be constrained by the new set point. To calculate the new WPS set points, the regulated power component of the WPGS should be determined and then distributed among the WPS having actual $P_{WPS} >= P^*_{MeanWPS}$, represented by N_{HiMean}. That is:

$$P^*_{WPS} = \frac{P^*_{DemandWPGS} - P_{LoMean}}{N_{HiMean}} \; ; \; \forall \left\{ NWPS_{Reg} = 0 \; \& \; P_{WPGS} >= P^*_{DemandWPGS} \right\} \qquad \textbf{(5.26)}$$

Where the WPGS production component given by fluctuating WPS, P_{LoMean}, is:

$$P_{LoMean} = \sum P_{WPS-i} \; ; \; \forall \left\{ P_{WPS-i} < P^*_{MeanWPS} \right\} \qquad \textbf{(5.27)}$$

And the number of WPS that will be regulated by P_{WPS}^* is:

$$N_{HiMean} = \sum i \; ; \; \forall \left\{ P_{WPS-i} >= P^*_{MeanWPS} \right\} \qquad \textbf{(5.28)}$$

Notice that, by adopting the set point from (**5.26**), the new state from the WPS after feedback will become $NWPS_{Reg} >= 1$ and the WPS set point in the next sample (*k*) in the digital controller will then be given then by (**5.19**).

As mentioned before, another operational condition is when the WPGS operator needs to reduce the power of just one WPS, while remaining WPS continue to operate normally. In this case it is sufficient to compare the P^*_{WPS} with the new value from the operator, $P^*_{OperatorWPSi}$, and then take the minimum of these to get the set point for that particular WPS-*i*, P^*_{WPS-i}:

$$P^*_{WPS-i} = \min\left\{ P^*_{WPS} \quad , \quad P^*_{OperatorWPS-i} \right\},$$ (5.29)

Expressions (**5.19**) to (**5.29**) can be discretized for implementation in a digital controller. Furthermore, they can be grouped in two types of calculation modules: i) one module for calculating WPGS values and ii) other modules for calculating individual WPS-*i* values (one module per WPS). The WPGS calculation module interchanges signals with each WPS-*i* calculation module.

Figure 5-28 exemplifies the arrangement of the calculation modules inside Dispatcher 1, and **Table 5-1** provides further signals description. **Figure 5-29** describes the complete algorithm for the WPS-*i* calculation module corresponding to each WPS. **Figure 5-30** describes the complete algorithm for the WPGS calculation module.

Figure 5-31 shows simulation results of the performance of this dispatching algorithm and **Figure 5-32** is a zooming-in around a set point change. The total WPGS production, P_{WPGS}, is regulated to $P^*_{DemandWPGS}$ as long as WPSs with surplus of power are available. A set point event is simulated at $t = 130$ p.u., where $P^*_{DemandWPGS}$ was increased 10 % from WPGS nominal. Observe that the P^*_{WPS} set point changes with $P^*_{DemandWPGS}$ but also compensating individual P^*_{WPS} fluctuations.

Individual WPS can experience a drop in power of **X** pu/s, therefore others WPS should increase power to compensate this reduction. Thus the individual WPS ramp limiters should not be less than **X**/(NWPS-1) pu/s.

Table 5-1: Further description of inputs and feedback signals in **Figure 5-28**

External inputs WPS-i	*Status feedback WPS-i*
$P^*_{OperatorWPS-i}$	*Is_Connected_WPS-i*
P_{WPS-i}	*Is_Regulated_WPS-i*
$P_{MaxWPS-i}$	*Is_Higher_than_Pmean_WPS-i*
$P_{MinWPS-i}$	$P_{WPSfluct-i}$
$P_{AvaWPS-i}$	$P_{WPSreg-i}$
$P_{MeanWPS-i}$	$P_{WPSloMean-i}$
$P_{elWPS-i}$	P_{WPS-i}
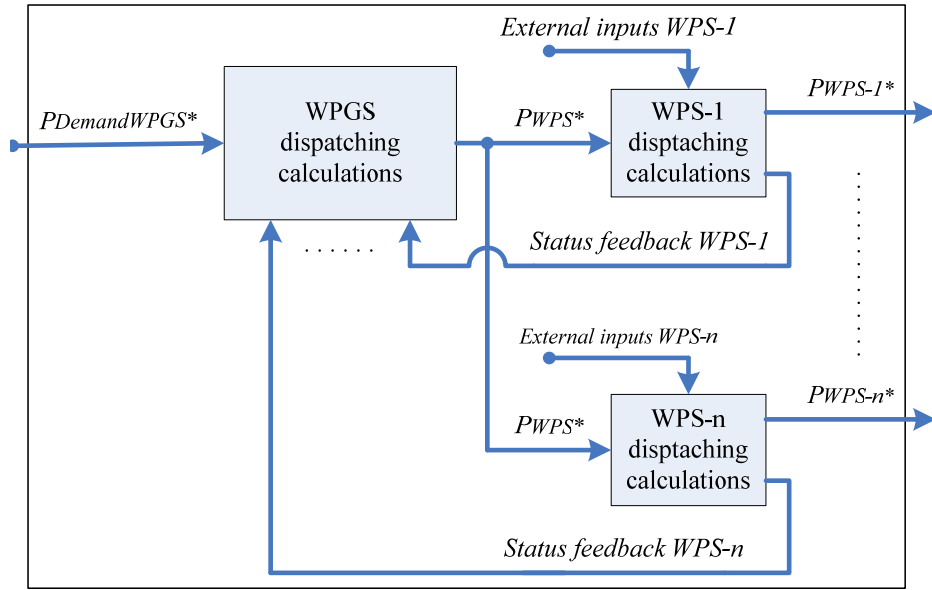
Figure 5-28: Arrangement of calculation modules in Dispatcher 1
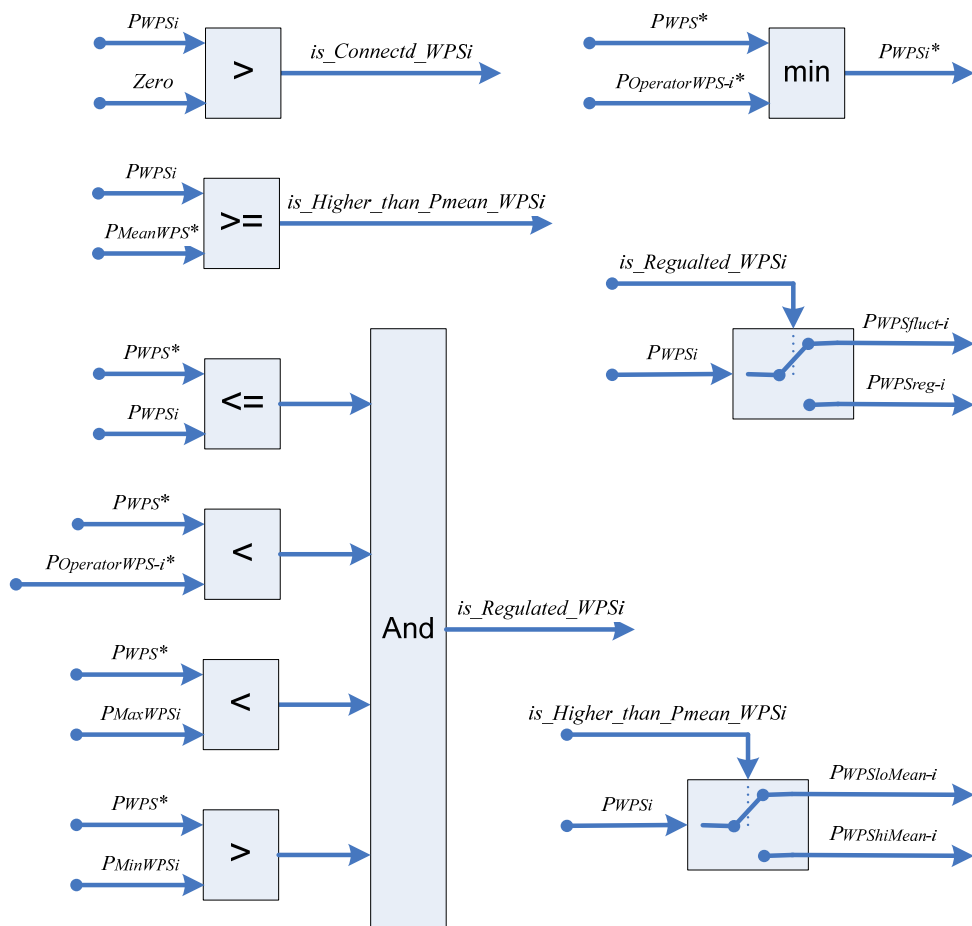
Figure 5-29: WPS-i dispatching calculations module
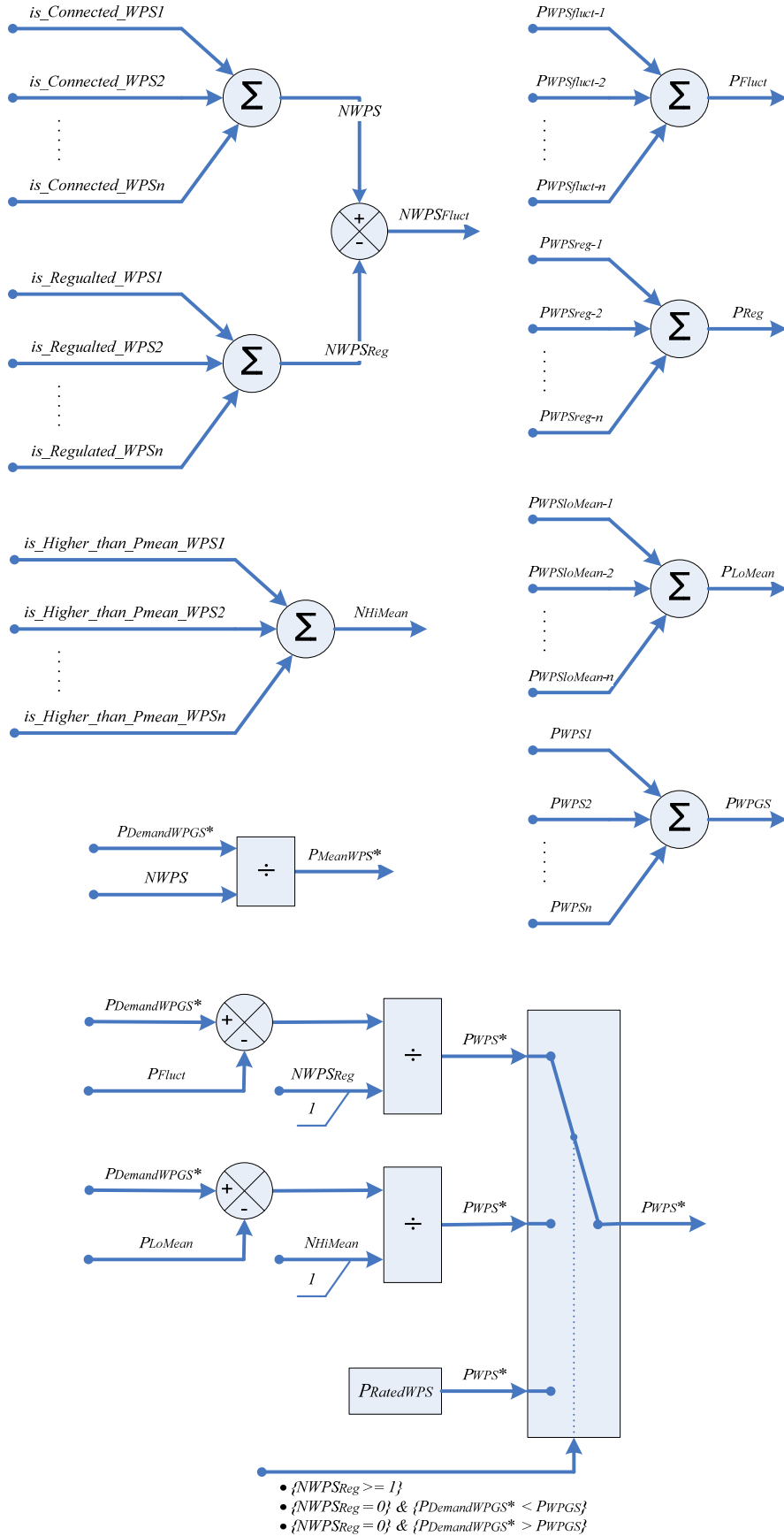
Figure 5-30: WPGS dispatching calculations module
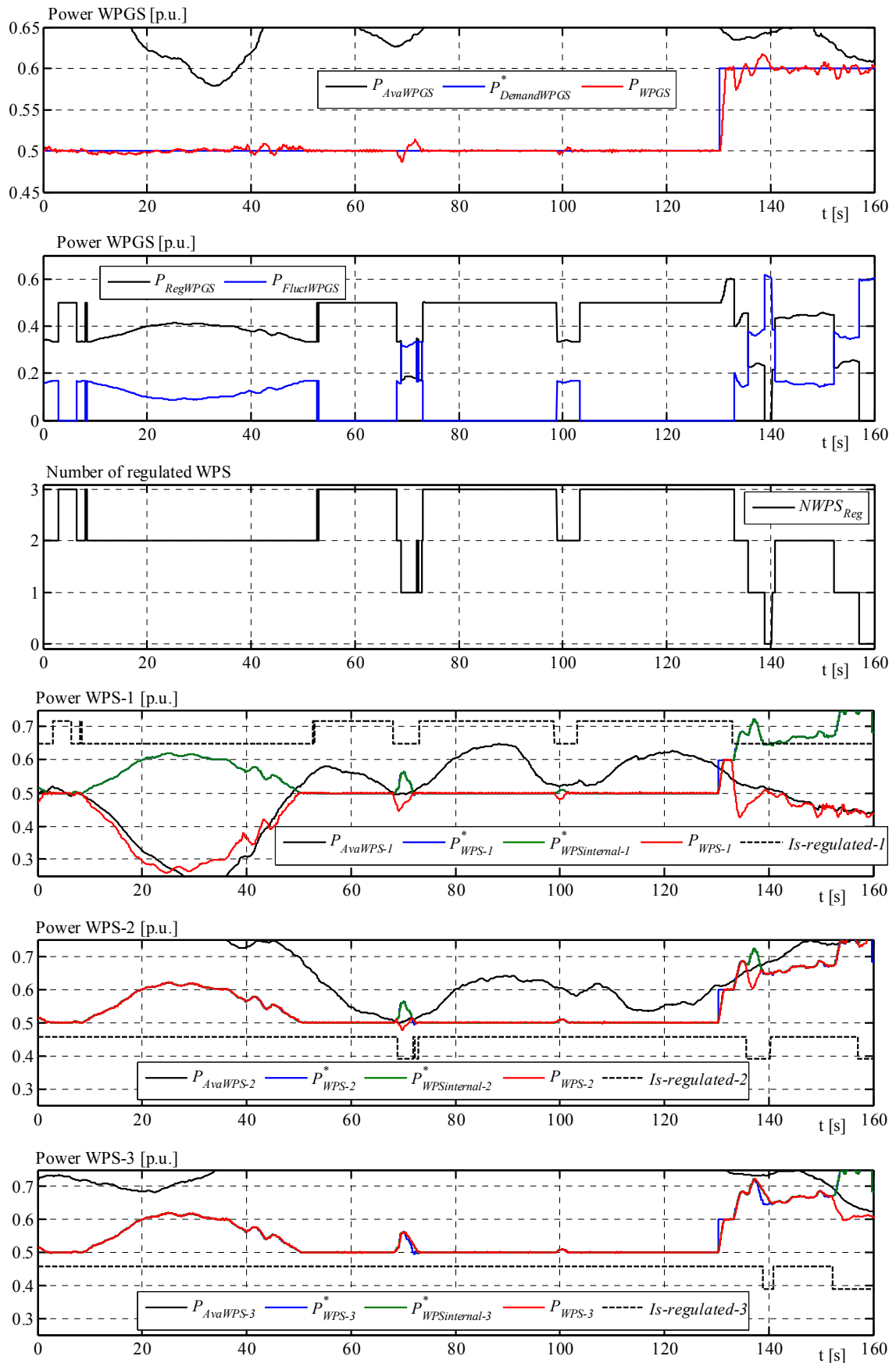
Figure 5-31: Dispatcher 1 working in a given WPGS made of three WPS.
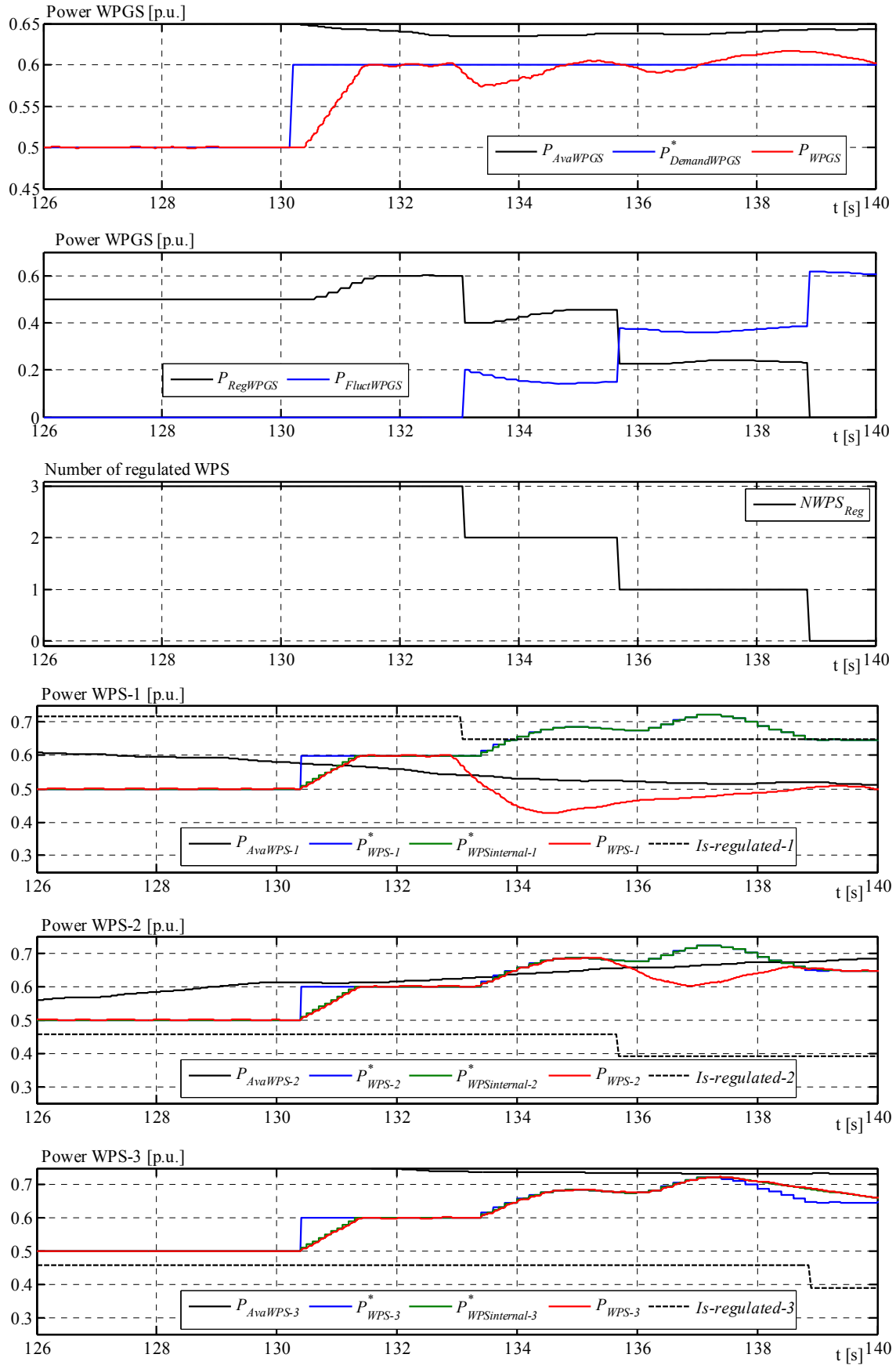
Figure 5-32: Zoom in. Dispatcher 1 working in a given WPGS made of three WPS.

5.3.4.2 Dispatcher 2

Here, only a basic description is done. The objective of this dispatching algorithm is to regulate the total WPGS production by constraining each WPS –when possible –with the same amount of power curtailment, $P_{CurtWPS-i}$. This dispatching algorithm is presented in other works e.g. [110]. Here it is extended to a generic implementation, i.e. PS, Cluster or WPP levels. **Figure 5-33** shows the dispatcher principle, and it works as follows:

- WPSs in the WPGS are curtailed in the same proportion.
- Total production of WPGS is maintained constant when possible.
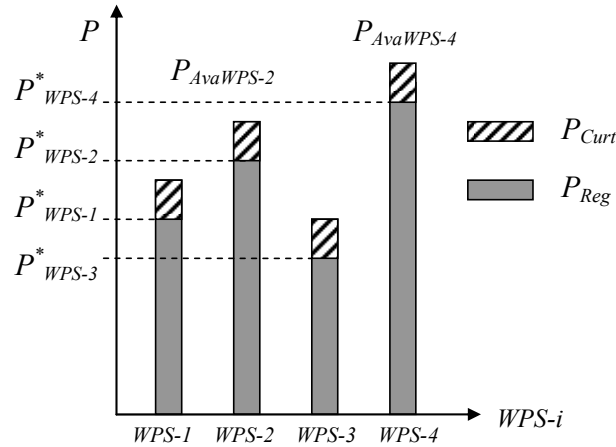
Figure 5-33: Dispatcher 2, principle. WPSs curtailed in the same proportion for generating a constant $P^*_{DemandWPGS}$ in the given WPGS.

Based on previous definitions, the following equations describe the dispatcher algorithm:

$$\frac{P^*_{WPS-1}}{P_{AvaWPS-1}} = \frac{P^*_{WPS-2}}{P_{AvaWPS-2}} = \ldots = \frac{P^*_{DemandWPGS}}{P_{AvaWPGS}} \tag{5.30}$$

Thus:

$$P^*_{WPS-i} = \frac{P_{AvaWPS-i}}{P_{AvaWPGS}} \cdot P^*_{DemandWPGS} \tag{5.31}$$

With:

$$P_{AvaWPGS} = \sum_{NWPS} P_{AvaWPS-i} \tag{5.32}$$

This algorithm is much simpler than Dispatcher 1.

5.3.5 Active power control

The Dispatchers 1 and 2 presented in previous sections (or any other dispatcher for wind power sources) are indeed *algebraic* power controllers. They receive a value of demanded power $P_{DemandWPGS}$ and communicate with actuators downstream sending suitable set points (calculated algebraically at each sampling step (k)) in order to obtain the demanded power. Actuators respond accordingly with their local dynamics. But the resulting overall power, controlled in this way, is only the summation of individual WPS powers (e.g. from each WTG or each WPP).

Grid Codes require the WPPs to be able to control the power flow at the point of common coupling, PCC (or point of interconnection, or point of measurement) [3]- [17]. In this case, the impedances between wind turbines and the PCC (cables and transformers) consume part of the generated power in the WPP, thus the $P_{DemandWPGS}$ cannot be obtained at the PCC by a dispatching control alone.

A close loop control power is necessary at WPP level in order to eliminate the error at the PCC caused by internal losses in the WPP grid. In the literature, the art of classical controllers and compensators is very well known [74]. In this work, a PI controller before the dispatcher for manipulating the $P_{DemandWPGS}$ is adopted. The integral action eliminates the internal losses upstream the PCC. This approach has been presented in works like [110] [111]. Figure 5-34 shows the block diagram of this compensator and its location in the WPP Controller. In this investigation, this power controller is used at WPP level only.
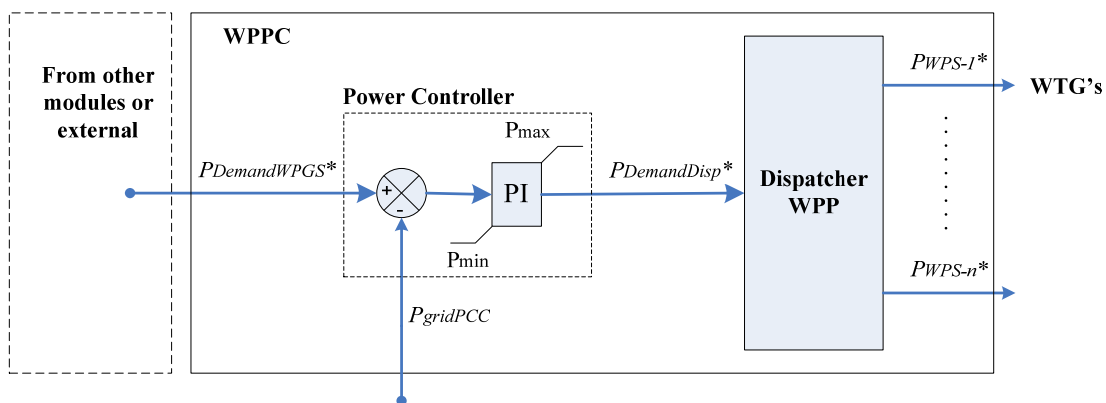
Figure 5-34: PI compensator for WPP losses.

5.4 Simulated performance of control architectures

The control functionalities proposed in the previous sections were tested together in different configurations (architectures). The objective was to identify the suitable architecture –among the candidates– that offers the best performance. The identification was accomplished by comparison of selected performance indicators. The performance of

the architectures is observed by accurate computational simulations. The architectures are implemented in a power system with high wind power penetration, where the inter-action with conventional generation is significant. Simulation results are also compared with a base case under no-controlled operation of wind power. The performance indica-tors are: i) error of the frequency fluctuation compared with the settings $\Delta F_{WindFluct}$ and ii) lost energy compared with the base case. The value of the nadir (minimum frequen-cy) is not taken as indicator here, since this is addressed in Chapter 6 where inertial re-sponse is combined with primary frequency response, therefore it can be observed that the nadir changes substantially in the simulations presented here.

5.4.1 Candidate architectures and simulation set up

The candidate architectures are three, described in **Figure 5-35**: (a) Power system level with Dispatcher 1 (PS-Dispatcher 1) and Dispatcher 2 (PS-Dispatcher 2); (b) wind pow-er plant level (WPP), and (c) wind turbine level (WTG). The simulations were carried out with two WPPs and three WTGs each. Observe carefully in this figure that each architecture contains the functionalities (blocks) developed in the previous sections, but located at the different levels.

The simulations were performed with the power system PS2 described in Chapter 3 and Appendix A.5. The simulation software was Power Factory DIgSILENT Gmb. The models for the wind turbines, wind speed, base case and wind power control character-istics (timings, measurements, etc.) are described in Chapter 3. This power system is relatively small, but presents high wind power penetration level and frequency sensitivi-ty to power fluctuations, as only one generator performs the normal regulation activity. Therefore it is expected a demanding activity for the wind power control as well as for the conventional frequency regulation.

Table 5-2 describes the simulation cases, **Table 5-3** presents the generation share for the simulated cases and **Table 5-4** presents the settings for the wind power control for the architectures. The values of $\Delta P_{WindFluct}$, R_{wind}, DB_{wind} and P_{ResWPS} were calculated considering: **Figure 5-10** (left), Δf_{min}, $\Delta f_{WindFluct}$, R_{SG1} and the size of generation loss SG3. The $Ramp_{Wind}$ was chosen according to the observed rate of change of system load (see measurements in Section 2.5.5.2), assuming this as the response speed of the SFC (worst case). In Chapter 6, a methodology for this calculation is presented.

Table 5-2: Simulation cases

Simulated case	Description	Results
Base case	Wind power generation with no restriction at all	Chapter 3, Figure 3-15
Case 1	Active power step response	Figure 5-36

Case 2	Power tracking and fluctuations limitation	Figure 5-37, Figure 5-38
Case 3	Power reserve and frequency control	Figure 5-40, Figure 5-41
Case 4	Frequency response to generation loss	Figure 5-42
Case 5	Frequency response to load loss	Figure 5-43

Table 5-3: Generation state for simulations

Power source	Initial power output condition			% share of total genera-tion capacity	H [s]	Comments
	% of consumption	% of name-plate capaci-ty	% of total capacity			
SG1	46	80	34	43	4.3	$R_{SG1} = 5\%$
SG2	23	62	17	28	4	-
SG3	11	100	8.5	8.5	2	*Tripped*
WPP1, WPP2	2 x 10	75	15.5	2 x 10.25	-	$Kp = 0.1$ $Ki = 0.1$ *Ramp = 7.5 %/s*
Consumption	100	82	75	95	-	-

Table 5-4: Parameters for architectures. Base power given by level capacity.

Parameter	Architecture (level)			
	PS-Dispatcher 1	PS-Dispatcher 2	WPP	WTG
$\Delta P_{windFluct}$	0.055 pu	0.055 pu	0.065 pu	0.15 pu
Δf_{min}	±0.3 Hz			
$\Delta f_{WindFluct}$	±0.05 Hz			
DB_{wind} $[Thr_{HF}, Thr_{LF}]$	±0.05 Hz			
R_{wind} $[R_{HF}, R_{LF}]$	2.5 %			
P_{ResWPS}	0.16 pu			
$Ramp_{Wind}$	3.3 %/10 min			

Figure 5-35: Candidate architectures analysed on the power system model PS2.

5.4.2 Case 1: Step Response

Figure 5-36 shows the simulation results with the description of the events. The wind power system was initially operating at available power (~0.7 pu) with each WPP at about the same production. All the control functionalities were disabled (fluctuations limitation, power tracking and frequency control), with the external reference, P_{ext}, at nominal value (max) and the wind turbines at optimal production. Three step changes were applied to the P_{ext} in the respective architecture, according to **Figure 5-35**. All the P_{ext} were stepped at the same time, independently of the architecture. As the other control functionalities were disabled, the P_{ext} passed through them, being communicated downstream through the respective dispatchers and affected by communication delays. For the implementation at PS and WPP levels, the P_{ext} ends as a reference for the PI controller, from where a demand reference for the Dispatcher 1, $P_{demandDisp}^{*}$, is generated (Figure **5-34**). But at WTG level, the P_{ext} is directly fed into the turbine. The response of the wind power production was observed here, whereas the performance of the power system was not interesting for the case.

At first view, it is clear to see the effect of the ramp rate limitation in all the tests, which was set to 7.5 %/s in each wind turbine and each PI controller. Thus, the response of the wind power to set point changes is mainly given by the imposed ramp rate value.

Due to the characteristics of Dispatcher 1, not all the "actuators" will initially respond to the demand from the dispatcher, because the signal sent from the PI controller is changing with the ramp rate, as seen in **Figure 5-36** bottom-right, with two turbines in WPP 1. Considering the concept described in **Figure 5-27**, the actuators with higher production will start deloading first, followed later by others. This produces a variable rate of change of produced power. This is applicable to WTGs as well as to WPPs, if they are controlled with a Dispatcher 1 and a ramp rate limiter on its input reference.

The test at the top-right shows a more clear response, since all the wind turbines were previously deloaded, therefore responding to an order for increase in production.

The attention should be paid at the total power at system level, since this is what is finally impacting in the frequency performance. From all the tested steps, it is clear that the implementation at WTG level shows the best performance. This is due to the lack of time delays in the signal communication. The only delay at WTG level is its sampling time of 100 ms. This characteristic implicates a better support to the power system during large frequency deviations, because the faster actuation. The worst performance was for the implementation PS-Dispatcher 1. This is due to the combination of time delays (300 ms in this example) and reduced number of actuators for responding. The resulting speed of actuation is proportional to the number of responding actuators. Considering this, Dispatcher 2 is in advantage over Dispatcher 1, because with Dispatcher 2 actuators are always following an external set point. The implementation at WPP level shows the second best performance due to the reduced delays, even though it is operating with a Dispatcher 1 topology.
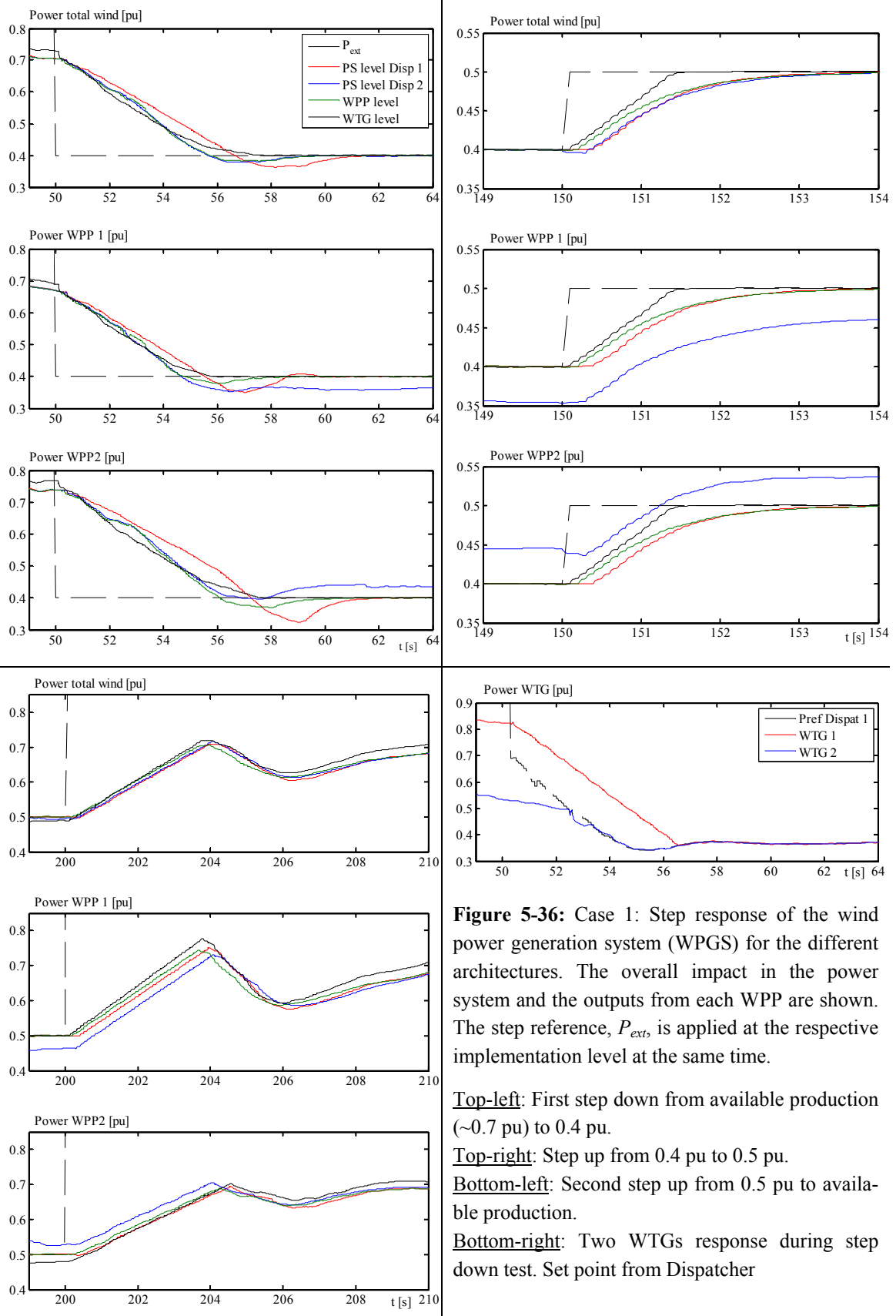
Figure 5-36: Case 1: Step response of the wind power generation system (WPGS) for the different architectures. The overall impact in the power system and the outputs from each WPP are shown. The step reference, P_{ext}, is applied at the respective implementation level at the same time.

Top-left: First step down from available production (~0.7 pu) to 0.4 pu.
Top-right: Step up from 0.4 pu to 0.5 pu.
Bottom-left: Second step up from 0.5 pu to available production.
Bottom-right: Two WTGs response during step down test. Set point from Dispatcher

203

5.4.3 Case 2: Fluctuations limitation and power tracking

Figure 5-37 and **Figure 5-38** show the simulation results including the impact on the power of conventional plant SG1 and the grid frequency. The base case of 30 min of continuous operation, previously defined in Chapter 3, Section 3.4.1, is used here. Initially, the system was operating at available power. Then, at $t = 150$ s the functionalities Fluctuations Limitation and Power Tracking were enabled. Observe in the results how the frequency fluctuations are effectively constrained about the specified value, but architectures take different times for settling it. The chosen ramp rate is almost not perceived during the simulated period. There is a permanent frequency deviation (according to discussion in Section 5.3.1) which is slowly eliminated by the power tracking. This frequency deviation can be easily corrected by a secondary frequency control (not simulated in this case). As the frequency *fluctuations* are limited satisfactorily (neglecting the permanent deviation), the question is: which architecture produces more energy? From the results it is obvious that the lost energy is larger when the control is implemented at WPP or WTG levels, in accordance with **Figure 5-10** right. Calculation of the produced energy during the last 15 min determined the architecture PS-Dispatcher 2 as the most efficient among the candidates. See **Figure 5-39** left, where generated energy, lost energy (compared to base case) and frequency fluctuations are shown.
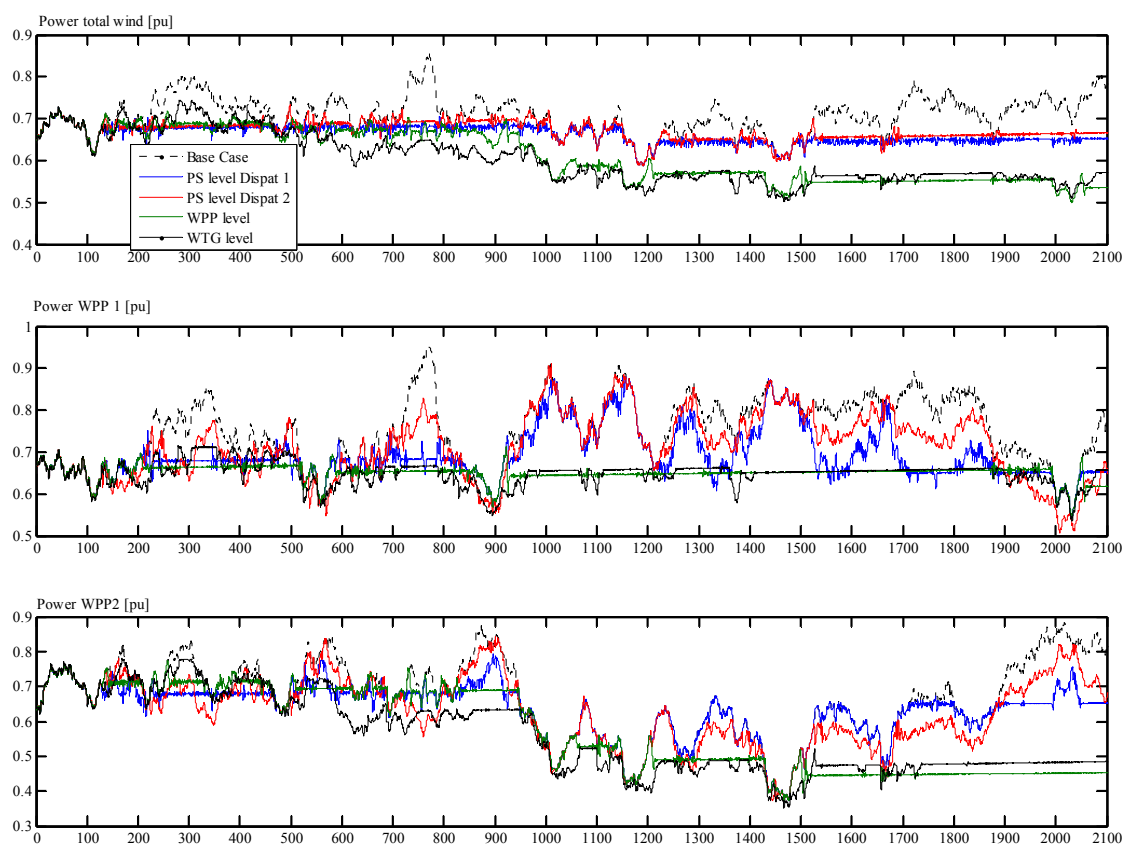
Figure 5-37: Case 2: Operation with fluctuation limitation and power tracking.
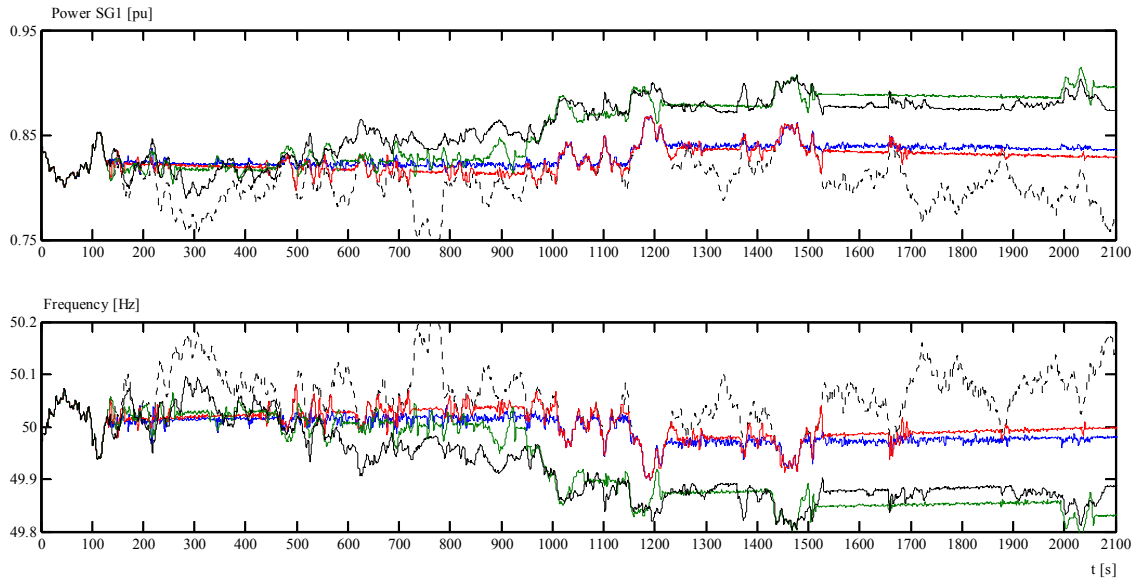
Figure 5-38: Case 2: Operation with fluctuation limitation and power tracking (cont.)
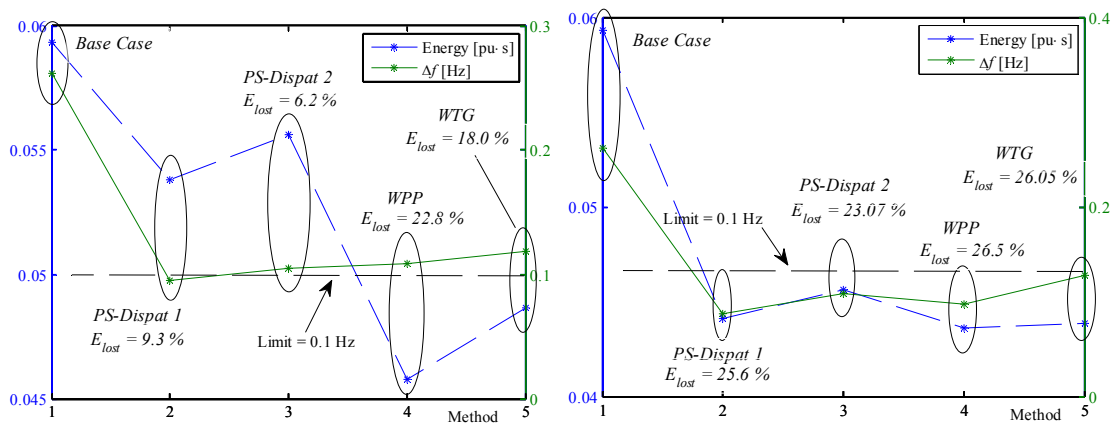
Figure 5-39: Comparison of generated and lost energies and amplitude of frequency fluctuations for Case 2 (left) and Case 3 (Reserve + F ctrl. enabled) (right).

5.4.4 Case 3: Power Reserve and Frequency Control

Figure 5-40 and **Figure 5-41** show the simulations results including the impact on the power system. The base case is as the previous, operating initially at available power. At $t = 150$ s the functionalities Fluctuations Limitation and Power Tracking were enabled (similarly to the previous case). At $t = 450$ s the allocation of Power Reserve was enabled. Finally, the Frequency Control was enabled at $t = 850$ s. Observe how the reserve of power is maintained in the period 450s $< t <$ 850s and, at the same time, the power fluctuations are limited to the specified value. The amount of generated energy during this period differs among architectures, being the highest for PS-Dispatcher 2 and PS-Dispatcher 1. The lower energy from the other two architectures is due to the lack of "coordination" among wind power production in the system. The implementation at PS level permits the allocation of the reserve by coordinating the production of

the wind plants. Observe in this period how wind power plants produce a variable output, while the combined production remains "constrained" at system level. This produces a direct (positive) impact on the system frequency. The same observations are valid for the previous case. The activation of the frequency control at $t = 850$ s produces a noticeable change in the system behaviour. Four mechanisms are active at this stage: i) fluctuations limitation, ii) power tracking, iii) power reserve and iv) frequency response (control). The frequency control is activated every time the frequency goes beyond the deadband, producing a self-stabilizing effect and keeping the grid frequency inside the deadband (i.e. 50±0.5 Hz). The fluctuations limitation still limits the power variations but one of these two mechanisms will actuate first, whichever reaches its setting first. The power tracking will slowly increase the power production following the increase in available power, unless the frequency controller is activated by over frequency. Obviously, the produced energy is much more less on all the architectures due to the amount of reserved power. **Figure 5-39** right shows the numbers for produced energy, lost energy and frequency fluctuations for the last 15 min simulated. The implementation PS-Dispatcher 2 shows the highest performance in terms of generated energy. Regarding fluctuations of frequency, it has to be considered that the implementation at WPP and WTG levels are "open loop" controls, being this performance dependant on the settings of individual $\Delta P_{WindFluct-i}$ as discussed in Section 5.3.1.1 and **Figure 5-10**.
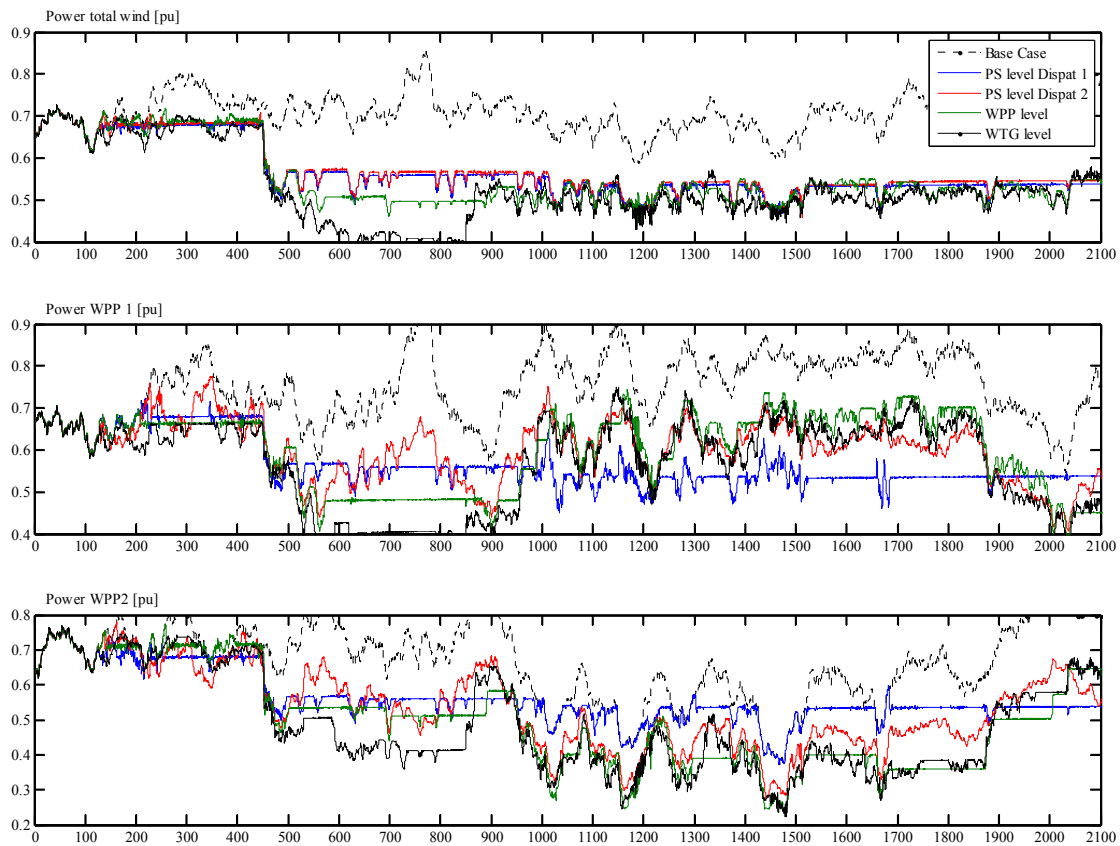
Figure 5-40: Case 3: Operation with power reserve and frequency control.
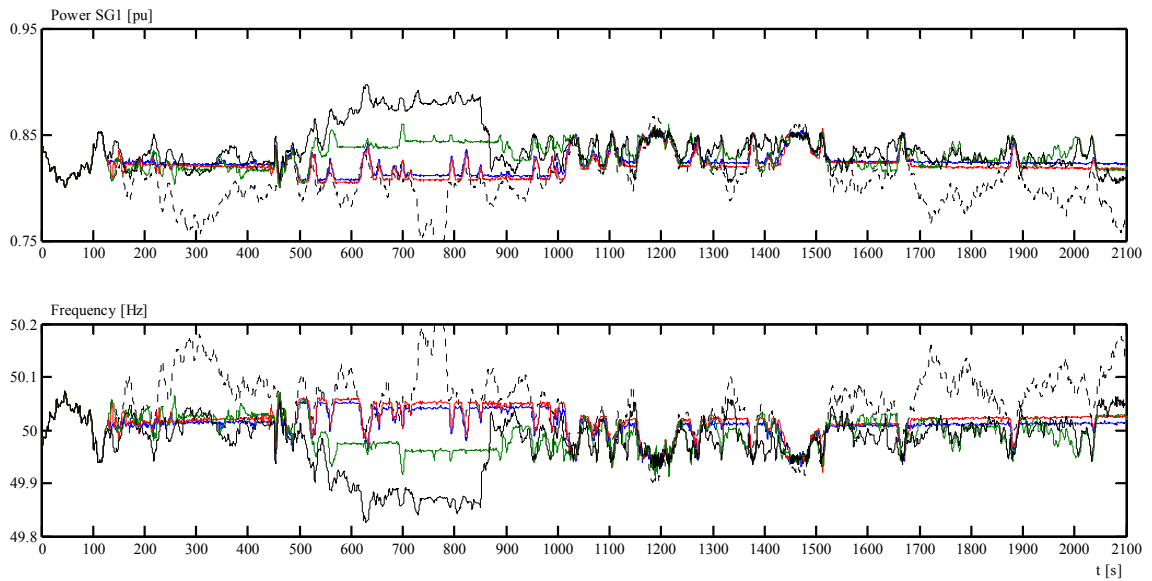
Figure 5-41: Case 3: Operation with power reserve and frequency control (cont.).

5.4.5 Case 4: Generation Loss Frequency Response

The initial conditions for this case are the final conditions from the previous case. A generation loss of SG3 = 11 % of demand was simulated for each candidate. The frequency response was compared with a similar event in the base case. Further data on power reserve, generation, regulation, etc. are in **Table 5-3** and **Table 5-4**. The **Figure 5-42** shows the simulations results.

From the results it can be seen that the frequency response of the system is adversely affected with the implementation level. The minimum nadir (maximum frequency deviation) is for the base case, where there is no frequency response from wind power. The maximum nadir is for the implementation at WTG level. This behaviour was expected from the observations in Case 1 and it is mainly due to the accumulation of time delays with the implementation level. **Table 5-5** shows the values of nadir for cases 4 and 5, with the % of degradation taking as reference the best response (WTG level). It is clear that at WTG level it is obtained the best frequency response (due to the delays), whereas the PS-Dispatcher 2 showed better performance than PS-Dispatch 1, due to the number of "actuators" responding to the reference. This is confirmed by the power drop at $t = $ ~4 s for the PS-Dispatcher 1 (looking from the total power point of view).
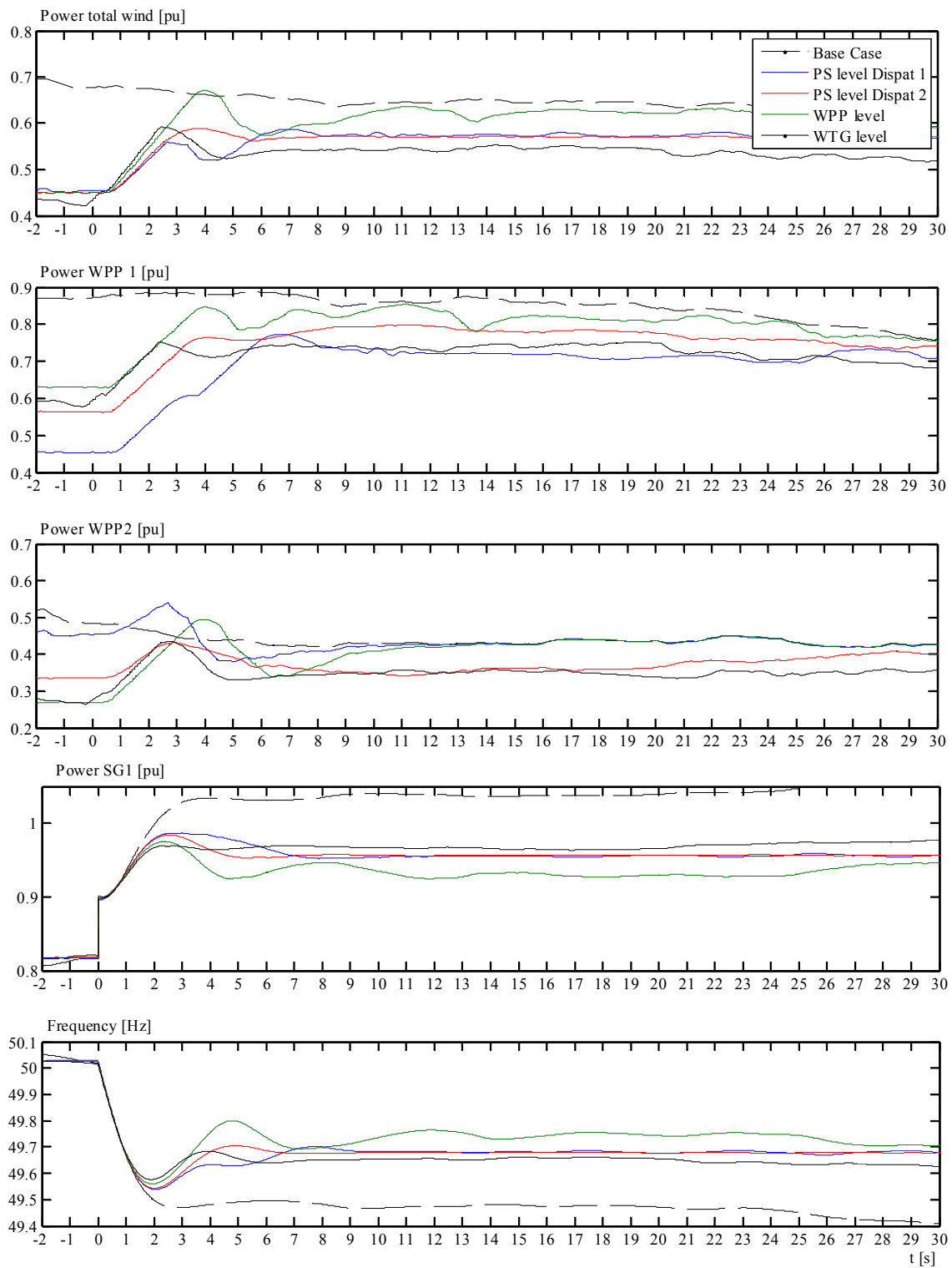
Figure 5-42: Case 4: generation loss frequency response.

Table 5-5: Comparison Case 4 & Case 5.

Case	Indicator	Architecture				
		Base case	PS-Dispat 1	PS-Dispat 2	WPP	WTG
Case 4	t_{fmin} [s]	3	2.05	2	1.95	1.9
	f_{min} [Hz] (degradation %)	49.47 (24.7%)	49.538 (8.7%)	49.545 (7.06%)	49.56 (3.53%)	49.575 (0%)
Case 5	t_{fmax} [s]	2.7	2.35	2.25	2.2	1.95
	f_{max} [Hz] (degradation %)	50.55 (26.43%)	50.518 (19.08%)	50.475 (9.2%)	50.457 (5.06%)	50.435 (0%)

5.4.6 Case 5: Load Loss Frequency Response

It is similar to the Case 4 but simulating a load loss of 11 % of demand instead of a generation loss. The initial conditions for this case were different than for Case 4. The wind power production was operating at 100% of available power before the event, similarly to the base case. The frequency response was compared with a similar event in the base case. Further data on power reserve, generation, regulation, etc. are in **Table 5-3** and **Table 5-4**.The **Figure 5-43** shows the simulations results. The results show a similar behaviour than previous case and similar conclusions can be drawn.

Table 5-5 shows the respective values of nadir and % of degradation taking as reference the best response (WTG level). It is clear that at WTG level it is obtained the best frequency response (due to the reduced delays), whereas the PS-Dispatcher 2 showed better performance than PS-Dispatch 1, due to the number of "actuators" responding quickly to the reference change. This is confirmed by the small power increase at $t = \sim 1$ s for the PS-Dispatcher 1 (looking from the total power point of view), which affected the rest of the response due to the ramp rate limiters in the PI controllers.
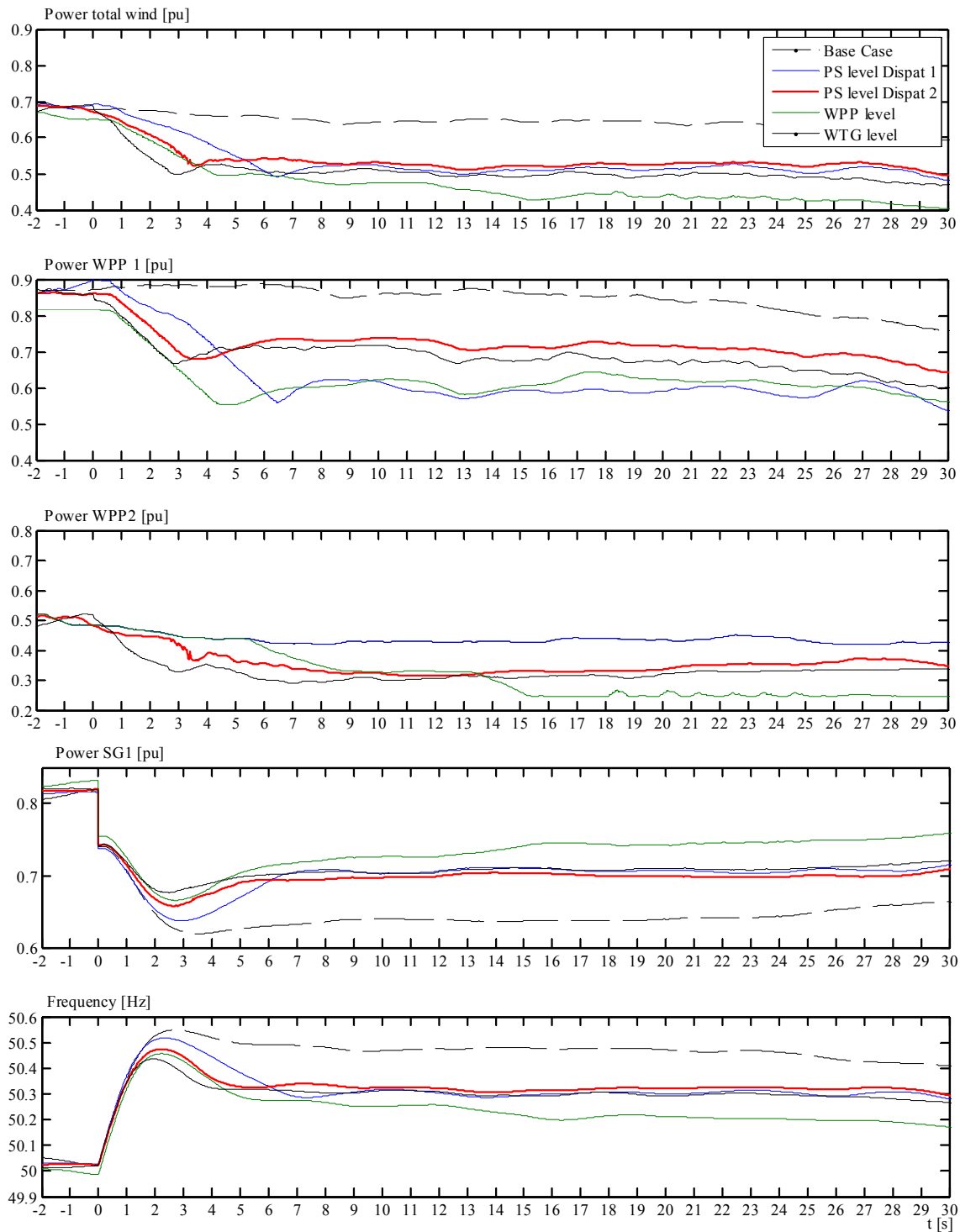
Figure 5-43: Case 5: load loss frequency response.

5.5 Conclusions

This chapter has proposed, developed and studied control architectures for the wind power production in the power system. The architectures are provided with control functionalities that perform in a combined manner. This combination of control functionalities aims at managing the variability of the generated wind power in order to re-

duce the impact on the grid frequency and to provide with suitable frequency regulation service to the system when required.

Firstly, the control objectives were defined based on requirements proposed in Chapter 2. Secondly, the control functionalities for meeting the objectives were defined, which are: i) fluctuations limitation control, ii) power tracking control, iii) frequency control, iv) active power control and v) dispatching algorithms 1 & 2. Thirdly, control architectures for implementing the control functionalities were proposed. The proposed architectures are classified according to the application level, which are: Power System level, Wind Power Plant level or Wind Turbine level.

By considering the system regulation constant (or system stiffness) it was possible to determine the amount of allowed wind power fluctuations in the power system. Thus, wind power fluctuations were kept restricted as well as grid frequency fluctuations. The frequency controller was developed by "combining" the frequency control methodologies from the Irish Grid Code and the British Grid Code, thus getting the benefits from both.

The performance of the control architectures were observed through computational simulations of a small real power system. Simulation results were compared with the measurements carried out on this power system under no-controlled operation of wind power, which was presented in Section 2.5. Architectures present different performance depending on the simulated operation.

To choose the most suitable architecture is not straightforward. It depends on many factors, especially on communication infrastructure. The recommended architecture is the implementation at power system level with power tracking Type 1 and Dispatcher 2. It provides the highest energy yield with an acceptable dynamic performance on dynamic events. The dispatching algorithm permits wind power plants to balance each other's fluctuations, keeping a constant power balance at system level. Its negative side is that it relies on the information of the "available power", which is estimated based on wind speed and aerodynamical models, introducing uncertainties in the estimated value. This architecture is used in Chapter 6 for studies of coordination with conventional plants and combination with inertial response functionality, which was addressed in Chapter 4.

6

COORDINATION AND PERFORMANCE OF WIND TURBINES FREQUENCY CONTROL

The aim of this chapter is to study the coordination between the frequency response mechanisms developed in the previous two chapters and the standard regulation mechanisms in power systems, in terms of regulating characteristics and power reserves. The combined contribution of wind power inertial and primary frequency control responses is assessed. The performance and the capability for supporting the grid during large load events are evaluated through computational simulations.

6.1 Introduction

In Chapter 4 the analysis, development and study of inertial response functionality (IR) for variable speed wind turbines (WTG) were carried out. Rather than studying the impact on the power system, focus was done exclusively on the capabilities of the WTG and the WPP for providing IR. One of the main characteristics of IR is the power drop in WTG output during its recovery period. This power drop is highly dependent on the wind and curtailment conditions: The power drop is more significant for wind speeds close to the nominal but it is largely reduced with relatively small curtailments. Other important characteristic of IR is that the individual power drops are masked inside a large WPP: As wind speeds are different for each turbine inside the WPP, the power drops are also different (and sometimes inexistent) and the final impact in the overall WPP output is reduced.

In Chapter 5 the analysis, development and study of active power and frequency control architecture for wind power generation were carried out. That study was not aimed to coordinate the wind power production with the power system. Rather, it was focused on the algorithms and functionalities to provide the desired responses at power system level. The performance of the architectures were studied on a given power system with high wind power penetration. From this, a suitable architecture (PS-Dispatcher 2) was identified.

In this chapter, the overall assessment of such functionalities working together (IR + PS-Dispatcher 2) is conducted. It is important to know how these functionalities interact with each other and, more important, how the impact on the power system is. For a giv-

en wind power forecast, penetration level and system conditions the wind power controller parameters should be adjusted in order to get a suitable coordination for both, power system stability and reduced energy loss. The necessary wind power reserve, frequency response characteristic (droop) and control dead bands need to be determined for the system conditions. A basic methodology for this coordination was developed in this work, which is described in this chapter.

6.2 Chosen control architecture

In Chapter 5 the architecture which implements the frequency control at system level with the Dispatcher 2 (PS-Dispatcher 2) was identified as the most suitable. Due to the time delays in communication, the implementation at WTG level offers faster response, but coordination during normal operation is difficult.

Figure 6-1 shows the chosen architecture for simulations in this chapter, which is based on the **Figure 5-35** (a). With this architecture, the combined response of the functionalities developed in Chapter 4 and Chapter 5 is tested to assess the performance on a power system with high wind power penetration.

The wind power system of **Figure 6-1** consists of two wind power plants located at different points in a power system, each containing 25 wind turbines and communicated to a central controller. As studied in Chapter 5, this architecture performs active power and frequency control functionalities that are split in tree levels, which are:

1- Power system level functionalities: i) absolute power constraint, ii) limitation of overall active power fluctuations, iii) power tracking type 1 for overall production increase, iv) total power reserve, v) primary frequency control and vi) dispatcher-2, which communicates downstream with the WPPs, sending set points and receiving WPP's status.
2- Wind power plant level functionalities: i) active power close loop control at PCC which receives set point from Dispatcher 2 and ii) dispatcher-1, which communicates downstream with the WTG's, sending set points and receiving WTG's status.
3- Wind turbine level functionalities: i) optimal production, ii) constrained production with external set point from Dispatcher 1 and iii) inertial response. All these performed by an active power close loop control in the WTG.
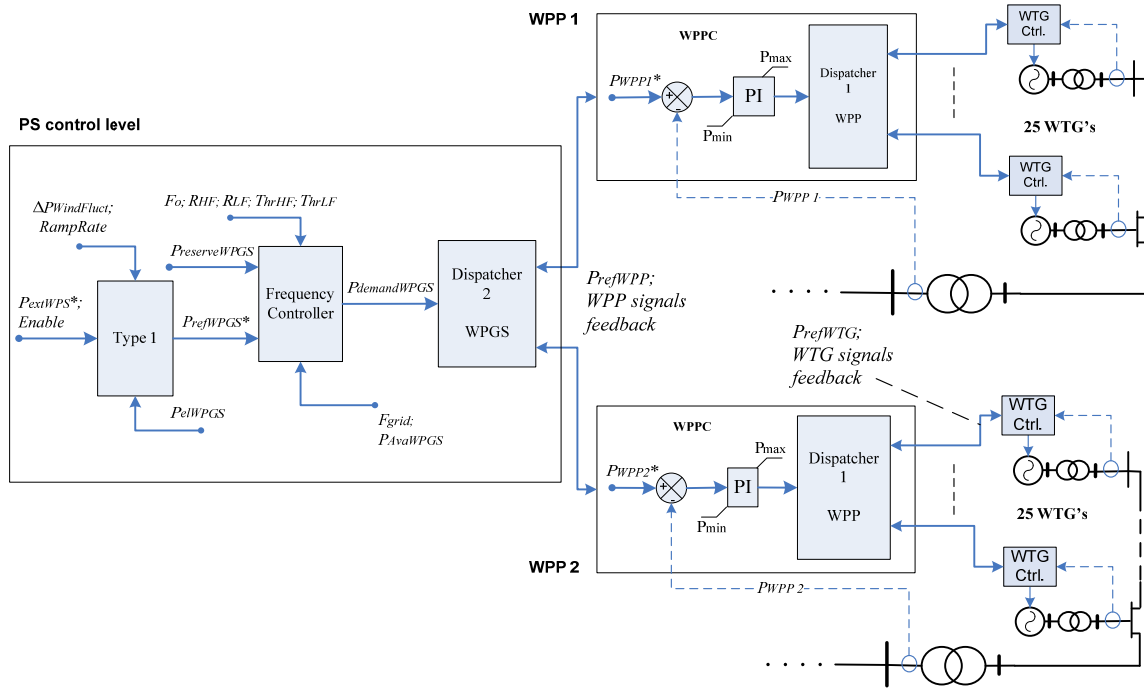
Figure 6-1: Control architecture at system level for wind power production

6.3 Coordination of wind power frequency control

The operation of relatively large amounts of wind power together with conventional power plants needs to be coordinated in terms of regulating characteristics and power reserves, aiming at the power balance and frequency stability of the grid. The need for coordination is more evident when the wind power production participates with regulation services for the system.

Taking into account the studied controls in the previous two chapters, in this work the coordination between wind and conventional production involves setting the parameters of the wind power controls for: i) normal operation regulation, ii) disturbance regulation (contingency) and iii) inertial response.

The coordination of normal and disturbance regulations requires setting the parameters of the control architecture developed in Chapter 5, shown in **Figure 6-1**. Those parameters are: frequency control deadband, DB_{Wind}; frequency response characteristic, R_{Wind} (droop); allowed overall wind power fluctuation, $\Delta P_{WindFluct}$; power tracking ramp rate, $Ramp_{Wind}$ and amount of wind power reserve P_{ReWPGS}. A basic algorithm for this coordination is proposed here.

In order to simplify the presentation of the concept, the distinction between normal regulation and disturbance regulation is not considered in the algorithm. This means that

the specified values of maximum frequency deviation and required power reserves can be thought as characterizing either operation of normal regulation or disturbance regulation (obviously, the respective values will be different). As grid codes specify a linear frequency response (static droop) from conventional plants, the combined (equivalent) response at system level is as shown in **Figure 6-2** left, where the maximum frequency deviation Δf_{Max} and the required conventional power reserve $\Delta P_{ResConv}$ are used. The wind power frequency response as defined in **Figure 5-21** (a) is also depicted here at the right. Because in the chosen wind power control architecture the frequency response is managed centrally, the **Figure 6-2** lumps the overall system frequency response in two main groups: a) conventional generation frequency response and b) wind power generation frequency response. The coordination between these two groups is carried out here and based on this figure.
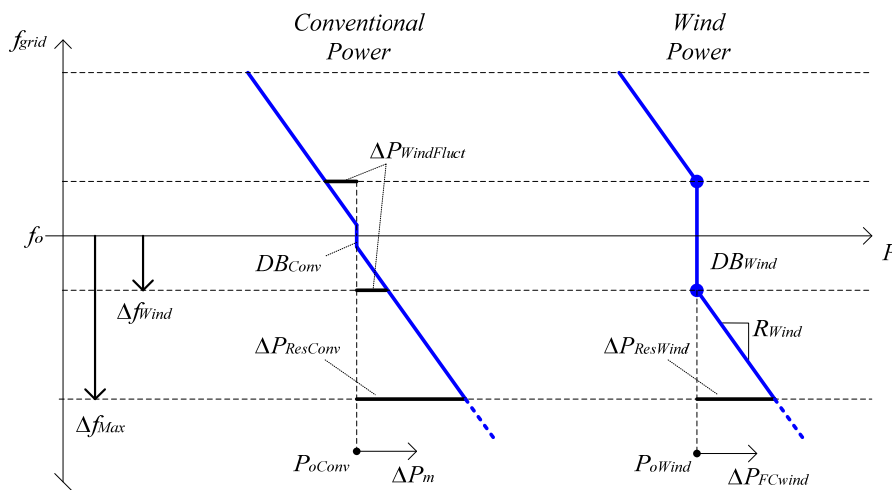
Figure 6-2: System frequency response characteristics from conventional generation (left) and wind power generation (right).

The proposed coordination algorithm is given by the following three steps:

1– Define:

   a. Maximum (allowed) static deviation of system frequency following a dimensioning load change, Δf_{Max}. This value is different among grid codes, as shown in e.g. **Table 2-2**.

   b. Amount of required system frequency activated reserves, ΔP_{ResSys}. This value also differs from system to system and it depends on the dimensioning load change and the load-frequency characteristic.

   c. Maximum allowed frequency deviation caused by wind power fluctuations, $\Delta f_{WindFluct}$. This was studied in Section 5.3.1 and in this work it is considered as a new specification from grid codes.

    d. Deadband of the speed-governors of conventional plants, DB_{Conv}, defined in the respective grid code.

2– Determine the power reserves form the individual generators, including WPPs, as a result from e.g. the trading in the regulation market. This gives:

    a. The *total* amount of reserve from conventional plants, $\Delta P_{ResConv}$.

    b. The *total* amount of reserve from wind power production, $\Delta P_{ResWind}$.

    c. The installed capacity $P_{N\text{-}WPPi}$ of wind plants WPP-*i* contributing with regulation reserves, i.e. connected to the control system as in **Figure 6-1**.

The following basic equation should be satisfied:

$$\Delta P_{ResSys} = \Delta P_{ResConv} + \Delta P_{ResWind} \tag{6.1}$$

3– Determine the parameters for the centralized wind power frequency control: DB_{Wind}, R_{Wind}, $\Delta P_{WindFluct}$, $\Delta P_{ResWind}$ and $Ramp_{Wind}$. Based on **Figure 6-2** and the previous steps, these parameters are given by:

$$DB_{Wind} = \Delta f_{WindFluct} \tag{6.2}$$

$$R_{Wind} = \frac{\Delta f_{Max} - \Delta f_{WindFluct}}{f_0} \cdot \frac{\sum_n P_{N-WPPi}}{\Delta P_{ResWind}} \tag{6.3}$$

$$\Delta P_{WindFluct} = \frac{\Delta f_{WindFluct} - DB_{Conv}}{\Delta f_{Max} - DB_{Conv}} \Delta P_{ResConv} \tag{6.4}$$

$$P_{ResWPGS} \geq \Delta P_{ResWind} \tag{6.5}$$

Setting a proper value for $Ramp_{Wind}$ is controversial, since the intention with this ramp is to follow an eventual increase in available power. This increase in production is feasible as long as: i) the wind power production is allowed to produce differently than the scheduled power, ii) the grid frequency is below ($f_o + DB_{Wind}$) –otherwise the frequency controller would be activated producing a self-constraining effect– and iii) the ramp rate setting is according to the *bandwidth of the secondary frequency control*. Nevertheless, there is no risk of creating an over-frequency by this ramp increase since the wind power frequency control is activated for frequencies beyond (+) DB_{Wind}, generating in this way a self-constraining effect. An obvious drawback of the ramp limiter is that it cannot constrain the wind power drops. But, as shown in Chapter 5 with the simulation Case 3, Section 5.4.4, if the wind power production is being operated with a certain $\Delta P_{ResWind}$, then the frequency drop caused by a drop in available wind power will make self-use of the frequency activated reserve from the $\Delta P_{ResWind}$. In this way the frequency deviation

caused by wind will be self-constrained to a (−) DB_{Wind}, giving time for the secondary frequency control actuation. Additionally, after an eventual power drop followed by an increase in available power, the wind power production would be restored automatically with a ramp rate. The value of $Ramp_{Wind}$ should be chosen according to some criteria from the TSO, but in general it should not be larger than the bandwidth of the secondary frequency control.

With respect to inertial response coordination, it requires setting the parameters of the control developed in Chapter 4, regarding grid event detection and activation. Those parameters are: activation frequency, *Thf*, and activation frequency rate of change, *Thdf*. The setting of these parameters is also controversial, since, as discussed in Sections 4.2.1 and 4.3.3: i) it is not necessary an IR contribution for small events and ii) the activation of IR at different moments in the process may result in different performances of the grid frequency stabilization. As a general rule, the setting of these parameters should aim to: i) activate the IR functionality only when it is necessary for the grid, e.g. with large grid events and ii) activate the IR functionality at the right moment, e.g. when prime movers have already started increasing powers (an excessively retarded activation will reduce the contribution effect of the IR though).

A study of the specific power system response, including governors and prime movers dynamics, as exemplified in **Figure 2-8** and **Figure 2-9** is useful for determining a suitable setting for *Thf*: The IR activation should be enabled at the moment that prime movers are activated, depending on the severity of the event. Additionally, measurements similar to the presented in **Figure 2-28** are useful for knowing the values of the normal ROCOF at which the IR should *not* be activated.

Regarding the other parameters of the IR functionality described in Chapter 4, this control should be already tuned to offer the best WTG inertial contribution depending on grid event characteristics, wind conditions, pre-event production (curtailment) and desired power drop during recovery period.

The combination of inertial and frequency responses improves the performance of the grid frequency deviation upon large events. The effectiveness of the proposed coordination is demonstrated in the next section by accurate computational simulations of power system cases with high wind power penetration.

6.4 Simulated performance

The power system model PS3 (a modified 9-bus system, as described in Chapter 3 and Appendix A.6) is used for simulations of two wind power penetration scenarios (Scenario A and Scenario B) and comparison with a Base Scenario, as shown in **Figure 6-3** and described as follows:

- **Base Scenario:** synchronous generators G1, G2, and G3 supplying ~28% of the load and G4 supplying ~15% of the load.
- **Scenario A:** wind plant 1 (WPP1) replacing G3 by supplying the same power at ~75 % WPP loading (30% wind penetration).
- **Scenario B:** wind plants 1 & 2 (WPP1 & WPP2) replacing G3 and G2 respectively by supplying the same power at ~75% loading each WPP (60% wind penetration).

The replacement of conventional generation introduces two effects in these Scenarios: i) reduction of regulation capacity from conventional plants and ii) reduction in system inertia.

For Scenarios A and B, three simulation cases were carried out:
- **Case 1:** Normal system operation. Continuous operation of the system with fluctuating wind power. A secondary frequency control loop is implemented in G1.
- **Case 2:** Primary frequency control response. The wind power is simulated providing primary frequency response only, as defined by **Figure 6-2** (right).
- **Case 3:** Inertia and primary frequency control combined response. The simulation is repeated with the wind power providing a combined response of inertial response plus primary frequency response.

Table 6-1 summarizes the load flow and settings for all the Scenarios. The settings were obtained by following the description in Section 6.3. The modelling is as described in Chapter 3. The simulation tool used was Power Factory DIgSILENT GmbH, with the modelling frames for the wind power control architecture as presented in Appendix D.
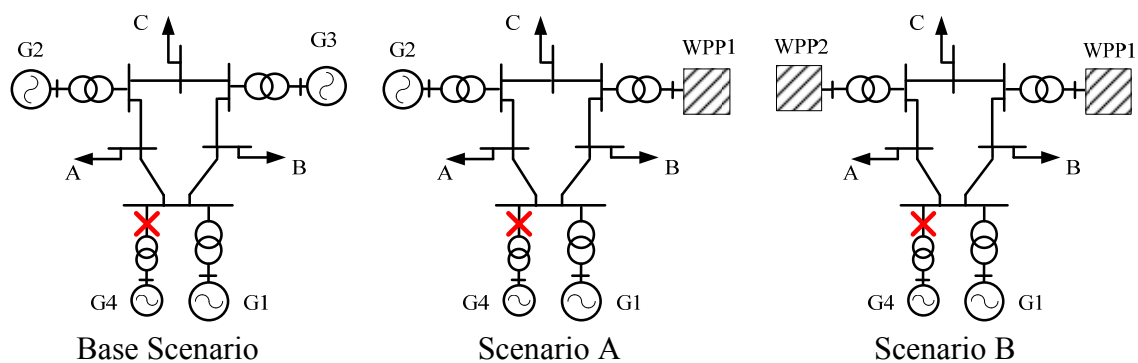
Figure 6-3: Simulated Scenarios with the modified 9-bus system

Table 6-1: Parameters of simulated Scenarios. Base power given by system load.

Data source	Parameter	Base Scenario	Scenario A ~30% WP$_I$	Scenario B ~60% WP$_I$
Power system conditions	P_{Load}	1 pu	1 pu	1 pu
	P_{oG1}	~0.283 pu	~0.283 pu	~0.283 pu
	P_{oG2}	~0.283 pu	~0.283 pu	-
	P_{oG3}	~0.283 pu	-	-
	$P_{oG4(Tripped)}$	0.15 pu	0.15 pu	0.15 pu
	P_{oWPP1}	-	**~0.283 pu**	**~0.283 pu**
	P_{oWPP2}	-	-	**~0.283 pu**
	H_{sys} (post event)	10.18 s	**8.02 s**	**4.15 s**
Power system requirements (Grid Code)	F_o	50 Hz	50 Hz	50 Hz
	Δf_{max}	±0.5 Hz	±0.5 Hz	±0.5 Hz
	$\Delta f_{windfluct}$	±0.05 Hz	±0.05 Hz	±0.05 Hz
	DB_{conv}	±0.015 Hz	±0.015 Hz	±0.015 Hz
	ΔP_{sysres}	0.15 pu	0.15 pu	0.15 pu
Regulating market	$\Delta P_{ResConv}$	0.15 pu	**0.10 pu**	**0.05 pu**
	$\Delta P_{ResWind}$	-	**0.05 pu**	**0.10 pu**
	P_{ava}	-	**~0.35 pu**	**~0.70 pu**
	K_{G1}	0.1 pu/Hz	0.1 pu/Hz	0.1 pu/Hz
	K_{G2}	0.1 pu/Hz	0.1 pu/Hz	-
	K_{G3}	0.1 pu/Hz	-	-
Wind power control settings	DB_{wind}	-	**±0.05 Hz**	**±0.05 Hz**
	R_{wind}	-	**7.2 %**	**7.2 %**
	$\Delta P_{windFluct}$	-	**~0.0073 pu**	**~0.005 pu**
	ΔP_{curt}	-	**0.05 pu**	**0.10 pu**
	$Ramp_{Wind}$	-	**1 %/min of $P_{oGTripped}$**	**1 %/min of $P_{oGTripped}$**

6.4.1 Case 1: Normal operation

6.4.1.1 Scenario A

Figure 6-4 and **Figure 6-5** show the simulation results. The grid frequency, shown here as the speed of G1, is bounded between ±0.05 Hz as established by $\Delta f_{WindFluct}$. The power contribution of the wind power frequency control is indicated by ΔP_{PFC} and the power contribution of the secondary frequency control of G1is indicated by ΔP_{SFC}. Observe how the ΔP_{SFC} balances the average wind power increase, while the wind power generation regulates the grid frequency inside the allowed range. The speed of increase in wind power is limited by the $Ramp_{Wind}$, which was chosen according to the SFC dynamics. The PFC of G1 and G2 (governors) actuate continuously. Power output fluctuations from wind turbines are balanced internally in the WPP by the Dispatcher 1 while the WPP production fluctuates according to $\Delta P_{WindFluct}$.
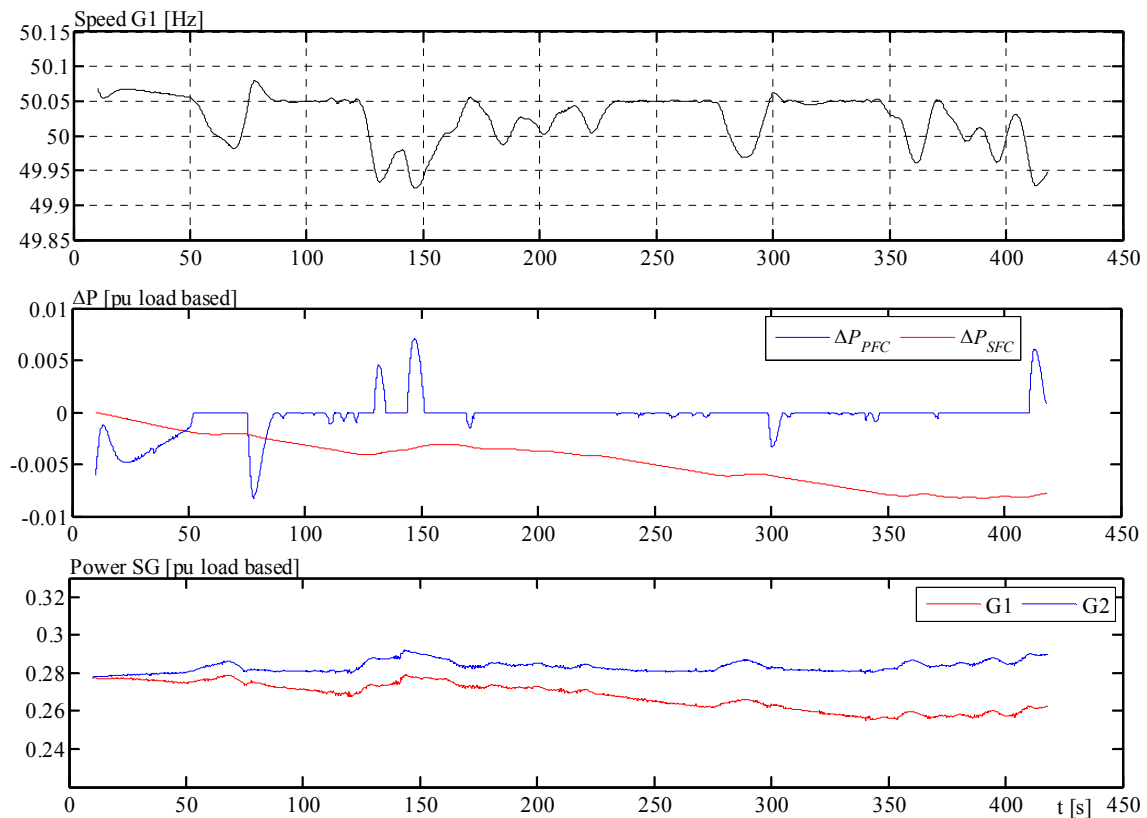
Figure 6-4: Case 1, Scenario A. Continuous system operation with 30 % wind power penetration.
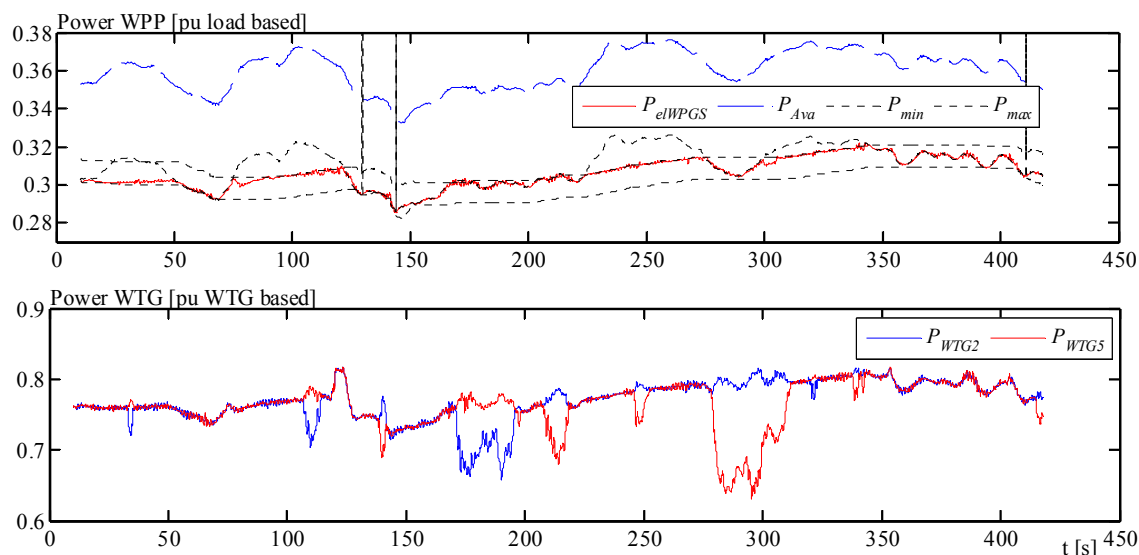
Figure 6-5: Case 1, Scenario A. Continuous system operation with 30 % wind power penetration (Cont.)

6.4.1.2 Scenario B

Figure 6-6 and **Figure 6-7** show the simulation results. Similarly to the Scenario A (30 % wind power penetration), the grid frequency shown here as the speed of G1 is bounded between ±0.05 Hz, as established by $\Delta f_{WindFluct}$. It can be noticed a higher activity of the wind power frequency controller to self-regulate the larger wind power fluctuations. Due to the number of conventional plants being reduced, the stiffness of the system is also reduced, thus wind power fluctuations need to be reduced in order to maintain the grid frequency inside the same boundaries than for the Scenario A. Observe in the figures how the WPPs production are regulated by the Dispatcher 2, while at the same time, the WTGs production in each WPP are regulated by the Dispatcher 1, respectively.
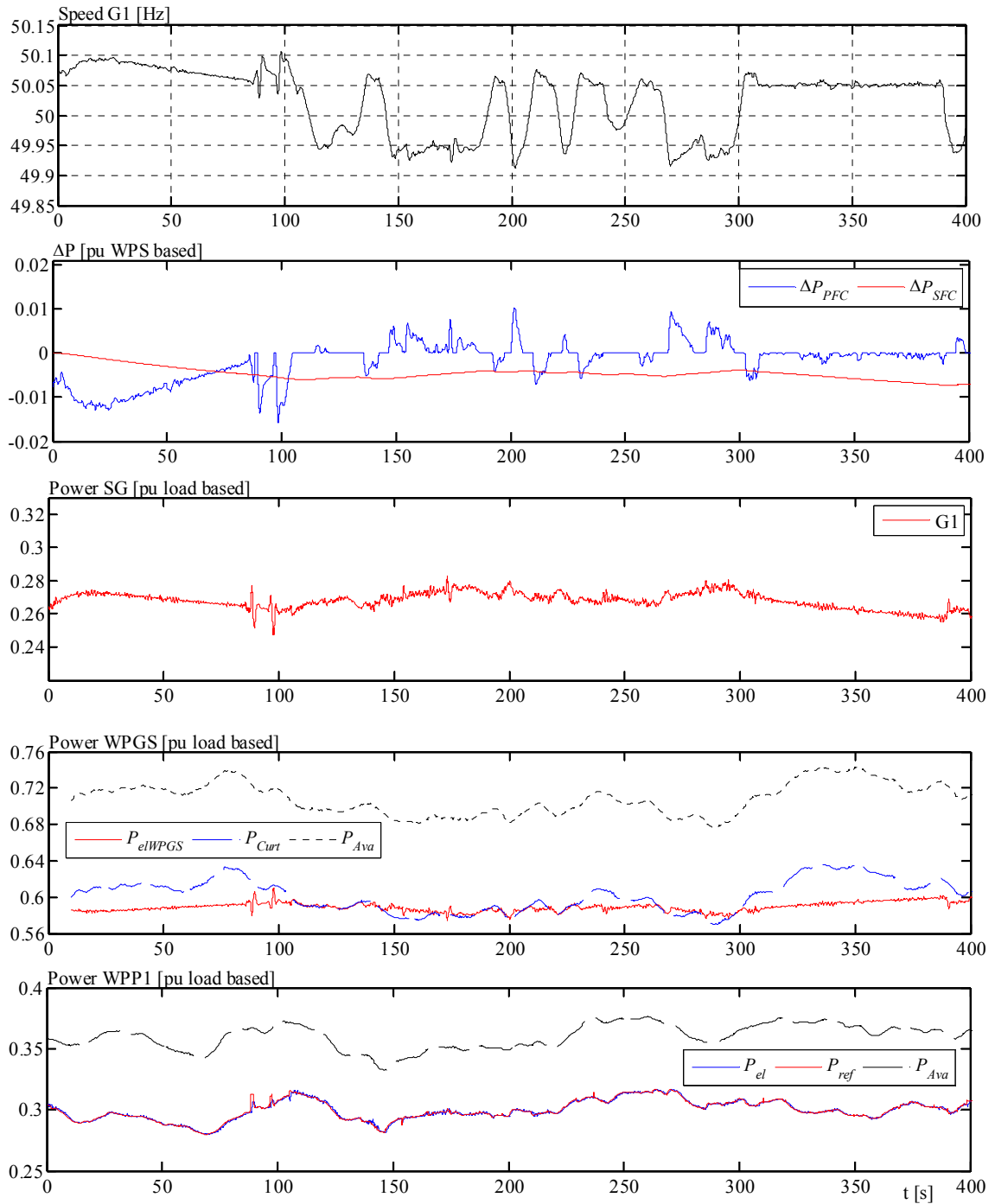
Figure 6-6: Case 1, Scenario B. Continuous system operation with 60 % wind power penetration.
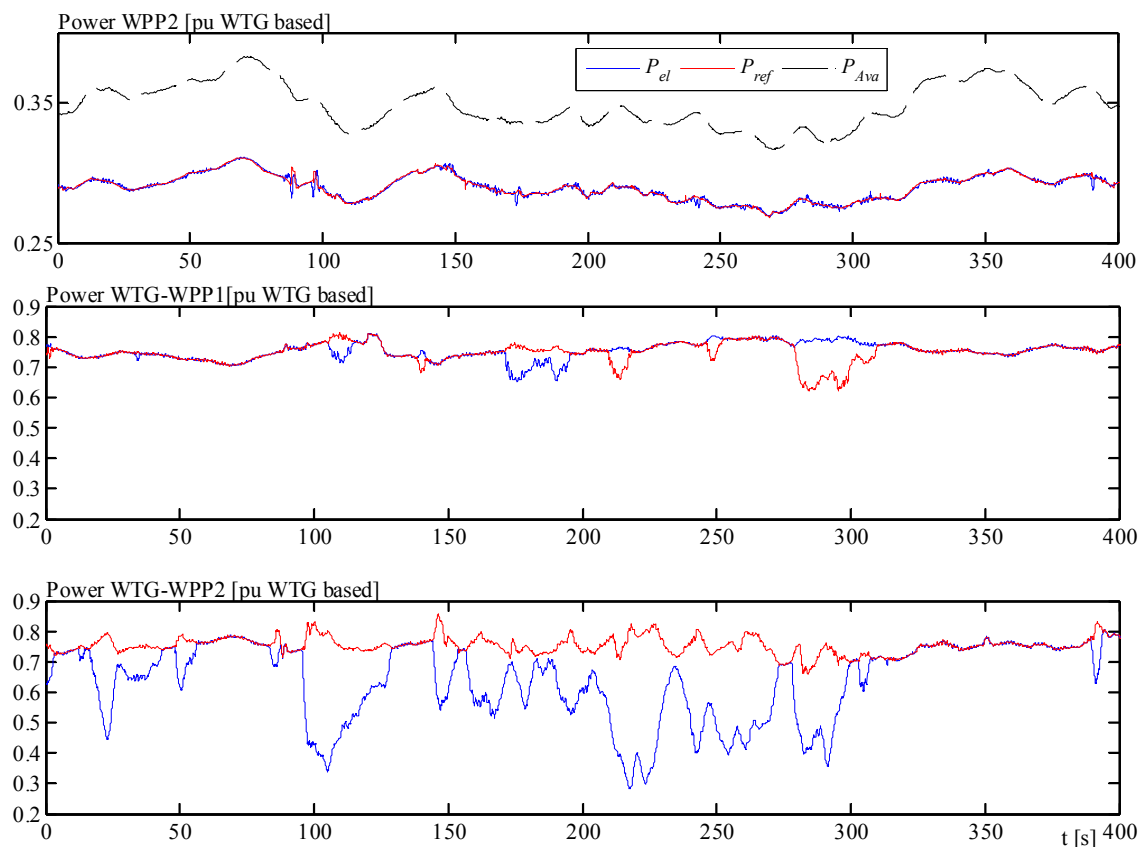
Figure 6-7: Case 1, Scenario B. Continuous system operation with 60 % wind power penetration (Cont.)

6.4.2 Case 2: Primary frequency control response

Figure 6-8 shows the results for primary frequency response from wind power. Scenarios A and B are compared with the Base Scenario. Observe how the steady state frequency deviation is the same in all Scenarios. However, the minimum frequency (nadir) is lower for high penetration degrees. The responses from the WPPS are constrained by the ramp rate limitation imposed to external set points, thus the response of the WPPs do not follow the demanded power reference according to grid frequency deviation. The initial power impact in remaining synchronous generators increases with high penetration degrees.
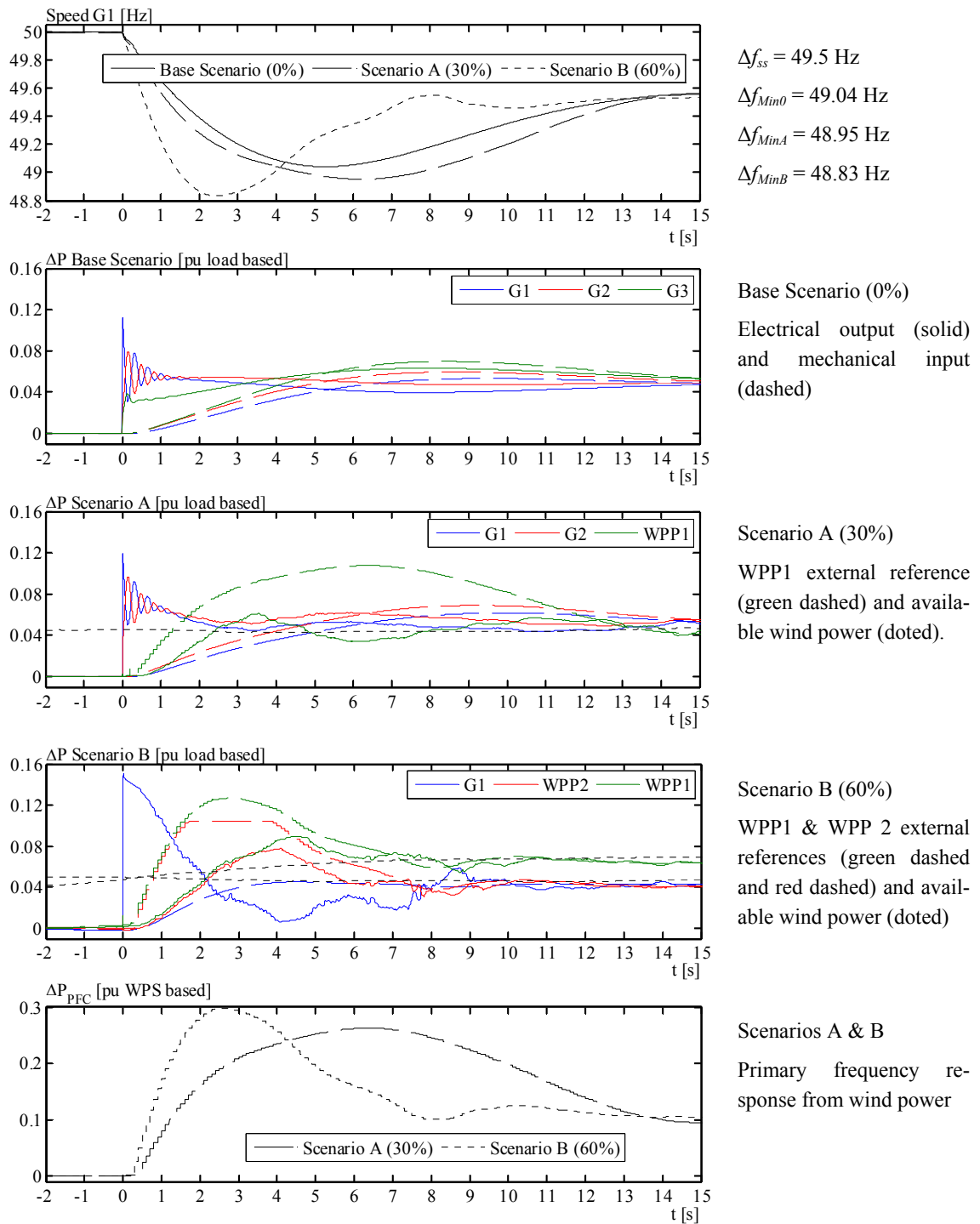
Figure 6-8: Case 2. Base Scenario, Scenario A (30 % penetration) and Scenario B (60 % penetration).

6.4.3 Case 3: Inertia and primary frequency control combined response

Figure 6-9 and **Figure 6-10** show the results for the combined actuation of inertial response plus primary frequency response from wind power. Base Scenario is used for comparison.

225

6.4.3.1 Scenario A (30% wind power penetration)

Δf_{ss} = 49.5 Hz

Δf_{Min0} = 49.04 Hz

Δf_{MinA} = 48.95 Hz

$\Delta f_{MinAinertia}$ = 48.99 Hz

Power G1: electrical output (solid) and mechanical input (dashed).

Power G2: electrical output (solid) and mechanical input (dashed).

Power G3 and WPP1: electrical output G3 (solid-blue) and mechanical input (dashed-blue). Electrical output WPP1 (red & green). Available wind power in WPP1 (dashed-black)

Powers WTG1 (solid) and WTG5 (dashed). External WTG reference (dashed-black).

Figure 6-9: Case 3 – Scenario A. Base Scenario, Scenario A and Scenario A with inertia from wind power

6.4.3.2 Scenario B (60% wind power penetration)
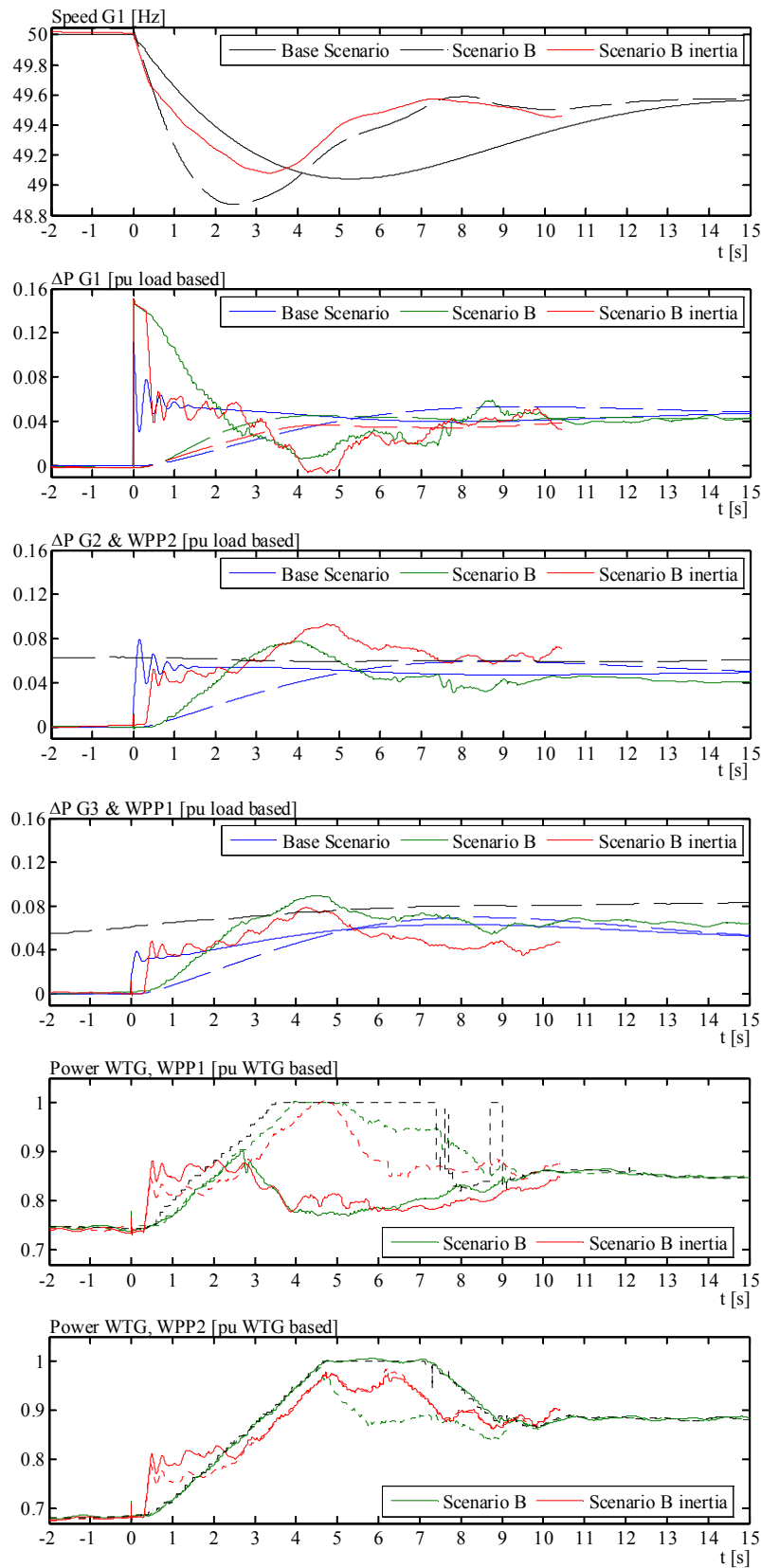
Δf_{ss} = 49.5 Hz

Δf_{Min0} = **49.04** Hz

Δf_{MinB} = 48.83 Hz

$\Delta f_{MinBinertia}$ = **49.08** Hz

Power G1: electrical output (solid) and mechanical input (dashed).

Power G2 and WPP2: electrical output G2 (solid-blue) and mechanical input (dashed-blue). Electrical output WPP2 (red & green). Available power WPP2 (dashed-black)

Power G3 and WPP1: electrical output G3 (solid-blue) and mechanical input (dashed-blue). Electrical output WPP1 (red & green). Available power in WPP1 (dashed-black)

Powers WTG1a (solid) and WTG5a (dashed) inside WPP1. External WTGa reference (dashed-black).

Powers WTG1b (solid) and WTG5b (dashed) inside WPP2. External WTGb reference (dashed-black).

Figure 6-10: Case 3 – Scenario B. Base Scenario, Scenario B and Scenario B with inertia from wind power

227

Figure 6-11 shows how is the inertial response (IR) reference generated in wind turbines WTG1 and WTG5 for the Scenarios A and B.
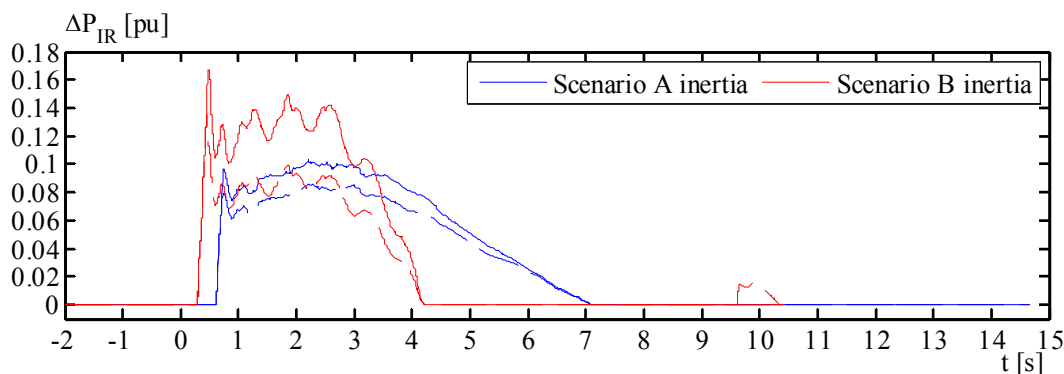
Figure 6-11: Case 3. Wind turbines inertial response reference (IR) in Scenario A & Scenario B. Two different wind turbines' responses are shown: WTG1 (solid) and WTG5 (dashed).

6.5 Conclusions

In this chapter the coordination between the controls for wind power frequency response developed in Chapter 4 and Chapter 5, together with standard regulation mechanisms in power systems, was analysed. A basic method for this coordination, which determines the controller deadband, frequency response characteristic (droop) and allowed wind power fluctuations at system level was presented. This coordination depends mainly on grid code requirements for frequency deviation and dimensioning contingency, wind power forecast, and regulating market outputs, where wind power also participates. The frequency control is handled by real-time balancing the wind power production in coordination with conventional power production. The method interplays with existing frequency reserves.

The specified maximum steady state frequency deviation is met satisfactorily with the wind power frequency control, with settling times equal or shorter than in the conventional system. However, for the same static regulation characteristic, the nadir is remarkably lower for high wind penetration levels. This is due to the combination of i) reduction in effective system inertia and ii) restriction imposed on ramp rates for external set points on wind power plants and wind turbines. The dynamic performance of the grid frequency is largely improved when the wind power combines inertial response from wind turbines and primary frequency control from the central controller, without need of increasing the ramp rates settings and/or communication/processing speeds. The power balance and the control of the grid frequency with high wind power penetration were shown to be satisfied when implementing the developed control methodology.

7

CONCLUSION AND SCOPE FOR FUTURE WORK

This thesis has studied modern wind power generation and its active power controls, aiming at integrating large amounts of wind power in power systems. New methods and solutions dealing specifically with the frequency stability problem with high wind power penetration or in islanding situations were developed.

7.1 Conclusions

- Detailed models based on a particular manufacturer's wind turbine and on a real islanded power system with large amounts of wind power generation, were developed in this work. The performance of these models was verified against field measurements showing a good matching in all cases. These models, together with others, were used for further studies in this work.

- Measurements on an isolated power system with large share of wind power generation were carried out. The main issue observed was the amount of wind power *fluctuation*, rather than the absolute power, since this characteristic was interplaying with the local regulation reserves. The installed wind power capacity was not able to be fully exploited. However, what is relevant for balancing the wind power is the collective behaviour of all wind power plants at system level. The developed control algorithms were inspired on the observed issues.

- Requirements for wind power control have been proposed, which are: i) constraint on the rate of change of wind power production at system level, ii) limitation on the amount of wind power fluctuations at system level, iii) power reserve and primary frequency response at system level and iv) inertial response for dynamic frequency support.

- The Study and characterization of the capability of variable speed wind turbines for providing inertial response was carried out. Issues such as drive train and tower impacts, amount of energy possible to deliver, power drop during recovery period and protection mechanisms on torque overload, electrical power overload and minimum rotor speed were considered. Simulations have shown that wind turbines are not abnormally stressed during this operation if suitable overloading limitations are imposed. The capability is reflected as a curve of amount of possible energy to be delivered. This energy is strongly dependent on wind speed and curtailment (deloading) conditions. It is largely reduced for wind speeds around nominal and close to the cut in speed. At rated wind speed, large power drop is experienced during recovery period due to the drop in aerodynamical efficiency. This is a drawback for the power sys-

tem in terms of frequency stability, but it can be largely improved when at least 2.5% to 3% curtailment is applied around rated wind speed. For medium or very high wind speeds, the capability increases without need of curtailment.

- A control algorithm for wind turbines inertial response was developed. This control algorithm generates a suitable power output waveform for grid stabilization. It takes into account not only the characteristics of the grid frequency but also the capability of the wind turbine and the impact during the recovery period. A gain scheduling based on operational conditions was implemented.

- The study and characterization of the capability of wind power plants (wind farms) for providing inertial response was carried out. This included detailed simulations of the individual turbine responses upon grid event, considering variable wind speeds. It was shown that single turbine inertial response output is in the same order of magnitude than normal variations due to wind speed fluctuations. Due to the differences in local wind speed, there is a diversification of inertial responses inside the wind plant, during the boosting period as well as during the recovery period, with different values of power drop. Nevertheless, the total power output of the wind plant is more "homogeneous" and, to some degree, less dependent on wind speed, compared to an individual wind turbine. Wind power is able to provide valuable inertial response but when combining a large number of wind turbines in a wind power plant.

- A frequency controller for wind power generation was proposed and studied. A particular frequency response for wind power systems has been identified as suitable for power systems with high wind power penetration, especially for isolated/small systems. This frequency controller mixes both the British and the Irish methodologies, taking the beneficial part from each other. Its response is given by comparing two references which depend on available power and pre event production.

- Control functionalities for wind power production aiming at reducing the overall power fluctuations injected to the grid were proposed and studied. Firstly, the control objectives were defined based on requirements previously elaborated. Then the control functionalities for meeting the objectives were defined, which are: i) fluctuations limitation control, ii) power tracking control, iii) frequency control, iv) active power control and v) dispatching algorithms 1 & 2. These control functionalities perform in a combined manner, aiming at managing the variability of the generated wind power in order to reduce the impact on the grid frequency and to provide with suitable frequency regulation service to the system when required.

- Several control architectures that implement the proposed functionalities were proposed and studied. These architectures are classified according to the application level, which are: Power System level, Wind Power Plant level or Wind Turbine level. The performance of the control architectures were observed through computational simulations of the modelled isolated power system. Architectures present different performance depending on the simulated operation. To choose the most suitable architecture is not straightforward. It depends on many factors, especially on communication infrastructure. The recommended architecture is the implementation at power system level with power tracking Type 1 and Dispatcher 2. It provides the highest energy yield with an acceptable dynamic performance on dynamic events. The dispatching algorithm permits wind power plants to balance each other's fluctuations,

keeping a constant power balance at system level. Its negative side is that it makes use of the "available power", which is estimated based on wind speed and aerodynamical models, introducing uncertainties in the estimated value

- A method for the coordination of the developed controls, i.e. wind turbine inertial response and wind power system active power and frequency control, was proposed and studied. The coordination is done considering the capability of the conventional regulation mechanism in the power system. This coordination depends mainly on grid code requirements for frequency deviations and dimensioning contingency, wind power forecast, and regulating market outputs, where wind power also participates. The frequency control is handled by real-time balancing the wind power production in coordination with conventional power production. The method interplays with existing frequency reserves. The specified maximum steady state frequency deviation is met satisfactorily with the wind power frequency control, with settling times equal or shorter than in the conventional system. However, for the same static regulation characteristic, the nadir is remarkably lower for high wind penetration levels when the turbines do not perform inertial response. This is due to the combination of i) reduction in effective system inertia and ii) restriction imposed on ramp rates for external set points on wind power plants and wind turbines. The dynamic performance of the grid frequency is largely improved when the wind power combines inertial response from wind turbines and primary frequency control from the central controller, without need of increasing the ramp rates settings and/or communication/processing speeds. The power balance and the control of the grid frequency with high wind power penetration were shown to be satisfied when implementing the developed control methodology.

7.2 Future Work

Some questions have been answered. Some others have been created. It was learned that there are many ways of operating the wind power generation, thanks to the technical advances in controllability of these power sources. Much work still remains to be done, particularly in the area of system operation and markets for wind power integration. But also work to be done on analyses and technical development. These are some suggestions for future work:

- It is necessary to study what would be the necessary modifications in the market rules for allowing coordination of generation of wind plants belonging to multiple owners. While, from one side, there is the technical problem of integrating wind power generation in the system, from the other side, there is the economic problem of this. To find a solution with good agreement with these two problems is not straightforward. Any kind of active power control applied directly to wind power generators, other than optimal power, produces a reduction on generated energy and, therefore, on revenues. This work studied the coordination of the generation from multiple wind plants, which are most likely to belong to

multiple owners. The studies were done regardless the economic implications and were focused on the technical problem. Today, the market is not designed for this kind of control, or coordination, of wind power.

- Generic wind turbine models for inertia response. It was found extremely difficult to study the grid impact using a detailed model of a wind turbine. Similarly when implementing control algorithms. A more generic representation is necessary. *But*, extremely care should be put in order to obtain a *realistic* response from the wind turbine. E.g., the response is very sensitive to the aerodynamics and overloads.

- Analysis of WPP with energy storage providing inertia response to improve the drawbacks created when inertia is provided solely with wind turbines.

- Studies involving reactive power control capability. Reactive power capability was not considered in this work.

- Development of WTG's and WPP's dispatching algorithms for maximizing the capability for grid support, e.g. by increasing the inertial response capability but minimizing the energy loss for the same curtailment.

- Analyse other configurations for architecture, e.g. locating the frequency controller in each WPP and having dispatcher at PS level, considering the benefit for faster response and higher yield.

- Use of wind power forecast in the control algorithm. Make the wind power forecast as an active part of the control algorithm in order to anticipate set points not only for market but also for system stability and balance. Each WPP with short term forecast may help to great extent the determination of the available power, hence the allocation of power reserve.

REFERENCES

[1]   EWEA, "Pure Power – Wind Energy Targets for 2020 and 2030", Report by the European Wind Energy Association, July 2011. Available online: www.ewea.org.

[2]   GWEC, "Global Wind Report –Annual Market Update 2010", Global Wind Energy Council, March 2011, available at www.gwec.net.

[3]   EirGrid, "EirGrid Grid Code Version 3.5". Into effect in March 2011. Available at: www.eirgrid.com/operations/gridcode.

[4]   Fagan E., Grimes S., McArdle J., Smith P., Stronge M., "Grid code provisions for wind generators in Ireland", Power Engineering Society General Meeting, 2005. IEEE, 12-16 June 2005.

[5]   Nordel, "The Nordic Grid Code 2007 (Nordic Collection of Rules)", 2007, Available at: www.nordel.org

[6]   Eltra/Elkraft, "Regulation TF 3.2.5, Wind turbines connected to grids with voltages above 100 kV", Eltra/Elkraft, Denmark, 2004.

[7]   REE, "P.O. 12.2 Instalaciones conectadas a la red de transporte y equipo generador: Requisitos mínimos de diseño, equipamiento, funcionamiento,puesta en servicio y seguridad", November 2009. Available online: www.ree.es

[8]   Johnson A., Tleis N., "The development of grid code requirements for new and renewable forms of generation in Great Britain", Wind Engineering, vol. 29, no. 3, pp. 201-215, 2005.

[9]   National Grid, "The Grid Code", UK, Aug 2011. Available online: www.nationalgrid.com/uk

[10]   EWEA, "Generic Grid Code Format for Wind Power Plants", EU, November 2009. Available online: www.ewea.org

[11]   Federal Energy Regulatory Commission – FERC, "Standard Interconnection Agreements for Wind Energy and Other Alternative Technologies, Appendix G", USA, Dec. 2005. Available online: www.ferc.gov

[12]   IOS Subcommittee, "Interconnected operations services reference document", North American Electric Reliability Council, 2001.

[13]   Abeyratne S., "Investigation 5: Effect of wind generation on management of frequency excursions", Utility report for Transpower, New Zealand System Operator, May 2007.

[14]   Transenergie, "Technical requirements for the connection of generation facilities to the hydro-quebec transmission system-supplementary requirements for wind generation", Utility report, Oct 2005.

[15]   Iov F., Hansen A., Cutulis N., Soerensen P., "A survey of interconnection requirements for wind power", in Proc. Nordic Wind Power Conf. (NWPC), Roskilde, Denmark, 2007.

[16]   Singh B. and Singh S. N., "Wind Power Interconnection into the Power System: A Review of Grid Code Requirements", Elsevier The Electricity Journal, vol. 22, no. 5, pp. 54-63, Jun. 2009.

[17]   Tsili M., Papathanassiou S., "A review of grid code technical requirements for wind farms", Renewable Power Generation, IET, vol.3, no.3, pp.308-332, Sept. 2009.

[18]   Ekanayake J. and Jenkins N., "Comparison of the response of doubly fed and fixed-speed induction generator wind turbines to changes in network frequency", IEEE Transactions on Energy Conversion, vol. 19, no. 4, pp. 800–802, 2004.

[19]   Vittal E., McCalley J. D., Ajarapu V. and Harbour T., "Wind penetration limited by thermal constraints and frequency stability", Power Symposium, 2007. NAPS '07. 39th North American, pp. 353–359, 2007.

[20]   Koch F. W., Erlich I., Shewarega F., and Bachmann U., "Dynamic interaction of large offshore wind farms with the electric power system", in Proc. 2003 IEEE Power Tech Conf., Bologna, Italy, 2003.

[21]   Lalor G., Mullane A. and O'Malley M., "Frequency Control and Wind Turbine Technologies", IEEE Trans. Power Syst., vol. 20, no. 4, pp. 1905-1913, Nov. 2005.

[22]   Morren J., Pierik J., and de Haan S. W. H., "Inertial response of variable speed wind turbines", Electric Power System Research, vol. 76, pp. 980–987, 2006.

[23]   Ramtharan G., Ekanayake J., and Jenkins N., "Frequency support from doubly fed induction generator wind turbines", IET Renewable Power Generation, vol. 1, no. 1, pp. 3–9, 2007.

[24]   Conroy J. and Watson R., "Frequency response capability of full converter wind turbine generators in comparison to conventional generation", IEEE Transactions on Power Systems, vol. 23, no. 2, May 2008.

[25]   Mullane A., and O'Malley M., "Modifying the inertial response of power-converter based wind turbine generators", Power Electronics, Machines and Drives, 2006. The 3rd IET International Conference on, vol. 20, no. 3, pp. 121–126, March 2006.

[26]   Keung P. K., Lei P., Banakar H., and Ooi B. T., "Kinetic energy of wind-turbine generators for system frequency support", IEEE Transactions on Power Systems, vol. 24, no. 1, pp. 279–287, 2009.

[27]   J. Morren, S. W. H de Haan, W. L. Kling, and J.A Ferreira, "Wind turbines emulating inertia and supporting primary frequency control", IEEE Transactions on Power Systems, vol. 21, no. 1, pp. 433–434, Februrary 2006.

[28]   N.Ullah, T. Thiringer, and D. Karlsson, "Temporary primary frequency control support by variable speed wind turbines – Potential and applications", IEEE Transactions on Power Systems, vol. 23, no. 2, pp. 601–612, May 2008.

[29]   Senjyu T., Ochi Y., Kikunaga Y., Tokudome M., Muhando E.B., Yona A., and Funabashi T, "Output power leveling of wind generation system using inertia of wind turbine", in Sustainable Energy Technologies, 2008. ICSET 2008. IEEE International Conference on, Nov. 24-27 2008, pp. 1217–1222.

[30]   L.Ran, J.R. Bumby, and P.J. Tavner, "Use of turbine inertia for power smoothing of wind turbines with a DFIG", in 11th International Conference on Harmonics and Quality of Power, Sept.12–15 2004, pp. 106–111.

[31]   C.L. Luo, H. Banakar, B. Shen, and B.T. Ooi, "Strategies to smooth wind power fluctuations of wind turbine generator", IEEE Transactions on Energy Conversion, vol. 22, no. 2, pp. 243–349, June 2007.

[32]   T.Luu, A.Abedini, and A. Nasiri, "Power smoothing of doubly fed induction generator wind turbines", Industrial Electronics, 2008. IECON 2008. 34th Annual Conference of IEEE, pp. 2365 – 2370, 2008.

[33]   B. Rawn, P.W. Lehn, and M. Maggiore, "A control methodology to mitigate the grid impact of wind turbines", IEEE Transactions on Energy Conversion, vol. 22, no. 2, pp. 431–438, June 2007.

[34]   B. Rawn, P.W. Lehn, and M. Maggiore, "Toward controlled wind farm output: adjustable power filtering", in IEEE Power Engineering Society General Meeting, 18-22 2006.

[35]   J Mauricio, A. Marano, A. Gomez-Exposito, and J. Ramos, "Frequency regulation contribution through variable-speed wind energy conversion systems", IEEE Transactions on Power Systems, vol. 24, no. 1, pp. 173–180, Feb 2009.

[36]   GE Energy, "Solutions for wind power performance: Windinertia control", Company Brochure, no. 1, pp. 3, March 2009.

[37]   B.H. Chowdhury and H.T. Ma, "Frequency regulation with wind power plants", PESGM 2008, pp. 21–35, 2008.

[38]   I. Erlich, K. Rensch, and F. Shewarga, "Impact of large offshore wind farms on frequency stability", IEEE Power Engineering Society General Meeting, 2006.

[39]   Nordel, "Description of Balance Regulation in the Nordic Countries", 2008, Available at: www.entsoe.eu

[40]   Ackermann, T., Abbad, J.R., Dudurych, I.M., Erlich, I., Holttinen, H., Kristoffersen, J.R., Sørensen, P.E., "European Balancing Act", IEEE Power and Energy Magazine, vol.5, no.6, pp.90-103, Nov.-Dec. 2007.

[41]   Dudurych I. M., "The Control of Power System with a High Wind Power Penetration", Power Tech, 2007 IEEE Lausanne, vol., no., pp.528-531, 1-5 July 2007.

[42]   Holttinen, H., "Impact of hourly wind power variations on the system operation in the Nordic countries", Wind Energy, vol. 8, no. 2, pp. 197–218, April/June 2005.

[43]   Holttinen, H. et al., "State of the art IEA Task 25 report: Design and operation of power systems with large amounts of wind power", VTT Working Papers 82, VTT Technical Research Centre of Finland, Espoo, 2007.

[44]   Holttinen, H., et al., "Impacts of large amounts of wind power on design and operation of power systems, results of IEA collaboration", in Proc. 8th International Workshop on Large-Scale Integration of wind Power into Power Systems as well as on Transmission Networks of Offshore Wind Farms, 14-15 Oct., Bremen, Germany, 2009.

[45]   Milligan, M. et.al., "Operating Reserves and Wind Power Integration: An International Comparison", In proc. 9th International Workshop on large-scale integration of wind power into power systems, 2010. 18-29 Oct., Québec, Canada, 2010.

[46]   Akhmatov, V., Gleditsch, M. and Gjengedal, T. "A regulation-caused bottleneck for regulating power utilization of balancing offshore wind power in hourly- and quarter-hourly-based power systems". Wind Eng., vol. 33, pp. 41–54, Jan. 2009.

[47]   Doherty, R., Mullane, A., Nolan, G., Burke, D.J., Bryson, A., O'Malley, M., "An Assessment of the Impact of Wind Generation on System Frequency Control", Power Systems, IEEE Transactions on, vol.25, no.1, pp.452-460, Feb. 2010.

[48]   Dany G., "Power reserve in interconnected systems with high wind power production", Power Tech Proceedings, 2001 IEEE Porto , vol.4, no., pp.6 pp. vol.4, 2001

[49]   Sørensen P., Cutululis N. A., "Wind farms' spatial distribution effect on power system reserves requirements", Industrial Electronics (ISIE), 2010 IEEE International Symposium on , vol., no., pp.2505-2510, 4-7 July 2010

[50]   Gibescu M., Ummels B.C., Kling W.L., "Statistical Wind Speed Interpolation for Simulating Aggregated Wind Energy Production under System Studies", Probabilistic Methods Applied to Power Systems, 2006. PMAPS 2006. International Conference on , vol., no., pp.1-7, 11-15 June 2006

[51]   Ortega-Vazquez, M.A., Kirschen, D.S., "Estimating the Spinning Reserve Requirements in Systems With Significant Wind Power Generation Penetration", Power Systems, IEEE Transactions on , vol.24, no.1, pp.114-124, Feb. 2009

[52]   A. Vigueras-Rodríguez, P. Sørensen, N. Cutululis, A. Viedma, E. Gomez, and S. Martin, "Application of ramp limitation regulations for smoothing the power fluctuations from offshore wind farms", in European Wind Energy Conference and Exhibition (EWEC09), Marseille (France), March 2009.

[53]   S. Martín-Martínez, E. Gómez-Lázaro, A. Vigueras-Rodríguez J. A. Fuentes-Moreno, A. Molina-García, "Regulation strategies for wind power fluctuations in a system depending on ramping power range", in European Wind Energy Conference and Exhibition (EWEC10), Warsaw, Poland, April 2010.

[54]   H. Holttinen, "Optimal electricity market for wind power", Energy Policy, vol. 33, no 16, Nov. 2005, pp. 2052-2063, 2004

[55]   Kabouris, J., Kanellos, F.D., "Impacts of Large-Scale Wind Penetration on Designing and Operation of Electric Power Systems", Sustainable Energy, IEEE Transactions on, vol.1, no.2, pp.107-114, July 2010.

[56]   IEEE Task Force Report, "Interconnected Power System Response to Generation Governing: Present Practice and Outstanding Concerns", Special publication 07TP180. Final report. May 2007.

[57]   E.Hirst and B. Kirby, "Electric power ancillary services", Oak Ridge National Laboratory Report ORNL/CON-426, 1996.

[58]   Wood, G.F., Hung, W.W., "Generating plant frequency control services", in Proc. IEE Frequency Control Capability of Generating Plant Colloquium on , vol., no., pp.1/1-1/5, 8 Feb 1995.

[59]   Tarnowski, G.C., Reginatto, R., "Adding Active Power Regulation to Wind Farms with Variable Speed Induction Generators". In Proc. Power Engineering Society General Meeting PES '07 IEEE, 24-28 June, Tampa, USA, 2007.

[60]   Tarnowski, G. C, Kjær, P. C., Sørensen, P. E., Østergaard, J., "Study on Variable Speed Wind Turbines Capability for Frequency Response", In Proc. European Wind Energy Conference EWEC 2009, 16-19 March, Marseille, France, 2009.

[61]   Tarnowski, G.C., Kjær, P.C., Sorensen, P.E., Østergaard, J., "Variable speed wind turbines capability for temporary over-production", In Proc. Power & Energy Society General Meeting PES '09 IEEE, 26-30 July, Calgary, Canada, 2009.

[62]   Tarnowski, G.C., Kjær, P.C., Dalsgaard, S., Nyborg, A., "Regulation and frequency response service capability of modern wind power plants", In Proc. Power and Energy Society General Meeting, 2010 IEEE , 25-29 July, Minneapolis, USA, 2010.

[63]   Tarnowski, G. C., Kjær, P. C., Østergaard, J. and Sørensen, P. E., "Frequency Control in Power Systems with High Wind Power Penetration", In proc. 9th International Workshop on large-scale integration of wind power into power systems, 2010. 18-29 Oct., Québec, Canada, 2010.

[64]   Tarnowski, G. C., "Wind Turbine Providing Grid Support". WO 2011/000531. Publication 06 Jan 2011.

[65]   Tarnowski, G. C., "Method for Emulation of Synchronous Machine", WO 2011/092193. Publication 04 Aug 2011.

[66]   Christensen, P. W., Tarnowski, G. C. "Inertia for Wind Power Plants – state of the art review – year 2011". In proc. 10th International Workshop on large-scale integration of wind power into power systems, 2011. Aarhus, Denmark, 2011.

[67]   Zeni, L., "Dynamic model of a CHP plant and its application to frequency control on island power systems with high penetration of wind power", Master thesis, Technical University of Denmark, June 2010.

[68]   Burton, T., Sharpe, D., Jenkins, N., Bossanyi, E. "Wind Energy Handbook", Chichester, England: John Wiley, 2001. 617p. ISBN: 0-471-48997-2.

[69]   EWEA, "Wind Energy – The Facts. A guide to the technology, economics and future of wind power", London: Earthscan, 2009, p. 568.

[70]   Kundur, P. "Power System Stability and Control", New York, USA: McGraw-Hill, Inc., 1994. 1776p. ISBN: 0-07-035958-X.

[71]   Anderson, P. M. and Fouad, A. A. "Power System Control and Stability", Iowa, USA: The Iowa State University Press, 1977. 392p. ISBN: 0-8138-1245-3.

[72]   Machowski, J., Bialek, J. W. and Bumby, J. R. "Power System Dynamics Stability and Control", Second Edition, Chichester, UK: John Wiley & Sons, Ltd., 2009. 629p. ISBN: 978-0-470-72558-0.

[73]   Wood, A. J. and Wollenberg, B. F., "Power Generation Operation and Control", Second Edition, New York, USA: John Wiley & Sons, Inc., 1996. 569p. ISBN: 978-0-471-58699-9.

[74]   Philips, C. L., "Basic Feedback Control Systems", Second Edition, New Jersey, USA: Prentice Hall, 1991. 478p. ISBN: 0-13-062845-X.

[75]   Haykin, S., Veen. B. van. "Signals and Systems", Second Edition, USA: Wiley, 2002. 802p. ISBN: 978-0471164746.

[76]   Slootweg J. G., Kling W. L. "Is the answer blowing on the wind?" IEEE Power&Energy Magazine, v.1, p.26–33, Nov./Dic. 2003.

[77]   Slootweg J. G., Haan S. W., Polinder H., Kling W. L., "General Model for Representing Variable Speed Wind Turbines in Power System Dynamics Simulations", IEEE Transactions on Power Systems, v.18, n.1, Feb. 2003.

[78]   Slootweg J. G., Polinder H., Kling W. L., "Dynamic Modelling of a Wind Turbine with Doubly Fed Induction Generator", In IEEE PES, SM, 2001, Vancouver, BC, Canada. Proceedings, 2001. vol.1, p.644–649.

[79]   Slootweg J. G., Poinder H., Kling W. L., "Representing wind turbine electrical generating systems in fundamental frequency simulations", IEEE Transactions on Energy Conversion, vol.18, no.4, Dec. 2003.

[80]   Lei Y., Mullane A., Lightbody G., Yacamini R., "Modelling of the Wind Turbine with a Doubly Fed Induction Generator for Grid Integration Studies", IEEE Transactions on Energy Conversion, vol.21, no.1, p.257–264, Mar. 2006.

[81]   Akhmatov V., "Analysis of Dynamic Behaviour of Electric Power Systems with Large Amount of Wind Power", 2003. 270p. PhD Thesis — Technical University of Denmark, Denmark.

[82]   Akhmatov V., Knudsen H., Nielsen A. H., "Advanced simulation of windmills in the electric power supply", Electrical Power and Energy Systems, vol.22, no.6, p.421–434, Aug. 2000.

[83]   Trudnowski D. J., Gentile A., Khan J. M., Petritz E. M., "Fixed-Speed Wind-Generator and Wind-Park Modelling for Transient Stability Studies", IEEE Transactions on Power Systems, vol.19, no.4, p.1911–19171, Nov. 2004.

[84]   R.G de Almeida, E. Castronuovo, and J.A. Pescas Lopez, "Optimum generation control in wind parks when carrying out system operator requests", IEEE Transactions on Power Systems, vol. 21, no. 2, pp. 718–725, 2006.

[85]   L. Chang-Chien, C. Hung, and Y. Yin, "Dynamic reserve allocation for system contingency by dfig wind farms", IEEE Transactions on Power Systems, vol. 23, no. 2, pp. 729–736, 2008.

[86]   van Engelen T. "Design model and load reduction assessment for multi-rotational mode individual pitch control (higher harmonics control)". In proceedings of the European Wind Energy Conference, Athens, Greece, 2006.

[87]   K. Selvam, S. Kanev, J. W. van Wingerden, T. van Engelen, and M. Verhaegen. "Feedback-feedforward individual pitch control for wind turbine load reduction". Int. J. Robust and Nonlinear Control, 2009.

[88]   E. Bossanyi, "Wind Turbine Control for Load Reduction", Wind Energy, vol. 6, no. 3, pp. 229-244, 2003.

[89]   Frandsen, S., Barthelmie, R.J., Pryor, S.C., Rathmann, O., Larsen, S.E., Højstrup, J., Thøgersen, M., "Analytical modelling of wind speed deficit in large offshore wind farms". Wind Energy, vol. 9, no. 1-2, pp. 39-53, 2006.

[90]   Barthelmie, R. J. and Jensen, L. E., "Evaluation of wind farm efficiency and wind turbine wakes at the Nysted offshore wind farm", Wind Energy, vol. 13, no. 6, pp. 573-586, 2010.

[91]   Mechali, M., L. Jensen, R. Barthelmie, et al. "Wake effects at Horns Rev and their influence on energy production", in EWEC 2006. Athens, Greece: p. 10.

[92]   S. Frandsen, R. Barthelmia, O. Rathmann, H. Jørgensen, J. Badger, K. Hansen, S. Ott, P. Rethore, S. Larsen, and L. Jensen, "Summary report: the shadow effect of large wind farms: measurements, data analysis and modelling", Risø National Laboratory, Technical University of Denmark, Roskilde, Denmark, Technical report, Oct. 2007.

[93]   N.O. Jensen, "A note on wind generator interaction", Risø M 2411, Denmark, November 1983.

[94]   Sørensen, Poul and Cutululis, Nicolaos Antonio and Vigueras-Rodríguez, Antonio and Madsen, Henrik and Pinson, Pierre and Jensen, Leo E. and Hjerrild, Jesper and Donovan, Martin. "Modelling of power fluctuations from large offshore wind farms", Wind Energy, vol. 11, no. 1, pp. 29-43, 2008.

[95]   P. Sørensen et al., "Simulation of Interaction Between Wind Farm and Power System", Risø National Laboratory, Risø-R-1281(EN), Roskilde, Denmark, Dec. 2001.

[96]   F. Koch, I. Erlich, and F. Shewarega, "Dynamic simulation of large wind farms integrated in a multi machine network", in IEEE PES Meeting, Toronto, Canada, July 2003.

[97]   Ch. Eping, J. Stenzel, M. Poller, and H. Muller, "Impact of large scale wind power on power system stability", in Fifth International Workshop on Large-Scale Integration of Wind Power and Transmission Networks for Offshore Wind Farms, Glasgow, Scotland, Apr. 7–8 2005.

[98]   J.G Slootweg andW.L Kling, "The impact of large scale wind power generation on power system oscillations", Electric Power Systems Research, vol. 67, no. 1, pp. 9–20, 2003.

[99]   C. Samarasinghe and D. Vowles, "Investigation 8: Effect of wind generation on small signal stability", Utility report for Transpower, New Zealand System Operator, March 2008.

[100]   Hagstrom E., Norheim I., and Uhlen K., "Large-scale wind power integration in Norway and impact on damping in the Nordic grid", Wind Energy, vol. 8, no. 3, pp. 375–384, 2005.

[101]   Hughes F. M., Anaya-Lara O., Jenkins N., and Strbac G., "A power system stabilizer for DFIG-based wind generation", IEEE Transactions on Power Systems, vol. 21, no. 2, pp. 763–772, 2006.

[102]   Jauch C., "Transient and dynamic control of a variable speed wind turbine with synchronous generator", Wind Energy, vol. 10, no. 3, pp. 247–269, May/June 2007.

[103]   Mann J., "Wind field simulation", Prob. Eng. Mech. Vol. 13, no. 4, pp. 269–282, 1998.

[104]   Sørensen P., Hansen A. D., Rosas P. A. C., "Wind models for simulation of power fluctuations from wind farms", Journal of Wind Engineering and Industrial Aerodynamics 2002, **90**: 1381–1402.

[105]   Oye S., "Unsteady wake effects caused by pitch-angle changes. In: IEA R&D WECS Joint action on aerodynamics of wind turbines, 1986, London, U.K. Proceedings, 1986. p.58–79.

[106]   Matsuura M., "Island breezes", IEEE Power and Energy Magazine, vol. 7, no. 6, pp. 59-64, Nov.-Dec. 2009.

[107]   Yu Chen, Zhao Xu, Østergaard J., "Frequency analysis for planned islanding operation in the Danish distribution system – Bornholm", Universities Power Engineering Conference, 2008. UPEC 2008. 43rd International, pp.1-5, 1-4 Sept. 2008.

[108]   Østergaard J., Nielsen J. E., "The Bornholm Power System. An overview", PowerLabDK, Kgs. Lyngby, Denmark, April 2011. Available online: www.powerlab.dk.

[109]   Østkraft Net A/S. "Årsrapport 2009", Østkraft Net A/S, Rønne, Bornholm, Denmark, 2009. Available online: www.oestkraft.dk.

[110]   Hansen A. D., Sørensen P., Iov F., Blaabjerg F., "Centralised power control of wind farm with doubly fed induction generators", Renewable Energy, Volume 31, Issue 7, June 2006, Pages 935-951.

[111]   Rodriguez-Amenedo J. L., Arnalte S., Burgos J. C., "Automatic Generation Control of a Wind Farm With Variable Speed Wind Turbines", IEEE Transactions on Energy Conversion, June 2002.

[112]   El Moursi M., Joos G., and Abbey C., "A secondary voltage control strategy for transmission level interconnection of wind generation", IEEE Transactions on Power Electronics, vol. 23, no. 3, pp. 1178–1190, 2008.

[113]   De Oliveira-De Jesus P. M., Castronuovo E. D., and Ponce de Leao M. T., "Reactive power response of wind generators under an incremental network-loss allocation approach", IEEE Transactions on Energy Conversion, vol. 23, no. 2, pp. 612–621, June 2008.

[114]   Ullah N., Bhattacharya K., and Thiringer T., "Wind farms as reactive power ancillary service providers-technical and economic issues", IEEE Transactions on Energy Conversion.

[115]   Kristoffersen J. R., "The Horns Rev wind farm and the operational experience with the wind farm main controller", in Copenhagen Offshore Wind, Oct. 26–28 2005.

[116]   Braun M., et.al. "Wind power plant capabilities – Operate wind farms like conventional power plants". European Wind Energy Conference 2009, Marseille, France, 16-19 Mar. 2009.

[117]   Gjengedal T., "System control of large scale wind power by use of automatic generation control (AGC)", Quality and Security of Electric Power Delivery Systems, 2003. CIGRE/PES 2003. CIGRE/IEEE PES International Symposium, pp. 15- 21, 8-10 Oct. 2003.

[118]   Suwannarat A., Bak-Jensen B., Chen Z., Nielsen H., Hjerrild J., Sørensen P., Hansen A. D., "Power Balancing Control with Large Scale Wind Power Integration in Denmark", in EuroPES. 2007. Palma De Mallorca, Spain.

[119]   Zhao Xu, Ostergaard J., Togeby M., "Demand as Frequency Controlled Reserve", Power Systems, IEEE Transactions on , vol.26, no.3, pp.1062-1071, Aug. 2011.

[120]   Larsen E., Chandrashekhara D.K., Ostergard J., "Electric Vehicles for Improved Operation of Power Systems with High Wind Power Penetration", Energy 2030 Conference, 2008. ENERGY 2008. IEEE , pp.1-6, 17-18 Nov. 2008

[121]   Pudjianto D., Ramsay C., Strbac G., "Virtual power plant and system integration of distributed energy resources", Renewable Power Generation, IET , vol.1, no.1, pp.10-16, March 2007.

[122]   Awad H., Svensson J., Bollen M. J., "Tuning software phase-locked loop for series-connected converters", Power Delivery, IEEE Transactions on , vol.20, no.1, pp. 300- 308, Jan. 2005

[123]   Chung S. -K., "Phase-locked loop for grid-connected three-phase power conversion systems", Electric Power Applications, IEE Proceedings, vol.147, no.3, pp.213-219, May 2000.

A
POWER SYSTEMS MODELLING

In this appendix, the different power system models used in this investigation are described.

A.1 Classical power system representation [70] [71]

The classical representation of a multimachine power system for load impact studies is briefly described. The final set of equations is useful for analysis of inertial response and intermachine oscillations of synchronous machines upon grid load change.

Assumptions:
- Negligible electromagnetic transients.
- Small load change ΔP_L applied at some bus L in the system.
- Load with negligible reactive component.
- Very high X/R ratio of the network with negligible conductances.
- Generators represented by the classical model of constant voltage E behind transient reactance.

Consider the n-machine system represented in Figure A-1. The *change* in electrical power output of machine i is:

$$\Delta P_{ei} = \sum_{\substack{j=1 \\ j \neq i,L}}^{n} \left[E_i E_j B_{ij} \cos \delta_{ij0} \right] \cdot \left(\Delta \delta_i - \Delta \delta_j \right) + \left[V_L E_i B_{iL} \cos \delta_{iL0} \right] \cdot \left(\Delta \delta_i - \Delta \delta_L \right) \quad \textbf{(A.1)}$$
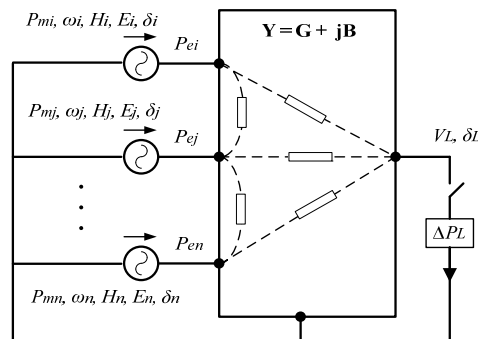

Figure A-1: Representation of a multimachine system for load impact (classical model)

For a given initial condition (0), the differences between rotor angles, δ_{ij0}, and between rotor and load busbar voltage angles, δ_{iL0}, are known and the terms in square brackets are constant. These terms are defined as the *synchronizing power coefficients*, P_{Sik}, for the given steady state condition:

$$P_{Sik} := \left.\frac{\partial P_{ik}}{\partial \delta_{ik}}\right|_{\delta_{ik0}} = E_i E_k B_{ik} \cos\delta_{ik0}, \tag{A.2}$$

The synchronizing power coefficient between a machine i and any other bus bar k in the system represents the active power change of that machine due to a change in the angle between its internal EMF and the voltage at bus k, with all other angles held constant.

Utilizing the concept of synchronizing power coefficients, the linearized model of active power changes and motion of generators in a multimachine system is:

$$\Delta P_{ei} = \sum_{\substack{j=1 \\ j \neq i,L}}^{n} P_{Sij} \cdot \left(\Delta\delta_i - \Delta\delta_j\right) + P_{SiL} \cdot \left(\Delta\delta_i - \Delta\delta_L\right) \tag{A.3}$$

$$\Delta P_L = \sum_{j=1}^{n} P_{SjL} \cdot \left(\Delta\delta_j - \Delta\delta_L\right) \tag{A.4}$$

$$\Delta\dot{\omega}_i = \frac{1}{2H'_i}\left(\Delta P_{mi} - \Delta P_{ei} - D_i \cdot \Delta\omega_i\right) \tag{A.5}$$

$$\Delta\dot{\delta}_i = \Delta\omega_i \tag{A.6}$$

A.2 Power system inertia

The equation (A.5) is expressed with a machine inertia constant H'_i which is referred to a system base power; thus it is not the generator's nameplate inertia constant H_i. A base transformation is necessary if the nameplate inertial constant is to be used in that expression.

By definition, the inertia constant H_i of a synchronous machine *is the amount of time in seconds that the machine should run at nominal power for generating an amount of energy equal to the kinetic energy stored in its rotating mass*. It is expressed as:

$$H_i := \frac{E_{Ki}}{S_{Ni}} = \frac{1}{2}J_i\left(\frac{\omega_{eN}}{p_i}\right)^2\frac{1}{S_{Ni}} \text{ [s]}, \tag{A.7}$$

where J is the moment of inertia of the rotational mechanical system in kg.m^2, ω_{eN} is the nominal electric frequency in rad/s, p is the pairs of poles of the machine and S_N is its nominal apparent power in VA.

Based on that definition, a similar can be elaborated for the power system: *The inertia constant H_{sys} of a power system is the amount of time in seconds in which the system supplies a base power generating an amount of energy equal to its total stored kinetic energy*.

$$H_{sys} := \frac{Total\ E_{Ksys}}{System\ Base\ Power} = \frac{\sum_{i=1}^{n} H_i \cdot S_{Ni}}{S_{Bsys}} = \sum_{i=1}^{n} H'_i \quad [s], \tag{A.8}$$

where n is the number of *synchronous* machines (generators and motors), H_i is the nameplate inertia constant in seconds of the machine i (according to (**A.7**)), S_{Bsys} is the chosen base power in MVA for the system and:

$$H'_i = \frac{S_{Ni}}{S_{Bsys}} H_i \quad [s], \tag{A.9}$$

is the base transformation for the inertia constant of machine i.

A.3 Reduced model for load-frequency response: PS1

This modelling was used for simulations in Chapter 2. Qualitative analysis of the mean frequency response and regulating characteristic of a power system due to a load change can be done by using a simple model as described in [70]. In this work, this simple power system model is referred as PS1. It represents the collective performance of all generators in the system. The intermachine oscillations and transmission system performance are not considered and a coherent response of all generators to changes in system load is assumed. Under such conditions, the system mean frequency response is given by the following linearized expression [70] [71] [72] [73]:

$$2H_{sys} \frac{d\Delta f}{dt} = \Delta P_{msys} - \Delta P_L - D_{sys} \Delta f = -\Delta P_{Inertia} \tag{A.10}$$

where Δf is the change in the mean grid frequency in pu, ΔP_{msys} is the change in all prime movers mechanical power output in pu, D_{sys} is the load-frequency sensitivity constant, $\Delta P_{Inertia}$ is the accelerating power (or system inertial response) in pu, and ΔP_L and H_{sys} were previously described.

The ΔP_{msys} is the summation of changes in mechanical power output, ΔP_{mi}, of all prime movers that contribute with governor response in the system. Different prime mover's governor response e.g. steam turbines, diesel engines, hydro turbines, etc., have different dynamic characteristics for ΔP_{mi} [56]. In order to simplify the complexity of modelling different types, it is assumed here just one equivalent representation for the overall mechanical response in the system. This further simplification should not affect the qualitative response of Δf when the system experiences a ΔP_L.

Figure A-2 shows the block diagram of this model. The ΔP_L can represent a large generator or load disconnection or a power imbalance caused by the wind power production.
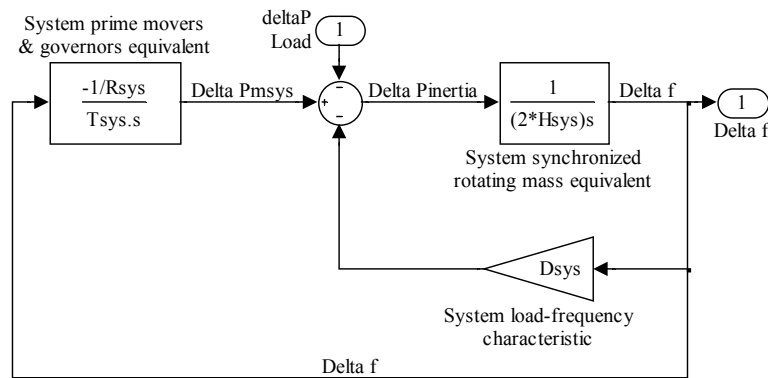

Figure A-2: Power system equivalent for composite load-frequency response analysis.

The equivalent governor-prime mover is represented by a first order transfer function with time constant T_{sys} and droop R_{sys}. This time constant should be such that produces an equivalent impact in the system frequency. The composite system droop R_{sys} is given by:

$$\frac{1}{R_{sys}} = \sum_{i=1}^{m} \left(\frac{1}{R_i} \frac{S_{Ni}}{S_{Bsys}} \right), \tag{A.11}$$

where m is the number of generators online contributing with primary frequency control (governor response), R_i is the droop of individual governors i based on nominal apparent power S_{Ni} in MVA and S_{Bsys} was previously defined. As defined in the classical power system literature, the droop R_i is the change in grid frequency in pu (or %) that produces 1 pu (or 100%) of change in prime mover power output, and it is a setting parameter for the respective governor. The D_{sys} is the change in system load in % of actual load per 1% change in grid frequency [70] [71] [72] [73].

Transfer functions

The transfer function relating the load change, $\Delta P_L(s)$, to the frequency change, $\Delta f(s)$, is:

$$\frac{\Delta f(s)}{\Delta P_L(s)} = \frac{-\dfrac{1}{2H_{sys}}\left(s + \dfrac{1}{T_{sys}}\right)}{s^2 + \dfrac{\left(D_{sys}T_{sys} + 2H_{sys}\right)}{2H_{sys}T_{sys}}s + \dfrac{\left(D_{sys} + \dfrac{1}{R_{sys}}\right)}{2H_{sys}T_{sys}}}, \tag{A.12}$$

and the transfer function relating $\Delta P_L(s)$ to the prime movers power change, $\Delta P_{msys}(s)$, is:

$$\frac{\Delta P_{msys}(s)}{\Delta P_L(s)} = \frac{\dfrac{1}{2H_{sys}T_{sys}R_{sys}}}{s^2 + \dfrac{\left(D_{sys}T_{sys} + 2H_{sys}\right)}{2H_{sys}T_{sys}}s + \dfrac{\left(D_{sys} + \dfrac{1}{R_{sys}}\right)}{2H_{sys}T_{sys}}} \tag{A.13}$$

Expression (**A.12**) represent a second order damped oscillator with a zero in $-1/T_{sys}$ and (**A.13**) represents a second order damped oscillator with no zero. Both can be written in the standard notation for these types of oscillators as follows [74]:

$$\frac{\Delta f(s)}{\Delta P_L(s)} = \frac{K_{\Delta f}\dfrac{\omega_0^2}{z}(s + z)}{s^2 + 2\xi\omega_0 s + \omega_0^2}, \tag{A.14}$$

and

$$\frac{\Delta P_{msys}(s)}{\Delta P_L(s)} = \frac{K_{\Delta P_{msys}}\omega_0^2}{s^2 + 2\xi\omega_0 s + \omega_0^2}, \tag{A.15}$$

where

$$K_{\Delta f} = \frac{1}{D_{sys} + \dfrac{1}{R_{sys}}}, \text{ steady state gain for the frequency deviation;} \tag{A.16}$$

$$K_{\Delta P_{msys}} = \frac{1}{D_{sys}R_{sys}+1}$$, steady state gain for the prime mover response; **(A.17)**

$$\omega_0 = \sqrt{\frac{D_{sys}+\dfrac{1}{R_{sys}}}{2H_{sys}T_{sys}}}$$, natural frequency of the fundamental oscillation; **(A.18)**

$$\xi = \frac{D_{sys}T_{sys}+2H_{sys}}{4H_{sys}T_{sys}\omega_0}$$, damping ratio of the fundamental oscillation; **(A.19)**

$$z = \frac{1}{T_{sys}}.$$ **(A.20)**

The inverse of $K_{\Delta f}$ is the composite frequency-response characteristic of the system, K_{sys}:

$$K_{sys} = \frac{1}{K_{\Delta f}} = D_{sys} + \frac{1}{R_{sys}}$$ **(A.21)**

The K_{sys} is also known as the *stiffness* of the system [70] [72] or system *regulation constant*, usually expressed in MW/Hz. Typically, frequency overshoots are experienced with large load imbalances [56], indicating that the system damping ratio is $0 \le \xi < 1$. Therefore the poles and zeros of the close loop system are [74]:

$$\left.\begin{array}{l} s_1 = -\xi\omega_0 + j\omega_d \\ s_2 = -\xi\omega_0 - j\omega_d \end{array}\right\}$$, poles of the close loop system; **(A.22)**

$$\omega_d = \omega_0\sqrt{1-\xi^2}$$, damped natural frequency; **(A.23)**

$$z_1 = -z$$, zero of the Δf response. **(A.24)**

Time response

It is important analyse the time response of the grid frequency when the system is perturbed with a step change in ΔP_L. The inverse Laplace transform of (**A.12**) when applying a step $\Delta P_L(s) = \Delta P_L/s$ gives the time response of $\Delta f(t)$ as:

$$\Delta f(t) = -\Delta P_L \, K_{\Delta f} \left(1 - \sqrt{1 + \frac{(\omega_0 - z\xi)^2}{z^2 (1 - \xi^2)}} \; e^{-\xi\omega_0 t} \; \cos(\omega_d t - \phi) \right) \tag{A.25}$$

with

$$\phi = \arctan\left(-\frac{\omega_0 - z\xi}{z \sqrt{1 - \xi^2}} \right) \tag{A.26}$$

The (**A.12**) and (**A.25**) can be used for determining useful values such as the peak of frequency change Δf_{peak} (usually referred as *nadir* in power systems nomenclature), the time to the peak frequency change t_{peak}, the maximum frequency overshoot $Mo_{\Delta f}$, the settling time $t_{98\%}$, the steady state frequency deviation Δf_{ss} and the initial rate of change of frequency (initial ROCOF) at the time of load change. By doing $d\Delta f(t)/dt = 0$:

$$\frac{d\Delta f(t)}{dt} = -\Delta P_L K_{\Delta f} \sqrt{1 + \frac{(\omega_0 - z\xi)^2}{z^2 (1 - \xi^2)}} \; \omega_0 \; e^{-\xi\omega_0 t} \; \cos(\omega_d t - \alpha) = 0 \tag{A.27}$$

we obtain

$$t_{peak} = \frac{\pi/2 + \alpha}{\omega_0 \sqrt{1 - \xi^2}} \; , \; \text{time to peak frequency.} \tag{A.28}$$

with

$$\alpha = \arctan\left(\frac{z - \omega_0 \xi}{\omega_0 \sqrt{1 - \xi^2}} \right) . \tag{A.29}$$

$$\Delta f_{peak} = \Delta f(t_{peak}) \; , \; \text{peak frequency.} \tag{A.30}$$

$$M_{o\Delta f} = 100 \frac{(-\Delta f_{peak}) - \Delta P_L K_{\Delta f}}{\Delta P_L K_{\Delta f}} \; [\%], \; \text{maximum frequency overshoot} \tag{A.31}$$

$$t_{98\%} = \frac{-\ln\left(\dfrac{1 - 0.98}{\sqrt{1 + \dfrac{(\omega_0 - z\xi)^2}{z^2 (1 - \xi^2)}}} \right)}{\xi\omega_0} \; , \; \text{settling time for 98\% of steady state value.} \tag{A.32}$$

251

$\Delta f_{ss} = -\Delta P_L \cdot K_{\Delta f}$, steady state frequency deviation. **(A.33)**

In the particular case of the instant of load change we have $t = +0$ and $\Delta P_{msys} = \Delta f = 0$. Thus:

$$\frac{d\Delta f(+0)}{dt} = -\frac{\Delta P_L}{2H_{sys}} = -\frac{\Delta P_{Inertia}(+0)}{2H_{sys}}$$, initial rate of change of frequency. **(A.34)**

A.4 Normalized case

In order to carry out a general analysis of the mean grid frequency impact when varying different parameters, a normalized case for the PS1 is defined. By normalizing the variables, it is easier to observe the deviations from a known case when changes in parameters are performed. This normalization is set for $\Delta P_L = 1$ pu, $\Delta f_{ss} = 1$ pu, $t_{peak} = 1$ pu, $\Delta f_{peak} = 1.5$ pu and $D_{sys} \Delta f_{ss} = 0.05\Delta P_L$, i.e. the peak frequency is 150% of the steady state deviation and the load reduction is 5% of the load change. Notice that in this normalized case the base power is the load change, the base frequency is the steady state deviation and the base time is the time to frequency peak. In such conditions, the main system parameters are $H_{sys} = H_0$, $R_{sys} = R_0$, $T_{sys} = T_0$ and $D_{sys} = D_0$. The respective values are shown in **Table A-1**. The **Figure A-3** shows the time response of the grid mean frequency deviation (Δf), the equivalent prime mover output (ΔP_{msys}), the net load change ($\Delta P_{Lnet} = \Delta P_L + D_{sys} \Delta f$) and the equivalent system inertial response ($\Delta P_{Inertia}$) (the electrical outputs of generators are always equal to the load).
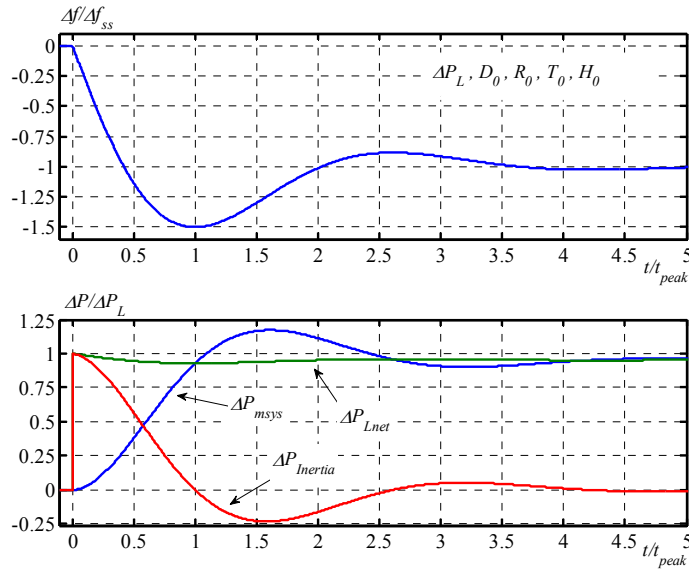

Figure A-3: Normalized Case: composite system frequency response (Δf) and equivalent primary frequency control activation (ΔP_{msys}) due to a system load change (ΔP_L). Notice the scales normalized to the steady state deviation (Δf_{ss}), the time for minimum frequency (t_{peak}) and the initial load change (ΔP_L).

Table A-1: Parameters for the normalized PS1 case

K_{sys0}	D_0	R_0	T_0	H_0
1.0	0.05	$1/(K_{sys0} - D_0)$	0.5915	0.1823

A.5 Islanded power system: PS2

This power system has been used for the control development and simulations in Chapter 5, and it is referred as PS2 in this work. It corresponds to the power system of the Danish island of Bornholm. Only a brief description is presented here, but detailed description can be found in [108] and [109]. The Bornholm power system is a unique facility for experiments with new SmartGrids technologies and it is part of PowerLabDK, an experimental platform for power and energy [108]. This Industrial PhD project was one of its research activities. Extensive data and measurements available at Centre for Electric Technology, Technical University of Denmark, which holds the rights of use and confidentiality, were used for the model development. Additional measurements carried out in this work, with high wind power penetration, were used for model enhancement and validation (see Section 2.5), aiming at dynamic simulations with wind power. The measurement activities were supported by Vestas Wind Systems A/S and by Centre for Electric Technology. The control algorithms for wind power production developed in this work were tested with this model together with the turbine model in Appendix B. In [63] and [67] other wind power studies were conducted on this power system.

The Bornholm power system is a Danish distribution system situated just south of Sweden in the Baltic Sea. Its surface can be fit in a square-shape area of approximately 20x30 km^2. It consists mainly of a ring-shape transmission system of 60 kV surrounding the island. Sixteen bus-bars spread over the island are connected to this transmission system, from where the voltage is reduced to 10 kV for each local distribution system (**Figure A-4**). ØSTKRAFT is the distribution system operator supplying electricity to more than 28,000 customers [109]. Bornholm is part of the Nordic interconnected power system (NPS) and power market [5] through a 60kV/70MVA submarine cable, which feeds the whole island. Considering area, electricity demand and population Bornholm corresponds to approximately 1% of Denmark and it has many of the characteristics of a typical Danish distribution system [108]. Loads are mainly homes and farms, but also industries.

The system can be operated isolated in islanding mode. Local generation consists of one conventional generator –steam turbine– with a permanently engaged governor, named SG1 in this work; one Combined Heat and Power unit (CHP) –steam turbine– with a normally disabled governor, named SG2; other diesel generators operated normally at constant power, which can be lumped in SG3, and other minor generators not operated

during the measurements performed in this work. The generators are concentrated in a main bus-bar, supplying power to the whole system when in islanding mode.

Additionally, two controllable wind power plants (WPP1 and WPP2) are located at two different bus-bars in the system –in parallel with local load– distant approximately 20 km from each other. The WPPs are composed respectively of 3xV80-2MW and 3xV66-1.75MW Vestas variable speed wind turbines, doubly-fed generator technology. They are supervised remotely and centrally via SCADA system, allowing operation at optimal production as well as deloaded by power limitation or curtailment. The wind turbines can be fully controlled remotely. Other wind turbines of old design (fixed speed, not controllable) can be found in the island. The system presents a large capacity penetration of $WP_C \approx 55\%$ and large share penetrations of $WP_{Sh} \approx 40\%$ when connected to the NPS. A large $WP_{Sh} \approx 200\%$ can be achieved during island operation, meaning that wind power may need to be curtailed during this mode.

Table A-2 highlights part of the basic generation/consumption data used for modelling. **Figure A-6** shows the modelling in Power Factory DIgSILENT GmbH. **Figure A-7** shows the main busbars where the modelled local generation and the two wind power plants are connected. All the wind turbines were modelled as V80-2MW type.
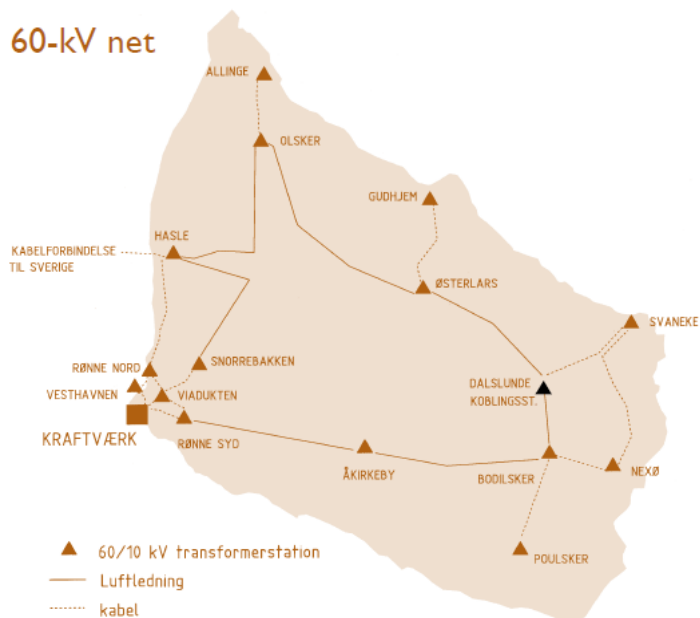

Figure A-4: Bornholm 60 kV transmission system in 2009 [109].

Table A-2: Part of the data of generation and consumption used in the modelling [108].

| Component	S_N [MVA]	P_N [MW]	V_N [kV]	Comments
SG1	29.5	25	10.5	Frequency regulation machine during islanding mode with a permanently engaged governor. Droop = 5%.
SG2	45	37.5	10.5	CHP plant supplying local heat demand, normally with no regulation activity [67].
SG3	6	5	10.5	Constant output diesel engine, tripped during simulations of low frequency events.
WPP1	6.12	6	10.5	WPP1 & WPP2 modelled with 3xV80-2MW Vestas wind turbines each.
WPP2	6.12	6	10.5	
Load	~56 MW maximum ~13 MW minimum		10.0	By year 2008 [63] [108]

Power system model verification
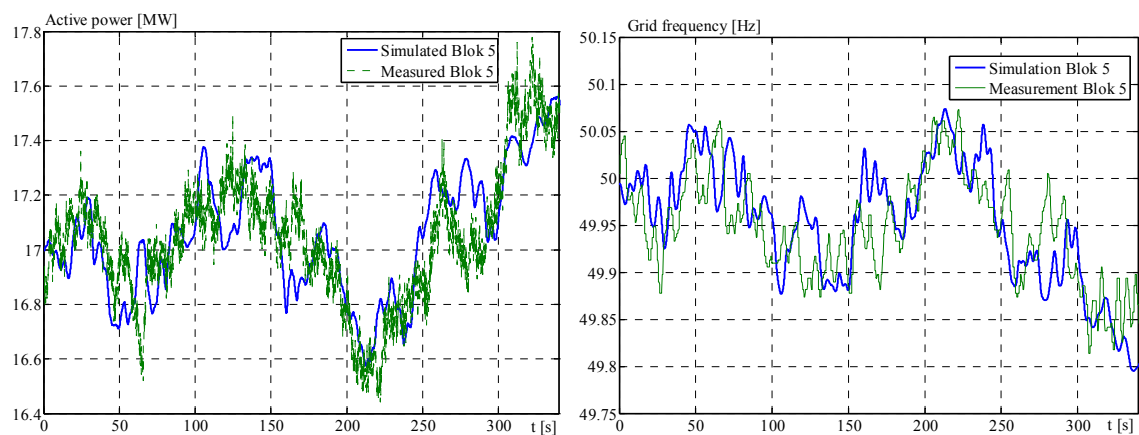
Figure A-5: Comparison of measured and simulated power output and speed of SG1 in the SP2 system (Island operation, Bornholm 17th Aug. 2009, sample record from 11:50 to 11:56)
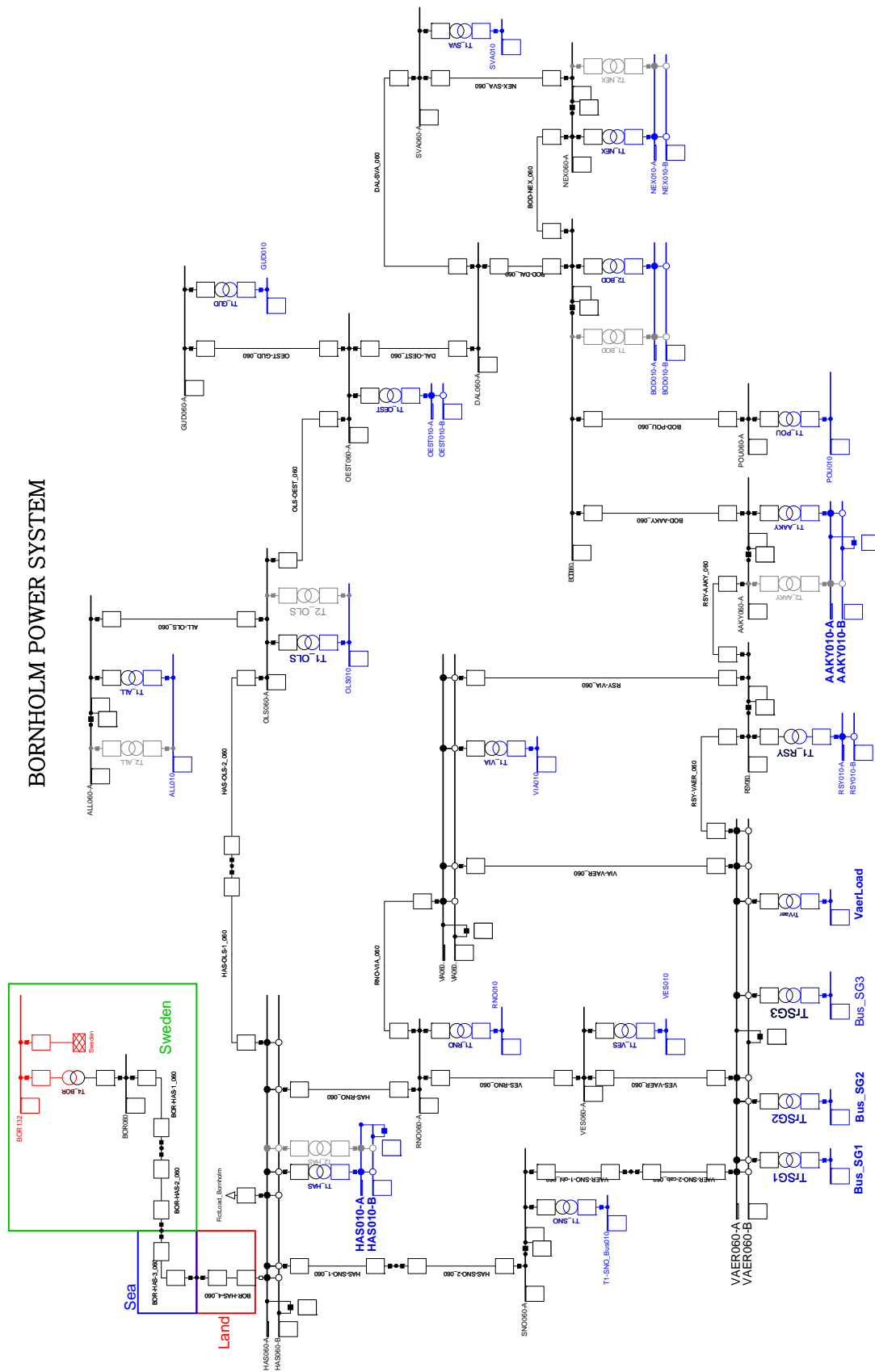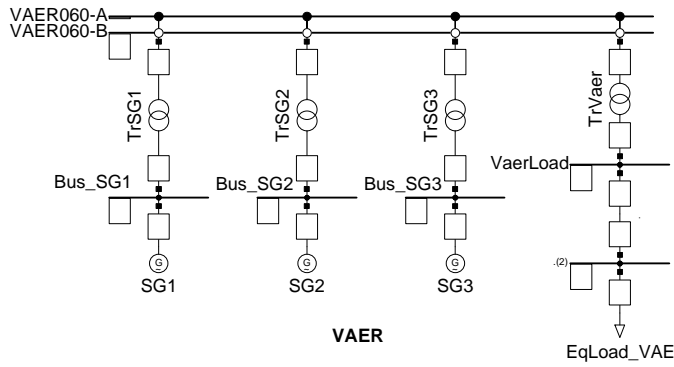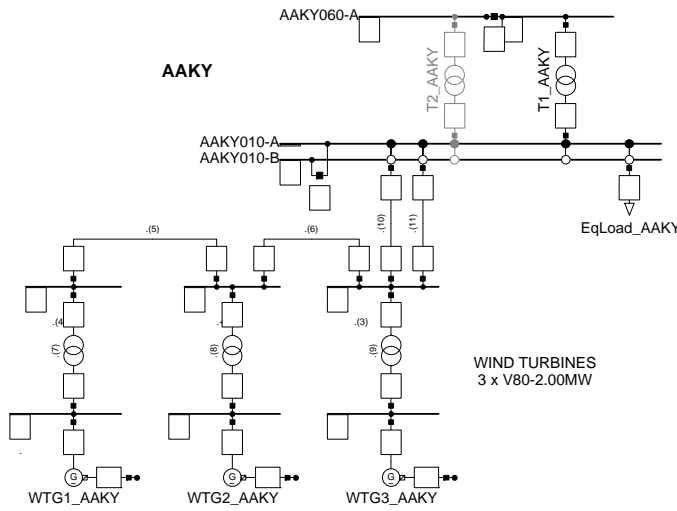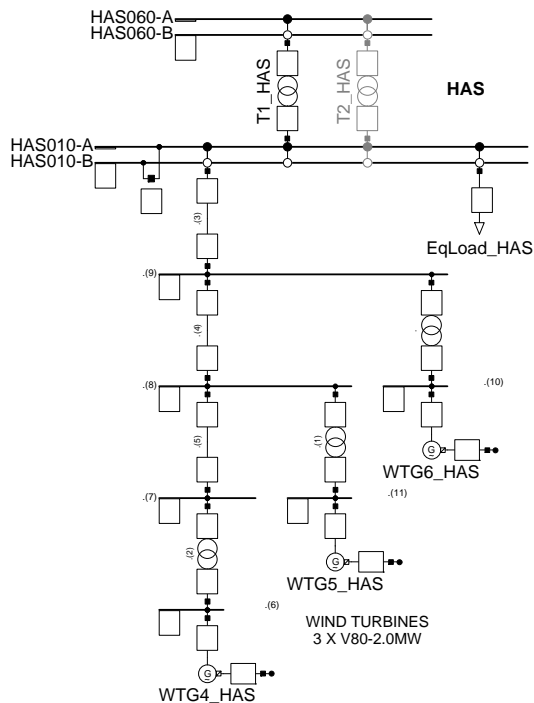
Figure A-6: Bornholm power system modeled in Power Factory DIgSILENT GmbH.

(a)

Conventional generators SG1, SG2 and SG3 in busbar VAER.

(b)

Wind turbines in WPP1, busbar AAKY.

(c)

Wind turbines in WPP2, busbar HAS.

Figure A-7: Busbars with modelled conventional generators and wind turbine generators

A.6 Nine-bus multimachine power system: PS3

This power system has been used for the performance simulations of coordinated frequency control in Chapter 6, and it is referred as PS3 in this work. It is a modification of the classical 9-bus power system model found in [71]. **Figure A-8** shows this power system, with a low flow case, implemented in Power Factory DIgSILENT GmbH. The modifications were changes only on the generators connected to the network, in order to make them comparable to the size of the modeled wind power plants (described in Appendix B). Additionally, the G4 machine was added to serve as a *tripping* machine, in order to create a power imbalance in the system. Therefore this machine does not participate during the dynamic response of the system. Only the load flow condition is necessary to specify for it. Finally, the simulations performed with this system are described in Chapter 6. **Table A-3**, **Table A-4** and **Table A-5** show the complete set of parameters and data of this power system (wind turbines and wind power plants are described in Appendix B). Data and nomenclature were taken from [71].
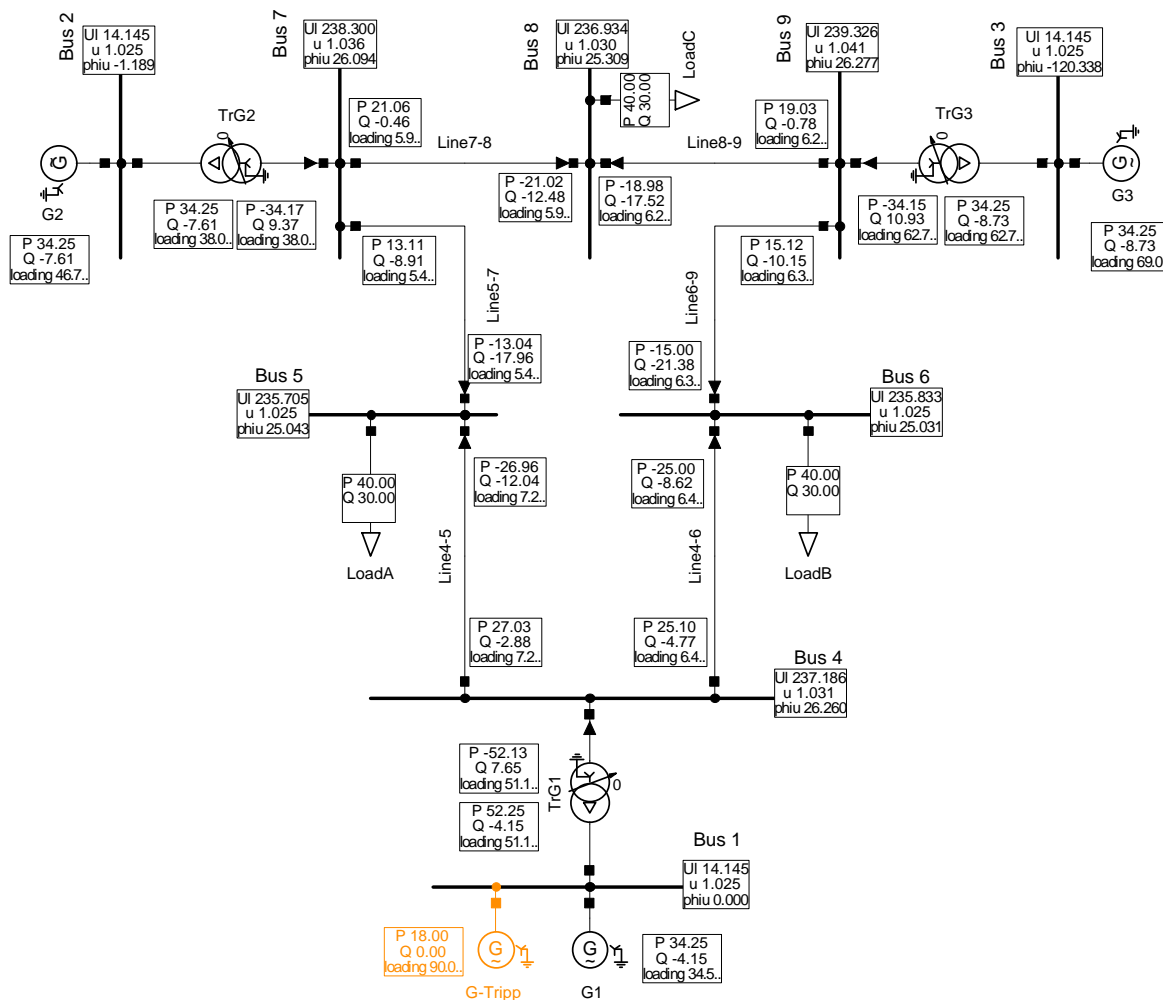

Figure A-8: Nine-bus system modified

Table A-3: Nine-bus system power plants parameters

Generator			G1 (Steam)	G2 (Steam)	G3 (Steam)
Parameter	**Unit**	**Description**	**Values**		
Sn	MVA	Machine-rated power; base value for impedances	100.00	75.00	51.20
Un	kV	Machine-rated line-to-line voltage; base value for impedances	13.80	13.80	13.80
PF	-	Machine-rated power factor	0.80	0.80	0.80
SCR	pu	Machine short circuit ratio	0.90	1.00	0.90
Xd''	pu	Unsaturated d axis subtransient reactance	0.145	0.130	0.105
Xd'	pu	Unsaturated d axis transient reactance	0.220	0.185	0.209
Xd	pu	Unsaturated d axis synchronous reactance	1.180	1.050	1.270
Xq''	pu	Unsaturated q axis subtransient reactance	0.145	0.130	0.116
Xq'	pu	Unsaturated q axis transient reactance	0.380	0.360	0.850
Xq	pu	Unsaturated q axis synchronous reactance	1.050	0.980	1.240
Ra	pu	Armature resistance	0.0035	0.0031	. . .
Xl	pu	Leakage or Potier reactance	0.075	0.070	0.108
R2	pu	Negative-sequence resistance	0.020	0.016	. . .
X2	pu	Negative-sequence reactance	0.095	0.085	0.105
X0	pu	Zero-sequence reactance	0.065	0.070	0.116
Td''	s	d axis subtransient short circuit time constant	. . .	. . .	. . .
Td'	s	d axis transient short circuit time constant	. . .	. . .	0.882
Td0''	s	d axis subtransient open circuit time constant	0.042	0.038	. . .
Td0'	s	d axis transient open circuit time constant	5.900	6.100	6.600
Tq''	s	q axis subtransient short circuit time constant	...	. . .	. . .
Tq'	s	q axis transient short circuit time constant	...	. . .	. . .
Tq0''	s	q axis subtransient open circuit time constant	0.092	0.099	. . .
Tq0'	s	q axis transient open circuit time constant	0.300	0.300	. . .
Ta	s	Armature time constant	0.140	0.140	. . .
Wr	MW.s	Kinetic energy of turbine + generator at rated speed	498.50	464.00	260.00
Rf	Ω	Machine field resistance	0.215	0.290	0.295
SG1.0	pu	Machine saturation at 1.0 pu voltage	0.0933	0.1000	0.2067
SG1.2	pu	Machine saturation at 1.2 pu voltage	0.4044	0.3928	0.7240

Efdfl	pu	Machine full load excitation	2.292	2.120	2.310
D	pu	Machine rotor damping coefficient	0.01	0.01	0.01
Exciter and AVR			**G1 (Steam)**	**G2 (Steam)**	**G3 (Steam)**
Parameter	**Unit**	**Description**	**Values**		
Type	-	Excitation system type [70]	DC1A	DC1A	DC1A
Name	-	Excitation system name	NA101	NA101	WMA
RR	-	Exciter response ratio (formerly ASA response)	0.50	0.50	1.50
Tr	s	Regulator input filter time constant	0.060	0.060	0.000
Ka	pu	Regulator gain	25.000	25.000	400.000
Ta or Ta1	s	Regulator time constant (#l)	0.200	0.200	0.050
Ta2	s	Regulator time constant (#2)	0.000	0.000	0.000
Vrmax	pu	Maximum regulator output, starting at full load field voltage	1.000	1.000	0.613
Vrmin	pu	Minimum regulator output, starting at full load field voltage	-1.000	-1.000	-0.613
Ke	pu	Exciter self-excitation at full load field voltage	-0.0582	-0.0516	-0.0769
Te	s	Exciter time constant	0.6544	0.5790	1.3700
SE.75max	-	Rotating exciter saturation at 0.75 ceiling voltage	0.0895	0.0794	0.1120
SEmax	-	Rotating exciter saturation at ceiling voltage	0.349	0.3093	0.2254
Aex	pu	Derived saturation constant for rotating exciter	0.0015	0.0013	0.0137
Bex	pu	Derived saturation constant for rotating exciter	1.5833	1.4015	0.6774
Efdmax	pu	Maximum field voltage or ceiling voltage	3.438	3.881	4.130
Efdmin	pu	Minimum field voltage	-3.438	-3.881	-4.130
Kf	pu	Regulator stabilizing circuit gain	0.105	0.093	0.040
Tf or Tf1	s	Regulator stabilizing circuit time constant (#l)	0.350	0.350	1.000
Tf2	s	Regulator stabilizing circuit time constant (#2)	0.000	0.000	0.000
Turbine and Governor			**G1 (Steam)**	**G2 (Steam)**	**G3 (Steam)**
Parameter	**Unit**	**Description**	**Values**		
Type	-	Type of governor block diagram	General	General	General
R	pu	Droop for regulation of 12 MW/Hz	0.166	0.125	0.0854
Pmax	MW	Maximum turbine output	100.00	75.00	51.20
T1	s	Governor response time	0.200	0.100	0.083

T2	s	Hydro reset time constant	0.000	0.000	0.000
T3	s	Servo time constant or hydro gate time constant	0.300	0.200	0.200
T4	s	Steam valve bowl time constant	0.090	0.050	0.050
T5	s	Steam reheat time constant or ½ hydro water starting time constant	10.000	8.000	5.000
F	-	Constant for unit type: pu shaft output ahead of re-heater for steam units or -2.0 for hydro units	0.250	0.300	0.280
Machines Transformers			**TrG1**	**TrG2**	**TrG3**
Parameter	**Unit**	**Description**	**Values**		
Sn	MVA	Rated power	100.00	90.00	55.00
U1/U2	kV	Nominal voltages	230/13.8	230/13.8	230/13.8
uk	%	Short circuit voltage	13.18	13.18	10.04
uk0	%	Zero sequence short circuit voltage	10.0	10.0	9.0
Po	kW	Copper losses	270	250	170

Table A-4: Nine-bus system transmission lines

Paramenter	Unit	Description	line 4-5	line 4-6	line 7-8	line 5-7	line 8-9	line 6-9
Ul-l	kV	Line to line voltage	230	230	230	230	230	230
R	Ω	Resistance	5.290	8.993	4.496	16.928	6.295	20.630
X	Ω	Reactance	44.965	48.668	38.088	85.169	53.323	89.930
C	μF	Capacitance	0.8830	0.7926	0.7475	1.5351	1.0485	1.7960

Table A-5: Nine-bus system base case load flow

Power		Load A	Load B	Load C	G1 (slack)	G2	G3	G4 (tripped)
Po	MW	40	40	40	34.25	34.25	34.25	18.00
Qo	MVAr	30	30	30	-4.15	-7.61	-8.73	0.00

B
WIND POWER PLANTS MODELLING

B.1 Aerodynamic power conversion

The aerodynamical power captured by the rotor blades, P_{Aero}, can be approximated by [68]:

$$P_{Aero} = \frac{1}{2} \rho \, A \, C_P(\lambda,\theta) \, V^3 \ [\text{W}] \tag{B.35}$$

where ρ [kg/m^3] is the air density, A [m^2] is the swept area by the rotor blades, V [m/s] is the wind speed relative to the rotor blades, $C_P(\lambda,\theta)$ is the power coefficient (or aerodynamical efficiency), λ is he tip-speed ratio and θ is the pitch angle of the blades. The C_P is *defined* by the ratio between P_{Aero} and the total power carried by the wind, P_{Wind} [68]:

$$C_P := \frac{P_{Aero}}{P_{Wind}} \tag{B.36}$$

The C_P is one of the main characteristics of a wind turbine and it depends on the specific aerodynamical design. The value of the C_P is variable with θ and with λ. The λ is defined as the ratio between the linear tip speed of the blade (m/s) and the wind speed (m/s):

$$\lambda := R\frac{\Omega_r}{V} \tag{B.37}$$

where R [m] is the rotor radius, Ω_r [rad/s] is the rotor speed. Thus captured mechanical power does not only depend on the wind speed but also on the rotor speed and pitch angle. The V is *relative* with respect to the turbine rotor, i.e. is the difference between the absolute wind speed (ground speed) and the *nacelle speed*. Due to the tower flexibility, its thrust-wise top displacement is largely changed during inertial response, as described in Section B.2. Therefore the nacelle speed contributes driving the turbine rotor. It is given by:

$$V = V_{Abs} - V_{nacY} \tag{B.38}$$

where V_{Abs} is the absolute wind speed and V_{nacY} is the nacelle speed in the y-axis direction. The V_{nacY} is determined with the mechanical model in (**B.50**) (in pu).

The aerodynamical torque developed in the turbine rotor can be approximated taking (**B.35**), dividing it by the rotor speed Ω_r and combining with (**B.37**), thus:

$$T_{Aero} = \frac{1}{2} \rho \, \pi \, R^3 \, \frac{C_P(\lambda,\theta)}{\lambda} \, V^2 \text{ [Nm]} \tag{B.39}$$

Besides knowing the aerodynamical power, it is also important to determine the thrust, F_T, caused by the wind on the turbines' rotor. Similarly to the aerodynamical power, the thrust depends not only on the wind speed but also on the rotors' speed and pitch angle. The thrust plays an important role in tower impact and must be assessed when performing critical control actions involving the blades. The thrust is transmitted to the tower through the main bearing, and yaw system, therefore producing tower deflections along the y-axis. The thrust can be calculated as [68]:

$$F_T = \frac{1}{2} \rho \, \pi \, R^2 \, C_T(\lambda,\theta) V^2 \text{ [N]} \tag{B.40}$$

where $C_T(\lambda,\theta)$ is the thrust coefficient.

For an existing wind turbine, the $C_P(\lambda,\theta)$ and $C_T(\lambda,\theta)$ should be provided by the blade manufacturer. This data can be obtained from advanced aerodynamical models in the form of 3D numerical arrays with λ and θ as independent variables.

The developed P_{Aero} and the captured wind energy E_{Aero} are very sensitive to C_P values thus is important to use accurate values. In the literature several approximations for the $C_P(\lambda,\theta)$ by means of analytical functions can be found, e.g. [78] [79] [80]. Those approximations are curves fitting on manufacturers' data. In this work, the $C_P(\lambda,\theta)$ and $C_T(\lambda,\theta)$ were provided by the manufacturer as 3D numerical array. These values were used directly in the simulations through a *look-up table* with λ and θ as inputs, which can be expressed as:

$$C_P(\lambda,\theta) = LookUpTable\{[\mathbf{C_P}, \boldsymbol{\lambda}, \boldsymbol{\theta}], \lambda, \theta\} \tag{B.41}$$

$$C_T(\lambda,\theta) = LookUpTable\{[\mathbf{C_T}, \boldsymbol{\lambda}, \boldsymbol{\theta}], \lambda, \theta\} \tag{B.42}$$

where $\mathbf{C_P}$, $\mathbf{C_T}$, $\boldsymbol{\lambda}$ and $\boldsymbol{\theta}$ are data arrays.

Appendix D.1 shows typical curves of the coefficients $C_P(\lambda,\theta)$ and $C_T(\lambda,\theta)$ used for the turbine WTG1. Each point in the curves in **Figure D-1** represents a steady state operation. In other words, this aerodynamic representation is based on the consideration of static aerodynamical equilibrium. The air distribution around the blades' profile adapts *instantaneously* to the new operational conditions, hence the aerodynamical power changes immediately from one value to another when changes in V, θ or Ω_r are experienced. Obviously, this assumption does not reflect the reality. The transition between two operational states is continuous but not instantaneous. The dynamic behaviour describing this transition is called *inflow phenomena* [105]. The inflow phenomena appear as an overshoot in the T_{Aero} when fast changes in θ are applied [81] [105]. If the pitch control system works properly, the speed changes of θ are limited thus the torque overshoots reduced. In this work, the pitch control system limits the speed of θ to ~2 deg/s; therefore the torque overshoots are kept very low by control action. Similarly, wind speed and rotational speed changes are not instantaneous and the C_P and C_T can be directly applied in the modelling without discussion [81].

Per-unit system

Expressions in per-unit system (pu) are defined. The nominal captured power P_{AeroN} is defined as the captured mechanical power corresponding to the nominal electrical power P_{eN} in steady state, with the nominal wind speed V_N and the nominal rotor speed Ω_{rN}.

The P_{AeroN} can be a value expressed in pu considering a base power P_b as following:

$$p_{AeroN} = \frac{1}{2} \cdot \frac{\rho \cdot A \cdot C_{PN}(\lambda_N, \theta_N) \cdot V_N^3}{P_b} \quad \text{[pu]} \tag{B.43}$$

Where C_{PN} is the nominal power coefficient, corresponding to the nominal tip speed ratio λ_N and nominal pitch angle θ_N. Considering nominal values and taking any base values P_b, V_b, Ω_{rb}, F_{Tb}, the aerodynamical modelling can be expressed in the per-unit system as:

$$v = v_{Abs} - v_{nacY} \quad \text{[pu]} \tag{B.44}$$

$$\lambda = \frac{\lambda_N \cdot v_N}{\omega_{rN}} \cdot \frac{\omega_r}{v} \quad \text{[pu]} \tag{B.45}$$

$$\tau_{Aero} = \frac{p_{AeroN}}{v_N^3 \cdot C_{PN}} \cdot C_P(\lambda,\theta) \cdot \frac{v^3}{\omega_r} \ [pu] \tag{B.46}$$

$$f_T = \frac{f_{TN}}{v_N^2 \cdot C_{TN}} \cdot C_T(\lambda,\theta) \cdot v^2 \ [pu] \tag{B.47}$$

$$p_{Aero} = \frac{p_{AeroN}}{v_N^3 \cdot C_{PN}} \cdot C_P(\lambda,\theta) \cdot v^3 \ [pu] \tag{B.48}$$

where the following variables are in pu: Absolute wind speed v_{Abs}, nacelle thrust-wise speed v_{nacY} and nominal wind speed v_N; rotor speed ω_r and its nominal ω_{rN}, aerodynamical torque τ_{Aero}, thrust force f_T and its nominal f_{TN}, aerodynamical power p_{Aero} and its nominal p_{AeroN}. Observe that no geometrical data is needed in this pu modelling; only aerodynamical efficiency and its nominal operational points. If the base values are chosen as the respective nominal ones, the previous expressions can be further simplified.

The expressions (**B.41**)-(**B.42**) and (**B.44**) to (**B.48**) determine the wind turbine aerodynamical model in per-unit system. **Figure B-9** shows the block diagram of aerodynamical model in pu with its inputs and outputs.
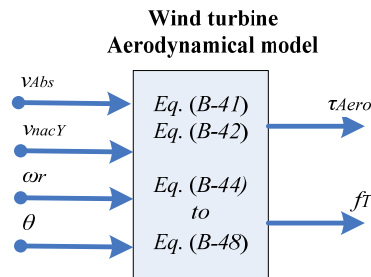

Figure B-9: Wind turbine aerodynamical model; inputs and outputs.

B.2 Drive train and tower

A gearbox-driven generator topology has been modeled in this work. **Figure B-10** shows a schematic of the main mechanical components in this type of wind turbine.
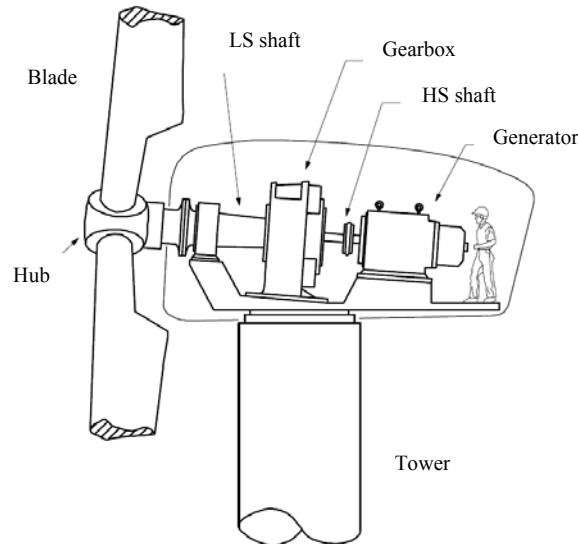
Figure B-10: Schematic of main mechanical components in a geared wind turbine.

The drive train is in charge of delivering the aerodynamical power captured in the blades to the generator's rotor in the form of torque and rotational speed. The mechanical system also provides structural support. The components of the mechanical system are generally subject to dynamical stress in the form of forces and displacements. Depending on the particular topology of the VSWT and its control characteristics, the electrical power output may contain (reflect) some of the mechanical oscillations, which are absorbed by the electricity network [81] [83].

In general, the study of the mechanical impact in the turbine is done through sophisticated computational models, for example based on Finite Elements Analysis [83]. This type of detailed modelling is not necessary for investigating the impact of wind power in the power system, giving place to simplifications. Nevertheless, the oscillatory behaviour in main components and in the turbine's power output cannot be observed if the mechanical model is excessively simplified. Thus the simulations aimed to the study of wind power impact in the grid or wind turbine controls would give incorrect results.

In this work, a particular active power response for grid stability is studied and its respective control algorithm is established. It is therefore necessary to assess, at least at a minimum level, the impact on the main components in the mechanical system. This will contribute to determine the feasibility of implementing the new functionality on commercial wind turbines.

Studies and measurements indicate that, for power system impact analysis, it is enough to consider just the 1st oscillatory mode in the modelling, which can be represented by the classical two-mass model for the drive train [82] [83]. The two-mass model provides

information of torques and speeds of rotor and generator, which is useful for simple assessment of the drive train impact. In this work the observations are extended to the tower top displacements and velocities in the fore-aft direction (wind speed direction) and sidewise direction (perpendicular to wind direction). The effects of the aerodynamical thrust and nacelle roll forces on the tower are included. The following main variables are observed: Rotor and generator speed, generator mechanical torque, tower top displacements, velocities and accelerations.

This model is based on the body diagram shown in **Figure B-11**. More detailed modelling (more oscillation modes) is described in [86] [87] [88]. Here the main assumptions are: Stiff connection of generator stator and gearbox-housing to the nacelle, therefore the inertias of the stator and gearbox-housing become part of the nacelle inertia (in the reality, the gearbox-housing presents an oscillation mode due to the soft coupling with the nacelle, but this mode is not represented here); drive train represented by two lumped masses connected by equivalent drive train stiffness and friction coefficient; stiff coupling between generator inertia and gearbox (i.e. drive train equivalent stiffness located in the low speed side); gearbox main shafts rotating in the same direction; nacelle receiving the torque reaction from generator stator and gearbox-housing; tower assumed as symmetrical slender bean with cylindrical section [86]; tower top equivalent displacements of only the first bending mode, in both the fore-aft direction (y-axis) and the sideward direction (x-axis); fore-aft displacement represented by a simple mass-spring-damper system; sideward direction coupled to the nacelle roll angle which depends on the reactions of drive train and generator stator.

The tower top rotation, the torsion deformation, the yawing effects and higher bending modes are neglected. Additionally, tilt related influences are ignored.
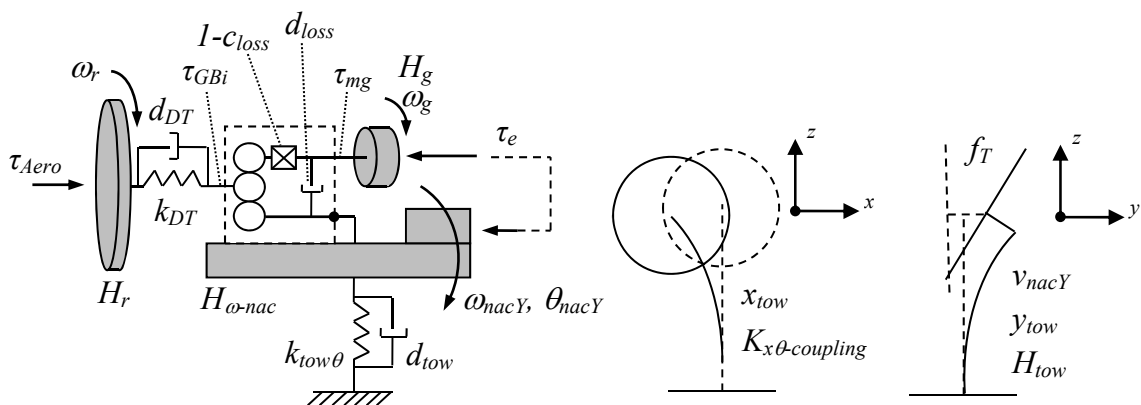

Figure B-11: Body diagram of wind turbine drive train, nacelle and tower.

The drive train losses are modeled as a torque τ_{loss} dependant on gearbox torque and speed, as follows:

$$\tau_{loss} = c_{loss} \cdot \tau_{mg} + d_{loss} \cdot \omega_g \tag{B.49}$$

where $c_{\tau loss}$ is the torque-dependant loss coefficient, d_{loss} is the speed-dependant loss coefficient, τ_{mg} [pu] is the generator mechanical torque (gearbox output) and ω_g [pu] is the generator speed. These losses are implicit in the formulation of the drive train model. The modelling of the drive train and tower are given in pu as follows:

$$\dot{\omega}_r = \frac{1}{2H_r} \left[\tau_{Aero} - k_{DT} \cdot \theta_{DT} - d_{DT} \cdot \left(\omega_r - \omega_g - \omega_{nacY} \right) \right]$$

$$\dot{\omega}_g = \frac{1}{2H_g} \left[\frac{1}{\left(1+c_{loss}\right)} \cdot \left\{ k_{DT} \cdot \theta_{DT} + d_{DT} \cdot \left(\omega_r - \omega_g - \omega_{nacY} \right) - d_{loss} \cdot \omega_g \right\} - \tau_e \right]$$

$$\dot{\omega}_{nacY} = \frac{1}{2H_{\omega - nac}} \left[\tau_e + k_{DT} \cdot \theta_{DT} + d_{DT} \cdot \left(\omega_r - \omega_g - \omega_{nacY} \right) - k_{tow\theta} \cdot \theta_{nacY} - d_{tow\theta} \cdot \omega_{nacY} \right]$$

$$\dot{\theta}_{DT} = \frac{\omega_B}{\theta_B} \left(\omega_r - \omega_g - \omega_{nacY} \right)$$

$$\dot{\theta}_{nacY} = \frac{\omega_B}{\theta_B} \cdot \omega_{nacY}$$

$$(\text{B.50})$$

$$\dot{v}_{nacY} = \frac{1}{2H_{tow}} \left[f_T - k_{towY} \cdot y_{tow} - d_{towY} \cdot v_{nacY} \right]$$

$$\dot{y}_{tow} = v_{nacY}$$

$$x_{tow} = \frac{\theta_{nacY}}{K_{x\theta - coupling}} \cdot$$

$$D_{tow} = \sqrt{x_{tow}^2 + y_{tow}^2}$$

$$\tau_{GBi} = k_{DT} \cdot \theta_{DT} + d_{DT} \cdot \left(\omega_r - \omega_g - \omega_{nacY} \right)$$

$$\tau_{mg} = \frac{1}{\left(1+c_{loss}\right)} \cdot \left(\tau_{GBi} - d_{loss} \cdot \omega_g \right)$$

where ω_r, ω_g and ω_{nacY} [pu] are respectively the rotor speed, the generator speed and the nacelle angular speed in the y-axis; θ_{DT} and θ_{nacY} [pu] are the equivalent torsion angles of the drive train and the nacelle in the y-axis; v_{nacY} [pu] is the nacelle linear speed on the y-axis (speed on the thrust-wise direction); y_{tow}, x_{tow} and D_{tow} [pu] are respectively the tower top displacements in the y-axis, the x-axis (sideward direction) and absolute; τ_{Aero}, τ_e, τ_{GBi} and τ_{mg} [pu] are respectively the aerodynamical torque (given by (**B.46**)), the electromagnetical torque in the generator windings, the gearbox torque input and the mechanical torque in the generator shaft; k_{DT}, $k_{tow\theta}$ and k_{towY} [pu] are respectively the equivalent stiffness of drive train torsion, tower bending and tower top linear displacement in the y-axis direction; d_{DT}, d_{loss}, $d_{tow\theta}$ and d_{towY} [pu] are the friction coefficients (based on damping factors) of the drive train shafts, the drive train losses, the tower bending and the tower displacement in the y-axis direction, respectively; H_r, H_g, $H_{\omega\text{-}nac}$ and H_{tow} [s] are respectively the inertia constants of turbine's rotor (including blades, hub and main shaft), generator's (including rotor, brake disk and high speed shaft), the nacelle plus tower rotating in the y-axis and the nacelle plus tower moving linearly on the y-axis; $K_{x\theta\text{-}coupling}$ the coupling between tower sideward displacement and nacelle rotated angle; and ω_B and θ_B the chosen base rotational speed [rad/s] and torsion angle [rad]. The thrust f_T [pu] is given by (**B.47**).
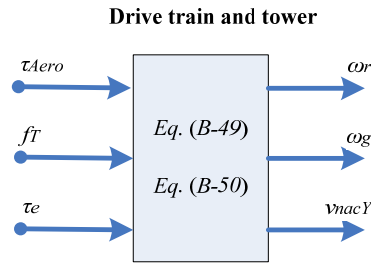
Drive train and tower

Figure B-12: Drive train and tower model; inputs and outputs.

Some of the parameters in (**B.50**) can be calculated as follows. Typical data is given in Appendix D.3:

$$K_{towY} = 4 \cdot \pi^2 \cdot f_{tow}^2 \cdot \left(M_{towTop} + M_{towEq}\right) \text{ [N/rad]}$$

$$k_{towY} = K_{towY} \cdot \frac{Y_{towB}}{F_{TB}} \text{ [pu]}$$

$$D_{towY} = 4 \cdot \pi \cdot \xi_{towY} \cdot f_{tow} \cdot \left(M_{towTop} + M_{towEq}\right) \text{ [N/rad/s]} \qquad \textbf{(B.1)}$$

$$d_{towY} = D_{towY} \cdot \frac{V_B}{F_{TB}} \text{ [pu]}$$

$$H_{tow} = \frac{1}{2} \cdot \left(M_{towTop} + M_{towEq}\right) \cdot \frac{V_B}{F_{TB}} \text{ [s]}$$

The tower top effective mass is determined by the summation of tower top mass (nacelle mass + rotor) and a top equivalent tower mass (equivalent tower mass assumed to be virtually concentrated at the tower top).

B.3 Wind speed in WPP

For the kind of studies conducted in this PhD, it is important to consider, at least to some degree, the effects of the wind speed distribution inside a WPP. Here a simplified (less accurate) approach is applied to generate this wind. In [90], [91], [92], measurements of wake effects were conducted in large offshore WPP. From the results, it can be seen that a number of 5 turbines in a row, separated by ~500 m can show the basic wake effects. This is reflected as a reduction on the average wind speed hitting the turbine, taking as reference the *free wind* (the wind that would exist if no WPP installation exists). A larger number of wind turbines would increase the simulation time, bringing little improvements in results and conclusions. For this reason, the WPP was chosen to be of 5x5 wind turbines.

Standing on the present bibliography, a simple set of equations was implemented to generate idealized wake *deficit* effects in the WPP, that is, the reduction on average wind speed from one turbine to another. The idealized wake deficit effects for an infinitely large number of wind turbines in a single row are given by [89]:

$$v_n = c_n \cdot v_0$$

$$v_{n+1} = c_{n+1} \cdot v_0$$

$$c_{n+1} = 1 - \left(\frac{A_n}{A_{n+1}} \cdot (1 - c_n) + 0.5 \cdot \frac{A_R}{A_{n+1}} \cdot c_n \cdot C_T \right)$$

$$A_{n+1} = 0.5 \cdot A_R \cdot \frac{c_w}{1 - c_w} \cdot C_T + A_n$$

$$c_w = \frac{\alpha}{\alpha + 0.5 \cdot C_T / s_r} \tag{B.51}$$

$$s_r = \frac{x_r}{D_R}$$

$$A_R = \frac{\pi \cdot D_R^2}{4}$$

$$c_1 = 1$$

$$A_1 = A_R$$

where v_0 is the free wind speed, v_n is the n turbine wind speed, c_n is the wake *deficit* for the turbine n, A_n is the wake area, A_R is the rotor area, D_R is the rotor diameter, C_T is the thrust coefficient for the given wind speed, c_w is the asymptotic value of the deficit, x_r is the distance between turbines, α is the decay factor. This simple wake effect model

needs to be adjusted with field measurements. In this work, the coefficient α was adjusted according to field measurements from Horns Rev wind power plant found in [92] for an average $C_T = 0.7$, obtaining α = 0.25 [89]. For the modeled WPP we have: $D_R = 80$ m, $x_r = 560$ m. This gives the deficits c as shown in **Figure B-13**. Note that this profile is very similar to the shown in e.g. [89]-[93].
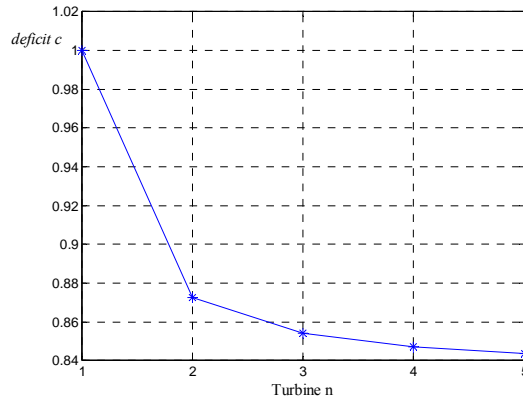

Figure B-13: Calculated wake deficit for one row in the modelled WPP.

For calculating the wind speed time series for the WPP, the following simplified procedure was implemented:

1- Using Kaimal spectrum, time series of free wind was created for the first column of the WPP (first line in the lateral) assuming Taylor's frozen turbulence hypothesis [103]. This assumption is not realistic for a large WPP, especially when the wind direction is along a row of wind turbines [104]. In this case, the generated wind speed series will be identical for all wind turbines in the row (coherence = 1). But, this assumption greatly simplifies the effort of generating a free wind field. It provides relatively simple equations for the wake effect models, which can be combined with the delay corresponding to the travel time for the wind from one turbine to the other. Errors are assumed by using this methodology, however practical results are obtained. The free wind field was generated with a length scale L = 600m, a turbulence intensity 8% and a frequency $f = 20$ Hz.

2- After generating the wind field for the first column of turbines, the next turbine in the line, $n+1$, receives a wind speed v_{n+1} which is derived from the previous turbine, but affected by a wake *deficit*: $v_{n+1} = (c_{n+1}) \cdot (v_o)$ and delayed by a time $\tau_{n+1} = x_r / v_{n+1}$. In this way, time series for all the wind turbines can be generated before simulating the WPP.

3- During the WPP simulation, the rotation of the wind turbines are introduced in the respective pre-generated wind speed, in order to introduce the 3p effect [104].

C
ENERGY BALANCE IN THE WIND TURBINE

This appendix presents some mathematical calculations for supporting the analysis described in Chapter 4, Section 4.2.3.

Determination of the aerodynamical energy change:

During the period T_{Boost} of delivering electric energy to the grid, the aerodynamical energy converted in the turbine's rotor and its variation Δ is (V_w is constant, so it can be put outside the integral):

$$E_{Aero} = K_{Aero} V_w^3 \int_0^{T_{Boost}} C_P(t) \, dt = K_{Aero} V_w^3 \int_0^{T_{Boost}} \left(C_P(0) + \Delta C_P(t) \right) dt \qquad \textbf{(C.1)}$$

$$\Delta E_{Aero} = K_{Aero} V_w^3 \int_0^{T_{Boost}} \Delta C_P(t) \, dt \qquad \textbf{(C.2)}$$

Following, the determination of ΔE_{Aero} is performed. First simplification: Taylor's series approximation:

$$\Delta C_P(t) = \left. \frac{\partial C_P}{\partial t} \right|_{t=0} t + \left. \frac{\partial^2 C_P}{\partial t^2} \right|_{t=0} \frac{t^2}{2} \qquad \textbf{(C.3)}$$

$$\left. \frac{\partial C_P}{\partial t} \right|_{t=0} = \left. \frac{\partial C_P}{\partial \lambda} \frac{\partial \lambda}{\partial \omega_t} \frac{\partial \omega_t}{\partial t} \right|_{t=0} = \left. \frac{R_t}{V_w} \frac{\partial C_P}{\partial \lambda} \frac{\partial \omega_t}{\partial t} \right|_{t=0} \qquad \textbf{(C.4)}$$

$$\left. \frac{\partial^2 C_P}{\partial t^2} \right|_{t=0} = \left(\frac{R_t}{V_w} \right)^2 \left. \frac{\partial^2 C_P}{\partial \lambda^2} \left(\frac{\partial \omega_t}{\partial t} \right)^2 \right|_{t=0} + \left. \frac{R_t}{V_w} \frac{\partial C_P}{\partial \lambda} \frac{\partial^2 \omega_t}{\partial t^2} \right|_{t=0} \qquad \textbf{(C.5)}$$

Considering Taylor's approximation, the coefficients at $t = 0$ are assumed constant:

$$\int_0^{T_{Boost}} \Delta C_P(t)\, dt \approx \frac{R_t}{V_w} \frac{\partial C_P}{\partial \lambda} \frac{\partial \omega_t}{\partial t}\Bigg|_{t=0} \int_0^{T_{Boost}} t\, dt$$

$$+ \frac{1}{2}\left(\frac{R_t}{V_w}\right)^2 \frac{\partial^2 C_P}{\partial \lambda^2}\left(\frac{\partial \omega_t}{\partial t}\right)^2\Bigg|_{t=0} \int_0^{T_{Boost}} t^2\, dt \qquad \textbf{(C.6)}$$

$$+ \frac{1}{2}\frac{R_t}{V_w}\frac{\partial C_P}{\partial \lambda}\frac{\partial^2 \omega_t}{\partial t^2}\Bigg|_{t=0} \int_0^{T_{Boost}} t^2\, dt$$

Solving the integrals we have:

$$\int_0^{T_{Boost}} \Delta C_P(t)\, dt \approx \frac{1}{2}\frac{R_t}{V_w}\frac{\partial C_P}{\partial \lambda}\frac{\partial \omega_t}{\partial t}\Bigg|_{t=0} T_{Boost}{}^2$$

$$+ \frac{1}{6}\left(\frac{R_t}{V_w}\right)^2 \frac{\partial^2 C_P}{\partial \lambda^2}\left(\frac{\partial \omega_t}{\partial t}\right)^2\Bigg|_{t=0} T_{Boost}{}^3 \qquad \textbf{(C.7)}$$

$$+ \frac{1}{6}\frac{R_t}{V_w}\frac{\partial C_P}{\partial \lambda}\frac{\partial^2 \omega_t}{\partial t^2}\Bigg|_{t=0} T_{Boost}{}^3$$

Second simplification: A further simplification can be done assuming constant speed acceleration and knowing that $\Delta t \cdot d\omega_t/dt = \Delta \omega_t$, therefore:

$$\int_0^{T_{Boost}} \Delta C_P(t)\, dt \approx \frac{1}{2}\frac{R_t}{V_w}\frac{\partial C_P}{\partial \lambda}\Bigg|_{t=0} T_{Boost}\,\Delta \omega_t + \frac{1}{6}\left(\frac{R_t}{V_w}\right)^2 \frac{\partial^2 C_P}{\partial \lambda^2}\Bigg|_{t=0} T_{Boost}\,\Delta \omega_t^2 \qquad \textbf{(C.8)}$$

Finally, the aerodynamical energy variation, for a rotational speed variation $\Delta \omega_t$ over a period T_{OP} at constant wind speed, can be estimated as:

$$\Delta E_{Aero} \approx \frac{1}{2}K_{Aero}V_w^3\frac{R_t}{V_w}\frac{\partial C_P}{\partial \lambda}\Bigg|_{t=0} T_{Boost}\,\Delta \omega_t$$

$$+ \frac{1}{6}K_{Aero}V_w^3\left(\frac{R_t}{V_w}\right)^2\frac{\partial^2 C_P}{\partial \lambda^2}\Bigg|_{t=0} T_{Boost}\,\Delta \omega_t^2 \qquad \textbf{(C.9)}$$

Determination of the electrical energy variation:

The electrical energy delivered to the grid and its variation is:

$$E_{Electric} = \int_0^{T_{Boost}} (P_0 + \Delta P_{Boost})\, dt = E_{Electric0} + \int_0^{T_{Boost}} \Delta P_{Boost}\, dt \qquad \textbf{(C.10)}$$

$$\Delta E_{Electric} = \Delta E_{Boost}.$$ **(C.11)**

As ΔE_{Boost} is a controlled variable, the variation law is given by the inertia controller.

Determination of the losses energy variation:
The lost energy in the machine after aerodynamical conversion, and its variation, are:

$$E_{Losses} = E_{Losses-Mech} + E_{Losses-Gen} + E_{Self}$$ **(C.12)**

$$E_{Losses} = \int_0^{T_{Boost}} \left(P_{Loss-Mech}(0) + \Delta P_{Loss-Mech}(t)\right)dt +$$

$$+ \int_0^{T_{Boost}} \left(P_{Loss-Gen}(0) + \Delta P_{Loss-Gen}(t)\right)dt$$ **(C.13)**

$$+ \int_0^{T_{Boost}} \left(P_{Self}(0) + \Delta P_{Self}(t)\right)dt$$

Mechanical losses are given by:

$$\int_0^{T_{Boost}} \left(P_{Loss-Mech}(0) + \Delta P_{Loss-Mech}(t)\right)dt$$

$$= \left(1 - \eta_{DT}\right) \int_0^{T_{Boost}} \left(P_{Aero}(0) + \Delta P_{Aero}(t)\right)dt + \eta_{DT}\, F_{DT} \int_0^{T_{Boost}} \left(\omega_t(0) + \Delta\omega_t(t)\right)^2 dt$$ **(C.14)**

First simplification: generator losses and self-consumption are considered constant during T_{Boost}, therefore $\Delta E_{Loss-Gen} = \Delta E_{Self} = 0$. Therefore:

$$\Delta E_{Losses} \approx \Delta E_{Loss-Mech}$$

$$= \left(1 - \eta_{DT}\right)\Delta E_{Aero} + 2\,\eta_{DT}\, F_{DT}\, \omega_t(0) \int_0^{T_{Boost}} \Delta\omega_t(t)\,dt + \eta_{DT}\, F_{DT} \int_0^{T_{Boost}} \Delta\omega_t(t)^2\,dt$$ **(C.15)**

Second simplification: Taylor's series approximation.

$$\Delta\omega_t(t) \approx \left.\frac{\partial\omega_t}{\partial t}\right|_{t=0} t$$ **(C.16)**

Considering Taylor's approximation, the coefficients at $t = 0$ are considered constant:

$$\Delta E_{Losses} \approx \left(1-\eta_{DT}\right)\Delta E_{Aero} + 2\ \eta_{DT}\ F_{DT}\ \omega_t(0)\left.\frac{\partial \omega_t}{\partial t}\right|_{t=0}\int_0^{T_{Boost}} t\ dt$$

$$+\ \eta_{DT}\ F_{DT}\left(\left.\frac{\partial \omega_t}{\partial t}\right|_{t=0}\right)^2\int_0^{T_{Boost}} t^2\ dt \qquad \text{(C.17)}$$

Solving the integrals:

$$\Delta E_{Losses} \approx \left(1-\eta_{DT}\right)\Delta E_{Aero} + \eta_{DT}\ F_{DT}\ \omega_t(0)\left.\frac{\partial \omega_t}{\partial t}\right|_{t=0} T_{Boost}^2$$

$$+\ \frac{1}{3}\eta_{DT}\ F_{DT}\left(\left.\frac{\partial \omega_t}{\partial t}\right|_{t=0}\right)^2 T_{Boost}^3 \qquad \textbf{(C.18)}$$

A further simplification can be done assuming constant speed acceleration and knowing that $\Delta t \cdot d\omega_t/dt = \Delta \omega_t$. Finally, the losses energy variation, for a rotational speed variation $\Delta \omega_t$ over a period T_{Boost} at constant wind speed, can be estimated as:

$$\Delta E_{Losses} \approx \left(1-\eta_{DT}\right)\Delta E_{Aero} + \eta_{DT}\ F_{DT}\omega_t(0)\ T_{Boost}\ \Delta \omega_t + \frac{1}{6}\eta_{DT}\ F_{DT}\ T_{Boost}\ \Delta \omega_t^2 \qquad \textbf{(C.19)}$$

Determination of the kinetic energy variation:

The variation of the kinetic energy stored in the turbine's rotating masses is:

$$\Delta E_{Kinetic} = \frac{1}{2}J_t\left(\omega_{t2}^2 - \omega_{t1}^2\right) \qquad \textbf{(C.20)}$$

$$\Delta E_{Kinetic} = J_t\ \omega_t(0)\Delta \omega_t + \frac{1}{2}J_t\ \Delta \omega_t^2 \qquad \textbf{(C.21)}$$

//

D
DATA WIND TURBINE WTG1

D.1 Aerodynamical data

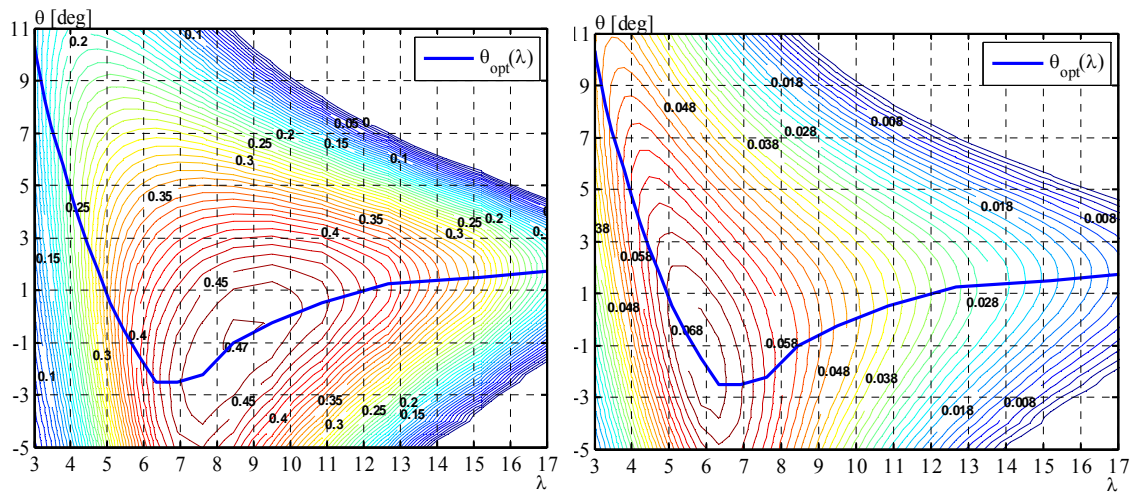**Figure D-1:** (right): contours of aerodynamic power coefficient $C_P(\lambda,\theta)$ and optimal pitch angle θ_{Opt} for different λ. (left): Level contours of aerodynamic torque coefficient $C_q(\lambda,\theta)$ and optimal pitch angle θ_{Opt} for different λ.
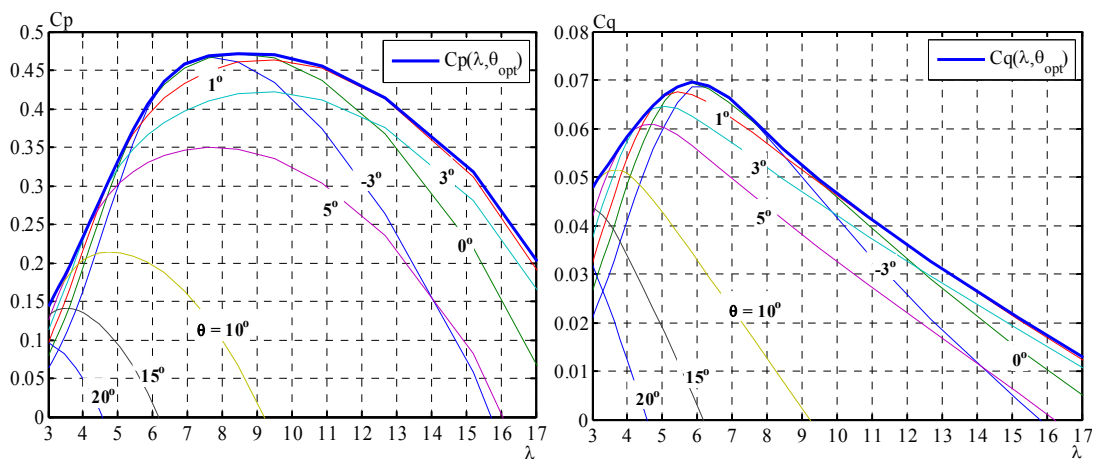

Figure D-2: (right): Aerodynamic power coefficient C_P vs. tip speed ratio λ, for different pitch angle θ and envelope of optimal $C_P(\lambda,\theta_{Opt})$. (left): Aerodynamic torque coefficient C_q vs. tip speed ratio λ, for different pitch angle θ and envelope of optimal $C_q(\lambda,\theta_{opt})$.

277

Figure D-1 and **Figure D-2** shows $\theta_{opt}(\lambda)$ and $C_{Popt}(\lambda)$. Observe, for a given λ, how the C_P changes with θ. The power coefficient has a maximum value $C_{Pmax} \approx 0.47$ for an optimum $\lambda_{opt} \approx 8.5$ and $\theta_{opt} \approx -1$ deg. The solid blue curve indicates optimum values of $\theta_{opt}(\lambda)$ at which the power coefficient is optimal: $C_P = C_{Popt}$.

$$C_{POpt}(\lambda_i) = \max\{Cp(\lambda_i, \theta)\}, \text{ for a given } \lambda_i. \qquad \textbf{(D.52)}$$

$$\theta_{Opt}(\lambda_i) = \theta_k, \ \forall \ Cp(\lambda_i, \theta_k) = C_{POpt-i}(\lambda_i), \text{ for a given } \lambda_i. \qquad \textbf{(D.53)}$$

Therefore optimum power coefficient, C_{Popt}, depends only on λ.

D.2 Approximation of $C_P(\lambda, \theta_{opt})$

Here, the approximation of $C_P(\lambda, \theta)$ when $\theta = \theta_{opt}$ is carried out by means of polynomial function. The points of C_{Popt} for different λ, shown in **Figure D-2** were used for fitting a polynomial function of order 15th as expressed in (**D.54**). Expressions (**D.55**) and (**D.56**) show respectively the first and second partial derivatives with respect to λ. The choosing of the 15th order polynomial for $C_{Popt}(\lambda)$ has been done by comparison of the second derivative functions for different polynomial order fittings. **Figure D-3** shows the $C_{Popt}(\lambda)$ fitting with polynomials of 7th, 15th and 25th order as comparisons. **Figure D-4** left shows the first derivative with respect to λ for polynomials of 7th, 15th and 25th order. **Figure D-4** right shows the second derivative with respect to λ for polynomials of 7th, 15th, 25th and 60th order. Observe carefully in this last figure that after the 25th order fitting there is no practical improvement in the second derivative function. Considering a reduction in the polynomial order and still acceptable errors, the 5th order function has been chosen. Nevertheless, for higher accuracy in calculations, a higher polynomial order can be adopted. The maximum and minimum possible λ for the turbine WTG1 in operation are $\lambda_{Max} \approx 18$ and $\lambda_{Min} \approx 3$, therefore these values were used for defining the valid range for the fitted function.

$$
\begin{aligned}
C_{Popt}(\lambda) \approx \\
-80.5947e-2 + 2.58949\,\lambda - 3.45986\,\lambda^2 + 2.63859\,\lambda^3 - 1.27185\,\lambda^4 + \\
+41.3875e-2\,\lambda^5 - 94.4685e-3\lambda^6 + 15.5047e-3\lambda^7 - 18.5862e-4\,\lambda^8 + \\
+16.3917e-5\lambda^9 - 10.6183e-6\,\lambda^{10} + 49.8998e-8\,\lambda^{11} - 16.5480e-9\,\lambda^{12} + \\
+36.7114e-11\lambda^{13} - 48.89e-13\,\lambda^{14} + 29.5e-15\,\lambda^{15}.
\end{aligned}
\qquad \textbf{(D.54)}
$$

$$\frac{\partial C_{Popt}(\lambda)}{\partial \lambda} \approx$$

$$2.58949 - 6.91972\,\lambda + 7.91576\,\lambda^2 - 5.08740\,\lambda^3 + 2.06937\,\lambda^4 -$$
$$- 56.6811e - 2\,\lambda^5 + 10.8533e - 2\,\lambda^6 - 14.8689e - 3\,\lambda^7 + 14.7525e - 4\,\lambda^8 -$$
$$- 10.6183e - 5\,\lambda^9 + 54.8898e - 7\,\lambda^{10} - 19.8577e - 8\,\lambda^{11} + 47.7248e - 10\,\lambda^{12} -$$
$$- 68.445e - 12\,\lambda^{13} + 44.3e - 14\,\lambda^{14}.$$

(D.55)

$$\frac{\partial^2 C_{Popt}(\lambda)}{\partial \lambda^2} \approx$$

$$- 6.91972 + 15.8315\,\lambda - 15.2622\,\lambda^2 + 8.27750\,\lambda^3 - 2.83405\,\lambda^4 +$$
$$+ 65.1198e - 2\,\lambda^5 - 10.4082e - 2\,\lambda^6 + 11.8020e - 3\,\lambda^7 - 95.5649e - 5\,\lambda^8 +$$
$$+ 54.8898e - 6\,\lambda^9 - 21.8434e - 7\,\lambda^{10} + 57.2698e - 9\,\lambda^{11} - 88.9786e - 11\,\lambda^{12}$$
$$+ 62.06e - 13\,\lambda^{13}.$$

(D.56)
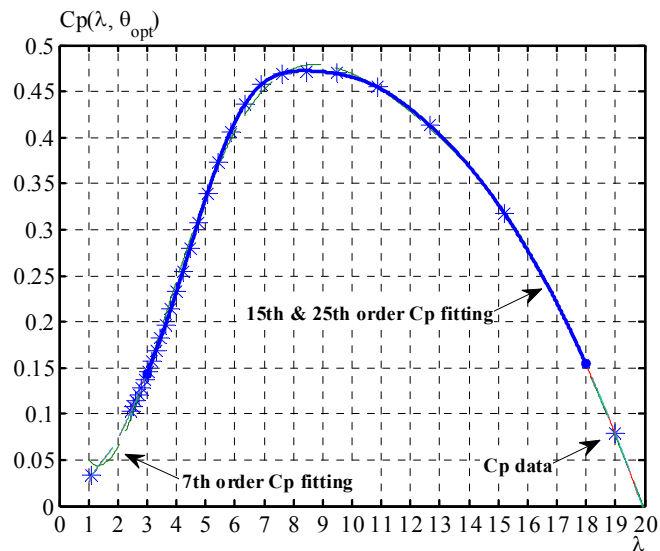
Figure D-3: Fitting of C_P for different order polynomial functions. The 15th order fitting was chosen showing valid range.
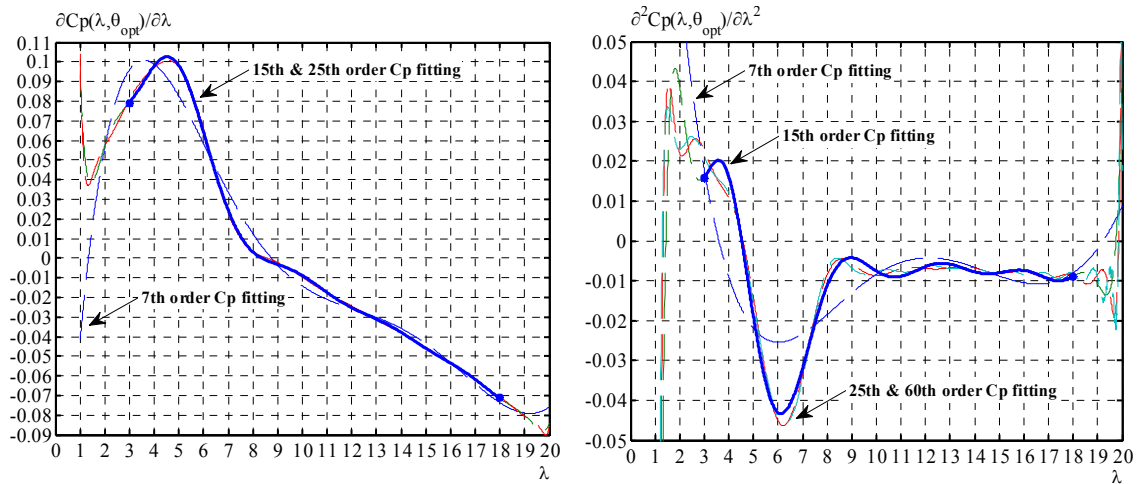
Figure D-4: (left) First derivative of C_P for different polynomial order fitting. The 15th order fitting was chosen showing valid range. (right): Second derivative of C_P for different polynomial order fitting. The 15th order fitting was chosen showing valid range.

D.3 Mechanical data

Table D-1: Main parameters of drive train and tower

Moment of inertia of generator's rotor plus break disk plus high speed shaft –all referred to the high speed shaft (J_g)	72 [kgm^2]
Moment of inertia of blades plus hub plus low speed shaft – all referred to the low speed shaft (J_r)	4.3073e6 [kgm^2]
Drive train stiffness –referred to the low speed shaft (K_{DT})	140e6 [Nm/rad]
Tower bending stiffness ($K_{tow\theta}$)	772e6 [Nm/rad]
Tower eigenfrequency (f_{tow})	0.4 [Hz]
Drive train damping coefficient (ξ_{DT})	0.004
Tower damping coefficient y-axis bending (ξ_{towY})	0.013
Tower damping coefficient x-axis bending (ξ_{towX})	0.015
Gearbox ratio ($iG = \Omega_g/\Omega_r$)	101.02
Tower high (h_{tow})	60 [m]
Mass of tower top (M_{towTop})	103644.5 [kg]
Equivalent tower mass (M_{towEq})	10500 [kg]

E
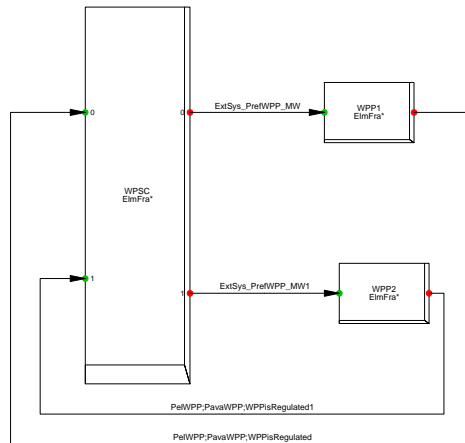# POWER FACTORY FRAMES WIND POWER

Figure E-5: Frame for wind power system, with control at power system level (WPSC) and two wind power plants (WPP1 & WPP2).
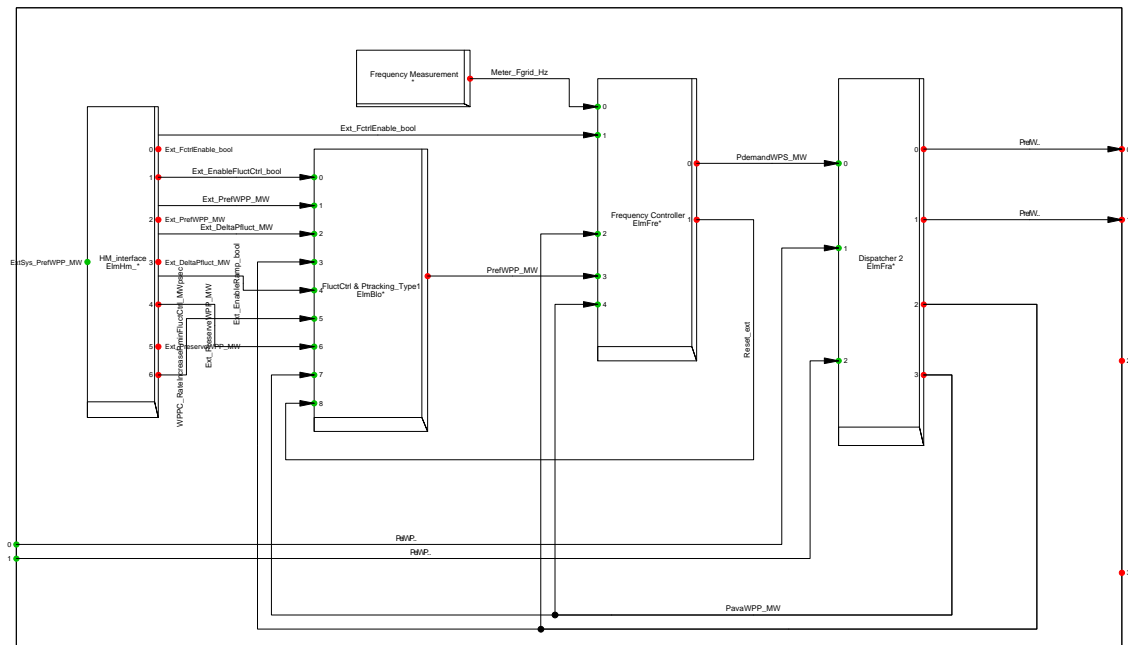

Figure E-6: Frame for controller at power system level (WPSC), with Human-Machine interface block, power tracking Type 1, frequency controller and Dispatcher 2, communicating with the wind power plants (WPP1 & WPP2).
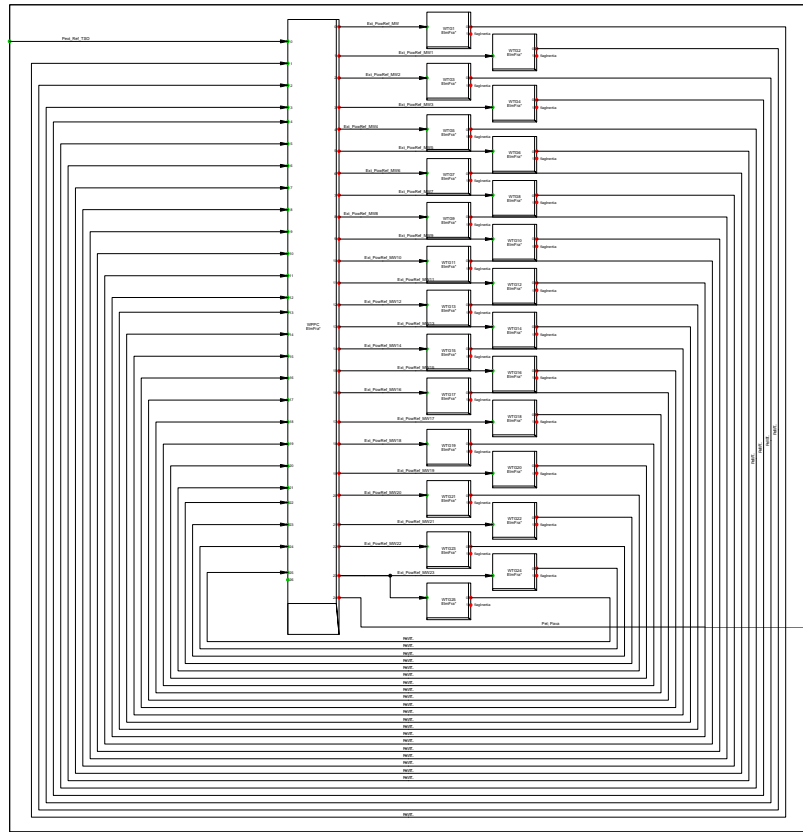
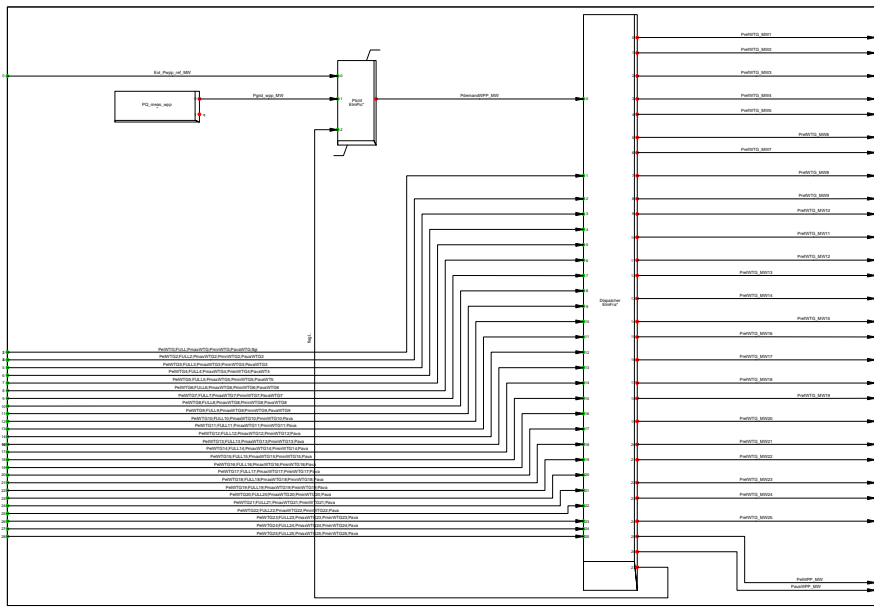**Figure E-7:** Frame for wind power plant (WPP), with a power plant controller (WPPC) and 25 wind turbines (WTG).

Figure E-8: Frame for wind power plant controller (WPPC), with PI controller and Dispatcher 1, communicating with the wind turbines (WTG).
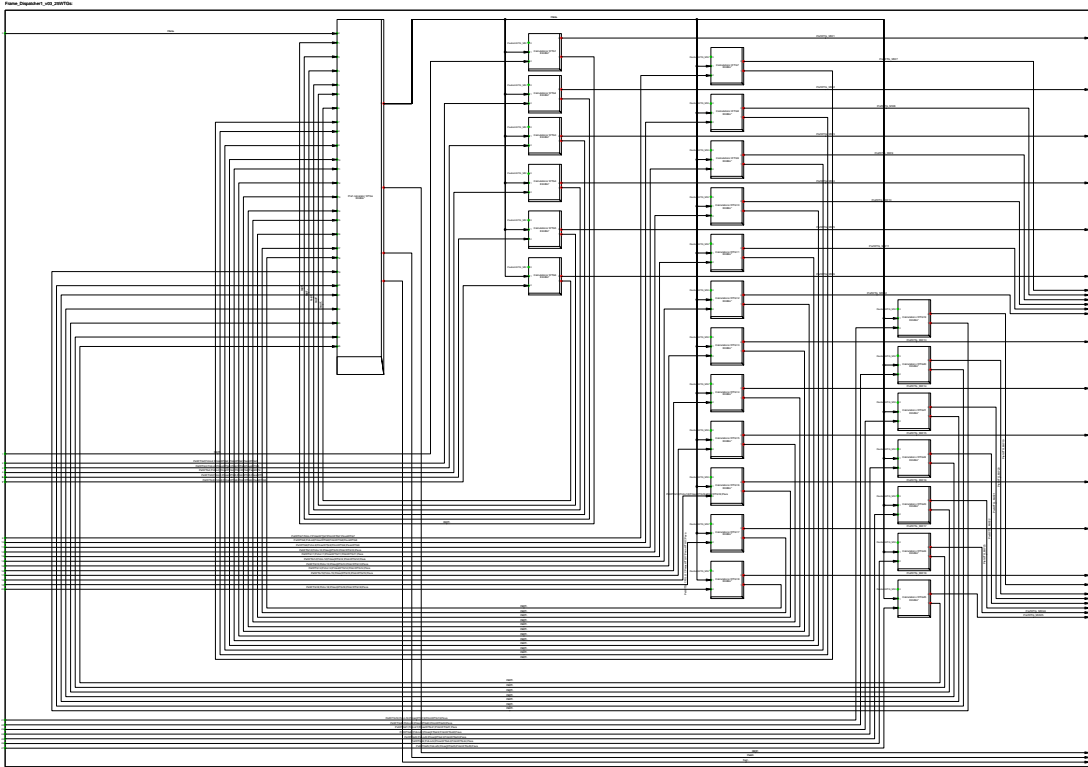
Figure E-9: Frame for Dispatcher 1 (in WPPC), receiving input from PI controller and communicating with wind turbines (WTG).
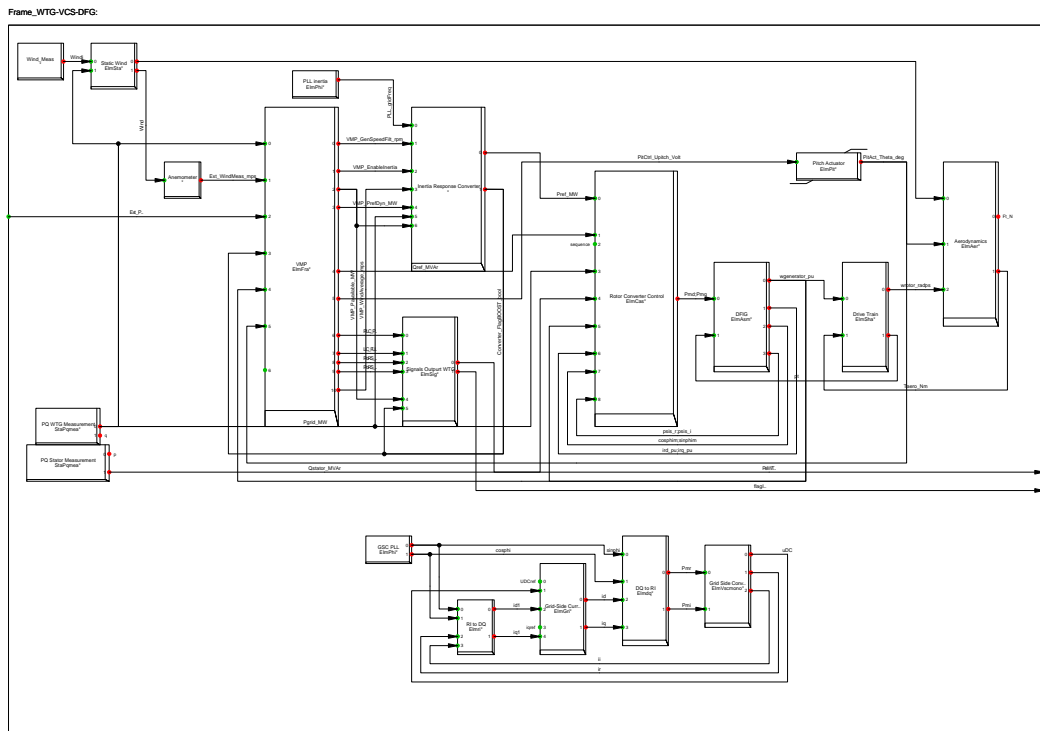

Figure E-10: Frame for wind turbine (WTG), communicating with the power plant controller (WPPC).